MONASH University

Application Of Synchrotron Microangiography To Functional Imaging Of Coronary Vessels *In Vivo*

Yi Ching (Peggy) Chen
Bachelor of Science

A thesis submitted for the degree of *Doctor of Philosophy* at
Monash University in 2016
Department of Physiology

Copyright notice

Table of Contents

List of Figures

CHAPTER 1

CHAPTER 2

CHAPTER 3

CHAPTER 4

CHAPTER 5

CHAPTER 6

APPENDIX 1

List of Tables

CHAPTER 1

CHAPTER 6

Abstract

Heart failure (HF) can be defined as a state in which the heart is unable to generate sufficient cardiac output to maintain normal body function. It can be caused by a variety of diseases or conditions that impair or overload the heart. HF usually develops slowly, often over many years (chronic HF), but it can also occur with rapid onset (acute HF). While mortality from acute myocardial infarction (MI) and chronic HF resulting from MI is on the decline in many countries, there is a secondary epidemic of HF with preserved ejection fraction (HFpEF) due at least partly to the global epidemic of obesity and diabetes. Additionally, various conditions, including hypertension, obesity, diabetes mellitus, sleep apnea, and coronary vascular disease (especially acute MI) are considered to accelerate the progression of HFpEF to end-stage HF.

Early diagnosis and prevention of HF is a crucial strategy for reducing cardiac remodeling and the other adverse compensatory pathophysiological changes associated with all subtypes of HF. This strategy is thus critical for improving survival of patients with HF. Assessment of coronary vascular function is a useful research tool to evaluate therapies for chronic HF, because coronary vascular disease or dysfunction are common causes of HF. Micro-angiography is a novel and minimally invasive technique for evaluation of coronary vascular function. In the experiments described in this thesis, synchrotron based micro-angiography was used to evaluate the efficacy of several therapies aimed at preventing the development of HF after MI. At the same time, micro-angiography was used to determine coronary vascular function in rodent models with various risk factors for development of HF, such as intermittent hypoxia, insulin resistance and vasospasm. This approach was aimed towards improving our understanding of the contributions of these risk factors to coronary vascular dysfunction and the progression of HF.

In the studies described in this thesis, we found that a regenerative therapy that combined stem cells with endogenous sources of angiogenic factors had a better potential to prevent and treat HF than either treatment as a monotherapy. The efficacy of combined therapy appeared to be due to its ability to increase and re-established coronary blood flow by increasing the number of functional coronary microvessels in the infarcted heart. In contrast, we found that a pharmacological therapy, the prostacyclin analogue ONO-1301, did not produce consistent and significant benefits in the rodent model of chronic HF we studied. We also found that risk factors for HF, such as insulin resistance and intermittent hypoxia, have additive effects on coronary function by exacerbating endothelial dysfunction. However, these two risk factors appear to affect coronary circulation through different mechanisms. Therefore, the strategies for preventing the onset of HFpEF and the

progression of chronic HF should not only be directed towards amelioration of symptoms, but should also be directed towards minimizing risk factors for HF.

In conclusion, in studies of rodents, using synchrotron microangiography, we were able to demonstrate how risk factors for HF and novel potential treatments for HF affect the function of the coronary circulation. These studies provide novel insights into the mechanisms that drive progression of coronary dysfunction, particularly the relative roles of major risk factors for HF. They also demonstrate that it is possible to assess the efficacy of potential therapies for HF in preclinical studies by evaluating coronary function *in vivo*.

Declaration

This thesis contains no material which has been accepted for the award of any other degree or diploma at any university or equivalent institution and that, to the best of my knowledge and belief, this thesis contains no material previously published or written by another person, except where due reference is made in the text of the thesis.

Chapter 1, 4 & 5 are unpublished manuscripts, and have not been submitted, accepted for submission, or published.

Chapter 1:
My contribution = 80%
Co-authors: Roger G Evans & James T Pearson

Chapter 4:
My contribution = 70%
Co-authors: Roger G Evans & James T Pearson

Chapter 5:
My contribution = 60%
Co-authors: Roger G Evans & James T Pearson

Student Print Names: Yi Ching (Peggy) Chen

Student signature: Chen Yi Ching **Date:** 22/08/2016

Main Supervisor Print Names: James T Pearson

Main Supervisor signature: **Date:** 22/08/2016

Publications during enrolment

Thesis including published works declaration

I hereby declare that this thesis contains no material which has been accepted for the award of any other degree or diploma at any university or equivalent institution and that, to the best of my knowledge and belief, this thesis contains no material previously published or written by another person, except where due reference is made in the text of the thesis.

This thesis includes 2 original papers published in peer reviewed journals and 0 unpublished publications. The core theme of the thesis is the application of synchrotron microangiography to functional imaging of coronary vessels *in vivo*. The ideas, development and writing up of all the papers in the thesis were the principal responsibility of myself, the candidate, working within the Department of Physiology under the supervision of Professor James T Pearson.

(The inclusion of co-authors reflects the fact that the work came from active collaboration between researchers and acknowledges input into team-based research.)

In the case of *Chapter 6 and Appendix 1*, my contribution to the work involved the following:

(If this is a laboratory-based discipline, a paragraph outlining the assistance given during the experiments, the nature of the experiments and an attribution to the contributors could follow.)

Thesis Chapter	**Publication Title**	**Status** *(published, in press, accepted or returned for revision)*	**Nature and % of student contribution**	**Co-author name(s) Nature and % of Co-author's contribution***	**Co-author(s), Monash student Y/N***
6	Chronic intermittent hypoxia accelerates coronary microcirculatory dysfunction in insulin-resistant Goto-Kakizaki rats	Published	*60%. Concept and collecting data and writing first draft*	*1) Tadakatsu Inagaki, input into manuscript 1%* *2) Yutaka Fujii, input into manuscript 1%* *3) Daryl O. Schwenke, input into manuscript 1%* *4) Hirotsugu Tsuchimochi, input into manuscript 1%* *5) Amanda J. Edgley, input into manuscript 1%* *6) Yuan Zhang, input into manuscript 1%* *7) Darren J. Kelly, input into manuscript 1%* *8) Misa Yoshimoto, input into manuscript 1%* *9) Hisashi Nagai, input into manuscript 1%* *10) Ichiro Kuwahira, input into manuscript 1%* *11) Mikiyasu Shirai, input into manuscript ~10%* *12) Roger G. Evans, input into manuscript ~10%* *13) James T. Pearson, input into manuscript ~10%*	*No*

Appendix 1	Cell-sheet Therapy With Omentopexy Promotes Arteriogenesis and Improves Coronary Circulation Physiology in Failing Heart	Published	*35%. Collecting data, analysis and writing first draft*	*1) Satoshi Kainuma, input into manuscript 35%* *2) Shigeru Miyagawa, input into manuscript ~1%* *3) Satsuki Fukushima, input into manuscript ~1%* *4) Atsuhiro Saito, input into manuscript ~1%* *5) Akima Harada, input into manuscript ~1%* *6) Motoko Shiozaki, input into manuscript ~1%* *7) Hiroka Iseoka, input into manuscript ~1%* *8) Tadashi Watabe, input into manuscript ~1%* *9) Hiroshi Watabe, input into manuscript ~1%* *10) Genki Horitsugi, input into manuscript ~1%* *11) Mana Ishibashi, input into manuscript ~1%* *12) Hayato Ikeda, input into manuscript ~1%* *13) Hirotsugu Tsuchimochi, input into manuscript ~1%* *14) Takashi Sonobe, input into manuscript ~1%* *15) Yutaka Fujii, input into manuscript ~1%* *16) Hisamichi Naito, input into manuscript ~1%* *17) Keiji Umetani, input into manuscript ~1%* *18) Tatsuya Shimizu, input into manuscript ~1%* *19) Teruo Okano, input into manuscript ~1%* *20) Eiji Kobayashi, input into manuscript ~1%* *21) Takashi Daimon, input into manuscript ~1%* *22) Takayoshi Ueno, input into manuscript ~1%* *23) Toru Kuratani, input into manuscript ~1%* *24) Koishi Toda, input into manuscript ~1%* *25) Nobuyuki Takakura, input into manuscript ~1%* *26) Jun Hatazawa input into manuscript ~1%* *27) Mikiyasu Shirai, input into manuscript ~1%* *28) Yoshiki Sawa, input into manuscript ~1%* *29) James T. Pearson input into manuscript 10%*	*No*

**If no co-authors, leave fields blank*

I have / have not renumbered sections of submitted or published papers in order to generate a consistent presentation within the thesis.

Student signature: **Date:** 22/08/2016

The undersigned hereby certify that the above declaration correctly reflects the nature and extent of the student's and co-authors' contributions to this work. In instances where I am not the responsible author I have consulted with the responsible author to agree on the respective contributions of the authors.

Main Supervisor signature: **Date:** 22/08/2016

Acknowledgements

First and foremost, I would like to show my deep and sincere gratitude to both of my supervisors Prof. James Pearson and Assoc. Prof. Roger Evans, whose guidance and support from the initial to the final level enabled me to develop an understanding of the subject. They have made available of their support in a number of ways with their wide knowledge, constructive criticism and excellent advice.

I have worked and met with a number of great individuals on my journey completing this thesis. It is a pleasure to thank the team from National Cardiovascular Centre, Osaka, Japan who made this thesis possible. Special thanks to the staff from Monash Cardiovascular and Renal Research Group for all the advice you guys given to help me prepare my seminar presentation.

To Connie, Debra and Jen, my family from HDR office and lab group, it is an honor for me to work and share these years with you. I would like to thank you all with the support and friendship. I also have learned a lot from all of you. Special thanks to Connie for all your advice, help and support during the time I was struggle. I would also like to thank my dearest friend and housemate, Jenny. I cannot thank you enough for giving me all the mental support and encouragement.

A great thank you to my Australian family, Kerrie for all your support and warmness during all these years. Also, a special thank to my dear two little friends, Piccolo and Monet for giving me the warm and pressure-releasing cuddle whenever I need. Woof Woof!!

I also would like to thank my friends from Taiwan for all the support during this journey.

Finally, I owe my deepest gratitude to my wonderful family, Mom and Dad in Taiwan and my dearest sis, Ivy in US for their support and selfless giving allowing me the opportunity to achieve my goals and aspirations. I cannot reach this great achievement without you.

Publications included in this PhD thesis

1. Kainuma S, Miyagawa S, Fukushima S, Pearson J, Chen YC, Saito A, Harada A, Shiozaki M, Iseoka H, Watabe T, Watabe H, Horitsugi G, Ishibashi M, Ikeda H, Tsuchimochi H, Sonobe T, Fujii Y, Naito H, Umetani K, Shimizu T, Okano T, Kobayashi E, Daimon T, Ueno T, Kuratani T, Toda K, Takakura N, Hatazawa J, Shirai M, and Sawa Y. Cell-sheet therapy with omentopexy promotes arteriogenesis and improves coronary circulation physiology in failing heart. *Mol Ther* 23: 374-386, 2015.

2. Chen YC, Inagaki T, Fujii Y, Schwenke DO, Tsuchimochi H, Edgley AJ, Umetani K, Zhang Y, Kelly DJ, Yoshimoto M, Nagai H, Evans RG, Kuwahira I, Shirai M, and Pearson JT. Chronic intermittent hypoxia accelerates coronary microcirculatory dysfunction in insulin resistant Goto-Kakizaki rats. *Am J Physiol Regul Integr Comp Physiol* 311: R426-439, 2016.

Conference abstracts

1. Chen Y-C, Shirai M, Kainuma S, Fujii Y, Inagaki T, Umetani K, Evans RG, Tsuchimochi H, Pearson JT. Does stem cell combination therapy enhance coronary vessel number in a rodent heart failure model more than monotherapy?

Conference: High Blood Pressure Research Council of Australia (HBPRCA) Annual Scientific Meeting

Conference paper published in *Hypertension* June 2014, Vol. 63, H-025

2. Pearson JT, Yoshimoto M, Chen Y-C, Sultani R, Nakaoka H, Nishida M, Yamashita S, Umetani K, Tsuchimochi H, Shirai M. Widespread coronary endothelial dysfunction in the absence of HDL receptor SRB1 in a mouse model of ischemic cardiomyopathy.

Conference: High Blood Pressure Research Council of Australia (HBPRCA) Annual Scientific Meeting

Conference paper published in *Hypertension* June 2014, Vol. 63, H-104

Presentations

1. Poster presentation at HBPRCA:

Chen Y-C, Shirai M, Kainuma S, Fujii Y, Inagaki T, Umetani K, Evans RG, Tsuchimochi H, Pearson JT. Does stem cell combination therapy enhance coronary vessel number in a rodent heart failure model more than monotherapy? *High Blood Pressure Research Council of Australia (HBPRCA)*, Melbourne, Australia (2013)

2. Poster presentation at MASR:

Y-C. Chen, T. Inagaki, Y. Fujii, D.O. Schwenke, A.J. Edgley, K. Umetani, Y. Zhang, D.J. Kelly, M. Yoshimoto, H. Tsuchimochi, H. Nagai, I. Kuwahira, R.G. Evans, M. Shirai, J.T. Pearson. Chronic intermittent hypoxia accelerate coronary microcirculatory dysfunction in young insulin resistant Goto-Kakizaki rats, *Medical Application of synchrotron Radiation (MASR)*, ESRF Grenoble & Villard de Lans, France (2015)

Symbols and abbreviations

SYMBOLS

±	plus or minus
×	times or multiples by
≤	at least or less than
≥	at least or greater than
<	less than
>	greater than
%	percent
~	approximately
µ	micro
cm	centimeter
L	liters
M	molar
mol	moles
°C	degrees Celsius

ABBREVIATIONS

AC	adenylyl cyclase
ACE	angiotensin-converting enzyme
APJ	apelin receptor
ARA	aldosterone receptor antagonists
ARB	angiotensin-receptors blockers
ARN	angiotensin receptor neprilysin inhibitor
ATP	adenosine triphosphate
BH4	tetrahydrobiopterin
BM	Bone marrow
cAMP	cyclic adenosine monophosphate
cGMP	cyclic guanosine monophosphate
COX	cyclooxygenase
CSC	cardiac stem cells
CT	computed tomography
CYP4502c	cytochrome P4502C
EDHF	endothelium-derived hyperpolarizing factors
EET	eicosatrienoic acids
EETs	eicosatrienoic acids
eNOS	endothelial nitric oxide synthase

ESCs	embryonic stem cells
Gap	myoendothelial gap junction
GTP	guanosine triphosphate
H_2O_2	hydrogen peroxide
HCN	hyperpolarization-activated cyclic nucleotide-gate
HF	heart failure
HFpEF	heart failure with preserved ejection fraction
HFrEF	heart failure with reduced ejection fraction
HIF-1α	hypoxia inducible factor 1α
HR	heart rate
IH	intermittent hypoxia
iNOS	inducible nitric oxide synthase
IP	prostacyclin receptor
iPSCs	induced pluripotent stem cells
ISDN	isosorbide dinitrate
KCa^+	calcium dependent potassium channels
K_{IR}^+	inwardly rectifying potassium channels
LV	left ventricle
MI	myocardial infarction
MLCK	myosin light chain kinase
MRI	magnetic resonance imaging
MSC	mesenchymal cells
NADPH	nicotinamide adenine dinucleotide phosphate
NF-$_K$B	nuclear factor kappa B
nNOS	neuronal nitric oxide synthase
NO	nitric oxide
NOS	nitric oxide synthase
O_2	oxygen
O_2^-	superoxide
$ONOO^-$	peroxynitrite
PGH_2	prostaglandin H_2
PGI_2	prostacyclin
PKA	protein kinase A
PKG	protein kinase G
PLA_2	phospholipase A_2

RAS	renin-angiotensin system
ROS	reactive oxygen species
sGC	soluble guanylate cyclase
SkM	skeletal myoblast cells
SNS	sympathetic nervous system
SOD	superoxide dismutase
SR	synchrotron radiation
TLRs	toll-like receptors
TNF-α	tumor necrosis factor-α
TRP	transient receptor potential
TRP V4	transient receptor potential vanilloid 4
VEGF	vascular endothelial growth factor
VSM	vascular smooth muscle

CHAPTER 1

General Introduction

Chapter 1

1.1 The Global International Problem of Heart Failure

Cardiovascular disease is the leading cause of mortality in developed countries such as the USA (188). It is also a major contributor (26%) to mortality in Australia (207). In past decades, treatments for acute coronary disease have dramatically improved. Patients who survive acute coronary disease often later develop chronic heart failure (HF) (83, 188). Consequently, chronic HF has become increasingly prevalent worldwide (225, 250). HF is not only the leading cause of death but also accounts for a large proportion of expenditure for health care in high-income countries (31). Hospitalization accounts for a large proportion of the health care expenditure (38%) required for management of patients with HF in Australia (134).

1.2 Characteristics of Heart Failure

HF can be defined as a state in which the heart is unable to generate sufficient cardiac output to maintain normal bodily function. It can be caused by a variety of diseases or conditions that impair or overload the heart. HF usually develops slowly, often over many years (chronic HF), but it can also occur with rapid onset (acute HF). In the clinical situation, acute end-stage HF commonly occurs in patients experiencing an acute exacerbation of chronic HF (187). Therefore, a better understanding of the development of chronic HF should also help in the effort to reduce the incidence of acute end-stage HF.

The ongoing cardiac dysfunction in chronic HF can be exacerbated by a combination of compensatory mechanisms including hypertrophy and apoptosis of cardiomyocytes, cardiac fibrosis, ventricular chamber dilation, tachycardia, peripheral vasoconstriction, and changes in sodium/water homeostasis due to altered renal function (149). Cardiac dysfunction can be categorized as systolic and/or diastolic dysfunction, and symptoms can be chiefly left-sided, right-sided or both (7). Chronic HF is associated with increased circulating levels of catecholamines, angiotensin II, tumor necrosis factor-α (TNF-α), and other neuroendocrine hormones and inflammatory cytokines (149). Short-term compensatory responses, driven by neurohumoral and hemodynamic changes,

lead to long-term deleterious effects. These include increased blood volume, increased systemic and pulmonary vascular resistance, and decreased cardiac contractility (165). These long-term effects then lead to impairment in cardiac output, which causes dyspnea and fatigue in patients with chronic HF (149). While mortality from acute myocardial infarction (MI) and chronic HF resulting from MI is on the decline in many countries, there is a secondary epidemic of HF with preserved ejection fraction (HFpEF) that has been exacerbated by the global epidemic of obesity and diabetes (223). A large number of young patients with diabetes have normal systolic function (ejection fraction >40%) but are intolerant of exercise (247). Hypertension, obesity, diabetes mellitus, sleep apnea, and coronary vascular disease (especially acute MI) all are considered to accelerate the progression of HFpEF to end-stage HF (28, 83, 149, 188).

Early diagnosis and prevention of HF is a crucial strategy for reducing cardiac remodeling and the other adverse compensatory pathophysiological changes associated with all subtypes of HF. This strategy is thus critical for improving survival of patients with HF. Evaluation of coronary vascular function is a useful research tool to evaluate therapies of chronic HF because coronary vascular disease or dysfunction are common causes of HF (203, 206). Microangiography is a novel and minimally invasive technique for evaluation of coronary vascular function as it requires arterial cannulation for assessment (220). In the experiments described in this thesis, microangiography was used to evaluate the efficacy of several therapies aimed at preventing the development of HF after MI. At the same time, microangiography was used to determine coronary vascular function in animal models with various risk factors for developing HF, such as intermittent hypoxia, insulin resistance and vasospasm, to allow us to understand the contributions of each risk factor to coronary vascular dysfunction and the progression of HF.

1.3 Myocardial Infarction and the Progression of Heart Failure

MI is the consequence of the interruption of blood supply to an area of the heart resulting in an irreversible loss of function of myocardial tissue. In the past, acute MI frequently resulted in mortality within several days, particularly if the MI was untreated or if the infarcted area was large (90). In the last few decades more patients are surviving acute MI, largely due to the introduction of modern interventions, such as thrombolytics and angioplasty (90). However, the patients

who survive acute MI often later develop HF (90, 206, 227). As many as 22% of those hospitalized in Australia between 1984 and 1993 with a first heart attack went on to develop chronic HF within 28 days of admission (4). In Australia, mortality of chronic HF is now twice that of acute MI (103, 159).

Necrosis associated with MI evokes an acute inflammatory response, which is a necessary process for healing and scar formation (52, 63). Following MI, impaired cardiac output leads to compensatory neurohormonal activation, which exacerbates the inflammatory response (53). Excessive activation of the renin-angiotensin system and sympathetic nervous system evoke left ventricle (LV) dysfunction and secondary ischemia (Fig 1.1). Furthermore, the change of chemical environment in the heart and a compensatory increase in contractility lead to apoptosis of cardiomyocytes (211). Ultimately, neurohormonal over activation causes pathological remodeling, leading to contractile failure (often referred to as decompensated HF) and death.

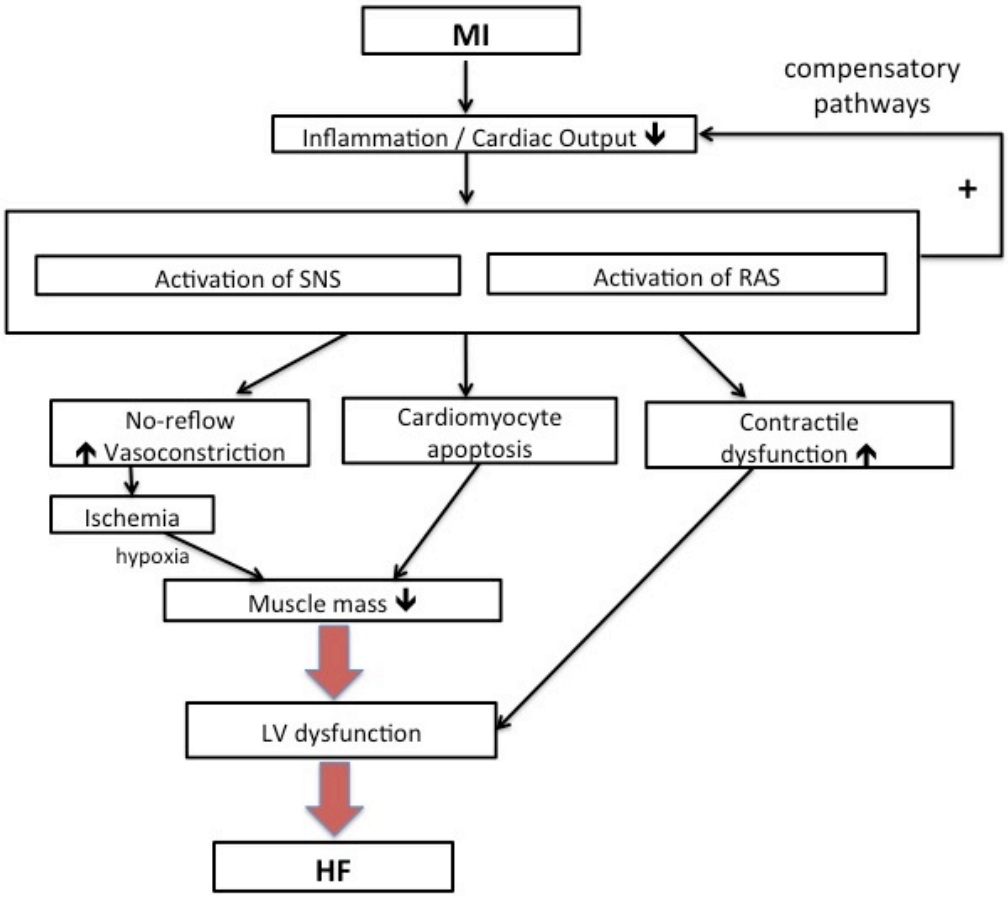

Figure 1.1 Schematic diagram of the progression from myocardial infarction to heart failure. Following myocardial infarction (MI), impaired cardiac output leads to compensatory neurohormonal activation which exacerbates the inflammatory response (53). Excessive activation of the renin-angiotensin system (RAS) and sympathetic nervous system (SNS) evoke left ventricle (LV) dysfunction and secondary ischemia. Furthermore, the change of chemical environment in the heart and a compensatory increase in contractility lead to apoptosis of cardiomyocytes (211). Ultimately, neurohormonal over activation causes pathological remodeling, leading to HF.

1.4 Normal Healing Process after Myocardial Infarction

The healing process after MI begins with an inflammatory response, which involves degradation of extracellular matrix, inhibition of tissue proliferation, and release of inflammatory mediators (63). Extracellular matrix is an important structure, in part because it provides an elastic structural support holding the myocytes in sheets. It consists of proteins and carbohydrates, and in particular collagen fibrils. In the first phase of healing, the matrix is dissolved, which allows the removal of debris by inflammatory cells (63). Degradation of collagen is significant at 24 h after

experimental coronary occlusion in rats. The normal collagen structure almost disappears during the first week after MI in mice (21, 99). Without collagen crosslinks between myocytes, as the cells lengthen the myocytes slip past each other leading to dilation of the muscle wall (238). This had been observed within hours of MI in man (34). Potential mediators that initiate the inflammatory response include reactive oxygen species (ROS are atoms or molecules with unpaired electrons in their outer orbit), heat shock proteins, and fibronectin released from necrotic cells (64). Certain products of necrosis, such as ROS and intracellular proteins, then activate pattern recognition receptors such as Toll-like receptors (TLRs), the transcription factor nuclear factor kappa B ($NF\text{-}_KB$) and complement (65). After triggering the inflammation, further inflammatory mediators are released, resulting in inflammatory cells being attracted to the site of infarct. Complement is an important mediator of neutrophil and monocyte recruitment to the injury site early after MI (49). Neutrophils are an important early mediator of the inflammatory response (98). Neutrophils release oxidants and proteases that phagocytose cellular debris and dead cells. They also secrete chemokines that attract other inflammatory cell types (63).

The healing process then turns to reparation, beginning approximately one week after MI in humans (53). This process involves increased synthesis of matrix, proliferation of fibroblasts and inflammatory cells, and release of fibrosis-promoting cytokines that lead to scar formation (53). Inflammatory cells, including macrophages, monocytes, and platelets, release cytokines and continue to contribute to the removal of necrotic tissue (53). The release of cytokines also stimulates expression of fibroblast growth factor and vascular endothelial growth factor (VEGF) (63). Fibroblast growth factor then causes myofibroblasts to appear in the wound, which reconstruct a new collagen network (53). The actions of myofibroblasts are essential for scar formation and the stabilization of the heart wall. These actions allow the walls of the heart to tolerate the hemodynamic stress associated with rhythmic contractions. On the other hand, VEGF promotes the inflammatory response and stimulates angiogenesis within infarct and peri-infarct regions (213).

Cardiomyocytes will continue to die if hypoxic conditions persist. Campbell *et al* showed that the size of an infarcted region progressively increased, over several hours after occlusion of coronary arteries in humans, due to the progressive loss of myocardium (34). Additionally, in a porcine model of MI, the infarcted region was found to further expand during the period from one day to one week after MI (87). Notably, another study has provided evidence that MI in human patients is associated with reduced microvascular density even in the myocardium remote from the site of infarction (35). Thus re-establishing adequate blood flow in the peri-infarct region is important for long-term survival of cardiac muscle and thus patients themselves. However, observations of vessel density provide no information about the functional impairment that also takes place in vessels that remain patent after MI. Therefore, direct assessment of coronary vascular function, using advanced imaging techniques, should provide important insights into ways to prevent ongoing ischemia after MI. In the experiments described in this thesis, two newly developed regenerative therapies were assessed. In the experiments described in Chapter 3, a combination therapy with stem cells and angiogenic factors was provided to the animals after MI to determine whether this regenerative therapy helps to increase infarct revascularisation. In the experiments described in Chapter 4, a new prostacyclin analogue (developed by ONO Pharmaceutical Pty Ltd, Japan) was administered to the animals after MI to examine whether this drug increases revascularization.

1.5 Angiogenesis and Vessel Recruitment in the Heart Post Myocardial Infarction

Humans and most mammals are born with a limited complement of cardiomyocytes, so that cells that die are not replaced (53). Therefore, after MI, damaged cardiomyocytes are not replaced whereas non-cardiomyocyte cell types are replaced, in a process driven by various intra- and intercellular pathways that contribute to myocardial wound healing (64). During the repair process, enhancement of blood flow to the infarct region can result from either angiogenesis or from the recruitment of pre-existing coronary collateral vessels (213). Angiogenesis can be defined as the budding of capillaries that leads to the formation of new microvessels from a pre-existing vascular structure. This process is different from vasculogenesis, which is the formation of new blood vessels from mesenchymal stem cells during embryogenesis (185). Collateral vessels can play

an important role in supplying oxygen and other nutrients to organs. They can help to supply blood flow to regions that are subject to infarction due to occlusion of epicardial arteries (190). However, the extent of coronary collateral vessels varies between species (84). For example, there is an extensive network of coronary collateral vessels in the dog (76), but it is very limited in the pig and human (109, 237).

Formation of new blood vessels involves several steps, including dissolution of the matrix underlying the endothelium; migration, adhesion, and proliferation of endothelial cells; and formation of a tubular structure which supports blood flow (185). The major triggers of angiogenesis post MI can be broadly separated into three categories: mechanical, chemical and molecular which will be described in the following passages (213). Firstly, the mechanical influence on angiogenesis is mainly due to shear stress. Augmentation of blood flow both stimulates vascular sprouting and maintains the newly formed collateral vessels due to enlargement of the endothelial cells (194). Shear stress on the endothelial cells up-regulates adhesion molecules in the endothelium, attracts inflammatory cells, and stimulates endothelial cells to produce growth factors (8). Secondly, hypoxia is one of the important chemical influences on angiogenesis. Hypoxia triggers vessel growth by signaling through hypoxia inducible factors which upregulated many angiogenic genes (112, 198). Of these genes, VEGF is probably the most essential gene for angiogenesis (41). This conclusion is supported by the observation that mice that constitutively express hypoxia inducible factor 1α (HIF-1α) in cardiomyocytes had a 3-4 fold greater increase expression of VEGF mRNA and augmented angiogenesis after MI, compared to wild-type mice (105). Finally, the molecular influences on angiogenesis after MI include inflammatory cytokines, angiogenic factors, growth factor receptors, angiogenic inhibitors, endothelial activation and extracellular matrix (37).

New vessels that originate from external stimulation due to MI do not necessarily have the normal capacity for blood flow control (27). Therefore, often the angiogenic capacity is not sufficient to prevent ongoing ischemia that leads to HF. Many approaches are being used to increase angiogenesis, but these are frequently used as monotherapies. The question of which regenerative approaches are best has been widely debated (see section 1.6.2). Importantly, the function of the

microvessels in regenerative therapy trials involving small animals has received little attention. This issue is the chief focus of the experiments described in Chapters 3 and 4 of this thesis.

1.6 Current Status of Therapies for Heart Failure

The major strategies for preventing the progression of chronic HF are to minimize risk factors of HF, improve status of symptoms, and increase survival rate. Following these strategies, various therapies have been used to prevent chronic HF, which are detailed in the following section. In general, pharmacological therapies are currently used to manage all forms of HF. However, the benefits of pharmacological therapies for HF with ejection fraction (HFrEF) have not been fully proven in HFpEF or in fact inadequately tested (162). Moreover, epidemiological analysis demonstrates that currently 50% of all patients with HF are diagnosed as HFpEF (223). Therefore, novel therapies are needed for patients with HFpEF. On the other hand, cell based regenerative therapies are continuing to be explored to improve cardiac function in end-stage HF.

1.6.1 Pharmacological Therapies

1.6.1.1 Angiotensin-converting Enzyme Inhibitors, Angiotensin-receptor Blockers and β-blockers

There is strong evidence that HF is driven by excessive activation of the renin-angiotensin system (RAS) and SNS (97, 170). Therefore, blockade of these systems has been used as a therapy to manage HF (Table 1.1). Inhibitors for angiotensin-converting enzyme (ACE) and angiotensin-receptors blockers (ARB) reduce activity of the RAS (131, 153). Reduction of RAS activity minimizes multiple pathophysiological effects of angiotensin II, and therefore leads to peripheral vasodilation, inhibition of LV hypertrophy and diuresis (104, 124, 153). ACE inhibitors have been shown to reduce mortality and morbidity in patients with HFrEF (70, 92). ARBs are normally only used in patients that do not tolerate ACE inhibitors, as they did not achieve superior benefits in reduction of mortality when compared with ACE inhibitors (44, 110, 138). On the other hand, β-blockers inhibit the activity of SNS through the β-adrenergic receptors. These slow the heart rate, decrease blood pressure, and have a beneficial effect on the myocardium through inhibition of remodeling (30, 75). Moreover, various studies show that treatment with β-blockers

reduces mortality and morbidity in patients with HFrEF (1, 166, 167). However, β-blockers can not be used in severe HF as they depress contractility of myocardium.

Table 1.1 Summary of current pharmacological therapies used to manage heart failure with reduced ejection fraction and primary outcomes from clinical trials.

Drugs	Primary Outcome	References
ACE inhibitors	↓↓ Mortality	
Captopril	↓↓ Hospitalization	(70, 92)
Enalapril		
Lisinopril		
Ramipril		
Trandolapril		
ARB	↓↓ Mortality	
Candesartan	↓↓ Hospitalization	(44, 110, 138)
Valsartan		
Losartan		
β-blockers	↓ Mortality	
Bisoprolol	↓ Hospitalization	(1, 166, 167)
Carvedilol		
Metoprolol		
Nebivolol		
Vasodilators	↓ Mortality	
Hydralazine	↓ Hospitalization	(43, 178, 244)
ISDN		
BiDil (hydralazine/ISDN)		
ARA	↓ Mortality	
Eplerenone	↓ Hospitalization	(176, 248)
Spironolactone	↓ LV remodeling	
If-channel blocker	↓ Heart rate	(62, 212)
Ivabradine	↑ Atrial fibrillation	
ARN inhibitor	↓↓↓ Mortality	
LCZ696 (valsartan/sacubritril)	↓↓↓ Hospitalization	(139)

ACE: angiotensin-converting enzyme, ARB: angiotensin-receptors blocker, ISDN: isosorbide dinitrate, ARA: aldosterone receptor antagonist, If-channel: current of funny channel and ARN: combined angiotensin receptor blocker and neprilysin inhibitor.

1.6.1.2 Vasodilators

Vasodilators, including hydralazine and isosorbide dinitrate (ISDN), were the very early agents used for the treatment of HF. Combination treatment with hydralazine and ISDN, in patients with HFrEF, was found to reduce mortality at 2 year follow-up

by 34%, but no effect on hospitalization was detected (42). In a clinical trial that compared this combination therapy to that with an ACE inhibitor (enalapril) in patients with HFrEF, the reduction in in mortality was found to be greater in the group treated with the ACE inhibitor (38.2% vs 32.8%) (43). Therefore, combined treatment with hydralazine and ISDN is now only recommended for patients unable to tolerate therapy with ACE inhibitors or ARBs (178, 244).

1.6.1.3 Aldosterone Receptor Antagonist and Digoxin

Drugs including aldosterone receptor antagonist and digoxin also have been used to treat HF (51, 77). Aldosterone receptor antagonists have been found to inhibit renal sodium retention, decrease renal potassium excretion, and reduce vascular and LV hypertrophy (5, 74). Furthermore, treatment with aldosterone receptor antagonists was found to reduce hospitalization and mortality in patients with HFrEF (176, 248). Digoxin increases myocardial contractility through inhibition of the Na^+/K^+ ATPase pump to increase intracellular sodium levels (51). However, digoxin is now rarely used for treating HF because it was found to be associated with increased mortality (222).

1.6.1.4 Hyperpolarization-activated, Cyclic Nucleotide-gated Channel Blocker

Ivabradine is an inhibitor of the hyperpolarization-activated, cyclic nucleotide-gated (HCN) channel. It is commonly used to manage HF in whom β-blockers have been ineffective (244). Blocking HCN channel leads to a reduction in funny channel current (I_f) in the sinus node (22). A reduction in I_f leads to decreased heart rate (22). Treatment with ivabradine was shown to improve contractility of the LV and reduce heart rate both in rats with HFrEF and in mice with HFpEF (150, 183). In patients with HFrEF, ivabradine reduced heart rate by 8 beats per minute, and reduced hospital admission by 18% (212). However, adverse events such as atrial fibrillation and symptomatic bradycardia were more frequently observed in patients treated with ivabradine than those with placebo (62).

1.6.1.5 Combined Angiotensin Receptor Blocker and Neprilysin Inhibitors

Recently, a new compound (LCZ696) that combines the moieties of an ARB (valsartan) and a neprilysin inhibitor (sacubitril) has been developed for treating HF (106). Treatment of rats with LCZ696 after MI attenuated cardiac remodeling and

dysfunction, at least partly by reducing cardiac fibrosis and hypertrophy (230). In a clinical trial, LCZ696 was found to be superior to an ACE inhibitor (enalapril) in reducing the risk of death and hospitalization in patients with HFrEF (139). Therefore, LCZ696 may be an alternative to ACE inhibitors or ARBs in patients with HFrEF.

Current pharmacological therapies have been shown to provide several beneficial effects to delay the progression of HF and increase survival rate (44, 51, 117). However, these drugs have multiple side effects, including hyperkalemia, hypotension and renal impairment (73, 139, 168). These side effects need to be carefully monitored in patients on combined treatment with a β-blocker and ACE inhibitor with an aldosterone antagonist. Furthermore, other concomitant medications should be used with caution to avoid adverse pharmacodynamic interactions. For example, combined use of β-blockers and calcium channel blockers can lead to atrioventricular block (96, 111). The pharmacological therapies mentioned above were only found to be effective in HF with HFrEF as opposed to HFpEF (162). Moreover, the drug therapies recommended by the current guidelines only help to manage chronic HF. They do not repair the damage to the heart. Therefore, there is growing interest in regenerative therapies for treating chronic HF.

1.6.2 Regenerative therapies

An alternative strategy for treating MI and chronic HF is to regenerate the myocardium to improve cardiac function. There is growing interest particularly in regenerative approaches aimed towards increasing the heart's contractile muscle mass. Various types of surgery have been employed including ventricular restoration (a procedure designed to restore or remodel the LV to its normal shape and size), implantation of a ventricular assist device, and heart transplantation for patients with end-stage HF (2). However, such procedures are limited by the highly complicated surgery, extremely high cost of medical resources and shortage of organ donors respectively. Hence, regenerative medicine has become one of the main research focuses in recent years, given its greater potential for wide spread use. Regenerative approaches have evolved from applications using differentiated cell lines to new approaches that utilize so-called progenitor cell lines. Each type of cell line used for regeneration has been found to have both advantages and disadvantages, as summarized below (Table 1.2).

Table 1.2 Summary of current stem cells therapies used to manage heart failure with reduced ejection fraction and outcomes from clinical trials.

Stem Cell Types	Studies reporting	
	Positive Outcome	Negative Outcome
Bone marrow derived stem cells	↑ LV ejection fraction (25) ↓ Scar size and infarct size (25)	No improvement in cardiac function (9)
Adipose tissue derived stem cells	↑ LV mass (88, 174) ↓ Scar size and infarct size (88, 174)	
Skeletal myoblast cells	↑ Cardiac function (141, 204) ↑ Cardiac contractility (141, 204)	No improvement in cardiac function (228) ↑ Risk of ventricular arrhythmia (204, 228)
Cardiac derived stem cells	↑ LV ejection fraction (23, 130) ↓ Infarct size (23, 130)	
ESCs/iPSCs	yet to be ascertained	

LV: left ventricle, ESCs: embryonic stem cells and iPSCs: induced pluripotent stem cells.

1.6.2.1 Bone Marrow Derived Stem Cells

Bone marrow (BM) cell lines were not only the first adult stem cells reported to differentiate into cardiomyocytes but have also been the most frequent source of cells used in clinical trials for cardiac repair in the past decade (79, 193). BM is derived from the embryonic mesoderm and is made up of a population of hematopoietic stem cells, which are supported by a mesenchymal stroma (172). BM stroma contains mesenchymal stem cells and endothelial progenitor cells, which have been reported to possess the potential to differentiate into cardiomyocytes by observing cardiomyocyte-like ultrastructure such as sarcomeres, a centrally positioned nucleus and atrial granules in the cells differentiated from BM stroma

under electron microscopy (13, 129). The studies of Orlic (160) and Taylor (217) both showed that implantation of BM stem cells improve myocardial contractility through myocardial regeneration and reduce infarcted size in animal models of MI. However, Scherschel showed that adult BM-derived cells do not acquire normal adult cardiomyocyte function (196). Clinical trials have not shown consistent positive outcomes associated with treatment with BM cells. For example, Ang *et al* were unable to detect improvements in regional or global LV function (end-systolic volume, end-diastolic volume stroke volume or ejection fraction), or a reduction in scar size using cardiac magnetic resonance imaging (MRI), after BM cells were delivered by intramyocardial injection or intracoronary infusion during coronary artery bypass grafting (9). On the other hand, a small clinical pilot study using MRI showed that infusion of BM derived multipotent stem cells preserved LV geometry and reduced infarcted size in patients who survived after MI (25). Furthermore, Poulin *et al* in their recent review conclude that treatment with BM derived cells improved perfusion defects, reduced infarcted size and increased myocardial viability in the short term in most of the published clinical trials (179). It is not clear whether the regenerated myocardium, in patients or animals treated with BM cell lines, is fully functional and can thus stave off HF in the long term (132). Additionally, harvesting of BM is painful and associated with potential morbidity. Therefore, alternative sources of stem cells are considered to be more attractive for direct implantation. Nonetheless, some consider it might be possible to harness the body's own ability to recruit BM progenitors to sites of cardiac injury with chemokines and other biochemical signals such as cytokines and adhesion molecules (108, 199). This new approach may provide a better way to recruit endogenous BM stem cells. However, it has not yet been trialed in patients.

1.6.2.2 Adipose Tissue Derived Regenerative Cells

Similar to BM cells, adipose tissue is also derived from the embryonic mesoderm and contains a heterogeneous stromal cell population (123). Adipose tissue is particularly advantageous as an autologous source for therapeutic regenerative cells due to the fact that cells can be harvested in large quantities by liposuction (251). Adipose tissue contains a pool of adipose-derived mesenchymal stem cells, which have been shown to be multipotent stem cells. Adipose-derived mesenchymal cells (MSC) can express cardiac marker genes, so may have the ability to differentiate into cardiomyocytes (177, 234). Miyahara *et al* showed that

transplantation of monolayered adipose-derived MSC into infarcted myocardium reversed wall thinning in the infarcted area and improved cardiac function (147). In addition, intramyocardial injection of adipose stem cells one week after coronary occlusion enhanced cardiac contractility and angiogenesis in the infarcted heart in rats (234). Several clinical studies on patients with MI show significant improvement in total LV mass and reduced infarct size after treatment with adipose-derived stem cells (88, 174). However, the ability of adipose-derived stem cells to differentiate into cardiomyocytes is still controversial and this might have a potential impact on future utilization of this cell source (161, 232).

1.6.2.3 Skeletal Myoblast Cells

Skeletal myoblast cells (SkM) are derived from satellite cells, which are a population of stem cells in skeletal muscle (240). Various animal studies have provided evidence that treatment with SkM improves cardiac function. This positive evidence quickly led to clinical studies showing that intramyocardial injection of SkM can improve cardiac function and increase contractility, albeit with an associated increased risk of ventricular arrhythmia (141, 204). On the other hand, Veltman *et al* found that intramyocardial injection with SkM did not improve function in patients, and might even induce the development of serious arrhythmias (228). Very early in this field of regenerative research Murry *et al* suggested that SkM were unlikely to regenerate into myocardium, based on their inability to detect myocardial gene expression in the cells regenerated from SkM, and the fact that the new muscle did not have the ability to contract spontaneously (155). Nevertheless, others have shown that SkM differentiate into myotubes *in vivo* and improve ventricular function (140). Moreover, SkM are amenable to culturing as cell sheets. Since implantation of a sheet of SkM improved cardiac function in part by attenuating the pathological remodeling in ischemic porcine myocardium (146), it now seems that growing SkM cell sheet constructs will offer a viable therapy for severe MI and thus prevention of the onset of HF. However, it is not clear if there is an optimum size limitation for such sheet constructs, as sheets are grown in an avascular state. Further, as coronary function is rarely assessed in preclinical studies utilizing small animal models, it is not known whether the vessels that revascularise at the sheet-myocardium interface have normal function. In the studies described in Chapter 3 of this thesis I examined whether SkM sheet therapy is improved by combining it with a source of angiogenic factors, by evaluating coronary function.

1.6.2.4 Cardiac Derived Stem Cells

Resident cardiac stem cells (CSC) in the heart have been reported to be able to differentiate into cardiomyocytes (119). Several cardiac resident stem cell populations have been characterized with the discovery of the expression of novel stem cell marker proteins. We now know that the c-Kit expressing cell population is able to differentiate into cardiomyocytes, smooth muscle cells and endothelial cells (16). Islet-1 expressing cells can differentiate into functional cardiomyocytes both *in vivo* and *in vitro* (115). Several animal studies have shown that intracoronary infusion of CSC after MI improves cardiac function with a decrease LV end-diastolic pressure and increase LV ejection fraction (24, 216). In clinical trials, patients with MI have also shown an increase in LV ejection fraction (8-12%) and reduced infarcted size (12-30%) after intracoronary infusion of CSC (23, 130). However, it is not clear from these studies if the regulation of coronary flow is normalized following CSC infusion. These results suggest that CSC is another potential cell source for cell therapy for treating MI.

1.6.2.5 Embryonic Stem Cells and Induced Pluripotent Stem Cells

Embryonic stem cells (ESCs) and induced pluripotent stem cells (iPSCs) are suggested to be the most promising source of cells for regenerative therapies. These cells are pluripotent, which means that they can differentiate into cells types from all germ layers indefinitely (6). ESCs are derived from the inner cell mass of blastocysts from mammals while iPSCs are derived from adult somatic cells after inducing the expression of specific transcription factors (54, 215). Mouse and human ESCs/iPSCs have been differentiated into various cell types, including cardiomyocytes, neuronal cells, and embryonic erythrocytes (47, 195). The efficiency of cardiomyocyte differentiation is improved by supplementation of growth media with signaling molecules, such as activin A and bone morphogenetic protein 4 (BMP4) (114, 245). Transplantations of human cardiomyocytes derived from ESC or iPSCs cells into infarcted hearts of rodents have been reported to enhance cardiac function (39, 86, 114). Although iPSCs show great promise for cardiac regeneration, the low efficiency of iPSCs generation must be improved for this approach to be clinically feasible (128). Furthermore, several preclinical studies showed that intramyocardial injection of iPSC resulted in growth of intramural

teratomas in rats and mice with MI (3, 233, 249). To date, iPSCs have not been used in clinical HF trials, but a trial that examines iPSC benefits for macular generation is underway in Japan (218).

1.7 Basic Anatomy and Physiology of Coronary Blood Vessels

Following MI, by its very nature, there is a region deprived of adequate blood flow. Neurohormonal activation after MI generally reduces myocardial perfusion further (175). In other forms of HF, for example HFpEF, there is a significant contribution of coronary microcirculatory dysfunction to the worsening of HF (26, 173). The coronary circulation is crucial for maintenance of cardiac function. In order to appreciate how coronary dysfunction contributes to HF we must consider the basic anatomy and physiology of the coronary circulation, which has been established in both human and animal studies.

The coronary vessels are the only source of blood, and thus oxygen, for the myocardium (55). The oxygen consumption of the heart is very high. Even in the resting subject, myocardial blood flow (~8 ml oxygen/100 g of myocardium) is around 20 times greater than that of resting skeletal muscle (19). Delivery of oxygen and nutrients is enhanced by the fact that the myocardium has a much greater capillary density (roughly 1 capillary per myocyte), and shorter diffusion path, than other peripheral tissues (19). In order to understand the components that regulate coronary vessel tone and flow, it is necessary to first consider the anatomy of the coronary circulation.

The walls of coronary arteries have three layers. From the luminal surface these are the intima, media and adventitia. These three layers are separated by layers of elastin; the internal elastic lamina separates the intima from media and the external elastic lamina separates the media from the adventitia (Fig 1.2). The adventitia is the outer-most layer, and is mainly formed by collagen, which anchors the artery to nearby tissue. The media of coronary arteries is mainly formed by vascular smooth muscle (VSM), contraction or relaxation of which mediates changes in their radius in response to vasoactive substances. Endothelial cells are the main component of the intima, which is directly exposed to the bloodstream.

Endothelial cells are highly active, highly differentiated cells with a multiplicity of functions. These include regulation of vascular tone, platelet activity and leukocyte adhesion (85, 102). The endothelium transduces various physiological stimuli by producing paracrine and autocrine signaling molecules that have effects on blood cells, smooth muscle cells and also the endothelium itself (40). The endothelium helps to regulate blood clotting, assists immune response, mediates the bulk flow of fluid and solutes between the plasma and extracellular compartments, and regulates vascular tone (40).

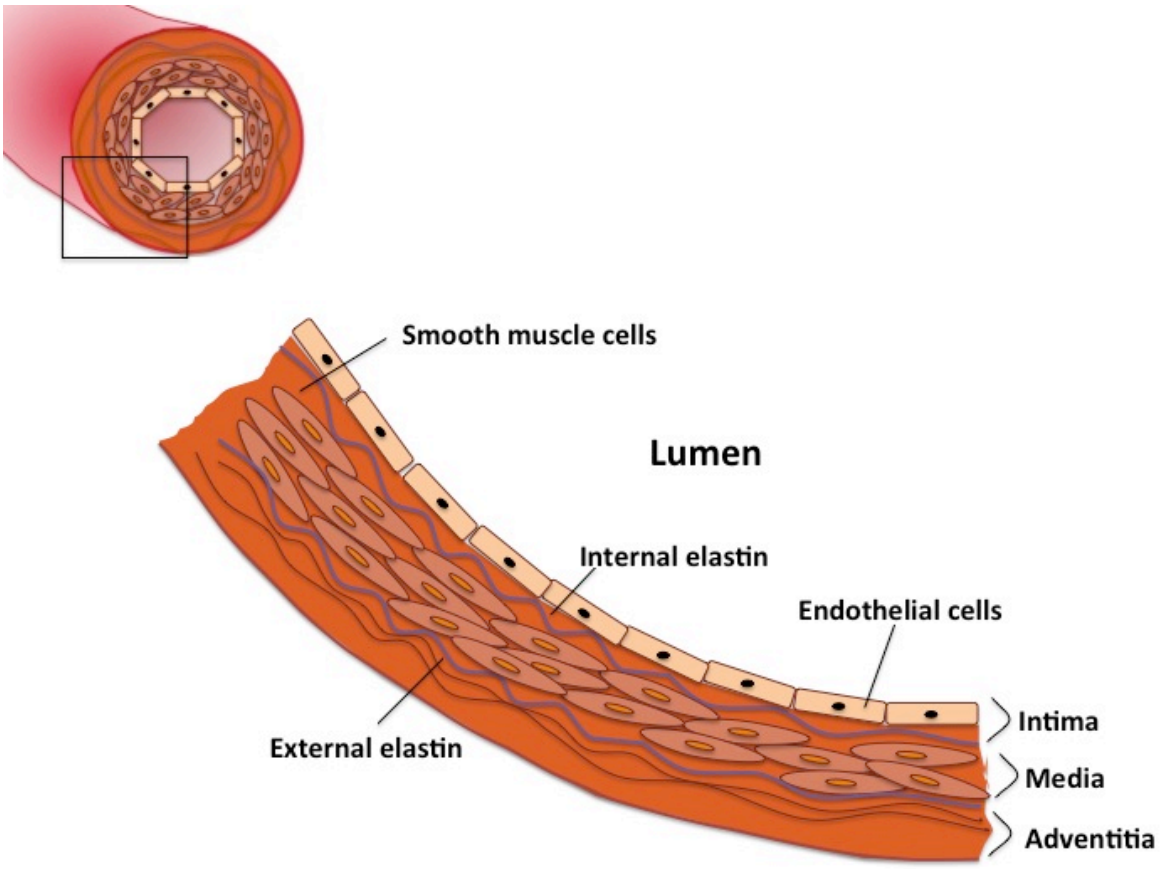

Figure 1.2 Internal structure of a coronary artery. The wall of a coronary artery has three layers, which are separated by layers of elastin. From the luminal surface these are the intima, media and adventitia. The vascular endothelium is the thin layer of cells that line the luminal surface, and is the main component of the intima. The media of blood vessel is mainly formed by vascular smooth muscle. The adventitia is chiefly composed of collagen fibers.

1.8 Control of Coronary Vascular Tone by Vascular Smooth Muscle

Contraction and relaxation of VSM evokes changes in vessel radius, which determines vascular resistance of that segment. Local vascular resistance regulates the distribution of blood flow within the myocardium. To understand how and what causes contraction and relaxation of VSM, we must first understand the structure of VSM. VSMs are spindle-shaped cells. They are joined by gap junctions that allow ionic currents to flow between them. Actin (thin) and myosin (thick) filaments are the basic contractile units in VSM cells. The actin filaments insert into dense bands on the inner surface of the cell and into dense bodies in the cytoplasm. There are no striations in VSM because the dense bodies are not aligned across the cell. The VSM cells can contract as a whole due to the function of the third kind of filament, the intermediate filament. The intermediate filament acts as a cytoskeleton and links up the dense bodies and the dense bands to produce the contraction of the whole cell.

Contraction of VSM can be triggered by a rise in the concentration of Ca^{2+} in the cytoplasm through the opening of voltage-dependent Ca^{2+} channels on the cell membrane. A complex of Ca^{2+} and calmodulin activates myosin light chain kinase (MLCK), which then phosphorylates the myosin light chain (part of the mobile head of myosin) (236). In the presence of adenosine triphosphate, phosphorylation of myosin light chain leads to formation of cross-bridges between myosin and actin, and thus the development of vascular contraction. On the other hand, relaxation of VSM can be induced by a reduction of Ca^{2+} concentration in the cytoplasm. A reduction in the Ca^{2+} concentration in the cytoplasm stops the progression of contraction, which then reduces the active tension in VSM.

The active tension exerted by VSM in a segment of wall is called vessel tone. Regulation of vascular tone is dependent on the balance of vasoconstriction and vasodilatation. The balance of vasoconstriction and vasodilatation is influenced by multiple competing vasoactive factors. The extrinsic factors that act on the vasculature to influence vessel tone include autonomic nerves (sympathetic, and in some vascular beds parasympathetic) and circulating hormones such as angiotensin, adrenaline and vasopressin (32). The intrinsic factors include myogenic mechanisms, local paracrine and autocrine hormones (such as

histamine), metabolites or hypoxia, and paracrine factors released from the endothelium. Of these factors, the secretion of vasoactive factors from the endothelium plays a dominant role in regulating vascular tone and blood flow in the coronary circulation, as described in detail below.

1.9 Influence of the Endothelium on Vascular Smooth Muscle

The endothelium regulates the transfer of nutrients, metabolites and signaling molecules between blood and tissue (158). Endothelial cells are also ideally situated to control the function of VSM to regulate blood flow (69). The endothelium regulates local vascular tone by synthesizing and secreting a number of vasoactive agents, including vasodilators (e.g. nitric oxide, prostacyclin and endothelium derived hyperpolarizing factors, Fig.1.3) and vasoconstrictors (endothelin-1 and a variety of metabolites of arachidonic acid) (133, 226). The pathways and functions of vasoactive agent secreted from endothelium are discussed below.

1.9.1 Nitric Oxide

Nitric oxide (NO) is a freely diffusible gas with several important cardiovascular functions. These include vascular relaxation and inhibition of platelet aggregation and adhesion (148, 169). When the concentration of Ca^{2+} is high in the endothelial cell, Ca^{2+} combines with calmodulin, which activates nitric oxide synthase (NOS). There are three isoforms of NOS, numbered in the order they were discovered. These are neuronal NOS (nNOS or NOS-I), inducible NOS (iNOS or NOS-II) and endothelial NOS (eNOS or NOS-III) (61, 148). NOS causes oxidation of L-arginine to L-citrulline to release NO (169). NO is generated continuously and has a short half life of only a few seconds (3-5 sec) (148).

After NO diffuses from the endothelium into the underlying VSM, NO induces vasodilation mainly through activating guanylyl cyclase. This enzymes catalyses the conversion of guanosine triphosphate (GTP) to cyclic guanosine monophosphate (cGMP), which activates protein kinase G (PKG) (80). PKG leads to the reduction of the cytosolic Ca^{2+} concentration through reuptake of cytosolic Ca^{2+} into sarcoplasmic reticulum. The cytosolic Ca^{2+} concentration decreases and MLCK can no longer phosphorylate myosin. The reduction of cytosolic Ca^{2+} concentration also activates myosin light chain phosphatase and thus leads to vasodilation (Fig. 1.3).

NOS blockade has been observed to blunt the increase in coronary flow produced by vasodilators such as ACh or bradykinin by 35-67% (93, 164, 241) Therefore, the generation of NO by the endothelium is important for the regulation of coronary blood flow.

1.9.2 Prostacyclin

Prostacyclin (PGI_2) has similar effects on coronary vascular function to NO, being a vasodilator and inhibitor of platelet aggregation (181). PGI_2 is produced from arachidonic acid (Fig 1.3). Arachidonic acid is metabolized by cyclooxygenase (COX) to prostaglandin H_2 (PGH_2), which then further transformed by prostacyclin synthase to PGI_2 (171).

PGI_2 then diffuses in the nearby VSM and acts on the prostacyclin receptor (IP), which is a member of the G-protein coupled receptor family present on VSM. IP-receptors mediate activation of adenylyl cyclase (AC) to generate cyclic adenosine monophosphate (cAMP) from adenosine triphosphate (ATP) (Fig 1.3) (80). The consequent increase in the intracellular concentration of cAMP activates protein kinase A (PKA), which decreases cytosolic Ca^{2+} concentration and causes vasodilation. The decrease in cytosolic Ca^{2+} concentration is mediated by an increase in the reuptake of Ca^{2+} into the sarcoplasmic reticulum through the Ca^{2+}-ATP pump (PKA mediated). In addition, PKA causes hyperpolarization by reducing the probability of opening of voltage-sensitive calcium channels by phosphorylation of K^+ channels (80). PGI_2 is normally considered less important than NO in vasodilation as inhibition of COX did not reduce coronary blood flow, but inhibition of NO production caused a significant reduction in coronary blood flow in both pigs and dogs (45, 118, 164).

1.9.3 Endothelium Derived Hyperpolarizing Factors

Even when the production of NO and PGI_2 is inhibited, vasodilation, accompanied by hyperpolarization of smooth muscle cells, can still be triggered by pharmacological stimulation of the endothelium (80). This observation indicates that there is at least one endothelium-derived hyperpolarizing factor (EDHF) that is independent of NO and PGI_2. The precise chemical identity of EDHF remain a matter of controversy. Indeed, it is likely that multiple EDHFs exist and that their nature differs across various vascular territories (see below). EDHF appears to play

a more important role in the small vessels than the large vessels, since ACh-induced vasodilation, observed in the presence of NOS and COX blockade, is relatively greater in smaller than larger vessels (71, 91, 201). EDHF hyperpolarizes the VSM through opening of K^+ channels (especially calcium-activated K^+ channels) to cause vasodilation in coronary vessels (81, 82). The evidence that EDHF hyperpolarizes the VSM through opening of K^+ channels was revealed by showing that stimulation of EDHF was strongly associated with the extracellular K^+ concentration (157, 200).

Several pathways have been proposed for EDHF-mediated vasodilation in the coronary circulation, including a pathway through metabolism of arachidonic acid by cytochrome P450 epoxygenase. Briefly, in response to shear stress or activation of certain receptors on the surface of endothelial cells, cytosolic Ca^{2+} increases. This activates PLA_2 and thus results in production of arachidonic acid (125). Catalyzed by cytochrome P450 epoxygenase, arachidonic acid is converted into eicosatrienoic acids (EETs) (59, 78). EETs then stimulate calcium dependent potassium channels (KCa^+) in endothelial and VSM resulting in hyperpolarization (10, 36, 145). EETs may directly activate the gap junctions between endothelial cells and VSM thereby transmitting hyperpolarization from endothelial cells to VSM (189). EETs also activate transient receptor potential vanilloid 4 (TRPV4) channels on endothelial cells, as evidenced by the observation that inhibition of EET degradation increased the TRPV4-dependent Ca^{2+} responses to arachidonic acid (231, 235). TRPV4 channels promote Ca^{2+} influx, which further increases the concentration of Ca^{2+} in the endothelial cells, and activates K^+ channels to release K^+ ions into the subendothelial space (235). The increase of K^+ in the subendothelial space leads to hyperpolarization in smooth muscle cells by activation of $K_{Ca}{}^+$ channels, inwardly rectifying potassium channels ($K_{IR}{}^+$) and the Na^+-K^+ pump. Hyperpolarization in VSM then further leads to relaxation by reducing the cytoplasmic concentration of Ca^{2+} (Fig. 1.3).

Another proposed pathway for EDHF-mediated vasodilation is through the production of hydrogen peroxide (H_2O_2), which can cause hyperpolarization by activating $K_{Ca}{}^+$ channels or myoendothelial gap junctions (18, 135, 143, 242). Superoxide dismutase (SOD) catalyzes of the production of H_2O_2 from superoxide (O_2^-) (11, 67). Vascular endothelial cells produce O_2^- and H_2O_2 from several

intracellular sources, including eNOS, COX, mitochondria, nicotinamide adenine dinucleotide phosphate (NADPH) oxidase, xanthine oxidase, and cytochrome P450 (15, 60, 100, 137, 192). Matoba *et al* showed that catalase, which dismutates H_2O_2 to form water and oxygen, inhibited EDHF-mediated relaxation and hyperpolarization in small mesenteric arteries in mice (136). Similar findings have been shown in peripheral arteries in pig, coronary arteries in canine, mesenteric arteries and coronary microvessels in human (113, 144, 242).

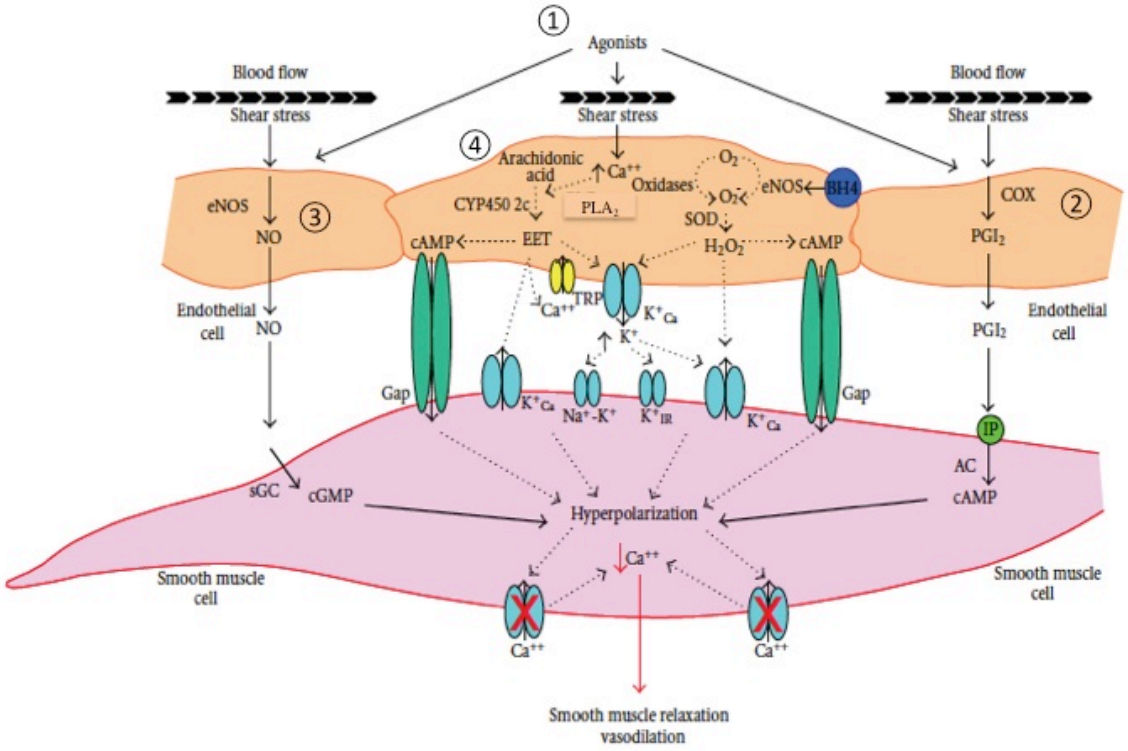

Figure 1.3 Mechanisms underlying endothelium-dependent vasodilatation. 1.) Agonist such as bradykinin and acetylcholine or shear stress increase the activity of endothelial nitric oxide synthase (eNOS) and cyclooxygenase (COX). These trigger nitric oxide (NO) and prostacyclin (PGI_2) mediated vasodilation. **2.)** PGI_2 acts via the prostacyclin receptor (IP) to activate adenylate cyclase (AC) causing an increase in cyclic adenosine monophosphate (cAMP) production. **3.)** NO activates soluble guanylate cyclase (sGC) leading to an increase in cyclic guanosine monophosphate (cGMP). **4.)** Endothelium derived hyperpolarizing factors mediate vasodilation through a number of pathways, including the opening of K^+ channels on the vascular smooth muscle cells. Calcium: Ca^{++}, phospholipase A_2: PLA_2, cytochrome P450 2C: CYP4502c, eicosatrienoic acids: EET, transient receptor potential: TRP, inwardly rectifying potassium channels: K_{IR}^+, calcium-activated potassium channels: K_{Ca}^+, myoendothelial gap junction: Gap, tetrahydrobiopterin: BH4, oxygen: O_2, oxygen produces superoxide: O_2^-, superoxide dismutase: SOD and hydrogen peroxide: H_2O_2. Images reproduced, with permission, from Ozkor *et al* (163).

1.10 Endothelial Dysfunction in the Coronary Circulation

The endothelium not only plays an important role in regulating vascular tone, platelet activity, and leukocyte adhesion but is also involved in thrombosis and the development of atherosclerosis in coronary vessels. Endothelial dysfunction in the coronary circulation is thus highly relevant to the development of HF (33, 85, 173, 178). Endothelial dysfunction is defined as a diminished ability of the endothelium to mediate its various functions, including vasodilation. The main feature of impaired endothelial function that is generally reported is a reduction of NO bioavailability, which is due to reduced NO production by the endothelium or increased inactivation of NO by reactive oxygen species (ROS), specifically the superoxide anion (68, 214). There is strong evidence that elevated levels of ROS lead to low NO bioavailability (68, 89, 182). Excessive production of ROS has been found in various disease states including hypertension, atherosclerosis and MI (29, 209). The low bioavailability of NO is most frequently attributed to the reaction of superoxide with NO to form peroxynitrite ($ONOO^-$), an important radical that triggers apoptosis in cardiomyocytes, endothelial and VSM cells (12, 46, 120, 121, 142). However, diminished NO-mediated dilation in HFpEF may also result from decreased phosphorylation of PKG (173, 219, 224). Indeed, patients with HFpEF have low PKG activity, low NO bioavailability and a blunted vasodilatory response to ACh (173, 219, 224).

Normally, coronary vessels are able to produce vasodilation in response to vasodilators, but in pathological states such as MI, hypertension and HF, coronary vessels produce vasoconstriction instead (66, 127, 229). It is well established that vasoconstriction, resulting largely from endothelial dysfunction, contributes to the no-reflow phenomenon associated with ischemia-reperfusion injury (205). Furthermore, changes in the surrounding normal myocardium after MI appear to arise from ongoing inflammation that can result in the spread of endothelial dysfunction (56). Indeed, it has been shown that in addition to diminished NO bioavailability, increased activation of constrictor factors occurs in chronic HF. Increased expression of RhoA/RhoKinase has been detected in hypertension, chronic HF, diabetes and vasospasm (48, 210, 239, 246). Activation of this pathway contributes to exaggerated constriction, which was reduced by selective RhoA-kinases (ROCK) inhibition (fasudil or Y-27632) (122, 156). Furthermore, others

have shown that, in hypertensive vascular dysfunction, RhoA/ROCK activation inhibits eNOS activity to exacerbate the reduced vasodilatory capacity of the coronary circulation due to endothelial dysfunction (116). Therefore, evaluation of vascular endothelial function in the coronary circulation plays an important role in preventing HF development.

1.11 Imaging Techniques for Assessing Vascular Function

Previous studies conducted in our laboratory have shown that visualization of coronary vascular beds with synchrotron radiation (SR), while administering vasoactive agents *in vivo*, is a useful method for evaluation of coronary vascular function (95, 202, 203). Intravital microscopy has the ability to directly image microvessels, and is commonly use to assess vascularization in tumour cells (126). However, it can only supply information on vascular calibre at a single location in a vascular network with limited imaging depth (less than 200 μm in the living tissue) (154). Various imaging techniques, such as magnetic resonance imaging (MRI) and computed tomography (CT) have been used to observe cardiovascular structure and function directly by providing images of the coronary vessels (17, 20, 57). MRI and CT can provide non-invasive visualization of coronary arteries, but they have limited resolution. Consequently, the microvessels, which are the vessels of greatest interest in diseased conditions, cannot be imaged in small animals (202). Microangiography utilizing SR provides high-resolution images of the microcirculation, even in small animals (202, 203). Importantly, this method allows repeated imaging of the vessel network (202). SR imaging can be performed with a temporal resolution of milliseconds at most of the third generation synchrotron facilities worldwide (202). SR is characterized by high directionality, variable polarization and brightness. The fine collimation of the X-ray beam for SR is 10^6 times brighter than laboratory and medical X-ray sources. The advantages and limitation of SR microangiography for imaging dynamic organs, such as heart and lung in anesthetized animals have been discussed in a recent review (203). SR is ideal for dynamic studies of small arterial vessels in small animals (203). In adult rats, utilizing this approach with available X-ray detectors capable of 10-15 μm pixel resolution, it is possible to visualize arterioles in vivo without motion artifacts (coronary ~40 μm, pulmonary vessels ~50 μm) (203). In the studies described in this thesis, I used this approach to evaluate vascular tone and its regulation in the coronary circulation.

1.12 Summary, Hypotheses and Aims

In the early hours after reperfusion caused by coronary artery occlusion, blood flow to the ischemic myocardium may still remain diminished, or even further deteriorate over time (184). This is known as the no-reflow phenomenon. The size of the no-reflow zone is approximately the same as that of the infarct size (101). Previous research has demonstrated that the obstruction of the microvasculature responsible for the no-reflow phenomenon is driven by swelling of the endothelium, infiltration of white blood cells, stagnation of red blood cells, and extravascular edema (107). No-reflow has been defined as an evolving process rather than an immediate event that occurs at the moment of reperfusion (184). Inflammation after MI can limit blood flow, due to migration of leukocytes into the injured microvasculature and the release of vasoactive amines from activated platelets (101). The no-reflow phenomenon is not the primary cause of myocardial cell damage but it can induce further loss in cardiac muscle mass (see Fig. 1.1). Therefore, there is a crucial need to investigate microvascular function after MI.

Coronary angiography is the most reliable technique for diagnosis of CVD and for optimizing treatment modalities for CVD (178, 186). Moreover, coronary angiography is essential for anatomical evaluation of the site and degree of coronary stenosis (178, 186). Importantly, SR allows microangiography of resistance vessels even in small animals (197). Thus, it can provide a powerful approach to facilitate basic and translational research on the coronary circulation. There have been studies demonstrating the utility of SR microangiography for *in vivo* coronary imaging in mice and rats (94, 203, 221, 243). However, there are very few studies that have applied this approach to the investigation of HF and the factors that drive it, such as coronary vasospasm. This approach has also been rarely applied to the assessment of the efficacy of cardiac regenerative therapies *in vivo*. These issues are the major focus of the current thesis.

SR overcomes many of the limitation of other techniques, used in previous studies, to investigate local control of blood flow *in vivo* (202). Magnetic resonance and micro-computed tomographic techniques have limited spatial and temporal resolution (17). The advantages of SR are that it provides images of the microcirculation in small animals with both high spatial and temporal resolution. The

images provide unrivalled insight into vasomotor regulation, particularly given the feasibility of repeated imaging of the vessel network (202). SR imaging can be performed in with a temporal resolution of milliseconds at most of the third generation synchrotron facilities worldwide (202). When combined with a fast X-ray detector system we consider that SR is ideal for dynamic studies of small arterial vessels in small animals and is also the best approach for imaging in cardiac regenerative medicine.

Assessment of endothelium-dependent and -independent vasodilator function in vivo has been used, in both clinical and preclinical studies, to establish how endothelial or VSM dysfunction might contribute to the progression of heart disease and various forms of HF (58, 95, 186, 203). However, coronary function is rarely assessed in studies of regenerative therapy. Rather, for the most part these studies have focused on evaluation of the effects of transplantation on LV function and remodeling (23, 72, 130, 191). Adequate perfusion is critical for the successful regeneration of the myocardium. Previous clinical trails also show attenuated therapeutic effects due to multiple factors such as generation of unstable and immature blood vessels with endothelial dysfunction (14, 38). Therefore, in my thesis one focus is the assessment of the vascular function of the coronary circulation to evaluate the efficacy of regenerative therapies. In the studies described in Chapter 3, my first aim was to generate an index of the number of coronary arterial vessels in the ischemic myocardium 2 weeks after treatment with either myoblast sheets, omentum or combined treatments. The second aim was to determine whether the existing and newly developed arterial vessels in the ischemic myocardium maintain normal vasomotor function after the treatments. I tested the hypothesis that combined therapy with myoblast sheets and omentum, improves coronary microvascular structure and function after MI, more than either treatment alone.

Inflammation contributes to the persistent vasoconstriction and endothelial dysfunction associated with the ongoing ischemia post MI, and so contributes to the development of chronic HF. Prostaglandins are a family of bioactive substances derived from arachidonic acid. They play an important role in maintaining local tissue homoeostasis and evoking the inflammatory response. Prostacyclin is a potent vasodilator in the heart, and potentiates nitric oxide release in various

vascular territories (180, 208). Furthermore, prostacyclin is thought to play a major role in tissue repair and modulation of inflammation (112, 208). However, endogenous prostacyclin is rapidly removed from the circulation by 15-hydroxyprostaglandin dehydrogenase. Therefore, in the experiments described in Chapter 4 of this thesis, I examined the effects of a prostacyclin analogue (ONO-1301) on revascularization in the myocardium adjacent to the infarct region following MI. The second aim was to determine whether the existing and newly developed arterial vessels within the infarct region maintain normal vasomotor function following ONO-1301 administration (Chapter 4). I tested the hypothesis that the vasodilatory capacity of arterial vessels of the anterior and lateral walls of the LV after MI is improved by ONO-1301.

Abnormal production of constrictor factors also contributes to coronary dysfunction in hypertensive disorders and HF. Angiotensin, RhoA/RhoKinase and endothelin-1 in particular are known contribute to chronic vasoconstriction. More recently, the endogenous peptide apelin and its receptor APJ, which shares close homology with the angiotensin II type 1 receptor, have been identified as potentially significant contributors to vasospasm and coronary heart disease. In particular it has been shown that delivery of apelin causes stenosis and focal vessel constriction in the hearts that overexpressed APJ in vascular smooth muscle *ex vivo* performed by our colleagues (Prof Fukamizu and Assoc Prof. Ishida from the University of Tsukuba). They performed the study by intraperitoneal injection of either apelin (296 μg/kg) or saline in wild type mice (WT) and a transgenic mouse model with overexpression of the APJ receptor. They then injected Microfil® (MV-112, Flow Tech Inc., Carver, MA, USA) directly into the left ventricle and clarified the heart to enable visualization of the coronary vessels in the intact hearts. It is not known whether APJ mediates vasospasm induced by apelin production *in vivo* from the previous study. Major limitations of the previous study discussed above were that (i) vascular caliber was assessed *ex vivo* rather than *in vivo*, and (ii) that only between-animal comparisons were made. Therefore, in the studies described in Chapter 5 of this thesis, I tested the hypothesis that APJ receptors mediate coronary vasoconstriction *in vivo*.

In this introduction I have described how many risk factors that are increasing in prevalence in society and contribute to the development of HF. It is now recognized that the combination of diabetes, obesity and hypertension in particular, leads to

HFpEF and often eventually end stage HF (173, 225, 247). In addition, there is strong evidence to suggest that insulin resistance creates an imbalance of vasoactive factors in favor of vasoconstriction (151, 152), increased oxidative stress, increased activation of the cardiac RAS and sympathetic overactivation, leading to endothelial dysfunction. Similarly, these same factors have been shown to important drivers of vascular dysfunction associated with sleep apnea syndrome (50). However, it is not known whether there is an additive effect of multiple risk factors on coronary dysfunction. In the studies described in Chapter 6 of this thesis, I tested the hypothesis that the onset of coronary vascular dysfunction in insulin resistant rats is accelerated by medium-term exposure to severe chronic intermittent hypoxia (IH). Our aim was to evaluate the effect of IH in coronary vasodilatory function in Wistar rats and insulin resistant (Goto Kakizaki) rats.

1.13 References

1. Effect of metoprolol CR/XL in chronic heart failure: Metoprolol CR/XL Randomised Intervention Trial in Congestive Heart Failure (MERIT-HF). *Lancet* 353: 2001-2007, 1999.
2. **Agnetti G, Piepoli MF, Siniscalchi G, and Nicolini F**. New Insights in the Diagnosis and Treatment of Heart Failure. *Biomed Res Int* 2015: 265260, 2015.
3. **Ahmed RP, Ashraf M, Buccini S, Shujia J, and Haider H**. Cardiac tumorigenic potential of induced pluripotent stem cells in an immunocompetent host with myocardial infarction. *Regen Med* 6: 171-178, 2011.
4. **AIHW**. Cardiovascular disease: Australian facts 2011. 232, 2011.
5. **Albert NM, Yancy CW, Liang L, Zhao X, Hernandez AF, Peterson ED, Cannon CP, and Fonarow GC**. Use of aldosterone antagonists in heart failure. *JAMA* 302: 1658-1665, 2009.
6. **Amabile G, and Meissner A**. Induced pluripotent stem cells: current progress and potential for regenerative medicine. *Trends Mol Med* 15: 59-68, 2009.
7. **America HFSo**. Executive summary: HFSA 2010 comprehensive heart failure practice guideline. *J Card Fail* 16: 475-539, 2010.
8. **Ando J, Nomura H, and Kamiya A**. The effect of fluid shear stress on the migration and proliferation of cultured endothelial cells. *Microvasc Res* 33: 62-70, 1987.
9. **Ang K-L, Chin D, Leyva F, Foley P, Kubal C, Chalil S, Srinivasan L, Bernhardt L, Stevens S, and Shenje LT**. Randomized, controlled trial of intramuscular or intracoronary injection of autologous bone marrow cells into scarred myocardium during CABG versus CABG alone. *Nat Clin Pract Cardiovasc Med* 5: 663-670, 2008.
10. **Archer SL, Gragasin FS, Wu X, Wang S, McMurtry S, Kim DH, Platonov M, Koshal A, Hashimoto K, and Campbell WB**. Endothelium-derived hyperpolarizing factor in human internal mammary artery is 11, 12-epoxyeicosatrienoic acid and causes relaxation by activating smooth muscle BKCa channels. *Circulation* 107: 769-776, 2003.
11. **Archibald FS, and Fridovich I**. The scavenging of superoxide radical by manganous complexes: in vitro. *Arch Biochem Biophys* 214: 452-463, 1982.
12. **Arstall MA, Sawyer DB, Fukazawa R, and Kelly RA**. Cytokine-mediated apoptosis in cardiac myocytes: the role of inducible nitric oxide synthase induction and peroxynitrite generation. *Circ Res* 85: 829-840, 1999.
13. **Badorff C, Brandes RP, Popp R, Rupp S, Urbich C, Aicher A, Fleming I, Busse R, Zeiher AM, and Dimmeler S**. Transdifferentiation of blood-derived human adult endothelial progenitor cells into functionally active cardiomyocytes. *Circulation* 107: 1024-1032, 2003.
14. **Banquet S, Gomez E, Nicol L, Edwards-Levy F, Henry JP, Cao R, Schapman D, Dautreaux B, Lallemand F, Bauer F, Cao Y, Thuillez C, Mulder P, Richard V, and Brakenhielm E**. Arteriogenic therapy by intramyocardial sustained delivery of a novel growth factor combination prevents chronic heart failure. *Circulation* 124: 1059-1069, 2011.
15. **Bayraktutan U, Blayney L, and Shah AM**. Molecular characterization and localization of the NAD(P)H oxidase components gp91-phox and p22-phox in endothelial cells. *Arterioscler Thromb Vasc Biol* 20: 1903-1911, 2000.
16. **Beltrami AP, Barlucchi L, Torella D, Baker M, Limana F, Chimenti S, Kasahara H, Rota M, Musso E, and Urbanek K**. Adult cardiac stem cells are multipotent and support myocardial regeneration. *Cell* 114: 763-776, 2003.
17. **Bentley MD, Ortiz MC, Ritman EL, and Romero JC**. The use of microcomputed tomography to study microvasculature in small rodents. *Am J Physiol Regul Integr Comp Physiol* 282: R1267-R1279, 2002.

18. **Beny JL, and Von der weid PY**. Hydrogen peroxide: an endogenous smooth muscle cell hyperpolarizing factor. *Biochem Biophys Res Commun* 176: 378-384, 1991.
19. **Berne R, and Rubio R**. Coronary circulation. *Handbook of Physiology, section* 2: 873-952, 1979.
20. **Bertrand B, Esteve F, Elleaume H, Nemoz C, Fiedler S, Bravin A, Berruyer G, Brochard T, Renier M, and Machecourt J**. Comparison of synchrotron radiation angiography with conventional angiography for the diagnosis of in-stent restenosis after percutaneous transluminal coronary angioplasty. *Eur Heart J* 26: 1284-1291, 2005.
21. **Blankesteijn WM, Creemers E, Lutgens E, Cleutjens JP, Daemen MJ, and Smits JF**. Dynamics of cardiac wound healing following myocardial infarction: observations in genetically altered mice. *Acta Physiol Scand* 173: 75-82, 2001.
22. **Bois P, Bescond J, Renaudon B, and Lenfant J**. Mode of action of bradycardic agent, S 16257, on ionic currents of rabbit sinoatrial node cells. *Br J Pharmacol* 118: 1051-1057, 1996.
23. **Bolli R, Chugh AR, D'Amario D, Loughran JH, Stoddard MF, Ikram S, Beache GM, Wagner SG, Leri A, Hosoda T, Sanada F, Elmore JB, Goichberg P, Cappetta D, Solankhi NK, Fahsah I, Rokosh DG, Slaughter MS, Kajstura J, and Anversa P**. Cardiac stem cells in patients with ischaemic cardiomyopathy (SCIPIO): initial results of a randomised phase 1 trial. *Lancet* 378: 1847-1857, 2011.
24. **Bolli R, Tang XL, Sanganalmath SK, Rimoldi O, Mosna F, Abdel-Latif A, Jneid H, Rota M, Leri A, and Kajstura J**. Intracoronary delivery of autologous cardiac stem cells improves cardiac function in a porcine model of chronic ischemic cardiomyopathy. *Circulation* 128: 122-131, 2013.
25. **Boonbaichaiyapruck S, Pienvichit P, Limpijarnkij T, Rerkpattanapipat P, Pongpatananurak A, Saelee R, Ungkanont A, and Hongeng S**. Transcoronary infusion of bone marrow derived multipotent stem cells to preserve left ventricular geometry and function after myocardial infarction. *Clin Cardiol* 33: E10-15, 2010.
26. **Borlaug BA**. Defining HFpEF: where do we draw the line? *Eur Heart J* 37: 463-465, 2016.
27. **Boulanger CM, Scoazec A, Ebrahimian T, Henry P, Mathieu E, Tedgui A, and Mallat Z**. Circulating microparticles from patients with myocardial infarction cause endothelial dysfunction. *Circulation* 104
: 2649-2652, 2001.
28. **Bradley TD, and Floras JS**. sleep apnea and heart failure Part II: central sleep apnea. *Circulation* 107: 1822-1826, 2003.
29. **Brieger K, Schiavone S, Miller FJ, Jr., and Krause KH**. Reactive oxygen species: from health to disease. *Swiss Med Wkly* 142: w13659, 2012.
30. **Bristow MR**. beta-adrenergic receptor blockade in chronic heart failure. *Circulation* 101: 558-569, 2000.
31. **Bui AL, Horwich TB, and Fonarow GC**. Epidemiology and risk profile of heart failure. *Nat Rev Cardiol* 8: 30-41, 2011.
32. **Büssemaker E, Pistrosch F, Förster S, Herbrig K, Gross P, Passauer J, and Brandes RP**. Rho kinase contributes to basal vascular tone in humans: role of endothelium-derived nitric oxide. *Am J Physiol Heart Circ Physiol* 293: H541-H547, 2007.
33. **Cai H, and Harrison DG**. Endothelial dysfunction in cardiovascular diseases: the role of oxidant stress. *Circ Res* 87: 840-844, 2000.
34. **Campbell DJ, Somaratne JB, Jenkins AJ, Prior DL, Yii M, Kenny JF, Newcomb AE, Kelly DJ, and Black MJ**. Differences in myocardial structure and coronary microvasculature between men and women with coronary artery disease. *Hypertension* 57: 186-192, 2011.

35. **Campbell DJ, Somaratne JB, Jenkins AJ, Prior DL, Yii M, Kenny JF, Newcomb AE, Kelly DJ, and Black MJ**. Reduced microvascular density in non-ischemic myocardium of patients with recent non-ST-segment-elevation myocardial infarction. *Int J Cardiol* 167: 1027-1037, 2013.
36. **Campbell WB, Gebremedhin D, Pratt PF, and Harder DR**. Identification of epoxyeicosatrienoic acids as endothelium-derived hyperpolarizing factors. *Circ Res* 78: 415-423, 1996.
37. **Carmeliet P**. Angiogenesis in health and disease. *Nat Med* 9: 653-660, 2003.
38. **Carmeliet P, and Jain RK**. Molecular mechanisms and clinical applications of angiogenesis. *Nature* 473: 298-307, 2011.
39. **Caspi O, Huber I, Kehat I, Habib M, Arbel G, Gepstein A, Yankelson L, Aronson D, Beyar R, and Gepstein L**. Transplantation of human embryonic stem cell-derived cardiomyocytes improves myocardial performance in infarcted rat hearts. *J Am Coll Cardiol* 50: 1884-1893, 2007.
40. **Channon KM**. The endothelium and the pathogenesis of atherosclerosis. *Medicine* 34: 173-177, 2006.
41. **Cochain C, Channon KM, and Silvestre JS**. Angiogenesis in the infarcted myocardium. *Antioxid Redox Signal* 18: 1100-1113, 2013.
42. **Cohn JN, Archibald DG, Ziesche S, Franciosa JA, Harston WE, Tristani FE, Dunkman WB, Jacobs W, Francis GS, Flohr KH, and et al.** Effect of vasodilator therapy on mortality in chronic congestive heart failure. Results of a Veterans Administration Cooperative Study. *N Engl J Med* 314: 1547-1552, 1986.
43. **Cohn JN, Johnson G, Ziesche S, Cobb F, Francis G, Tristani F, Smith R, Dunkman WB, Loeb H, Wong M, and et al.** A comparison of enalapril with hydralazine-isosorbide dinitrate in the treatment of chronic congestive heart failure. *N Engl J Med* 325: 303-310, 1991.
44. **Cohn JN, Tognoni G, and Valsartan Heart Failure Trial I**. A randomized trial of the angiotensin-receptor blocker valsartan in chronic heart failure. *N Engl J Med* 345: 1667-1675, 2001.
45. **Dai X, and Bache RJ**. Effect of indomethacin on coronary blood flow during graded treadmill exercise in the dog. *Am J Physiol Heart Circ Physiol* 247: H452-H458, 1984.
46. **Dickhout JG, Hossain GS, Pozza LM, Zhou J, Lhotak S, and Austin RC**. Peroxynitrite causes endoplasmic reticulum stress and apoptosis in human vascular endothelium: implications in atherogenesis. *Arterioscler Thromb Vasc Biol* 25: 2623-2629, 2005.
47. **Doetschman TC, Eistetter H, Katz M, Schmidt W, and Kemler R**. The in vitro development of blastocyst-derived embryonic stem cell lines: formation of visceral yolk sac, blood islands and myocardium. *J Embryol Exp Morphol* 87: 27-45, 1985.
48. **Dong M, Liao JK, Fang F, Lee AP, Yan BP, Liu M, and Yu CM**. Increased Rho kinase activity in congestive heart failure. *Eur J Heart Fail* 14: 965-973, 2012.
49. **Dreyer WJ, Michael LH, Nguyen T, Smith CW, Anderson DC, Entman ML, and Rossen RD**. Kinetics of C5a release in cardiac lymph of dogs experiencing coronary artery ischemia-reperfusion injury. *Circ Res* 71: 1518-1524, 1992.
50. **Dumitrascu R, Heitmann J, Seeger W, Weissmann N, and Schulz R**. Obstructive sleep apnea, oxidative stress and cardiovascular disease: lessons from animal studies. *Oxid Med Cell Longev* 2013: 234631, 2013.
51. **Eichhorn EJ, Lukas MA, Wu B, and Shusterman N**. Effect of concomitant digoxin and carvedilol therapy on mortality and morbidity in patients with chronic heart failure. *Am J Cardiol* 86: 1032-1035, A1010-1031, 2000.

52. **Entman ML, and Smith CW**. Postreperfusion inflammation: a model for reaction to injury in cardiovascular disease. *Cardiovasc Res* 28: 1301-1311, 1994.
53. **Ertl G, and Frantz S**. Healing after myocardial infarction. *Cardiovasc Res* 66: 22-32, 2005.
54. **Evans M, and Kaufman M**. Establishment in culture of pluripotential cells from mouse embryos. *Nature* 292: 154-156, 1981.
55. **Feigl E**. Coronary physiology. *Physiol Rev* 63: 1-205, 1983.
56. **Fichtenbaum CJ**. Inflammatory Markers Associated with Coronary Heart Disease in Persons with HIV Infection. *Curr Infect Dis Rep* 13: 94-101, 2011.
57. **Flachskampf FA, Schmid M, Rost C, Achenbach S, DeMaria AN, and Daniel WG**. Cardiac imaging after myocardial infarction. *Eur Heart J* 32: 272-283, 2011.
58. **Flammer AJ, Anderson T, Celermajer DS, Creager MA, Deanfield J, Ganz P, Hamburg NM, Luscher TF, Shechter M, Taddei S, Vita JA, and Lerman A**. The assessment of endothelial function: from research into clinical practice. *Circulation* 126: 753-767, 2012.
59. **Fleming I**. Cytochrome p450 and vascular homeostasis. *Circ Res* 89: 753-762, 2001.
60. **Fleming I, Michaelis UR, Bredenkötter D, Fisslthaler B, Dehghani F, Brandes RP, and Busse R**. Endothelium-derived hyperpolarizing factor synthase (Cytochrome P450 2C9) is a functionally significant source of reactive oxygen species in coronary arteries. *Circ Res* 88: 44-51, 2001.
61. **Förstermann U, Boissel J, and Kleinert H**. Expressional control of the 'constitutive'isoforms of nitric oxide synthase (NOS I and NOS III). *FASEB J* 12: 773-790, 1998.
62. **Fox K, Ford I, Steg PG, Tardif JC, Tendera M, Ferrari R, and Investigators S**. Ivabradine in stable coronary artery disease without clinical heart failure. *N Engl J Med* 371: 1091-1099, 2014.
63. **Frangogiannis NG, Smith CW, and Entman ML**. The inflammatory response in myocardial infarction. *Cardiovasc Res* 53: 31-47, 2002.
64. **Frantz S, Bauersachs J, and Ertl G**. Post-infarct remodelling: contribution of wound healing and inflammation. *Cardiovasc Res* 81: 474-481, 2009.
65. **Frantz S, Ertl G, and Bauersachs J**. Mechanisms of disease: Toll-like receptors in cardiovascular disease. *Nat Clin Pract Cardiovasc Med* 4: 444-454, 2007.
66. **Freiman PC, Mitchell GG, Heistad DD, Armstrong ML, and Harrison DG**. Atherosclerosis impairs endothelium-dependent vascular relaxation to acetylcholine and thrombin in primates. *Circ Res* 58: 783-789, 1986.
67. **Fridovich I**. Superoxide radical and superoxide dismutases. *Annu Rev Biochem* 64: 97-112, 1995.
68. **Fukai T, and Ushio-Fukai M**. Superoxide dismutases: role in redox signaling, vascular function, and diseases. *Antioxid Redox Signal* 15: 1583-1606, 2011.
69. **Furchgott RF, and Zawadzki JV**. The obligatory role of endothelial cells in the relaxation of arterial smooth muscle by acetylcholine. *Nature* 288: 373-376, 1980.
70. **Garg R, and Yusuf S**. Overview of randomized trials of angiotensin-converting enzyme inhibitors on mortality and morbidity in patients with heart failure. Collaborative Group on ACE Inhibitor Trials. *JAMA* 273: 1450-1456, 1995.
71. **Ge ZD, and He GW**. Altered endothelium-derived hyperpolarizing factor–mediated endothelial function in coronary microarteries by St Thomas' hospital solution. *J Thorac Cardiovasc Surg* 118: 173-180, 1999.
72. **George JC**. Stem cell therapy in acute myocardial infarction: a review of clinical trials. *Transl Res* 155: 10-19, 2010.

73. **Gheorghiade M, and Bonow RO**. Introduction and overview: beta-blocker therapy in the management of chronic heart failure. *Am J Med* 110 Suppl 7A: 1S-5S, 2001.
74. **Grandi AM, Imperiale D, Santillo R, Barlocco E, Bertolini A, Guasti L, and Venco A**. Aldosterone antagonist improves diastolic function in essential hypertension. *Hypertension* 40: 647-652, 2002.
75. **Groenning BA, Nilsson JC, Sondergaard L, Fritz-Hansen T, Larsson HB, and Hildebrandt PR**. Antiremodeling effects on the left ventricle during beta-blockade with metoprolol in the treatment of chronic heart failure. *J Am Coll Cardiol* 36: 2072-2080, 2000.
76. **Guan Y, Cai B, Liu Z, Ye F, Deng P, Cai WJ, Schaper J, and Schaper W**. The Formation of Aberrant Collateral Vessels during Coronary Arteriogenesis in Dog Heart. *Cells Tissues Organs* 201: 118-129, 2016.
77. **Guthrie RM**. Review of diuretic and ultrafiltration strategies in patients with acute decompensated heart failure. *Hosp Pract* 41: 129-131, 2013.
78. **Halcox JP, Narayanan S, Cramer-Joyce L, Mincemoyer R, and Quyyumi AA**. Characterization of endothelium-derived hyperpolarizing factor in the human forearm microcirculation. *Am J Physiol Heart Circ Physiol* 280: H2470-2477, 2001.
79. **Hansson EM, and Lendahl U**. Regenerative medicine for the treatment of heart disease. *J Intern Med* 273: 235-245, 2013.
80. **He GW**. Nitric oxide release, EDHF, and the role of potassium channels in coronary circulation. *Drug Dev Res* 58: 23-27, 2003.
81. **He GW, and Yang CQ**. Hyperkalemia alters endothelium-dependent relaxation through non—nitric oxide and noncyclooxygenase pathway: A mechanism for coronary dysfunction due to cardioplegia. *Ann Thorac Surg* 61: 1394-1399, 1996.
82. **He GW, and Yang CQ**. Inhibition of vasoconstriction by potassium channel opener aprikalim in human conduit arteries used as bypass grafts. *Br J Clin Pharmacol* 44: 353-359, 1997.
83. **He J, Ogden LG, Bazzano LA, Vupputuri S, Loria C, and Whelton PK**. Risk factors for congestive heart failure in US men and women: NHANES I epidemiologic follow-up study. *Adv Intern Med* 161: 996-002, 2001.
84. **Hearse DJ**. Species variation in the coronary collateral circulation during regional myocardial ischaemia: a critical determinant of the rate of evolution and extent of myocardial infarction. *Cardiovasc Res* 45: 213-219, 2000.
85. **Heitzer T, Schlinzig T, Krohn K, Meinertz T, and Münzel T**. Endothelial dysfunction, oxidative stress, and risk of cardiovascular events in patients with coronary artery disease. *Circulation* 104: 2673-2678, 2001.
86. **Higuchi T, Miyagawa S, Pearson JT, Fukushima S, Saito A, Tsuchimochi H, Sonobe T, Fujii Y, Yagi N, Astolfo A, Shirai M, and Sawa Y**. Functional and Electrical Integration of Induced Pluripotent Stem Cell-Derived Cardiomyocytes in a Myocardial Infarction Rat Heart. *Cell Transplant* 24: 2479-2489, 2015.
87. **Holmes JW, Yamashita H, Waldman LK, and Covell JW**. Scar remodeling and transmural deformation after infarction in the pig. *Circulation* 90: 411-420, 1994.
88. **Houtgraaf JH, Wijnand K, van Dalen BM, Springeling T, de Jong R, van Geuns RJ, Geleijnse ML, Fernandez-Aviles F, Zijlsta F, and Serruys PW**. First experience in humans using adipose tissue-derived regenerative cells in the treatment of patients with ST-segment elevation myocardial infarction. *J Am Coll Cardiol* 59: 539-540, 2012.
89. **Hsieh HJ, Liu CA, Huang B, Tseng AH, and Wang DL**. Shear-induced endothelial mechanotransduction: the interplay between reactive oxygen species (ROS) and nitric oxide (NO) and the pathophysiological implications. *J Biomed Sci* 21: 3, 2014.
90. **Hung J, Teng THK, Finn J, Knuiman M, Briffa T, Stewart S, Sanfilippo FM, Ridout S, and Hobbs M**. Trends From 1996 to 2007 in Incidence and Mortality

Outcomes of Heart Failure After Acute Myocardial Infarction: A Population‐Based Study of 20 812 Patients With First Acute Myocardial Infarction in Western Australia. *J Am Heart Assoc* 2: e000172, 2013.
91. **Hwa JJ, Ghibaudi L, Williams P, and Chatterjee M**. Comparison of acetylcholine-dependent relaxation in large and small arteries of rat mesenteric vascular bed. *Am J Physiol Heart Circ Physiol* 35: H952, 1994.
92. **Investigators TS**. Effect of enalapril on mortality and the development of heart failure in asymptomatic patients with reduced left ventricular ejection fractions. The SOLVD Investigattors. *N Engl J Med* 327: 685-691, 1992.
93. **Ishizaka H, Okumura K, Yamabe H, Tsuchiya T, and Yasue H**. Endothelium-derived nitric oxide as a mediator of acetylcholine-induced coronary vasodilation in dogs. *J Cardiovasc Pharmacol Ther* 18: 665-669, 1991.
94. **Jenkins MJ, Edgley AJ, Sonobe T, Umetani K, Schwenke DO, Fujii Y, Brown RD, Kelly DJ, Shirai M, and Pearson JT**. Dynamic synchrotron imaging of diabetic rat coronary microcirculation in vivo. *Arteriosclerosis, thrombosis, and vascular biology* 32: 370-377, 2012.
95. **Jenkins MJ, Edgley AJ, Sonobe T, Umetani K, Schwenke DO, Fujii Y, Brown RD, Kelly DJ, Shirai M, and Pearson JT**. Dynamic synchrotron imaging of diabetic rat coronary microcirculation in vivo. *Arterioscler Thromb Vasc Biol* 32: 370-377, 2012.
96. **Jessup M, and Brozena S**. Medical progress. *Heart failure N Engl J Med* 348: 2007-2018, 2003.
97. **Johnston CI, Fabris B, and Yoshida K**. The cardiac renin-angiotensin system in heart failure. *Am Heart J* 126: 756-760, 1993.
98. **Jolly SR, Kane WJ, Hook BG, Abrams GD, Kunkel SL, and Lucchesi BR**. Reduction of myocardial infarct size by neutrophil depletion: Effect of duration of occlusion* 1. *American heart journal* 112: 682-690, 1986.
99. **Jugdutt BI**. Ventricular remodeling after infarction and the extracellular collagen matrix: when is enough enough? *Circulation* 108: 1395-1403, 2003.
100. **Katusic ZS**. Superoxide anion and endothelial regulation of arterial tone. *Free Radic Biol Med* 20: 443-448, 1996.
101. **Kaul S, and Ito H**. Microvasculature in acute myocardial ischemia: part II: evolving concepts in pathophysiology, diagnosis, and treatment. *Circulation* 109: 310-315, 2004.
102. **Keaney JF**. Atherosclerosis: from lesion formation to plaque activation and endothelial dysfunction. *Mol Aspects Med* 21: 99-166, 2000.
103. **Keeley EC, Boura JA, and Grines CL**. Primary angioplasty versus intravenous thrombolytic therapy for acute myocardial infarction: a quantitative review of 23 randomised trials. *Lancet* 361: 13-20, 2003.
104. **Khalil ME, Basher AW, Brown EJ, Jr, and Alhaddad IA**. A remarkable medical story: benefits of angiotensin-converting enzyme inhibitors in cardiac patients. *J Am Coll Cardiol* 37: 1757-1764, 2001.
105. **Kido M, Du L, Sullivan CC, Li X, Deutsch R, Jamieson SW, and Thistlethwaite PA**. Hypoxia-inducible factor 1-alpha reduces infarction and attenuates progression of cardiac dysfunction after myocardial infarction in the mouse. *J Am Coll Cardiol* 46: 2116-2124, 2005.
106. **King JB, Bress AP, Reese AD, and Munger MA**. Neprilysin Inhibition in Heart Failure with Reduced Ejection Fraction: A Clinical Review. *Pharmacotherapy* 35: 823-837, 2015.
107. **Kloner R, Rude R, Carlson N, Maroko P, DeBoer L, and Braunwald E**. Ultrastructural evidence of microvascular damage and myocardial cell injury after coronary artery occlusion: which comes first? *Circulation* 62: 945-952, 1980.

108. **Ko IK, Lee SJ, Atala A, and Yoo JJ**. In situ tissue regeneration through host stem cell recruitment. *Exp Mol Med* 45: e57, 2013.
109. **Koerselman J, van der Graaf Y, de Jaegere PP, and Grobbee DE**. Coronary collaterals: an important and underexposed aspect of coronary artery disease. *Circulation* 107: 2507-2511, 2003.
110. **Konstam MA, Neaton JD, Dickstein K, Drexler H, Komajda M, Martinez FA, Riegger GA, Malbecq W, Smith RD, Guptha S, Poole-Wilson PA, and Investigators H**. Effects of high-dose versus low-dose losartan on clinical outcomes in patients with heart failure (HEAAL study): a randomised, double-blind trial. *Lancet* 374: 1840-1848, 2009.
111. **Krum H, and Driscoll A**. Management of heart failure. *Med J Aust* 199: 334-339, 2013.
112. **Kuwabara K, Ogawa S, Matsumoto M, Koga S, Clauss M, Pinsky DJ, Lyn P, Leavy J, Witte L, and Joseph-Silverstein J**. Hypoxia-mediated induction of acidic/basic fibroblast growth factor and platelet-derived growth factor in mononuclear phagocytes stimulates growth of hypoxic endothelial cells. *Proc Natl Acad Sci USA* 92: 4606-4610, 1995.
113. **Lacza Z, Puskar M, Kis B, Perciaccante JV, Miller AW, and Busija DW**. Hydrogen peroxide acts as an EDHF in the piglet pial vasculature in response to bradykinin. *Am J Physiol Heart Circ Physiol* 283: H406-411, 2002.
114. **Laflamme MA, Chen KY, Naumova AV, Muskheli V, Fugate JA, Dupras SK, Reinecke H, Xu C, Hassanipour M, and Police S**. Cardiomyocytes derived from human embryonic stem cells in pro-survival factors enhance function of infarcted rat hearts. *Nat Biotechnol* 25: 1015-1024, 2007.
115. **Laugwitz KL, Moretti A, Lam J, Gruber P, Chen Y, Woodard S, Lin LZ, Cai CL, Lu M, and Reth M**. Postnatal isl1+ cardioblasts enter fully differentiated cardiomyocyte lineages. *Nature* 446: 934-945, 2007.
116. **Lee DL, Webb RC, and Jin L**. Hypertension and RhoA/Rho-kinase signaling in the vasculature: highlights from the recent literature. *Hypertension* 44: 796-799, 2004.
117. **Lee VC, Rhew DC, Dylan M, Badamgarav E, Braunstein GD, and Weingarten SR**. Meta-analysis: angiotensin-receptor blockers in chronic heart failure and high-risk acute myocardial infarction. *Ann Intern Med* 141: 693-704, 2004.
118. **Lefroy DC, Crake T, Uren NG, Davies GJ, and Maseri A**. Effect of inhibition of nitric oxide synthesis on epicardial coronary artery caliber and coronary blood flow in humans. *Circulation* 88: 43-54, 1993.
119. **Leri A, Kajstura J, and Anversa P**. Role of cardiac stem cells in cardiac pathophysiology: a paradigm shift in human myocardial biology. *Circ Res* 109: 941-961, 2011.
120. **Levrand S, Vannay-Bouchiche C, Pesse B, Pacher P, Feihl F, Waeber B, and Liaudet L**. Peroxynitrite is a major trigger of cardiomyocyte apoptosis in vitro and in vivo. *Free Radic Biol Med* 41: 886-895, 2006.
121. **Li J, Li W, Su J, Liu W, Altura BT, and Altura BM**. Peroxynitrite induces apoptosis in rat aortic smooth muscle cells: possible relation to vascular diseases. *Exp Biol Med* 229: 264-269, 2004.
122. **Liao JK, Seto M, and Noma K**. Rho kinase (ROCK) inhibitors. *J Cardiovasc Pharmacol* 50: 17-24, 2007.
123. **Löffler G, and Hauner H**. Adipose tissue development: The role of precursor cells and adipogenic factors. *Klin Wochenschr* 65: 812-817, 1987.
124. **London GM, Pannier B, Guerin AP, Marchais SJ, Safar ME, and Cuche JL**. Cardiac hypertrophy, aortic compliance, peripheral resistance, and wave reflection in end-stage renal disease. Comparative effects of ACE inhibition and calcium channel blockade. *Circulation* 90: 2786-2796, 1994.

125. **Luckhoff A, Zeh R, and Busse R**. Desensitization of the bradykinin-induced rise in intracellular free calcium in cultured endothelial cells. *Pflugers Arch* 412: 654-658, 1988.
126. **Lunt SJ, Gray C, Reyes-Aldasoro CC, Matcher SJ, and Tozer GM**. Application of intravital microscopy in studies of tumor microcirculation. *J Biomed Opt* 15: 011113, 2010.
127. **Lüscher T, and Vanhoutte PM**. Endothelium-dependent contractions to acetylcholine in the aorta of the spontaneously hypertensive rat. *Hypertension* 8: 344-348, 1986.
128. **Ma T, Xie M, Laurent T, and Ding S**. Progress in the reprogramming of somatic cells. *Circ Res* 112: 562-574, 2013.
129. **Makino S, Fukuda K, Miyoshi S, Konishi F, Kodama H, Pan J, Sano M, Takahashi T, Hori S, and Abe H**. Cardiomyocytes can be generated from marrow stromal cells in vitro. *J Clin Invest* 103: 697-705, 1999.
130. **Makkar RR, Smith RR, Cheng K, Malliaras K, Thomson LE, Berman D, Czer LS, Marban L, Mendizabal A, Johnston PV, Russell SD, Schuleri KH, Lardo AC, Gerstenblith G, and Marban E**. Intracoronary cardiosphere-derived cells for heart regeneration after myocardial infarction (CADUCEUS): a prospective, randomised phase 1 trial. *Lancet* 379: 895-904, 2012.
131. **Mancini GB, Etminan M, Zhang B, Levesque LE, FitzGerald JM, and Brophy JM**. Reduction of morbidity and mortality by statins, angiotensin-converting enzyme inhibitors, and angiotensin receptor blockers in patients with chronic obstructive pulmonary disease. *J Am Coll Cardiol* 47: 2554-2560, 2006.
132. **Martinez de Ilarduya O, Barallobre Barreiro J, Moscoso I, Anon P, Fraga M, Centeno A, Lopez E, and Domenech N**. Gene expression profiles in a porcine model of infarction: differential expression after intracoronary injection of heterologous bone marrow mesenchymal cells. *Transplant Proc* 41: 2276-2278, 2009.
133. **Mas M**. A close look at the endothelium: its role in the regulation of vasomotor tone. *Eur Urol Suppl* 8: 48-57, 2009.
134. **Mathers C, and Penm R**. *Health system costs of cardiovascular diseases and diabetes in Australia 1993-94*. Australian Institute of Health and Welfare, 1999.
135. **Matoba T, Shimokawa H, Kubota H, Morikawa K, Fujiki T, Kunihiro I, Mukai Y, Hirakawa Y, and Takeshita A**. Hydrogen peroxide is an endothelium-derived hyperpolarizing factor in human mesenteric arteries. *Biochem Biophys Res Commun* 290: 909-913, 2002.
136. **Matoba T, Shimokawa H, Nakashima M, Hirakawa Y, Mukai Y, Hirano K, Kanaide H, and Takeshita A**. Hydrogen peroxide is an endothelium-derived hyperpolarizing factor in mice. *J Clin Invest* 106: 1521-1530, 2000.
137. **Matoba T, Shimokawa H, Nakashima M, Hirakawa Y, Mukai Y, Hirano K, Kanaide H, and Takeshita A**. Hydrogen peroxide is an endothelium-derived hyperpolarizing factor in mice. *J Clin Invest* 106: 1521-1530, 2000.
138. **McMurray JJ, Ostergren J, Swedberg K, Granger CB, Held P, Michelson EL, Olofsson B, Yusuf S, Pfeffer MA, Investigators C, and Committees**. Effects of candesartan in patients with chronic heart failure and reduced left-ventricular systolic function taking angiotensin-converting-enzyme inhibitors: the CHARM-Added trial. *Lancet* 362: 767-771, 2003.
139. **McMurray JJ, Packer M, Desai AS, Gong J, Lefkowitz MP, Rizkala AR, Rouleau JL, Shi VC, Solomon SD, Swedberg K, and Zile MR**. Angiotensin-neprilysin inhibition versus enalapril in heart failure. *N Engl J Med* 371: 993-1004, 2014.
140. **Menasche P**. Skeletal myoblasts as a therapeutic agent. *Prog Cardiovasc Dis* 50: 7-17, 2007.

141. **Menasche P, Hagege AA, Vilquin JT, Desnos M, Abergel E, Pouzet B, Bel A, Sarateanu S, Scorsin M, Schwartz K, Bruneval P, Benbunan M, Marolleau JP, and Duboc D**. Autologous skeletal myoblast transplantation for severe postinfarction left ventricular dysfunction. *J Am Coll Cardiol* 41: 1078-1083, 2003.
142. **Mihm MJ, Jing L, and Bauer JA**. Nitrotyrosine causes selective vascular endothelial dysfunction and DNA damage. *J Cardiovasc Pharmacol* 36: 182-187, 2000.
143. **Miura H, Bosnjak JJ, Ning G, Saito T, Miura M, and Gutterman DD**. Role for hydrogen peroxide in flow-induced dilation of human coronary arterioles. *Circ Res* 92: e31-e40, 2003.
144. **Miura H, Bosnjak JJ, Ning G, Saito T, Miura M, and Gutterman DD**. Role for hydrogen peroxide in flow-induced dilation of human coronary arterioles. *Circ Res* 92: e31-40, 2003.
145. **Miura H, and Gutterman DD**. Human coronary arteriolar dilation to arachidonic acid depends on cytochrome P-450 monooxygenase and Ca2+-activated K+ channels. *Circ Res* 83: 501-507, 1998.
146. **Miyagawa S, Saito A, Sakaguchi T, Yoshikawa Y, Yamauchi T, Imanishi Y, Kawaguchi N, Teramoto N, Matsuura N, and Iida H**. Impaired myocardium regeneration with skeletal cell sheets-a preclinical trial for tissue-engineered regeneration therapy. *Transplantation* 90: 364-372, 2010.
147. **Miyahara Y, Nagaya N, Kataoka M, Yanagawa B, Tanaka K, Hao H, Ishino K, Ishida H, Shimizu T, Kangawa K, Sano S, Okano T, Kitamura S, and Mori H**. Monolayered mesenchymal stem cells repair scarred myocardium after myocardial infarction. *Nat Med* 12: 459-465, 2006.
148. **Moncada S, and Higgs E**. Nitric oxide and the vascular endothelium. In: *The Vascular Endothelium I.* Springer Berlin Heidelberg, 2006, p. 213-254.
149. **Morrissey RP, Czer L, and Shah PK**. Chronic Heart Failure. *Am J Cardiovasc Drugs* 11: 153-171, 2011.
150. **Mulder P, Barbier S, Chagraoui A, Richard V, Henry JP, Lallemand F, Renet S, Lerebours G, Mahlberg-Gaudin F, and Thuillez C**. Long-term heart rate reduction induced by the selective I(f) current inhibitor ivabradine improves left ventricular function and intrinsic myocardial structure in congestive heart failure. *Circulation* 109: 1674-1679, 2004.
151. **Muniyappa R, Iantorno M, and Quon MJ**. An integrated view of insulin resistance and endothelial dysfunction. *Endocrinol Metab Clin North Am* 37: 685-711, ix-x, 2008.
152. **Muniyappa R, and Sowers JR**. Role of insulin resistance in endothelial dysfunction. *Rev Endocr Metab Disord* 14: 5-12, 2013.
153. **Münzel T, and Keaney JF**. Are ACE inhibitors a "magic bullet" against oxidative stress? *Circulation* 104: 1571-1574, 2001.
154. **Muriello P, Clendenon S, and Dunn K**. Practical Limitations in Intravital Multiphoton Microscopy of the Kidney. *Microsc Microanal* 15: 850-851, 2009.
155. **Murry CE, Wiseman RW, Schwartz SM, and Hauschka SD**. Skeletal myoblast transplantation for repair of myocardial necrosis. *J Clin Invest* 98: 2512-2523, 1996.
156. **Nagaoka T, Fagan KA, Gebb SA, Morris KG, Suzuki T, Shimokawa H, McMurtry IF, and Oka M**. Inhaled Rho kinase inhibitors are potent and selective vasodilators in rat pulmonary hypertension. *Am J Respir Crit Care Med* 171: 494-499, 2005.
157. **Nakashima Y, Toki Y, Fukami Y, Hibino M, Okumura K, and Ito T**. Role of K+ channels in EDHF-dependent relaxation induced by acetylcholine in canine coronary artery. *Heart Vessels* 12: 287-293, 1997.

158. **Nilius B, Viana F, and Droogmans G**. Ion channels in vascular endothelium. *Ann Rev Physiol* 59: 145-170, 1997.
159. **O'Flaherty M, Allender S, Taylor R, Stevenson C, Peeters A, and Capewell S**. The decline in coronary heart disease mortality is slowing in young adults (Australia 1976–2006): a time trend analysis. *Int J Cardiol* 158: 193-198, 2012.
160. **Orlic D, Kajstura J, Chimenti S, Jakoniuk I, Anderson SM, Li B, Pickel J, McKay R, Nadal-Ginard B, and Bodine DM**. Bone marrow cells regenerate infarcted myocardium. *Nature* 410: 701-705, 2001.
161. **Otto Beitnes J, Oie E, Shahdadfar A, Karlsen T, Muller RM, Aakhus S, Reinholt FP, and Brinchmann JE**. Intramyocardial injections of human mesenchymal stem cells following acute myocardial infarction modulate scar formation and improve left ventricular function. *Cell Transplant* 21: 1697-1709, 2012.
162. **Owens AT, Brozena SC, and Jessup M**. New Management Strategies in Heart Failure. *Circ Res* 118: 480-495, 2016.
163. **Ozkor MA, and Quyyumi AA**. Endothelium-derived hyperpolarizing factor and vascular function. *Cardiol Res Pract* 2011: 156146, 2011.
164. **Pacicca C, von der Weid PY, and Beny JL**. Effect of nitro-L-arginine on endothelium-dependent hyperpolarizations and relaxations of pig coronary arteries. *J Physiol* 457: 247-256, 1992.
165. **Packer M**. The neurohormonal hypothesis: a theory to explain the mechanism of disease progression in heart failure. *J Am Coll Cardiol* 20: 248-254, 1992.
166. **Packer M, Coats AJ, Fowler MB, Katus HA, Krum H, Mohacsi P, Rouleau JL, Tendera M, Castaigne A, Roecker EB, Schultz MK, and DeMets DL**. Effect of carvedilol on survival in severe chronic heart failure. *N Engl J Med* 344: 1651-1658, 2001.
167. **Packer M, Fowler MB, Roecker EB, Coats AJ, Katus HA, Krum H, Mohacsi P, Rouleau JL, Tendera M, Staiger C, Holcslaw TL, Amann-Zalan I, and DeMets DL**. Effect of carvedilol on the morbidity of patients with severe chronic heart failure: results of the carvedilol prospective randomized cumulative survival (COPERNICUS) study. *Circulation* 106: 2194-2199, 2002.
168. **Palmer BF**. Managing hyperkalemia caused by inhibitors of the renin-angiotensin-aldosterone system. *N Engl J Med* 351: 585-592, 2004.
169. **Palmer RM, Ashton D, and Moncada S**. Vascular endothelial cells synthesize nitric oxide from L-arginine. *Nature* 333: 664-666, 1988.
170. **Parati G, and Esler M**. The human sympathetic nervous system: its relevance in hypertension and heart failure. *Eur Heart J* 33: 1058-1066, 2012.
171. **Parkington HC, Coleman HA, and Tare M**. Prostacyclin and endothelium-dependent hyperpolarization. *Pharmacol Res* 49: 509-514, 2004.
172. **Paul S, Yang Y-C, Donahue R, Goldring S, and Williams D**. Stromal cell-associated hematopoiesis: immortalization and characterization of a primate bone marrow-derived stromal cell line. *Blood* 77: 1723-1733, 1991.
173. **Paulus WJ, and Tschope C**. A novel paradigm for heart failure with preserved ejection fraction: comorbidities drive myocardial dysfunction and remodeling through coronary microvascular endothelial inflammation. *J Am Coll Cardiol* 62: 263-271, 2013.
174. **Perin EC, Sanz-Ruiz R, Sánchez PL, Lasso J, Pérez-Cano R, Alonso-Farto JC, Pérez-David E, Fernández-Santos ME, Serruys PW, and Duckers HJ**. Adipose-derived regenerative cells in patients with ischemic cardiomyopathy: The PRECISE Trial. *Am Heart J* 168: 88-95. e82, 2014.
175. **Persson H, Andreasson K, Kahan T, Eriksson SV, Tidgren B, Hjemdahl P, Hall C, and Erhardt L**. Neurohormonal activation in heart failure after acute myocardial infarction treated with beta-receptor antagonists. *Eur J Heart Fail* 4: 73-82, 2002.

176. **Pitt B, Zannad F, Remme WJ, Cody R, Castaigne A, Perez A, Palensky J, and Wittes J**. The effect of spironolactone on morbidity and mortality in patients with severe heart failure. Randomized Aldactone Evaluation Study Investigators. *N Engl J Med* 341: 709-717, 1999.
177. **Planat-Benard V, Menard C, André M, Puceat M, Perez A, Garcia-Verdugo J-M, Pénicaud L, and Casteilla L**. Spontaneous cardiomyocyte differentiation from adipose tissue stroma cells. *Circ Res* 94: 223-229, 2004.
178. **Ponikowski P, Voors AA, Anker SD, Bueno H, Cleland JG, Coats AJ, Falk V, Gonzalez-Juanatey JR, Harjola VP, Jankowska EA, Jessup M, Linde C, Nihoyannopoulos P, Parissis JT, Pieske B, Riley JP, Rosano GM, Ruilope LM, Ruschitzka F, Rutten FH, and van der Meer P**. 2016 ESC Guidelines for the diagnosis and treatment of acute and chronic heart failure: The Task Force for the diagnosis and treatment of acute and chronic heart failure of the European Society of Cardiology (ESC). Developed with the special contribution of the Heart Failure Association (HFA) of the ESC. *Eur J Heart Fail* 2016.
179. **Poulin MF, Deka A, Mohamedali B, and Schaer GL**. Clinical Benefits of Stem Cells for Chronic Symptomatic Systolic Heart Failure A Systematic Review of the Existing Data and Ongoing Trials. *Cell Transplant* 2016.
180. **Raczka E, and Quintana A**. Effects of intravenous administration of prostacyclin on regional blood circulation in awake rats. *Br J Pharmacol* 126: 1325-1332, 1999.
181. **Radomski MW, Palmer R, and Moncada S**. The anti‐aggregating properties of vascular endothelium: interactions between prostacyclin and nitric oxide. *Br J Pharmacol* 92: 639-646, 1987.
182. **Rajendran P, Rengarajan T, Thangavel J, Nishigaki Y, Sakthisekaran D, Sethi G, and Nishigaki I**. The vascular endothelium and human diseases. *Int J Biol Sci* 9: 1057-1069, 2013.
183. **Reil JC, Hohl M, Reil GH, Granzier HL, Kratz MT, Kazakov A, Fries P, Muller A, Lenski M, Custodis F, Graber S, Frohlig G, Steendijk P, Neuberger HR, and Bohm M**. Heart rate reduction by If-inhibition improves vascular stiffness and left ventricular systolic and diastolic function in a mouse model of heart failure with preserved ejection fraction. *Eur Heart J* 34: 2839-2849, 2013.
184. **Rezkalla SH, and Kloner RA**. No-reflow phenomenon. *Circulation* 105: 656-662, 2002.
185. **Risau W**. Mechanisms of angiogenesis. *Nature* 386: 671-674, 1997.
186. **Roffi M, Patrono C, Collet JP, Mueller C, Valgimigli M, Andreotti F, Bax JJ, Borger MA, Brotons C, Chew DP, Gencer B, Hasenfuss G, Kjeldsen K, Lancellotti P, Landmesser U, Mehilli J, Mukherjee D, Storey RF, Windecker S, Baumgartner H, Gaemperli O, Achenbach S, Agewall S, Badimon L, Baigent C, Bueno H, Bugiardini R, Carerj S, Casselman F, Cuisset T, Erol C, Fitzsimons D, Halle M, Hamm C, Hildick-Smith D, Huber K, Iliodromitis E, James S, Lewis BS, Lip GY, Piepoli MF, Richter D, Rosemann T, Sechtem U, Steg PG, Vrints C, and Luis Zamorano J**. 2015 ESC Guidelines for the management of acute coronary syndromes in patients presenting without persistent ST-segment elevation: Task Force for the Management of Acute Coronary Syndromes in Patients Presenting without Persistent ST-Segment Elevation of the European Society of Cardiology (ESC). *Eur Heart J* 37: 267-315, 2016.
187. **Roger VL**. Epidemiology of heart failure. *Circ Res* 113: 646-659, 2013.
188. **Roger VL, Go AS, Lloyd-Jones DM, Benjamin EJ, Berry JD, Borden WB, Bravata DM, Dai S, Ford ES, and Fox CS**. Heart disease and stroke statistics—2012 update a report from the American heart association. *Circulation* 125: e2-e220, 2012.

189. **Sandow SL, and Hill CE**. Incidence of myoendothelial gap junctions in the proximal and distal mesenteric arteries of the rat is suggestive of a role in endothelium-derived hyperpolarizing factor–mediated responses. *Circ Res* 86: 341-346, 2000.
190. **Sasayama S, and Fujita M**. Recent insights into coronary collateral circulation. *Circulation* 85: 1197-1204, 1992.
191. **Satessa GD, Lenjisa JL, Gebremariam ET, and Woldu MA**. Stem Cell Therapy for Myocardial Infarction: Challenges and Prospects. *J Stem Cell Res Ther* 2015: 2015.
192. **Sato A, Sakuma I, and Gutterman DD**. Mechanism of dilation to reactive oxygen species in human coronary arterioles. *Am J Physiol Heart Circ Physiol* 285: H2345-2354, 2003.
193. **Schachinger V, Tonn T, Dimmeler S, and Zeiher AM**. Bone-marrow-derived progenitor cell therapy in need of proof of concept: design of the REPAIR-AMI trial. *Nat Clin Pract Cardiovasc Med* 3: S23-S28, 2006.
194. **Schaper W, and Ito WD**. Molecular mechanisms of coronary collateral vessel growth. *Circ Res* 79: 911-919, 1996.
195. **Schenke Layland K, Rhodes KE, Angelis E, Butylkova Y, Heydarkhan Hagvall S, Gekas C, Zhang R, Goldhaber JI, Mikkola HK, and Plath K**. Reprogrammed mouse fibroblasts differentiate into cells of the cardiovascular and hematopoietic lineages. *Stem Cells* 26: 1537-1546, 2008.
196. **Scherschel JA, Soonpaa MH, Srour EF, Field LJ, and Rubart M**. Adult bone marrow°Vderived cells do not acquire functional attributes of cardiomyocytes when transplanted into peri-infarct myocardium. *Mol Ther* 16: 1129-1137, 2008.
197. **Schwenke DO, Pearson JT, Umetani K, Kangawa K, and Shirai M**. Imaging of the pulmonary circulation in the closed-chest rat using synchrotron radiation microangiography. *Journal of Applied Physiology* 102: 787-793, 2007.
198. **Semenza GL, Agani F, Iyer N, Kotch L, Laughner E, Leung S, and Yu A**. Regulation of cardiovascular development and physiology by hypoxia inducible factor 1a. *Ann N Y Acad Sci* 874: 262-268, 1999.
199. **Shafiq M, Lee SH, Jung Y, and Kim SH**. Strategies for recruitment of stem cells to treat myocardial infarction. *Curr Pharm Des* 21: 1584-1597, 2015.
200. **Sharma NR, and Davis MJ**. Mechanism of substance P-induced hyperpolarization of porcine coronary artery endothelial cells. *Am J Physiol Heart Circ Physiol* 266: H156-H164, 1994.
201. **Shimokawa H, Yasutake H, Fujii K, Owada MK, Nakaike R, Fukumoto Y, Takayanagi T, Nagao T, Egashira K, Fujishima M, and Takeshita A**. The importance of the hyperpolarizing mechanism increases as the vessel size decreases in endothelium-dependent relaxations in rat mesenteric circulation. *J Cardiovasc Pharmacol* 28: 703-711, 1996.
202. **Shirai M, Schwenke DO, Eppel GA, Evans RG, Edgley AJ, Tsuchimochi H, Umetani K, and Pearson JT**. Synchrotron based angiography for investigation of the regulation of vasomotor function in the microcirculation in vivo. *Clin Exp Pharmacol Physiol* 36: 107-116, 2009.
203. **Shirai M, Schwenke DO, Tsuchimochi H, Umetani K, Yagi N, and Pearson JT**. Synchrotron radiation imaging for advancing our understanding of cardiovascular function. *Circ Res* 112: 209-221, 2013.
204. **Siminiak T, Kalawski R, Fiszer D, Jerzykowska O, Rzezniczak J, Rozwadowska N, and Kurpisz M**. Autologous skeletal myoblast transplantation for the treatment of postinfarction myocardial injury: phase I clinical study with 12 months of follow-up. *Am Heart J* 148: 531-537, 2004.
205. **Singhal AK, Symons JD, Boudina S, Jaishy B, and Shiu YT**. Role of Endothelial Cells in Myocardial Ischemia-Reperfusion Injury. *Vasc Dis Prev* 7: 1-14, 2010.

206. **Solomon SD, Zelenkofske S, McMurray JJ, Finn PV, Velazquez E, Ertl G, Harsanyi A, Rouleau JL, Maggioni A, and Kober L**. Sudden death in patients with myocardial infarction and left ventricular dysfunction, heart failure, or both. *N Engl J Med* 352: 2581-2588, 2005.
207. **Statistics ABo**. Australian Health Survey: first results, 2011-12. *ABS cat no 4364055001* 2013a.
208. **Stitham J, Midgett C, Martin KA, and Hwa J**. Prostacyclin: an inflammatory paradox. *Front Pharmacol* 2: 24, 2011.
209. **Sugamura K, and Keaney JF, Jr.** Reactive oxygen species in cardiovascular disease. *Free Radic Biol Med* 51: 978-992, 2011.
210. **Surma M, Wei L, and Shi J**. Rho kinase as a therapeutic target in cardiovascular disease. *Future Cardiol* 7: 657-671, 2011.
211. **Sutton MGSJ, and Sharpe N**. Left ventricular remodeling after myocardial infarction pathophysiology and therapy. *Circulation* 101: 2981-2988, 2000.
212. **Swedberg K, Komajda M, Bohm M, Borer JS, Ford I, Dubost-Brama A, Lerebours G, Tavazzi L, and Investigators S**. Ivabradine and outcomes in chronic heart failure (SHIFT): a randomised placebo-controlled study. *Lancet* 376: 875-885, 2010.
213. **Tabibiazar R, and Rockson S**. Angiogenesis and the ischaemic heart. *Eur Heart J* 22: 903-918, 2001.
214. **Taddei S, Ghiadoni L, Virdis A, Versari D, and Salvetti A**. Mechanisms of endothelial dysfunction: clinical significance and preventive non-pharmacological therapeutic strategies. *Curr Pharm Des* 9: 2385-2402, 2003.
215. **Takahashi K, and Yamanaka S**. Induction of pluripotent stem cells from mouse embryonic and adult fibroblast cultures by defined factors. *Cell* 126: 663-676, 2006.
216. **Tang XL, Rokosh G, Sanganalmath SK, Yuan F, Sato H, Mu J, Dai S, Li C, Chen N, Peng Y, Dawn B, Hunt G, Leri A, Kajstura J, Tiwari S, Shirk G, Anversa P, and Bolli R**. Intracoronary administration of cardiac progenitor cells alleviates left ventricular dysfunction in rats with a 30-day-old infarction. *Circulation* 121: 293-305, 2010.
217. **Taylor DA, Atkins BZ, Hungspreugs P, Jones TR, Reedy MC, Hutcheson KA, Glower DD, and Kraus WE**. Regenerating functional myocardium: improved performance after skeletal myoblast transplantation. *Nat Med* 4: 929-933, 1998.
218. **Trounson A, and DeWitt ND**. Pluripotent stem cells progressing to the clinic. *Nat Rev Mol Cell Biol* 17: 194-200, 2016.
219. **Tschope C, Bock CT, Kasner M, Noutsias M, Westermann D, Schwimmbeck PL, Pauschinger M, Poller WC, Kuhl U, Kandolf R, and Schultheiss HP**. High prevalence of cardiac parvovirus B19 infection in patients with isolated left ventricular diastolic dysfunction. *Circulation* 111: 879-886, 2005.
220. **Umetani K, Fukushima K, Tsurusaki M, Uotani K, Yamasaki K, and Sugimura K**. Synchrotron radiation coronary microangiography in isolated perfused rat heart for evaluation of coronary vascular response. In: *Proc IEEE Int Symp Biomed Imaging* 2002, p. 561-564.
221. **Umetani K, Fukushima K, Tsurusaki M, Uotani K, Yamasaki K, and Sugimura K**. Synchrotron radiation coronary microangiography in isolated perfused rat heart for evaluation of coronary vascular response. In: *Biomedical Imaging, 2002. Proceedings. 2002 IEEE International Symposium on*IEEE, 2002, p. 561-564.
222. **Vamos M, Erath JW, and Hohnloser SH**. Digoxin-associated mortality: a systematic review and meta-analysis of the literature. *Eur Heart J* 36: 1831-1838, 2015.
223. **van der Velden J, van der Wall EE, and Paulus WJ**. Heart failure with preserved ejection fraction: current status and challenges for the future. *Neth Heart J* 24: 225-226, 2016.

224. **van Heerebeek L, Hamdani N, Falcao-Pires I, Leite-Moreira AF, Begieneman MP, Bronzwaer JG, van der Velden J, Stienen GJ, Laarman GJ, Somsen A, Verheugt FW, Niessen HW, and Paulus WJ**. Low myocardial protein kinase G activity in heart failure with preserved ejection fraction. *Circulation* 126: 830-839, 2012.
225. **van Riet EE, Hoes AW, Wagenaar KP, Limburg A, Landman MA, and Rutten FH**. Epidemiology of heart failure: the prevalence of heart failure and ventricular dysfunction in older adults over time. A systematic review. *Eur J Heart Fail* 18: 242-252, 2016.
226. **Vanhoutte PM**. Vascular biology: old-timer makes a comeback. *Nature* 396: 213-216, 1998.
227. **Vasan RS, Sullivan LM, Roubenoff R, Dinarello CA, Harris T, Benjamin EJ, Sawyer DB, Levy D, Wilson PW, and D'Agostino RB**. Inflammatory markers and risk of heart failure in elderly subjects without prior myocardial infarction the Framingham Heart Study. *Circulation* 107: 1486-1491, 2003.
228. **Veltman CE, Soliman OII, Geleijnse ML, Vletter WB, Smits PC, Ten Cate FJ, Jordaens LJ, Balk AHHM, Serruys PW, and Boersma E**. Four-year follow-up of treatment with intramyocardial skeletal myoblasts injection in patients with ischaemic cardiomyopathy. *Eur Heart J* 29: 1386-1396, 2008.
229. **Vita JA, Treasure CB, Nabel EG, McLenachan JM, Fish RD, Yeung AC, Vekshtein VI, Selwyn AP, and Ganz P**. Coronary vasomotor response to acetylcholine relates to risk factors for coronary artery disease. *Circulation* 81: 491-497, 1990.
230. **von Lueder TG, Wang BH, Kompa AR, Huang L, Webb R, Jordaan P, Atar D, and Krum H**. Angiotensin receptor neprilysin inhibitor LCZ696 attenuates cardiac remodeling and dysfunction after myocardial infarction by reducing cardiac fibrosis and hypertrophy. *Circ Heart Fail* 8: 71-78, 2015.
231. **Vriens J, Owsianik G, Fisslthaler B, Suzuki M, Janssens A, Voets T, Morisseau C, Hammock BD, Fleming I, Busse R, and Nilius B**. Modulation of the Ca2 permeable cation channel TRPV4 by cytochrome P450 epoxygenases in vascular endothelium. *Circ Res* 97: 908-915, 2005.
232. **Wang H, Shi J, Wang Y, Yin Y, Wang L, Liu J, Liu Z, Duan C, Zhu P, and Wang C**. Promotion of cardiac differentiation of brown adipose derived stem cells by chitosan hydrogel for repair after myocardial infarction. *Biomaterials* 35: 3986-3998, 2014.
233. **Wang H, Xi Y, Zheng Y, Wang X, and Cooney AJ**. Generation of electrophysiologically functional cardiomyocytes from mouse induced pluripotent stem cells. *Stem Cell Res* 16: 522-530, 2016.
234. **Wang L, Deng J, Tian W, Xiang B, Yang T, Li G, Wang J, Gruwel M, Kashour T, Rendell J, Glogowski M, Tomanek B, Freed D, Deslauriers R, Arora RC, and Tian G**. Adipose-derived stem cells are an effective cell candidate for treatment of heart failure: an MR imaging study of rat hearts. *Am J Physiol Heart Circ Physiol* 297: H1020-1031, 2009.
235. **Watanabe H, Vriens J, Prenen J, Droogmans G, Voets T, and Nilius B**. Anandamide and arachidonic acid use epoxyeicosatrienoic acids to activate TRPV4 channels. *Nature* 424: 434-438, 2003.
236. **Webb RC**. Smooth muscle contraction and relaxation. *Adv Physiol Ed* 27: 201-206, 2003.
237. **White FC, Carroll SM, Magnet A, and Bloor CM**. Coronary collateral development in swine after coronary artery occlusion. *Circ Res* 71: 1490-1500, 1992.
238. **Whittaker P, Boughner DR, and Kloner RA**. Role of collagen in acute myocardial infarct expansion. *Circulation* 84: 2123-2134, 1991.
239. **Wirth A**. Rho kinase and hypertension. *Biochim Biophys Acta* 1802: 1276-1284, 2010.

240. **Wollert KC, and Drexler H**. Clinical applications of stem cells for the heart. *Circ Res* 96: 151-163, 2005.
241. **Woodman OL, and Dusting GJ**. N-nitro L-arginine causes coronary vasoconstriction and inhibits endothelium-dependent vasodilatation in anaesthetized greyhounds. *Br J Pharmacol* 103: 1407-1410, 1991.
242. **Yada T, Shimokawa H, Hiramatsu O, Kajita T, Shigeto F, Goto M, Ogasawara Y, and Kajiya F**. Hydrogen peroxide, an endogenous endothelium-derived hyperpolarizing factor, plays an important role in coronary autoregulation in vivo. *Circulation* 107: 1040-1045, 2003.
243. **Yamashita T, Kawashima S, Ozaki M, Namiki M, Shinohara M, Inoue N, Hirata K-i, Umetani K, and Yokoyama M**. In vivo angiographic detection of vascular lesions in apolipoprotein E-knockout mice using a synchrotron radiation microangiography system. *Circ J* 66: 1057, 2002.
244. **Yancy CW, Jessup M, Bozkurt B, Butler J, Casey DE, Jr., Colvin MM, Drazner MH, Filippatos G, Fonarow GC, Givertz MM, Hollenberg SM, Lindenfeld J, Masoudi FA, McBride PE, Peterson PN, Stevenson LW, and Westlake C**. 2016 ACC/AHA/HFSA Focused Update on New Pharmacological Therapy for Heart Failure: An Update of the 2013 ACCF/AHA Guideline for the Management of Heart Failure: A Report of the American College of Cardiology/American Heart Association Task Force on Clinical Practice Guidelines and the Heart Failure Society of America. *Circulation* 2016.
245. **Yang L, Soonpaa MH, Adler ED, Roepke TK, Kattman SJ, Kennedy M, Henckaerts E, Bonham K, Abbott GW, and Linden RM**. Human cardiovascular progenitor cells develop from a KDR+ embryonic-stem-cell-derived population. *Nature* 453: 524-528, 2008.
246. **Yao L, Romero MJ, Toque HA, Yang G, Caldwell RB, and Caldwell RW**. The role of RhoA/Rho kinase pathway in endothelial dysfunction. *J Cardiovasc Dis Res* 1: 165-170, 2010.
247. **Zacharias M, Joffe S, Konadu E, Meyer T, Kiernan M, Lessard D, and Goldberg RJ**. Clinical epidemiology of heart failure with preserved ejection fraction (HFpEF) in comparatively young hospitalized patients. *Int J Cardiol* 202: 918-921, 2016.
248. **Zannad F, McMurray JJ, Krum H, van Veldhuisen DJ, Swedberg K, Shi H, Vincent J, Pocock SJ, and Pitt B**. Eplerenone in patients with systolic heart failure and mild symptoms. *N Engl J Med* 364: 11-21, 2011.
249. **Zhang Y, Wang D, Chen M, Yang B, Zhang F, and Cao K**. Intramyocardial transplantation of undifferentiated rat induced pluripotent stem cells causes tumorigenesis in the heart. *PLoS One* 6: e19012, 2011.
250. **Ziaeian B, and Fonarow GC**. Epidemiology and aetiology of heart failure. *Nat Rev Cardiol* 13: 368-378, 2016.
251. **Zuk PA, Zhu M, Mizuno H, Huang J, Futrell JW, Katz AJ, Benhaim P, Lorenz HP, and Hedrick MH**. Multilineage cells from human adipose tissue: implications for cell-based therapies. *Tissue Eng* 7: 211-228, 2001.

CHAPTER 2

General Methods

Chapter 2 General Methods

2.1 Synchrotron Radiation and the Microangiography

All coronary microangiography for the studies described in this thesis was conducted at the 28B2 beam line, SPring-8, Japanese Synchrotron Radiation Research Institute, Hyogo, Japan. All procedures involving animals received prior approval of the SPring-8 Animal Experiment Review Committee and the National Cerebral and Cardiovascular Center Animal Experiment Committee in accordance with the guidelines of the Physiological Society of Japan.

Synchrotron radiation microangiography was used for visualizing the coronary circulation and has been described in detail previously (6, 7). Imaging of the coronary circulation was performed with monochromatic synchrotron radiation at 33.2 keV, just above the iodine K-edge energy for producing maximal absorption contrast of the iodine contrast agent in the vascular lumen. A single-crystal monochromator selects a single energy of a very narrow energy bandwidth (20-30 eV) and produces high flux X-rays (~10^{10} photons/mm^2/s). The monochromic X-ray beam from the synchrotron source is highly collimated due to the small size of the X-ray source and the very long source to object distance, which ensures that distortion of the image is avoided. The monochromatic X-rays transmitted through the specimen under study (i.e. the experimental animal) were detected by the X-ray detector (Hitachi Denshi Techno-System, Ltd., Tokyo, Japan), which included a SATICON X-ray pick-up tube (Hamamatsu Photonics, Shizuoka, Japan). X-rays absorbed in the photoconductive layer of the tube are directly converted into electron-hole pairs. Charge carriers generated by X-rays are transported across the photoconductive layer by an electric field that forms a charge density pattern on the photoconductive layer surface. Scanning beams of low-velocity electrons read out the electrostatic image on the surface to generate a video signal (7). The SATICON X-ray camera has a resolution of 1050 scanning lines and has the potential to record images at a maximum rate of 30 frames per second with 1.5-2 ms/frame shutter open time. The detector features a 10 μm equivalent pixel size that captures sequence images with the field of view of 10 x 10 mm. High resolution images with 1024 x 1024 pixel format and a 10-bit resolution were stored and used for coronary vessel count and arterial caliber measurement.

2.1.1 Surgical Protocols for Microangiography of Rats

Rats were anesthetized with pentobarbital sodium (50 mg/kg i.p). Supplementary doses of anesthetic (~20 mg/kg/h) were periodically administered to maintain the level of anesthesia. After induction of anesthesia, the rats were intubated by tracheotomy for artificial ventilation with a rodent ventilator (tidal volume = 1 ml/100 g body weight, 70 strokes/min, ~40% oxygen, Shinano, Tokyo, Japan). A rectal thermistor coupled with a thermostatically controlled heating pad was used to maintain body temperature at ~37 °C (Fig 2.1).

A 20 gauge Angiocath catheter (Becton Dickinson, Inc., Sandy, Utah, USA) was used to cannulate the right carotid artery near the aortic valve for selective angiography of the coronary circulation. Arterial pressure and heart rate were recorded from a catheter filled with heparinized saline (12 units/ml) inserted into the femoral artery, and connected to a pressure transducer (MLT0699, AD Instruments, NSW, Australia). The analogue arterial pressure signal was digitized at 1000 Hz and recorded by CHART software (v5.4.1, AD Instruments, NSW, Australia) to determine mean arterial pressure and heart rate. Body fluid was maintained during the period of imaging by sodium lactate (Otsuka, Tokyo, Japan) infused via a catheter inserted into the jugular vein (3 ml/h). Drug infusions were also delivered via the jugular venous catheter.

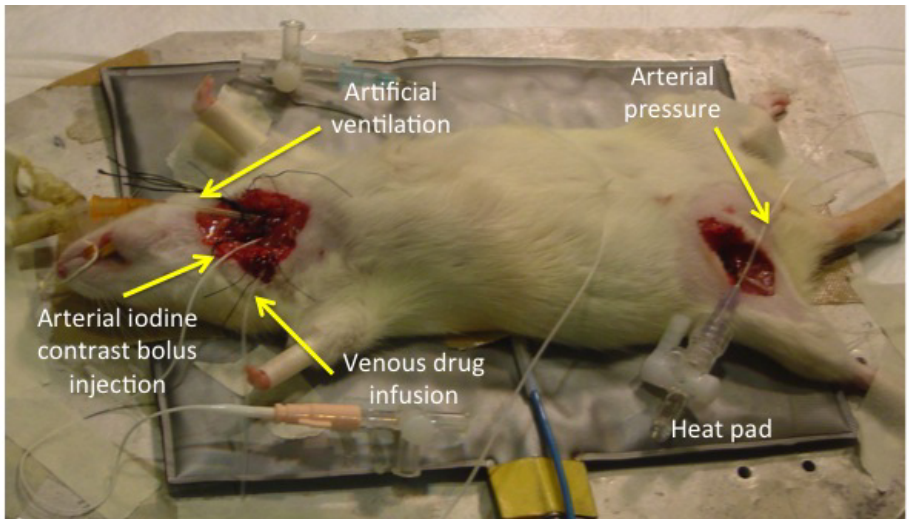

Figure 2.1 Surgical preparations for coronary microangiography of rats. Iodine contrast was injected through the carotid artery, drugs were infused into the jugular vein, and heart rate and blood pressure were measured from the femoral artery. The heating pad was placed under the rat's body to maintain body temperature.

2.1.2 Surgical Protocols for Microangiography of Mice

Each mouse was anesthetized with sodium pentobarbital (1:10 dilution with sodium lactate, 50 mg/kg) intraperitoneally, and supplementary doses of anesthetic (~20 mg/kg/h) were periodically administered to maintain the level of anesthesia. After induction of anesthesia, the mice were intubated for artificial ventilation (~40% oxygen) with a MiniVent rodent ventilator (Hugo-Sachs, Germany). A rectal thermistor coupled with a thermostatically controlled heating pad was used to maintain body temperature at approximately 37 °C.

A Funnel polyurethane catheter (1.2 to 3Fr, Instech-Solomon, Plymouth Meeting, PA, United States) was used to cannulate the right carotid artery. The tip of the catheter was positioned close to left descending coronary artery, near the aortic valve, to facilitate selective injection of contrast media into the coronary circulation. Arterial pressure and heart rate were also recorded from the modified Instech-Solomon catheter inserted into the carotid artery. The analogue arterial pressure signal was digitized at 1000 Hz and recorded by CHART software (Version 5.4.1, AD Instruments, NSW, Australia) to allow determination of mean arterial pressure and heart rate. Body fluids were maintained during the period of imaging by infusion of sodium lactate (Otsuka, Tokyo, Japan) via a catheter inserted into the jugular vein.

2.1.3 General Angiography Protocols for Rats

After the preparatory surgery, each animal was moved into the X-ray hutch at BL28B2 for coronary microangiography. The rat was placed in a supine position in front of the X-ray detector in the path of the X-ray beam. Iodinized contrast medium (Iomeron 350, Bracco-Eisai Co. Ltd., Tokyo, Japan) was delivered through the carotid artery using a high-speed injector (0.3-0.5 ml bolus ~25 ml/s, Nemoto Kyorindo, Tokyo, Japan). The ventilator was turned off for a period of approximately 3 seconds immediately before the start of each cine recording of 100 frames at 30 frames/s. A SATICON detector (Hitachi Denshi Techno-System, Ltd., Tokyo, Japan) with 1.5-2 ms/frame shutter open time was used. Images with 1024 x 1024 pixel format and 10-bit resolution were recorded from a ~10 mm^2 field of view (Fig. 2.2). Approximately 10 min was allowed between each imaging sequence for renal clearance of the contrast.

Contrast images were recorded from the upper LV during all experiments. In each rat, vessel calibers were determined after 5 minutes of vehicle infusion (sodium lactate 3 ml/h), and then during infusion of acetylcholine (ACh; Ovisot, Daiichi Sankyo, Japan, 5 μg/kg/min), sodium nitroprusside (SNP; Sigma-Aldrich, Japan, 5 μg/kg/min) and dobutamine (Dob; Eli Lilly Japan, Kobe, Japan 4-8 μg/kg/min, a cardiac specific β-adrenergic agonist).

Currently available preclinical imaging techniques do not permit imaging of the microcirculation of dynamic organs under conscious conditions. Within the limitations of the controlled substances regulations of the Japanese synchrotron facilities we have utilized pentobarbitone anesthesia in our studies (2, 5, 8), which is known to depress myocardial contractility (3). I report here only the responses of rats after a similar period of stable anesthesia that has been shown to slightly reduce coronary and pulmonary vascular resistances in anesthetized dogs relative to conscious conditions (3, 4). Therefore basal coronary flow in our anesthetized rats is likely to be slightly enhanced compared to conscious rats.

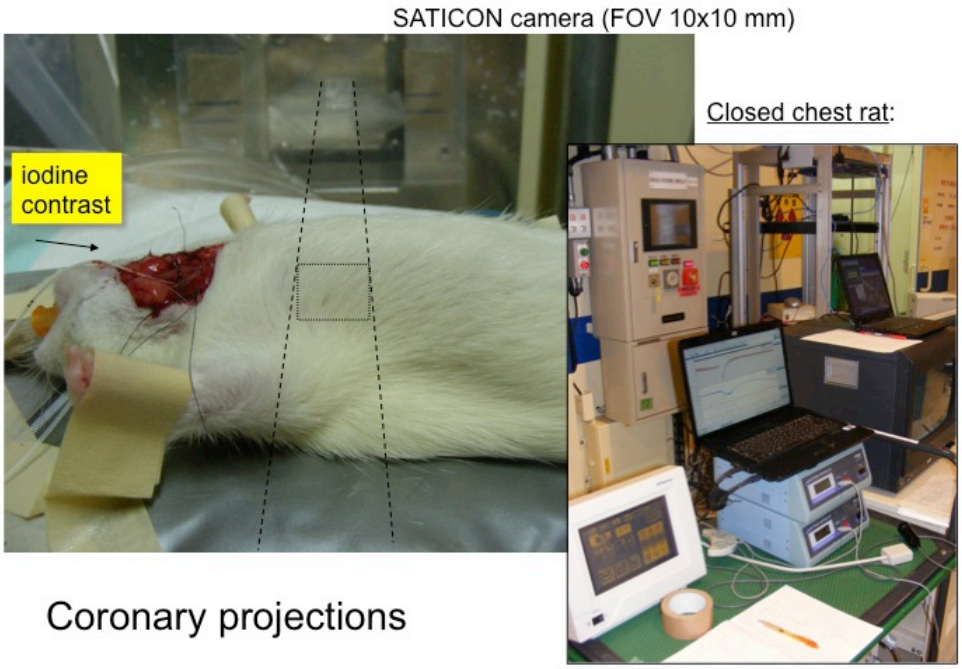

Figure 2.2 Microangiography setup for rats at the BL28B2 beamline. The left part of the diagram shows the path of the horizontal X-ray (33.2 KeV, black dashed lines) radiation and the field of view (10mm x 10mm, black square) used for coronary imaging of supine anesthetized rats within the radiation hutch. The right part of the diagram demonstrates the systems used for recording of data and injection of contrast agent remotely from the radiation hutch.

2.1.4 General Angiography Protocols for Mice

A similar protocol, to that applied for coronary microangiography in rats, was applied in mice. Briefly, the iodinized contrast medium (Iomeron 350, Bracco-Eisai Co. Ltd., Tokyo, Japan) was delivered through the carotid artery using a PHD200 syringe pump (0.1-0.2 ml bolus 11 ml/min, Harvard Apparatus, Holliston, Massachusetts, United States). Microangiograms for baseline were recorded after 5 minutes of vehicle infusion (sodium lactate 0.2 ml/h). There was no vasoactive agent used in the study described in this thesis.

2.2 Assessment of Vessel Caliber and Vessel Number

After recording the image sequence, the freeware software Image-J (ver. 1.41, NIH Bethesda, USA) was used to measure the internal diameter of vessels and to count the visible vessel number. The frame with the clearest image of vessels appearing at the baseline and each drug treatment was selected for vessel identification and classification. The vessels were labeled and classified into different branching orders based on a system for branching order classification (Fig. 2.3). The visible vessel number for each branching order was simply counted and recorded from the frame. The internal diameter of each vessel was measured by manually drawing a line across the vessel from edge to edge, perpendicular to the direction of the vessel using Image-J (Fig. 2.4). The processes for measuring internal diameter of each vessel were repeated over 15 consecutive frames in the baseline and other drug treatments.

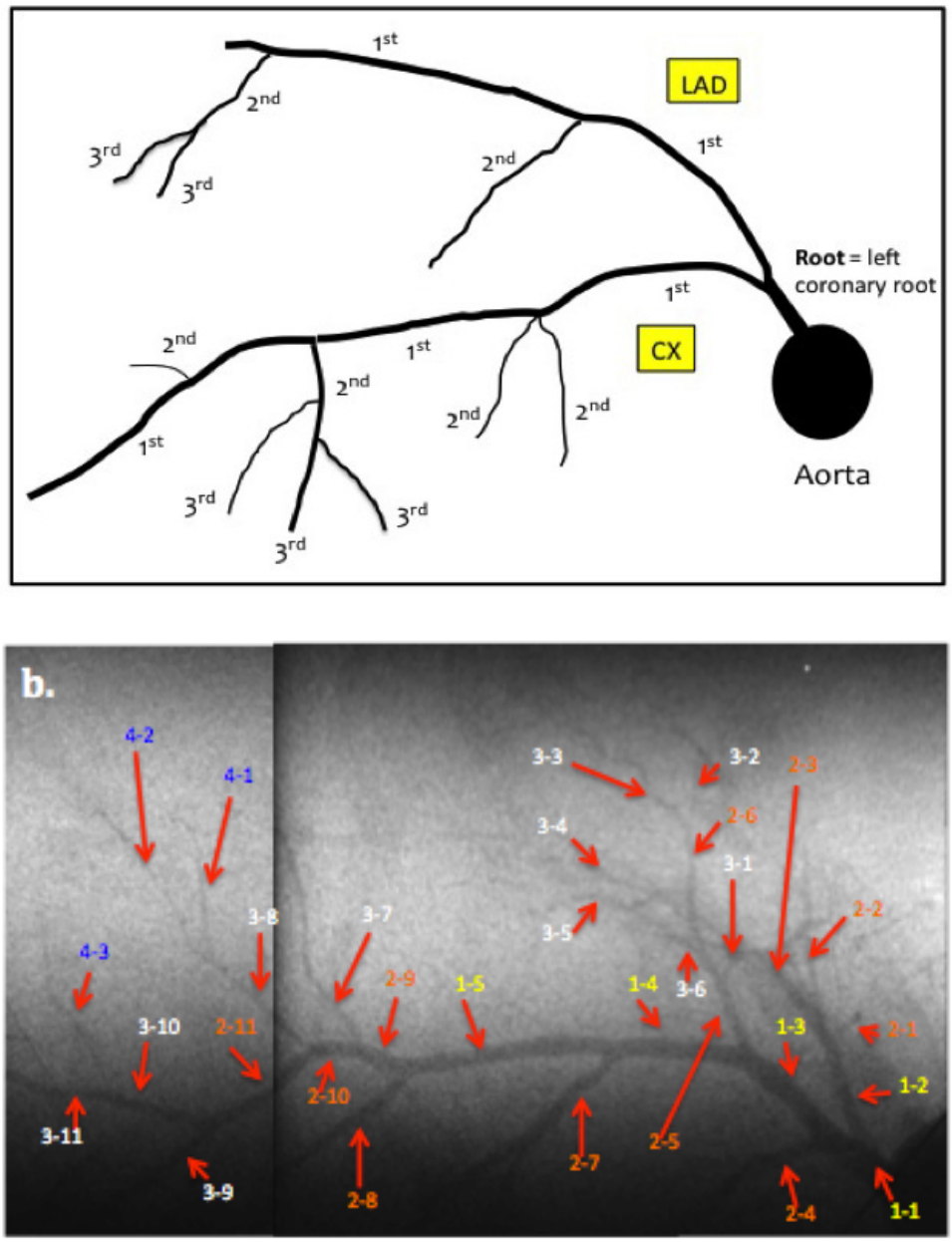

Figure 2.3 Example of nomenclature for angiography a.) Angiogram branching order classification system. Our angiograms generally show a large internal diameter step down from the 1st order segment to 2nd order segments that form the main arteries of the left anterior descending artery (LAD) and left circumflex artery (LCX). Therefore, 2nd order main segments were considered equal daughter branches from the main root segment. **b.)** An image of the coronary circulation of a rat at baseline. Each segment is labelled with a number indicating the branching order, followed by a vessel count number.

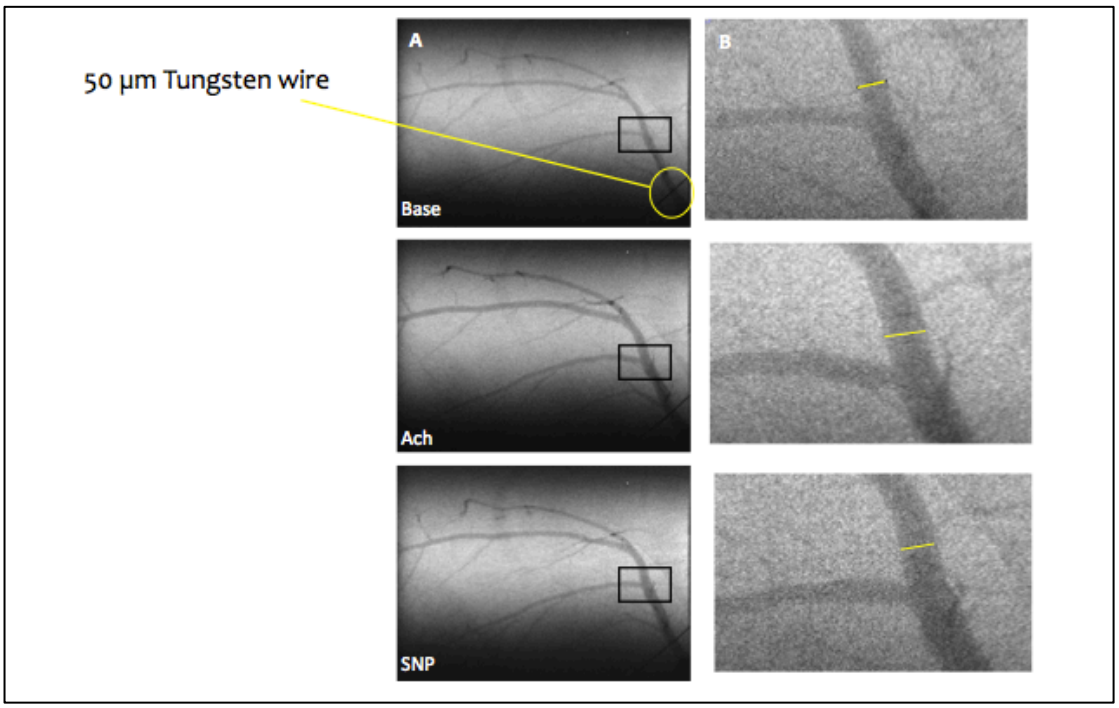

Figure 2.4 Examples of images used with Image-J measurement of the internal diameter of coronary arteries of a rat. Images were captured during intravenous infusion of the vehicle (sodium lactate, 3 ml/h), acetylcholine (ACh, 5 µg/kg/min) and sodium nitroprusside (SNP, 5 µg/kg/min). **A.)** A 50 µm thick tungsten filament was present at the right bottom corner of all the images and was used for calibration. **B.)** The yellow line drawn across the vessel, from edge to edge perpendicular to vessel direction, was used to quantify internal diameter.

2.3 Histology and Immunohistochemistry

The hearts of rats were fixed with paraformaldehyde (Wako Pure Chemical Industries, Ltd., Osaka, Japan), and stored in 70% ethanol (Wako Pure Chemical Industries, Ltd., Osaka, Japan). Paraffin sections (4 µm thick) were then stained with picrosirus red to examine the extent of fibrosis as described previously (2). All non-round vessels were excluded from analysis. Immunohistochemical staining with the endothelial cell marker isolectin B4 (Vector Laboratories, Inc, Burlingame, CA, USA; diluted 1:100) was performed to assess capillary density (2). Capillary density was evaluated by histological examination of the myocardium to detect positively stained endothelial cells from 10 non-overlapping fields randomly selected from within two sections of the sub-epicardial region of the middle of the LV. After using proteinase K (Dako, Golstrup, Denmark) to digest the tissues for 4 min, sections were then incubated with biotinylated isolectin B4 (Vector Laboratories, Inc, Burlingame, CA, USA; diluted 1:100) at room temperature for an hour, followed by streptavidin-HRP (Dako,

Golstrup, Denmark) for 30 min and diaminobenzidine (Dako, Golstrup, Denmark) as described previously (2). An Aperio ScanScope XT Slide Scanner (Aperio Technologies Inc., CA, USA) system was used to capture digital images with a 20x objective. Quantification was performed automatically with Aperio Imagescope (v11.0.2.725, Aperio Technologies) using the Positive Pixel Count v9 algorithm (Aperio Technologies) for perivascular fibrosis and capillary density (1).

2.4 Reference

1. **Campbell DJ, Somaratne JB, Jenkins AJ, Prior DL, Yii M, Kenny JF, Newcomb AE, Kelly DJ, and Black MJ**. Differences in myocardial structure and coronary microvasculature between men and women with coronary artery disease. *Hypertension* 57: 186-192, 2011.
2. **Jenkins MJ, Edgley AJ, Sonobe T, Umetani K, Schwenke DO, Fujii Y, Brown RD, Kelly DJ, Shirai M, and Pearson JT**. Dynamic synchrotron imaging of diabetic rat coronary microcirculation in vivo. *Arterioscler Thromb Vasc Biol* 32: 370-377, 2012.
3. **Manders WT, and Vatner SF**. Effects of sodium pentobarbital anesthesia on left ventricular function and distribution of cardiac output in dogs, with particular reference to the mechanism for tachycardia. *Circ Res* 39: 512-517, 1976.
4. **Nyhan DP, Chen BB, Fehr DM, Goll HM, and Murray PA**. Pentobarbital augments pulmonary vasoconstrictor response to cyclooxygenase inhibition. *Am J Physiol* 257: H1140-1146, 1989.
5. **Schwenke DO, Pearson JT, Umetani K, Kangawa K, and Shirai M**. Imaging of the pulmonary circulation in the closed-chest rat using synchrotron radiation microangiography. *J Appl Physiol* 102: 787-793, 2007.
6. **Shirai M, Schwenke DO, Eppel GA, Evans RG, Edgley AJ, Tsuchimochi H, Umetani K, and Pearson JT**. Synchrotron-based angiography for investigation of the regulation of vasomotor function in the microcirculation in vivo. *Clin Exp Pharmacol Physiol* 36: 107-116, 2009.
7. **Shirai M, Schwenke DO, Tsuchimochi H, Umetani K, Yagi N, and Pearson JT**. Synchrotron radiation imaging for advancing our understanding of cardiovascular function. *Circ Res* 112: 209-221, 2013.
8. **Shirai M, Tsuchimochi H, Nagai H, Gray E, Pearson JT, Sonobe T, Yoshimoto M, Inagaki T, Fujii Y, Umetani K, Kuwahira I, and Schwenke DO**. Pulmonary vascular tone is dependent on the central modulation of sympathetic nerve activity following chronic intermittent hypoxia. *Basic Res Cardiol* 109: 1-10, 2014.

CHAPTER 3

Application Of Combined Stem Cells Therapy After Myocardial Infarction In the Rat

Chapter 3

3.1 Chapter Preface and Author Contribution

This chapter describes a study performed in collaboration with our colleagues from Osaka University, Osaka, Japan, the National Cerebral & Cardiovascular Center, Osaka, Japan and the SPring-8 Synchrotron Radiation Research Institute, Harima, Hyogo, Japan.

Dr. Kainuma from Osaka University performed the surgery on rats to induce MI, and to provide the allocated treatments. Furthermore, he performed the positron emission tomography imaging and gene regulation studies that were included in the final journal publication (attachment). My primary supervisor, Dr. Pearson, performed the preparative surgery on the rats on the day of the terminal imaging experiment and subsequent contrast angiography of the coronary circulation. I was responsible for assisting in the angiography and I was principally responsible for analyzing and interpreting the data, generated by coronary microangiography, in this study.

3.2 Abstract

In this study, I tested the hypothesis that combined therapy, with myoblast sheets and omentum, improves coronary microvascular structure and function after MI, more than either treatment alone. The first aim for the current study was to investigate the number of perfused coronary arterial vessels in the ischemic myocardium two weeks after initiating treatment with either myoblast sheets or omentum or combined treatment. The second aim was to determine whether the existing and newly developed arterial vessels in the ischemic myocardium maintain normal vasomotor function after these treatments. Synchrotron-based contrast angiography was used to allow assessment of endothelial function of pre-existing and newly formed micro- and macro- vessels. The rats treated with omentum plus myoblast sheets had a greater number of 3^{rd} and 4^{th} order vessels (resistance arterial vessels) than did control animals. There was also greater increase in the caliber of 3^{rd} order vessels in the rats treated with both omentum and myoblast sheets than the rats in the control group during both infusion of acetylcholine (28 ± 8% versus 3 ± 3% in the control group, P = 0.03) and sodium nitroprusside (25 ± 8% versus 3 ± 6% in the control group, P = 0.03). Our current findings provide evidence that treatment with combined omentum and myoblast sheets improves the function of the coronary circulation post MI. Notably, we did not observe the same improvement in rats treated with either treatment alone. These findings indicate that combined treatment provides a better outcome for the coronary circulation post MI than do omentum or myoblast sheets alone.

3.3 Introduction

Heart failure following myocardial infarction (MI) is a major cause of death around the world (7). The myocardial cells lost after MI are replaced by non-contractile scar tissue due to the adult human heart's limited capacity for regeneration. Cell-based therapies for myocardial regeneration have been widely studied for treatment of MI (4, 12, 13). Various cell types have been considered as candidates for cardiac regenerative therapy. For example, there is evidence that various cell types such as skeletal myoblast cells (SkM) (19), bone marrow cells (BM) (21, 29), endogenous cardiac stem cells (1, 5), embryonic stem cells (ESCs) (16) and induced pluripotent stem cells (iPSCs) (3, 14) can improve myocardial function and reduces infarct area in animal models of MI. However, in a number of these cases the experimental findings revealed challenges that must be overcome for development of effective cardiac regenerative therapy. Firstly, targeted cell delivery should be achievable with little risk of extraneous diffusion; the phenomenon where transplanted cells do not stay within the transplantation site (6, 8, 9). Secondly, the therapy must enhance the survival of the transplanted cells. Therefore, the optimal approach must deliver sufficient cell numbers to the adjacent myocardium within the infarct region.

To date, various techniques for cell delivery (e.g. cell infusion, cell injection and cell sheets) have been tested in animals to determine whether myocardial function and or microvessel density can be improved (20, 22, 31). Among all of these techniques, stem cell sheet transplantation has been reported to provide better outcome of engraftment and survival of delivered cells than using other techniques (17, 26). However, the therapeutic efficacy of transplanted sheets, for animals with severe HF, is limited (20, 22, 31). The limited therapeutic effect is possibly due to insufficient capillary maturation in addition to limited retention of donor cells (2). Therefore, in the current study, our team (Dr. Kainuma) designed a new tissue delivery technique by combining large sheets of myoblast cells with omentum (a fat rich fold of the peritoneum attached to the stomach and transverse colon), which provides a rich source of endogenous angiogenic factors (24). Such sheets can be transplanted to the heart following experimentally induced MI in rodents. In the current study, myoblast cells were chosen as a stem cell source since they are relatively easy to collect, and have been reported to improve cardiac function, by attenuating cardiac remodeling, in a porcine model of myocardial ischemia (23). However, it is not known

whether the new vessels, and microvessels in particular, function normally in the transplanted regions. Therefore, in this study, I tested the hypothesis that combined therapy with myoblast sheets and omentum, improves coronary microvascular structure and function after MI, more than either treatment alone. The first aim for the current study was to investigate the number of perfused coronary arterial vessels in the ischemic myocardium 2 weeks after providing the treatments (with either myoblast sheets or omentum or combined treatment). The second aim was to determine whether the existing and newly developed arterial vessels in the ischemic myocardium maintain normal vasomotor function after these treatments. Synchrotron-based contrast microangiography was used to allow the assessment of endothelial function of pre-existing and newly formed micro- and macro- vessels.

3.4 Methods

The experiment was conducted on 4 groups of 8-week old male Lewis rats (Seac Yoshitomi Ltd, Fukuoka, Japan) at the SPring-8 Synchrotron Radiation Research Institute in Hyogo, Japan. All procedures were approved in advance by the SPring-8 Animal Experiment Review Committee and the National Cerebral and Cardiovascular Center Animal Experiment Committee.

Experimental treatment groups:

1. Rats without treatment post MI, (Control, n = 11)
2. Rats treated with myoblast cells sheets + omentum post MI (O+M, n = 11)
3. Rats treated with myoblast cells sheets post MI (Myoblast, n = 6)
4. Rats treated with omentum post MI (Omentum, n = 5)

3.4.1 Pre-experimental Model Preparation

Surgical preparation of the rats used in this study was conducted by our colleague from Osaka University (Dr Kainuma), using methods described previously (11). Briefly, a medial sternotomy was performed on rats (LEW/SsN rats, 8 weeks of age) under anesthesia after oral intubation for artificial ventilation (11). Animals were pretreated with lignocaine (1 mg/kg) to prevent the development of lethal arrhythmias. Then the left coronary artery was permanently ligated with 6-0 silk sutures. After

confirming normal heart rhythm the chest was closed, and the rats were allowed to recover over 2 weeks.

At the same time, several grams of skeletal muscle were harvested from the gastrocnemius of separate 3-week old male Lewis rats. Muscle cells were then cultured as previously described (23). Briefly, the muscle cells were incubated at 37°C in a shaker bath with 0.5% w/v type 1 collagenase (Gibco, Grand Island, NY) in Dulbecco's modified Eagle solution (Gibco, Grand Island, NY) for around 4 days. The cells were collected by centrifugation, and the skeletal cells were seeded into 150 mm dishes (Iwaki, Tokyo, Japan) for 3 days after removal of fibroblasts. The cells were dissociated from the flasks with trypsin-ethylenedinetetraacetic acid (Dojindo laboratories, Kumamoto, Japan) and re-incubated on the 35 mm temperature-responsive polymer poly *N*-isopropylacrylamide (PIPAAm) dishes (Cellseed, Tokyo, Japan) at 37°C with the cell numbers around 3×10^6 per dish when the cells became approximately 70% confluent after 7 days.

The dishes were then incubated at 20°C for approximately 30 minutes. The myoblast sheets detached spontaneously from the surface due to the low temperature. Immediately after detachment, the cell sheet with media was gently aspirated into the tip of a 10 ml pipet and transferred onto appropriate culture surfaces. Media was dropped onto the center of the sheet to spread folded parts of the transferred sheet. After sheet spreading, media was then aspirated to adhere the cell sheet to the culture surface. Within 30 minutes, the transferred sheet reattached and new media was then added for further culture. To layer cell sheets, another myoblast sheet was detached from a PIPAAm-grafted dish and transferred into the first dish in the same way. The second sheet was positioned above the first sheet and placed onto the original sheet by slow aspiration of media. Then the same process was performed again until the three-layered sheet was produced.

In the group with combined treatment with omentum and myoblast sheets, the myoblast cell sheets were transplanted onto the LV wall surface together with omentum 2 weeks after MI. Omentum was not cut or harvested, but separated from the spleen of the same animal and stretched up to the thorax and through an incision in the diaphragm under anesthesia. The same surgery was performed, but with stem cell sheet or omentum only, in the remaining two groups. Rats were then allowed to

recover for about 2 weeks before being transported to SPring-8 for terminal experimentation.

3.4.2 Surgical Preparation for Angiography

All coronary microangiography was conducted at Beamline 28B2 of SPring-8, the Synchrotron Radiation Research Institute in Hyogo, Japan. Microangiography was performed with synchrotron radiation to visualize the coronary circulation *in vivo* and has been described in detail previously (10). Imaging of the coronary circulation was performed with monochromatic synchrotron radiation at 33.2 KeV, just above the iodine K-edge energy for producing maximal absorption of the iodine contrast agent in the vascular lumen.

Rats were anesthetized with pentobarbital sodium (50 mg/kg i.p.). Supplementary doses of anesthetic (~20 mg/kg/h) were periodically administered to maintain the level of anesthesia. After induction of anesthesia, the rats were intubated by tracheotomy for artificial ventilation with a rodent ventilator (tidal volume = 1 ml/100 g body weight, 70 strokes/min, ~40% oxygen, Shinano, Tokyo, Japan). A rectal thermistor coupled with a thermostatically controlled heating pad was used to maintain body temperature at ~37 °C.

A 20 gauge Angiocath catheter (Becton Dickinson, Inc., Sandy, Utah, USA) was used to cannulate the right carotid artery near the aortic valve for selective angiography of the coronary circulation. Arterial pressure and heart rate were recorded from a catheter filled with heparinized saline (12 units/ml) inserted into the femoral artery, and connected to a pressure transducer (MLT0699, AD Instruments, NSW, Australia). The analogue arterial pressure signal was digitized at 1000 Hz and recorded by CHART software (v5.4.1, AD Instruments, NSW, Australia) to determine mean arterial pressure and heart rate. Body fluid was maintained during the period of imaging by sodium lactate (Otsuka, Tokyo, Japan) infused via a catheter inserted into the jugular vein (3 ml/h). Drug infusions were also delivered via the jugular venous catheter.

3.4.3 Angiography Protocols

After the preparatory surgery, each animal was moved into the X-ray hutch at BL28B2 for coronary microangiography. The rat was placed in a supine position in front of the X-ray detector in the path of the X-ray beam. Iodinized contrast medium (Iomeron 350, Bracco-Eisai Co. Ltd., Tokyo, Japan) was delivered through the carotid artery using a high-speed injector (0.3-0.5 ml bolus 25 ml/s, Nemoto Kyorindo, Tokyo, Japan). The ventilator was turned off for a period of approximately 3 seconds immediately before the start of each cine recording of 100 frames at 30 frames/s, recorded on a SATICON detector (Hitachi Denshi Techno-System, Ltd., Tokyo, Japan) with 1.5-2 ms/frame shutter open time. Images with 1024 x 1024 pixel format and 10-bit resolution were recorded from a ~10 mm^2 field of view. Approximately 10 min was allowed between each imaging sequence for renal clearance of the contrast.

Contrast images were recorded from the upper LV during all experiments. In each rat, vessel calibers were determined after 5 minutes of infusion of vehicle (sodium lactate 3 ml/h), acetylcholine (ACh; Ovisot, Daiichi Sankyo, Japan, 5 μg/kg/min), sodium nitroprusside (SNP; Sigma-Aldrich, Japan, 5 μg/kg/min) and dobutamine (Dob; Eli Lilly Japan, Kobe, Japan 4-8 μg/kg/min, a cardiac specific β-adrenergic agonist).

3.4.4 Statistical Analysis

Data are expressed as mean ± SEM unless otherwise stated and n represents the number of rats in each group. For each individual rat, within-rat mean vessel ID and vessel number for each branching order were calculated and the between-rat means were then used for group comparisons. Student's paired t-test was used to assess differences between the baseline period and the period of drug infusion (ACh, SNP or Dob). One-way ANOVA was used to assess differences between groups during the baseline period (GraphPad Software, Inc., La Jolia, CA, USA). Two-way ANOVA following with Dunnett's multiple comparisons was also used, with factors treatment and branching order. Two-sided $P \leq 0.05$ was considered statistically significant.

3.5 Results

3.5.1 General Characteristics and Hemodynamics

Body weight (g) was measured on the day of experiment prior to synchrotron angiography. There was no significant between-group difference in body weight (Control: 189 ± 3.7 g, O+M: 181 ± 5.9 g, Myoblast: 184 ± 5.3 g and Omentum: 182 ± 3.9 g, *P* = 0.63). There were also no significant differences in either heart rate (HR) or mean arterial pressure (MAP) between the treatment groups at baseline (Fig. 3.1)

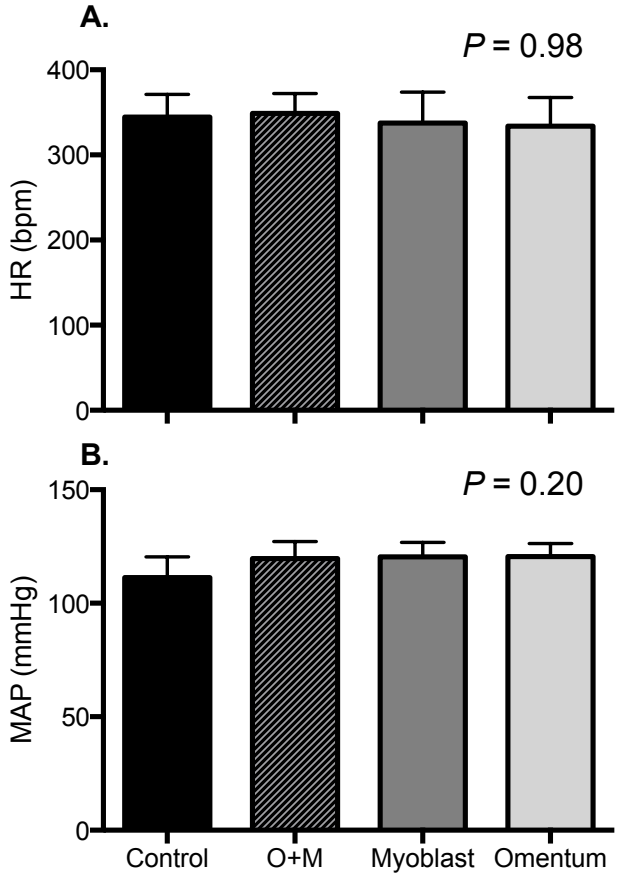

Figure 3.1 (A) **Heart rate and (B) mean arterial pressure at baseline.** The four groups were: rats subjected to myocardial infarction (MI) but no other treatment (Control, n =11), MI plus treatment with omentum plus myoblast cell sheets post MI (O+M, n = 11), treatment with myoblast cell sheets only post MI (Myoblast, n = 5), and treatment with omentum only post MI (Omentum, n = 6). Data are shown as mean ± SEM. *P* values are the outcomes of one-way ANOVA. MAP = mean arterial pressure; HR = heart rate.

In control animals ACh reduced MAP (by 36 ± 8 mmHg) and HR (by 48 ± 27 bpm), SNP also induced reductions in MAP (by 38 ± 8 mmHg) and HR (by 59 ± 27 bpm), and Dob increased HR (by 35 ± 16 bpm) but had little effect on MAP. In rats with monotherapy or combined therapy, the effects of ACh, SNP and Dob on MAP and HR were similar to those observed in control rats (see Fig. 3.2).

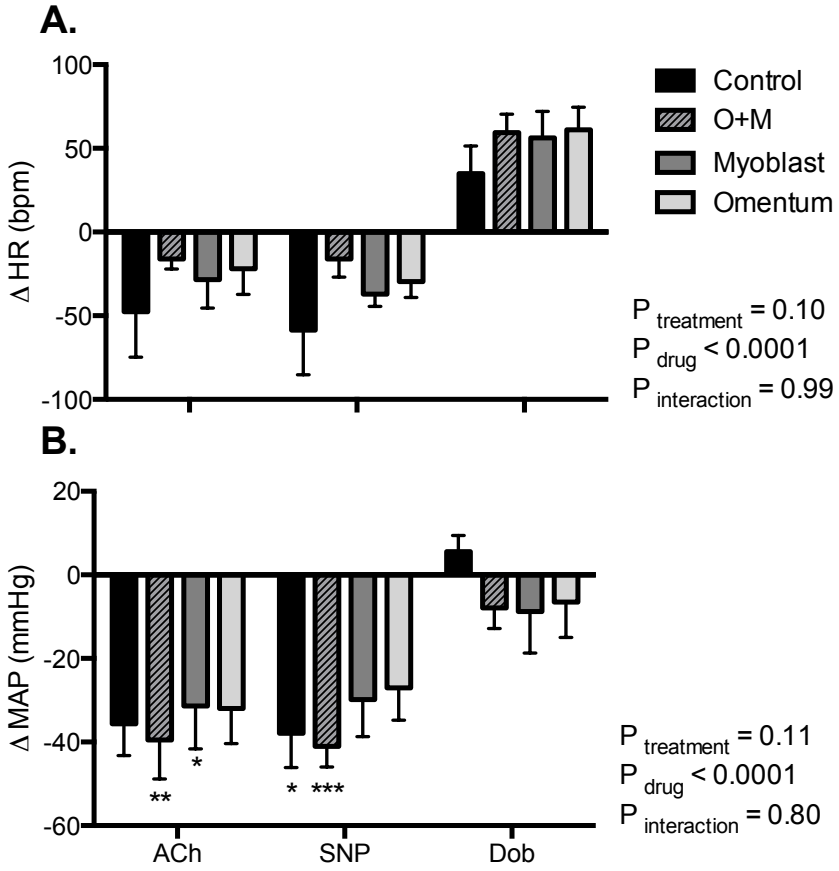

Figure 3.2 Relative changes of heart rate and mean arterial pressure in response to vasoactive agents in the various treatment groups. The four groups were: rats subjected to myocardial infarction (MI) but no other treatment (Control, n =11), MI plus treatment with omentum plus myoblast cell sheets post MI (O+M, n = 11), treatment with myoblast cell sheets only post MI (Myoblast, n = 5), and treatment with omentum only post MI (Omentum, n = 6). Data are shown as mean ± SEM. P values are the outcomes of two-way analysis of variance. * denotes $P < 0.05$, ** $P < 0.01$, *** $P < 0.001$ vs baseline (Student's paired t-test). Acetylcholine = ACh; sodium nitroprusside = SNP, dobutamine = Dob; MAP = mean arterial pressure; HR = heart rate.

3.5.2 Revascularisation

3.5.2.1 Number and Caliber of Vessels Visible in the Ischemic Myocardium During the Baseline Period

Representative angiograms of the coronary circulation showed differences between the groups at baseline and during drug administration (Fig. 3.3). The number of visualized vessels progressively increased across order 1-3, but fewer 4th order vessels were observed than 3rd order vessels (Fig. 3.4). The rats treated with O+M had a greater number of 3rd and 4th order vessels (resistance arterial vessels) than did control animals. As expected vessel ID at baseline progressively decreased with branching order (P < 0.001) across the four groups. Notably, the rats treated with O+M had larger 1st order arteries than did control rats (Fig. 3.4).

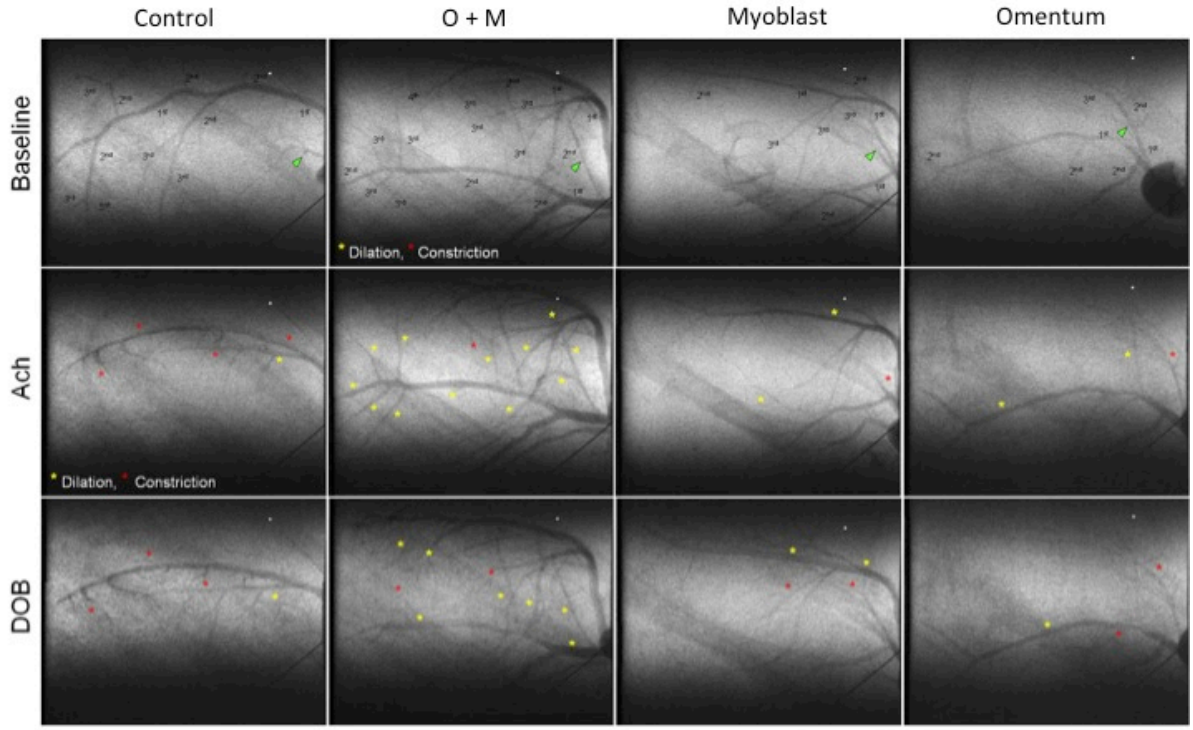

Figure 3.3 Representative synchrotron radiation angiograms of the coronary vasculature. Images were captured during infusion of the vehicle, acetylcholine (ACh), and dobutamine (Dob). Rats were subjected to myocardial infarction (MI) but no other treatment (Control), MI plus treatment with omentum plus myoblast cell sheets post MI (O+M), treatment with myoblast cell sheets only post MI (Myoblast), or treatment with omentum only post MI (Omentum). Vertically aligned images are from the same rat. Yellow and red asterisks indicate vessels showing dilation and constriction, respectively, in response to ACh and Dob.

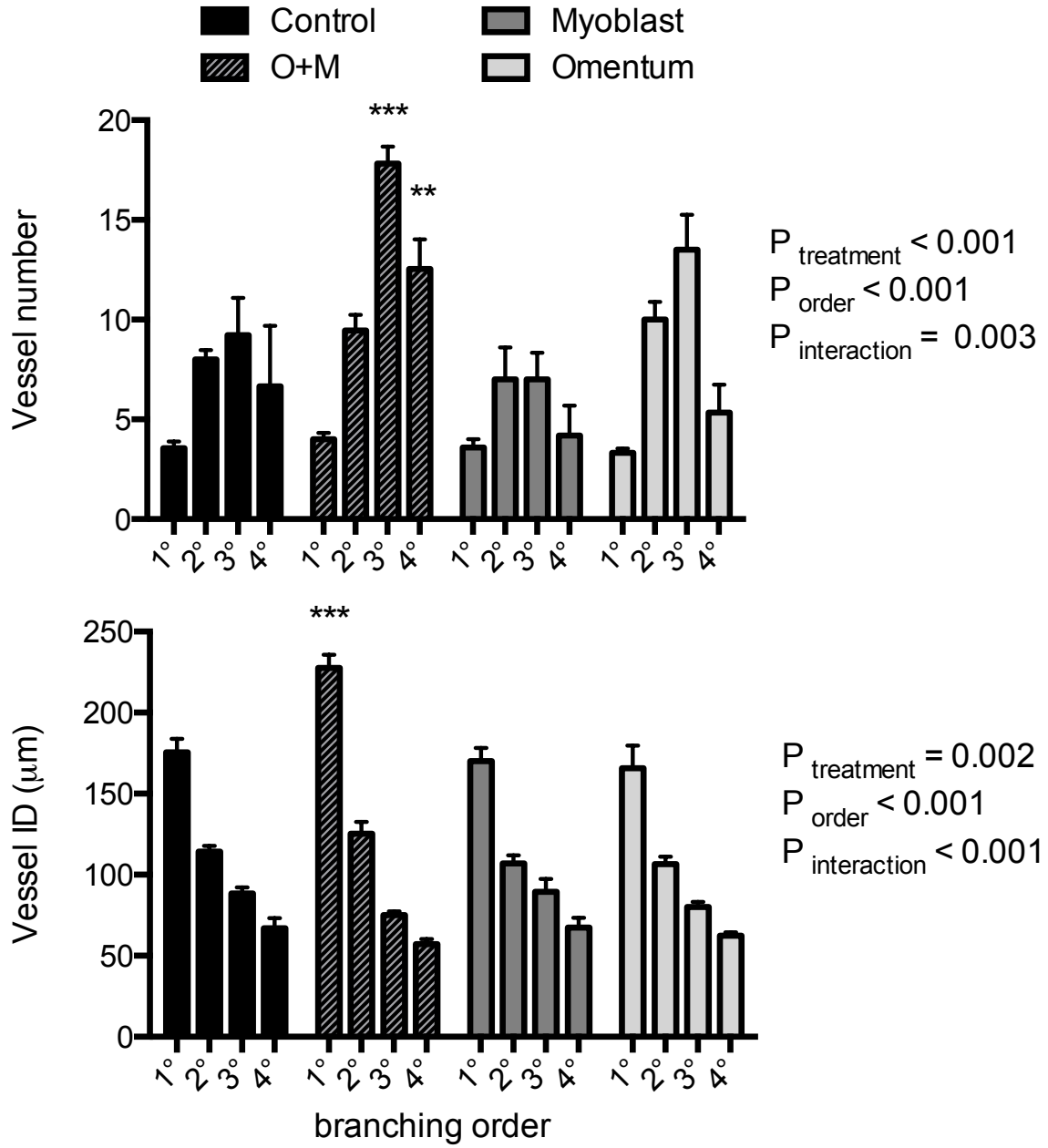

Figure 3.4 The number of visible vessels and internal diameter (ID) in the field of view categorized by branching order in all the treatment groups. The four groups were: rats subjected to myocardial infarction (MI) but no other treatment (Control, n =11), MI plus treatment with omentum plus myoblast cell sheets post MI (O+M, n = 11), treatment with myoblast cell sheets only post MI (Myoblast, n = 5), and treatment with omentum only post MI (Omentum, n = 6). Data are shown as mean ± SEM. *P* values are the outcomes of two-way ANOVA. ** denotes $P < 0.01$, *** $P < 0.001$ vs corresponding vessels in control animals (Dunnett's multiple comparisons).

3.5.2.2 *Number and Caliber of Newly Formed Vessels in the Infarct and Peri-infarct Regions*

Newly formed arterioles and small arteries were identified in our images based on possession of any of the following characteristics: i) apparent sprouting of vessels from the occlusion point (see Fig 3.5), ii) lengthening of vessels and extension towards the infarct zone, iii) formation of vessels originating from a projecting vessel extension, and iv) change in flow direction from normal coronary flow patterns (from the aorta towards the apex and from the surface towards the LV lumen) (Fig 3.6). In many cases, the lengthening of circumflex and right coronary artery branches towards the anterior wall area subtended by the left coronary artery can be seen. One example presented is the circumflex branch seen to be extending from the middle of each frame of Fig 3.6, towards the top of the frame, before abruptly changing direction towards the apex (left of frame). New vessels with flow in a direction counter to the pre-existing circumflex, from which they originate, are indicated by the red arrows within the yellow circle (Fig 3.6).

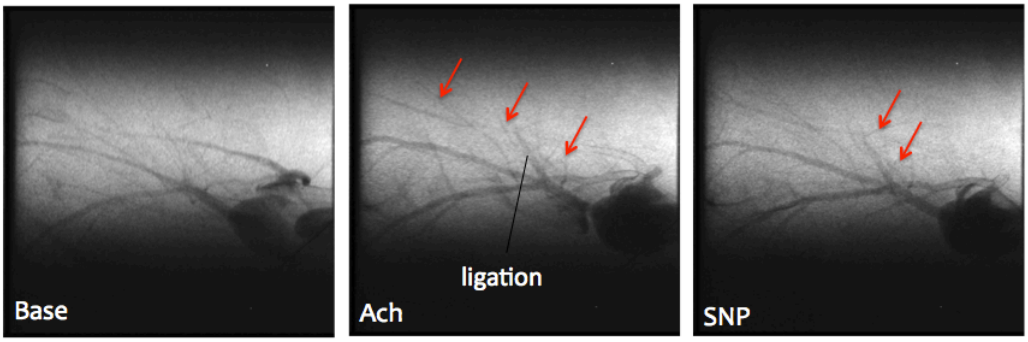

Figure 3.5 Images of newly developed coronary vessels. The red arrows in the images indicate the newly developed vessels that sprout from the segments of existing vessels around the occlusion point. Images were captured during infusion of the vehicle (Base), acetylcholine (ACh), and sodium nitroprusside (SNP).

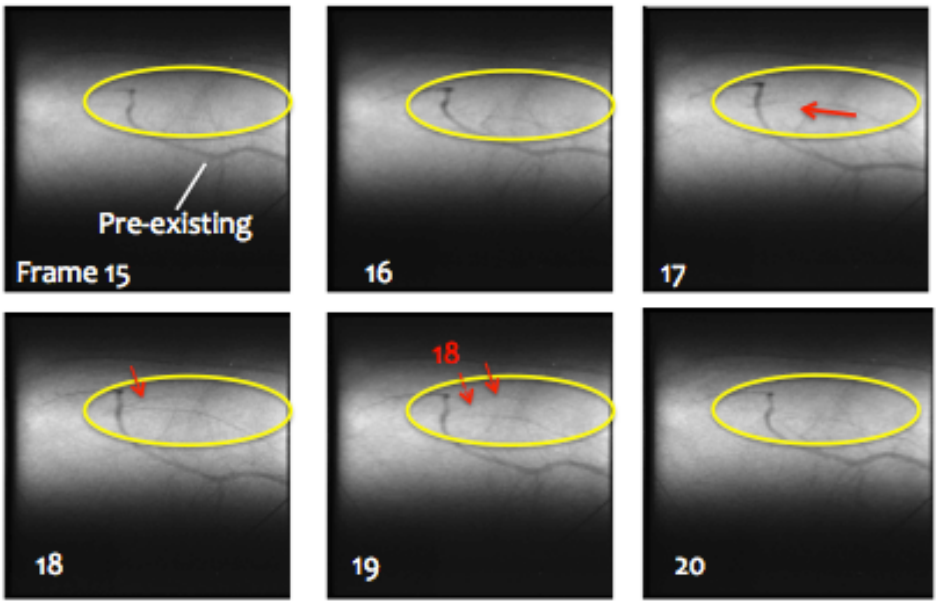

Figure 3.6 Image sequence of contrast flow in newly developed vessels towards the aorta during baseline. A large pre-existing artery is evident as a vessel in the middle of each frame from 15 to 20. In frame 18 and 19, it is clear that flow is from left to right in the segment indicated by red arrows. This blood vessel was defined as a newly developed vessel.

To take into account individual variability in the number of vessels visualized we examined the proportion of newly developed vessels observed under baseline conditions by dividing the total number of newly developed vessels by the total number of visible vessels. There was only a small number of newly developed vessels visible in the fourth branching order, and they were only found in a minority of the rats we studied. Therefore we only examined the proportion of newly developed vessels in the second and third branching orders. The proportion of newly developed vessels was similar across the four treatment-groups. There was a significantly greater proportion of newly developed vessels in the 3rd branching order (24.5 ± 7.8%) than the 2nd branching order; a pattern seen consistently in all treatment groups (Fig 3.7).

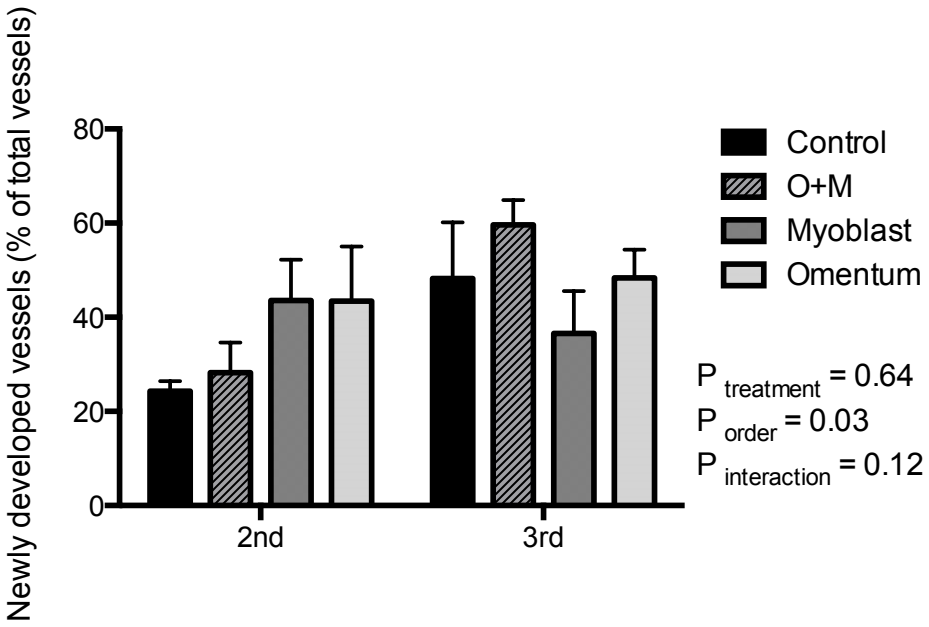

Figure 3.7 The prevalence of newly developed vessels in second and third branching orders. The four groups were: rats subjected to myocardial infarction (MI) but no other treatment (Control, n =11), MI plus treatment with omentum plus myoblast cell sheets post MI (O+M, n = 11), treatment with myoblast cell sheets only post MI (Myoblast, n = 5), and treatment with omentum only post MI (Omentum, n = 6). Data are shown as mean ± SEM. *P* values are the outcomes of two-way analysis of variance.

3.5.3 Assessment of Endothelial Function

3.5.3.1 Changes in Number of Perfused Vessel During Drug Stimulation

We examined relative change in vessel number in response to administration of ACh, SNP and the β_1-adrenergic agonist (Dob). Infusion of ACh, SNP and Dob did not significantly alter the number of visible 1st, 2nd, 3rd, or 4th order coronary vessels in angiograms in any of the groups (Fig. 3.8).

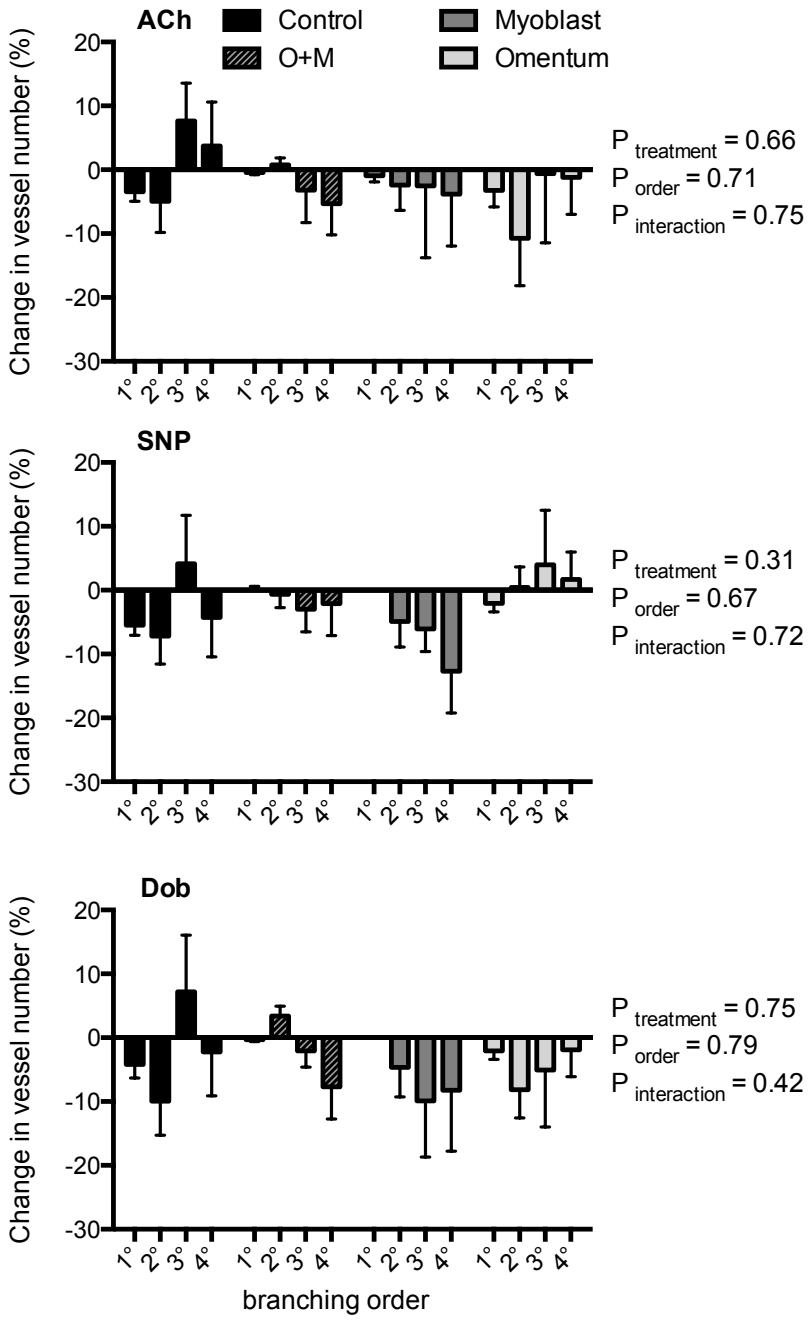

Figure 3.8 Relative changes of vessel number in response to vasoactive agents in the various treatment groups. The four groups were: rats subjected to myocardial infarction (MI) but no other treatment (Control, n =11), MI plus treatment with omentum plus myoblast cell sheets post MI (O+M, n = 11), treatment with myoblast cell sheets only post MI (Myoblast, n = 5), and treatment with omentum only post MI (Omentum, n = 6). Data are shown as mean ± SEM. P values are the outcomes of two-way analysis of variance. Acetylcholine = ACh; sodium nitroprusside = SNP, dobutamine = Dob.

3.5.3.2 Changes in Vessel Caliber During Drug Stimulation

ACh increased the calibers of coronary vessels in all four groups. The calibers were increased to a similar degree across the four groups in 1st (17 ± 4%) and 2nd (19 ± 5%) order vessels. In contrast to the 1st and 2nd order vessels, ACh mediated vasodilation in the 3rd and 4th order vessels was significantly different among the groups (Fig. 3.9). There was greater increase in the caliber of 3rd (mean difference vs control = 24 ± 9%, *P* = 0.03) order vessels in the rats treated with both omentum and myoblast sheets than the rats in the control group (3 ± 3%) during infusion of ACh. A similar pattern was observed in the caliber of 4th order vessels (mean difference vs control = 15 ± 11%, *P* = 0.37). Similarly, in response to infusion of SNP, the caliber of 3rd order vessels increase more in rats treated with O+M (25 ± 8%, *P* = 0.03 vs control) than the control group (3 ± 6%). During infusion of Dob, there was a trend of greater increase in the caliber of 3rd (31 ± 7%, *P* = 0.06 vs control) in the rats treated with O+M than in the control group (11 ± 6%), and rats treated with O+M also had a greater increase in the caliber of 4th (34 ± 7%, *P* = 0.05 vs control) order vessels than did the control group (9 ± 3%, see Fig. 3.9).

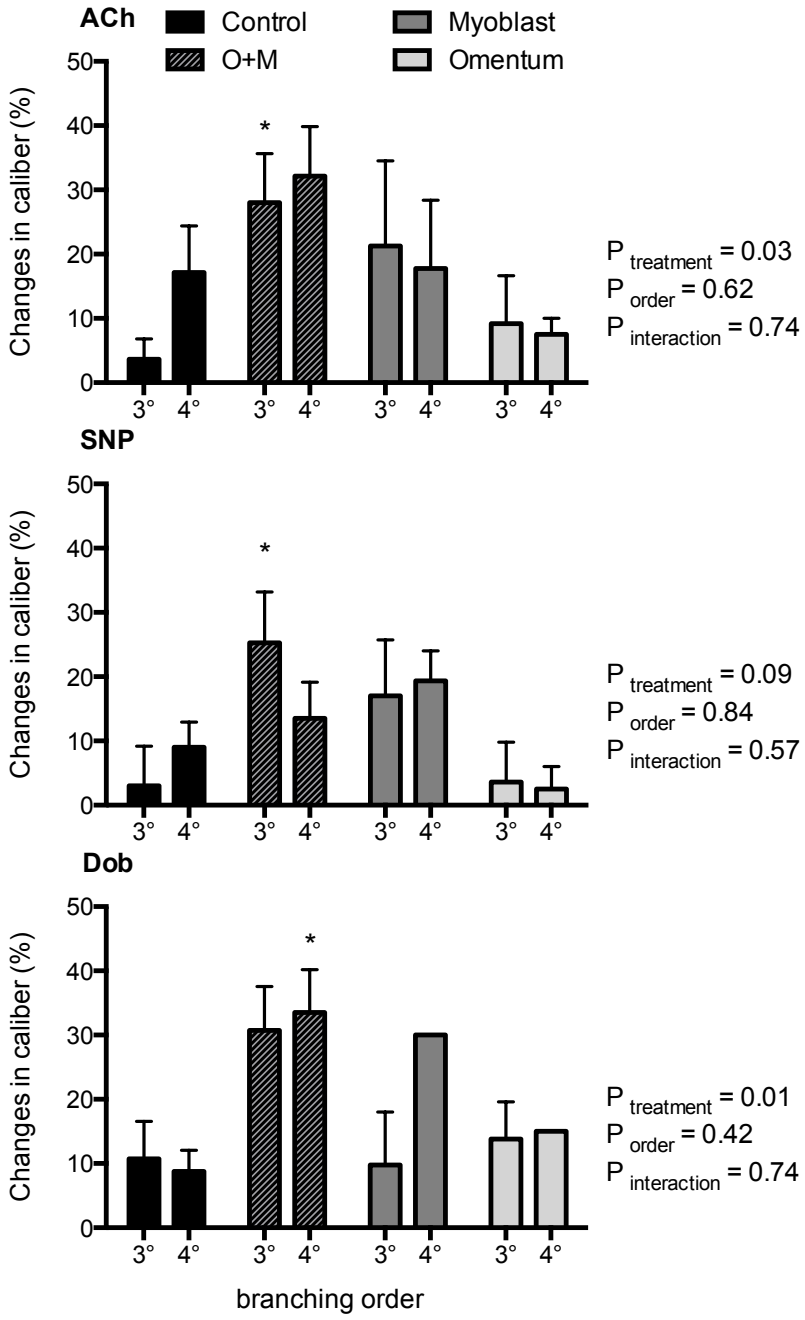

Figure 3.9 Relative changes of vessel caliber in response to vasoactive agents in the various treatment groups. The four groups were: rats subjected to myocardial infarction (MI) but no other treatment (Control, n =11), MI plus treatment with omentum plus myoblast cell sheets post MI (O+M, n = 11), treatment with myoblast cell sheets only post MI (Myoblast, n = 5), and treatment with omentum only post MI (Omentum, n = 6). Data are shown as mean ± SEM. P values are the outcomes of two-way analysis of variance. * denotes $P < 0.05$ vs control (Dunnett's multiple comparisons). Acetylcholine = ACh; sodium nitroprusside = SNP, dobutamine = Dob.

3.6 Discussion

In our current study, we found that combined treatment with omentum and myoblast cell sheets post MI increased revascularization of the ischemic myocardium with arterial microvessels. Resistance vessels in the myocardium in rats given the combined treatment also had better dilatory responses to endothelium-dependent agents than did control rats. In addition, the assessment of cardiac function parameters such as LV ejection fraction and LV dimension collected by our colleagues shows that the group that received combined treatment had sustained improvements in cardiac function parameters and better functional capacity than the other groups (11). These beneficial effects were not observed when the omentum and myoblast cell sheet therapies were administered individually. Thus, myoblast cell sheets together with omentum has potential as a therapy for treating MI.

Our data provide evidence that combined treatment with omentum and myoblast sheets in rats post MI can improve endothelial vasodilator function of coronary microvessels. There is strong evidence for severe vasodilator dysfunction after MI, involving not only resistance vessels in the infarcted myocardium, but also those in normal myocardium perfused by coronary vessels that were not exposed to ischemia (30). When this vasomotor dysfunction is present and vessels degenerate after acute MI, this loss of vessels increases the extent of the ischemic region and necrosis in the areas not directly injured by infarction (30). In the current study, the group with combined treatment (with omentum and myoblast sheets) effectively improved endothelial function in the resistance vessels as they showed pronounced dilatory responses to the endothelium-dependent vasodilator ACh. Our current findings also show that there were more visible resistance vessels in the rats treated with both omentum and myoblast sheets than others during baseline. Moreover, the visible perfused vessels were similar in the monotherapy treatment groups with only myoblast sheets or omentum, and did not increase the number of perfused vessels compared to the control group during baseline imaging. Our findings closely corresponded to the PET/CT results provided by our colleagues (11). They showed that rats treated with combined treatment had a substantial improvement in coronary flow reserve, which indicated the ability of the myocardium to increase blood flow in response to increasing myocardial oxygen demand was maintained (11). These observations provide evidence that treatment with both omentum and myoblast sheet

provides beneficial effects on the coronary dilatory response in rats with MI, but that either treatment as a monotherapy is less beneficial. Thus, treatment with omentum and myoblast sheets together provided beneficial effects on coronary flow in ischemic myocardium additively.

The proportion of visible newly developed vessels determined by dynamic imaging in the animals treated with omentum and myoblast sheets together in our study was not significantly greater than that in the control group. However, the immunohistochemistry results from our colleague, obtained from the same animals, did provide evidence for a greater number of mature vessels in the group with combined treatment of omentum and myoblast sheets (11). They also found new vessels in the control group and the groups with monotherapy (either myoblast sheets or omentum), but these vessels were highly immature (11). In our study, there were only very few fourth order newly developed vessels visualized in any treatment group. The likely reason for this might be that the fourth order vessels present within the ischemic region are very small (< 30 μm) and below the detection limit for our approach (27). Furthermore, the high resistance of these small vessels would be expected to restrict entry of the contrast agent. Therefore, in the rats we studied, there might have many small newly developed vessels, which we were not able to detect with the current protocol. Additionally, previous estimates of vessel density, generated using histological methods, indicate that the hearts of rats with MI that had been treated with implanted hepatic tissue combined with omentum wrapping show greater coronary vascular density than rats treated with only omentum or with no treatment after MI (25). Further, data from another recently reported study documented greater coronary vascular density, in a porcine model of MI treated with myoblast sheets and omentum wrapping, than in corresponding animals that did not receive this treatment after MI (28). All published studies that have employed histological methods to assess vascular density provide evidence consistent with the notion that omentum increases angiogenesis. Taken collectively with our current observations, it appears that providing myoblast sheets together with omentum increases the number of mature vessels in the ischemic myocardium.

An important limitation of the study is that the outcome was only evaluated at one time point; two weeks after commencing the treatments in this study. Ideally multiple time points should be evaluated longitudinally, with the same cohorts of animals, to

establish whether there is more arteriolar/small artery development beyond 2 weeks post MI. This would also allow us to determine the time window during which the benefits of combination therapy are maximal and the size of the benefit that can be obtained with this regenerative approach. We also should consider studies in older animals to evaluate the effect of these treatments on recovery from MI, since the potential for angiogenesis is blunted with age (15, 18).

To conclude, our current findings provide evidence that treatment with combined omentum and myoblast sheets improved coronary circulation post MI. Notably, we did not observe the same improvement in rats treated with either treatment alone. These indicate that combined treatment provides better outcomes for the coronary circulation post MI than do the individual treatments. It will be important, in the future, to evaluate these therapeutic effects at multiple time points to establish the true scope of the beneficial effects.

3.7 Reference

1. **Barile L, Messina E, Giacomello A, and Marban E**. Endogenous cardiac stem cells. *Prog Cardiovasc Dis* 50: 31-48, 2007.
2. **Cao Y, Hong A, Schulten H, and Post MJ**. Update on therapeutic neovascularization. *Cardiovasc Res* 65: 639-648, 2005.
3. **Caspi O, Huber I, Kehat I, Habib M, Arbel G, Gepstein A, Yankelson L, Aronson D, Beyar R, and Gepstein L**. Transplantation of human embryonic stem cell-derived cardiomyocytes improves myocardial performance in infarcted rat hearts. *J Am Coll Cardiol* 50: 1884-1893, 2007.
4. **Dimmeler S, Burchfield J, and Zeiher AM**. Cell-based therapy of myocardial infarction. *Arterioscler Thromb Vasc Biol* 28: 208-216, 2008.
5. **Fuentes T, and Kearns-Jonker M**. Endogenous cardiac stem cells for the treatment of heart failure. *Stem Cells Cloning* 6: 1-12, 2013.
6. **George J, Goldberg J, Joseph M, Abdulhameed N, Crist J, Das H, and Pompili VJ**. Transvenous intramyocardial cellular delivery increases retention in comparison to intracoronary delivery in a porcine model of acute myocardial infarction. *J Interv Cardiol* 21: 424-431, 2008.
7. **Gerber Y, Weston SA, Enriquez-Sarano M, Berardi C, Chamberlain AM, Manemann SM, Jiang R, Dunlay SM, and Roger VL**. Mortality Associated With Heart Failure After Myocardial Infarction: A Contemporary Community Perspective. *Circ Heart Fail* 9: e002460, 2016.
8. **Hale SL, Dai W, Dow JS, and Kloner RA**. Mesenchymal stem cell administration at coronary artery reperfusion in the rat by two delivery routes: a quantitative assessment. *Life Sci* 83: 511-515, 2008.
9. **Hayashi M, Li TS, Ito H, Mikamo A, and Hamano K**. Comparison of intramyocardial and intravenous routes of delivering bone marrow cells for the treatment of ischemic heart disease: an experimental study. *Cell Transplant* 13: 639-647, 2004.
10. **Jenkins MJ, Edgley AJ, Sonobe T, Umetani K, Schwenke DO, Fujii Y, Brown RD, Kelly DJ, Shirai M, and Pearson JT**. Dynamic synchrotron imaging of diabetic rat coronary microcirculation in vivo. *Arterioscler Thromb Vasc Biol* 32: 370-377, 2012.
11. **Kainuma S, Miyagawa S, Fukushima S, Pearson J, Chen YC, Saito A, Harada A, Shiozaki M, Iseoka H, Watabe T, Watabe H, Horitsugi G, Ishibashi M, Ikeda H, Tsuchimochi H, Sonobe T, Fujii Y, Naito H, Umetani K, Shimizu T, Okano T, Kobayashi E, Daimon T, Ueno T, Kuratani T, Toda K, Takakura N, Hatazawa J, Shirai M, and Sawa Y**. Cell-sheet therapy with omentopexy promotes arteriogenesis and improves coronary circulation physiology in failing heart. *Mol Ther* 23: 374-386, 2015.
12. **Krishna KA, Krishna KS, Berrocal R, Rao KS, and Sambasiva Rao KR**. Myocardial infarction and stem cells. *J Pharm Bioallied Sci* 3: 182-188, 2011.
13. **Kwon YW, Yang HM, and Cho HJ**. Cell therapy for myocardial infarction. *Int J Stem Cells* 3: 8-15, 2010.
14. **Laflamme MA, Chen KY, Naumova AV, Muskheli V, Fugate JA, Dupras SK, Reinecke H, Xu C, Hassanipour M, and Police S**. Cardiomyocytes derived from human embryonic stem cells in pro-survival factors enhance function of infarcted rat hearts. *Nat Biotechnol* 25: 1015-1024, 2007.
15. **Lahteenvuo J, and Rosenzweig A**. Effects of aging on angiogenesis. *Circ Res* 110: 1252-1264, 2012.

16. **Laugwitz KL, Moretti A, Lam J, Gruber P, Chen Y, Woodard S, Lin LZ, Cai CL, Lu M, and Reth M**. Postnatal isl1+ cardioblasts enter fully differentiated cardiomyocyte lineages. *Nature* 446: 934-945, 2007.
17. **Masuda S, Shimizu T, Yamato M, and Okano T**. Cell sheet engineering for heart tissue repair. *Adv Drug Deliv Rev* 60: 277-285, 2008.
18. **Min JY, Chen Y, Malek S, Meissner A, Xiang M, Ke Q, Feng X, Nakayama M, Kaplan E, and Morgan JP**. Stem cell therapy in the aging hearts of Fisher 344 rats: synergistic effects on myogenesis and angiogenesis. *J Thorac Cardiovasc Surg* 130: 547-553, 2005.
19. **Miyagawa S, Saito A, Sakaguchi T, Yoshikawa Y, Yamauchi T, Imanishi Y, Kawaguchi N, Teramoto N, Matsuura N, and Iida H**. Impaired myocardium regeneration with skeletal cell sheets-A preclinical trial for tissue-engineered regeneration therapy. *Transplantation* 90: 364-372, 2010.
20. **Miyahara Y, Nagaya N, Kataoka M, Yanagawa B, Tanaka K, Hao H, Ishino K, Ishida H, Shimizu T, and Kangawa K**. Monolayered mesenchymal stem cells repair scarred myocardium after myocardial infarction. *Nat Med* 12: 459-465, 2006.
21. **Orlic D, Kajstura J, Chimenti S, Jakoniuk I, Anderson SM, Li B, Pickel J, McKay R, Nadal-Ginard B, and Bodine DM**. Bone marrow cells regenerate infarcted myocardium. *Nature* 410: 701-705, 2001.
22. **Sekine H, Shimizu T, Hobo K, Sekiya S, Yang J, Yamato M, Kurosawa H, Kobayashi E, and Okano T**. Endothelial cell coculture within tissue-engineered cardiomyocyte sheets enhances neovascularization and improves cardiac function of ischemic hearts. *Circulation* 118: S145-S152, 2008.
23. **Sekiya N, Matsumiya G, Miyagawa S, Saito A, Shimizu T, Okano T, Kawaguchi N, Matsuura N, and Sawa Y**. Layered implantation of myoblast sheets attenuates adverse cardiac remodeling of the infarcted heart. *J Thorac Cardiovasc Surg* 138: 985-993, 2009.
24. **Shah S, Lowery E, Braun RK, Martin A, Huang N, Medina M, Sethupathi P, Seki Y, Takami M, Byrne K, Wigfield C, Love RB, and Iwashima M**. Cellular basis of tissue regeneration by omentum. *PLoS One* 7: e38368, 2012.
25. **Shao ZQ, Kawasuji M, Takaji K, Katayama Y, and Matsukawa M**. Therapeutic angiogenesis with autologous hepatic tissue implantation and omental wrapping. *Circ J* 72: 1894-1899, 2008.
26. **Sheng CC, Zhou L, and Hao J**. Current stem cell delivery methods for myocardial repair. *Biomed Res Int* 2013: 2012.
27. **Shirai M, Schwenke DO, Eppel GA, Evans RG, Edgley AJ, Tsuchimochi H, Umetani K, and Pearson JT**. Synchrotron based angiography for investigation of the regulation of vasomotor function in the microcirculation in vivo. *Clin Exp Pharmacol Physiol* 36: 107-116, 2009.
28. **Shudo Y, Miyagawa S, Fukushima S, Saito A, Shimizu T, Okano T, and Sawa Y**. Novel regenerative therapy using cell-sheet covered with omentum flap delivers a huge number of cells in a porcine myocardial infarction model. *J Thorac Cardiovasc Surg* 142: 1188-1196, 2011.
29. **Taylor DA, Atkins BZ, Hungspreugs P, Jones TR, Reedy MC, Hutcheson KA, Glower DD, and Kraus WE**. Regenerating functional myocardium: improved performance after skeletal myoblast transplantation. *Nat Med* 4: 929-933, 1998.
30. **Uren NG, Crake T, Lefroy DC, de Silva R, Davies GJ, and Maseri A**. Reduced coronary vasodilator function in infarcted and normal myocardium after myocardial infarction. *N Engl J Med* 331: 222-227, 1994.

31. **Zakharova L, Mastroeni D, Mutlu N, Molina M, Goldman S, Diethrich E, and Gaballa MA**. Transplantation of cardiac progenitor cell sheet onto infarcted heart promotes cardiogenesis and improves function. *Cardiovasc Res* 87: 40-49, 2010.

CHAPTER 4

Effects Of A Slow-release Formulation Of The Prostacyclin Analog ONO-1301 On Coronary Microvascular Function After Myocardial Infarction In the Rat

Chapter 4

4.1 Chapter Preface and Author Contribution

This chapter describes a study performed in collaboration with the Ono Pharmaceutical Co Ltd., Osaka, Japan and the SPring-8 Synchrotron Radiation Research Institute, Harima, Hyogo, Japan. Previously, the lead prostacyclin analog ONO-1301 was found to produce functional improvement, including increased left ventricular contractility, in mice after myocardial infarction (MI) (Ono Pharmaceutical Co Ltd, personal communication). The aim of the current study was to determine whether these beneficial effects are due to improved coronary vascular function and thus reduced vulnerability to cardiac ischemia. Therefore, we used synchrotron-based contrast microangiography to assess endothelial function in pre-existing and newly formed micro- and macro- vessels.

This study was performed with the financial support of a small grant to Prof. Mikiyasu Shirai (Department of Cardiac Physiology, NCVC) from Ono Pharmaceutical Co Ltd. Staff of Ono Pharmaceutical Co Ltd. performed the surgery on rats to induce MI. However, Ono Pharmaceutical had no involvement in the conduct of the microangiography study or subsequent analysis of the images. My primary supervisor, Dr. Pearson, performed the preparative surgery on the rats on the day of the acute experiment and subsequent contrast angiography of the coronary circulation. I assisted with the angiography and analyzed and, with the help of my supervisors, interpreted the data generated in this study.

4.2 Abstract

In the current study, I tested the hypothesis that the vasodilator capacity of arterial vessels of the anterior and lateral walls of the left ventricle is improved by ONO-1301 treatment after myocardial infarction. The first aim of the current study was to determine whether angiogenesis is increased, in the myocardium adjacent to the infarct region, following ONO-1301 administration. The second aim was to determine whether the existing and newly developed arterial vessels in the myocardium adjacent to the infarct region maintain normal vasomotor function following ONO-1301 administration. We used synchrotron radiation microangiography to assess endothelial function of the micro- and macro-vessels in the infarcted heart of the rat *in vivo*. Furthermore, we also determined whether the increase in coronary blood flow induced by a graded infusion of dobutamine (increased heart work simulating an exercise stress test) is also improved by ONO-1301. Across all 4 orders, similar number of vessels were observed in rats treated with ONO-1301 compared with rats treated with vehicle. Acetylcholine increased the calibers of coronary vessels to a similar degree in all branching orders in the control animals (1^{st}: 25.7 ± 10.8 %, 2^{nd}: 24.7 ± 8.5 % and 3^{rd}: 17.5 ± 6.1 %). In response to infusion of sodium nitroprusside, the calibers of coronary vessel in the control animals increased by a similar magnitude to that in response to acetylcholine. In these vessels the response to dobutamine was similar to those to acetylcholine and sodium nitroprusside. In rats treated with ONO-1301, the effects of acetylcholine, sodium nitroprusside and dobutamine on vessel caliber were similar to those in control rats. To conclude, we were not able to detect a beneficial effect of ONO-1301, on revascularization and vasodilatory responses to endothelium-dependent and endothelium-independent agents, after myocardial infarction that was significantly different from that of untreated control animals.

4.3 Introduction

Myocardial infarction (MI) is the consequence of interruption of the blood supply to an area of the heart, resulting in an irreversible loss of function of myocardial tissue. MI causes activation of resident immune cells and accumulation of circulating immune cells within the ischemic zone (6). The healing process then turns to reparation, beginning approximately one week after MI in humans (4). This process involves increased synthesis of matrix, proliferation of fibroblasts and inflammatory cells, and release of fibrosis-promoting cytokines that lead to scar formation (4). These responses consequently determine the size of the infarct; the region in which cardiac myocytes become lysed and replaced by fibrous components (1, 5). In addition, the border between the infarct area and the remote areas with insufficient blood supply is associated with persistent ischemia that can progressively widen the infarct region (1). Therefore, treatment for MI is chiefly focused on achieving reperfusion of the ischemic area to supply sufficient oxygen and other nutrients to the tissue and efficiently remove metabolic wastes (9).

There has recently been considerable interest in development of therapies that target the mechanisms underlying the progression of MI into cardiac failure, in particular the potential for enhancement of cardiac tissue salvage or regeneration (3). Previous studies have provided evidence that many growth factors and cytokines are involved in the development of new functional vessels that restore perfusion in many ischemic cardiovascular diseases (18). In animal models of cardiac failure, the up-regulation of pro-angiogenic or anti-inflammatory factors appears to promote some level of recovery in cardiac function (14, 15, 29). This is largely thought to be due to the enhanced salvage and regeneration of cardiac tissues (5). Therefore, treatments targeting up-regulation of angiogenic cytokines and growth factors may be a viable and attractive strategy for increasing perfusion to infarcted areas of the heart following an ischemic event. However, it is not clear which growth factors are most effective in driving angiogenesis after MI. Notably, cardiac ischemia evokes the release of prostacyclin, which has been demonstrated to stimulate release of multiple growth factors, including hepatocyte growth factor (HGF) and vascular endothelial growth factor (VEGF) (17).

Prostaglandins are a family of bioactive substances derived from arachidonic acid. They play an important role in maintaining local tissue homoeostasis and evoking the inflammatory response. Prostacyclin is a potent vasodilator in the heart, and potentiates nitric oxide release in various vascular territories (22, 24). Furthermore, prostacyclin is thought to play a major role in tissue repair and modulation of inflammation (17, 24). However, endogenous prostacyclin is rapidly removed from the circulation by 15-hydroxyprostaglandin dehydrogenase. ONO-1301 (Ono Pharmaceuticals), is a synthetic prostacyclin agonist lacking the typical prostanoid structures which allow prostanoids to be rapidly metabolized by 15-hydroxyprostaglandin dehydrogenase *in vivo* (27). Thus, ONO-1301 is a chemically stable prostacyclin agonist. In addition, ONO-1301 has a 3-pyridine radical that exerts inhibitory activity against thromboxane synthase, thus reducing the production of thromboxanes (25). Thromboxanes promote both vasoconstriction and aggregation of platelets (10), so lead to disruption of vascular homeostasis and thrombosis (2, 8). ONO-1301 has several potential advantages over other synthetic prostaglandin agonists, such as beraprost, epoprostenol, iloprost or treprostinil (27). Firstly, ONO-1301 has a long plasma half-life (12). Secondly, a poly-lactic co-glycolic acid (PLGA)-polymerised form of ONO-1301 has been developed which provides sustained-release of ONO-1301 (26, 27). Moreover, Nakamura and associates (20) found that intra-cardiac injection of ONO-1301 not only increased angiogenesis in the border of the infarct area in the heart, but also prevented enlargement of the left ventricle (LV) and extended survival in mice.

A previous study provided evidence for a severe vasodilator abnormality after MI, involving not only resistance vessels in the myocardium in the infarcted region, but also those in the myocardium perfused by normal coronary vessels (28). When this vasomotor dysfunction is present after acute MI, it is thought to influence the extent of ischemia and necrosis in the areas not directly injured by infarction (28). Therefore, it is necessary to evaluate the function of coronary vessels after delivering potential treatments for MI. In the current study, I tested the hypothesis that the vasodilator capacity of arterial vessels of the anterior and lateral walls of the LV is improved by ONO-1301 treatment after MI. To test this hypothesis, rats that had been subjected to MI in the anterior-lateral wall of the left ventricle (region supplied by the anterior descending left coronary artery) were studied after treatment with either ONO-1301 or its vehicle. The first aim of current study was to determine whether angiogenesis is

increased, in the myocardium adjacent to the infarct region, following ONO-1301 administration. The second aim was to determine whether the existing and newly developed arterial vessels in the myocardium adjacent to the infarct region maintain normal vasomotor function following ONO-1301 administration. We used synchrotron radiation (SR) angiography to assess endothelial function of the micro- and macro-vessels in the infarcted heart of the rat. Furthermore, we also determined whether the increase in coronary blood flow induced by a graded infusion of dobutamine (increased heart work simulating an exercise stress test) is also improved by ONO-1301.

4.4 Methods

4.4.1 Preparation of the Experimental Model

All rats were prepared by a staff of ONO Pharmaceutical Co Ltd., Osaka. All procedures were approved in advance by the SPring-8 Animal Experiment Review Committee and the National Cerebral and Cardiovascular Center Animal Experiment Committee. Rats received a medial sternotomy under anesthesia (Nembutal; pentobarbital sodium 50 mg/kg by intraperitoneal injection). MI was induced by permanent ligation of the left coronary artery with a 6-0 nylon suture. Rats then were allocated to one of the three groups, as described below, to receive a single dose of ONO 1301 or vehicle 3 hours after MI, or a single dose of ONO 1301 on day 3 post MI. After 4 weeks the treated rats were transported to SPring-8 for imaging experiments. ONO-1301 was polymerized with poly (D, L-lactic-co-glysolic acid) microspheres (MS) for a single subcutaneous injection (10 mg/kg). This preparation has been demonstrated to achieve sustained, slow release (21). These biodegradable and biocompatible microspheres release the drug through degradation of their polymeric matrix (Fig 4.1).

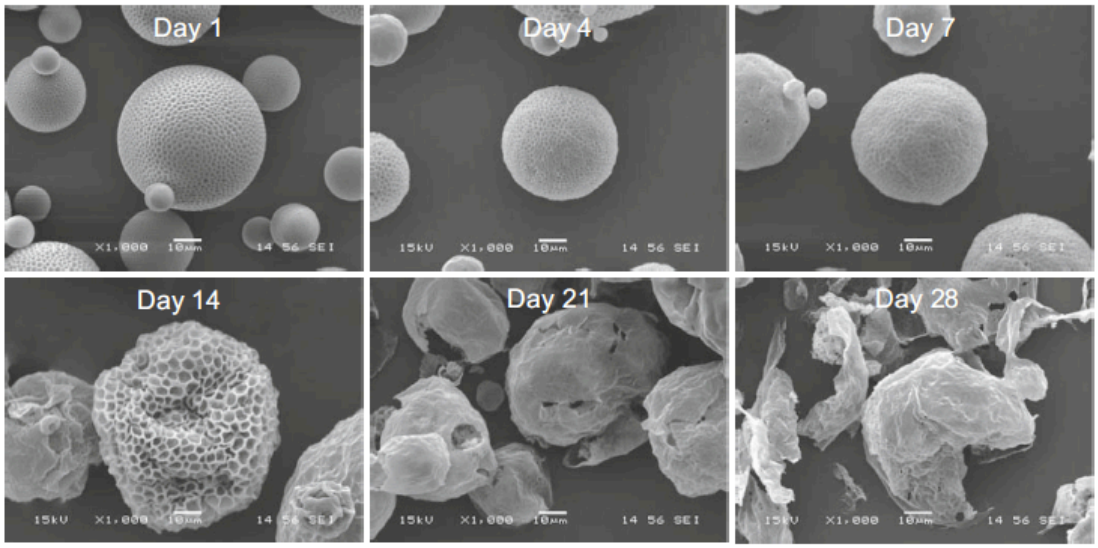

Figure 4.1 Representative electron micrographic images of ONO-1301. This, polymerized form (poly D, L-lactic-co-glysolic acid) of ONO-1301 is gradually degraded over 28 days at 37 °C *in vitro.* Images reproduced from Fukushima *et al* (7).

Experimental treatment groups (n = 9 in each group) evaluated by SR angiography were:

Group 1 (Control): Sprague Dawley (male) rats 12 wks of age, received vehicle MS post MI (subcutaneous).
Group 2 (3h): Sprague Dawley (male) rats 12 wks of age, received ONO-1301MS (10 mg/kg subcutaneous) 3 hours post MI.
Group 3 (72h): Sprague Dawley (male) rats 12 wks of age, received ONO-1301MS (10 mg/kg subcutaneous) 72 hours post MI.

The final number of animals included in each analysis was, in some instances, fewer than this, because the quality of some micro-angiograms was poor. Final values of n are provided in the legends to each figure.

4.4.2 Surgical Preparation for Angiography

All coronary microangiography was conducted at Beamline 28B2 of SPring-8, the Synchrotron Radiation Research Institute in Hyogo, Japan. Microangiography was performed with SR to visualize the coronary circulation *in vivo* and has been described in detail previously (13). Imaging of the coronary circulation was performed with monochromatic synchrotron radiation at 33.2 KeV, just above the iodine K-edge

energy for producing maximal absorption of the iodine contrast agent in the vascular lumen.

Rats were anesthetized with pentobarbital sodium (50 mg/kg i.p.). Supplementary doses of anesthetic (~20 mg/kg/h) were periodically administered to maintain a surgical level of anesthesia. After induction of anesthesia, the rats were intubated by tracheotomy, to permit artificial ventilation with a rodent ventilator (tidal volume = 1 ml/100 g body weight, 70 strokes/min, ~40% oxygen, Shinano, Tokyo, Japan). A rectal thermistor coupled with thermostatically controlled heating pad was used to maintain body temperature at ~37 °C.

A 20 gauge Angiocath catheter (Becton Dickinson, Inc., Sandy, Utah, USA) was used to cannulate the right carotid artery near the aortic valve for selective angiography of the coronary circulation. Arterial pressure and heart rate were recorded from a catheter filled with heparinized saline (12 units/ml) inserted into the femoral artery, and connected to a pressure transducer (MLT0699, AD Instruments, NSW, Australia). The analogue arterial pressure signal was digitized at 1000 Hz and recorded by CHART software (v5.4.1, AD Instruments, NSW, Australia) to determine mean arterial pressure and heart rate. Body fluid was maintained during the period of imaging by sodium lactate (Otsuka, Tokyo, Japan) infused via a catheter inserted into the jugular vein (3 ml/h). Drug infusions were also delivered via the jugular vein catheter.

4.4.3 Angiography Protocol

After the preparatory surgery, each animal was moved into the X-ray hutch at BL28B2 for coronary microangiography. The rat was placed in a supine position in front of the X-ray detector in the path of the X-ray beam. Iodinized contrast medium (Iomeron 350, Bracco-Eisai Co. Ltd., Tokyo, Japan) was delivered through the carotid artery using a high-speed injector (0.3-0.5 ml bolus 25 ml/s, Nemoto Kyorindo, Tokyo, Japan). The ventilator was turned off for a period of approximately 3 seconds immediately before the start of each cine recording, of 100 frames at 30 frames/s, recorded on a SATICON detector (Hitachi Denshi Techno-System, Ltd., Tokyo, Japan) with 1.5-2 ms/frame shutter open time. Images with 1024 x 1024 pixel format and 10-bit resolution were recorded from a ~10 mm^2 field of view. Approximately 10 min was allowed between each imaging sequence for renal clearance of the contrast.

Contrast images were recorded from the upper LV during all experiments. In each rat, the calibers of vessels were determined sequentially during 5 minutes of infusion of vehicle (sodium lactate 3 ml/h), acetylcholine (ACh; Ovisot, Daiichi Sankyo, Japan, 5 μg/kg/min), sodium nitroprusside (SNP; Sigma-Aldrich, Japan, 5 μg/kg/min) and dobutamine (Dob; Eli Lilly Japan, Kobe, Japan 4-8 μg/kg/min, a cardiac specific β-adrenergic agonist).

4.4.4 Statistical Analysis

Data are expressed as mean ± SEM unless otherwise stated and n represents the number of rats in each group. For each individual rat, within-rat mean vessel ID and vessel number for each branching order were calculated and the between-rat means were then used for group comparisons. Student's paired t-test was used to assess differences between vessel number and diameter during the baseline period (vehicle infusion) and the later drug infusion periods (ACh, SNP or Dob). One-way ANOVA was used to assess differences between groups during the baseline period (GraphPad Software, Inc., La Jolla, CA, USA). Two-way ANOVA was also used, with factors treatment and branching order. The Dunn-Sidak multiple comparison procedure was used to reduce the probability of type 1 error.

4.5 Results

4.5.1 General Characteristics and Hemodynamics

Body weight was measured on the day of experiment prior to microangiography. There were no significant differences between the groups (Control: 260 ± 4.9 g, 3 h: 260 ± 3.9 g, 72 h: 259 ± 5.8 g, *P* = 0.99). There were also no significant differences in either heart rate (HR) or mean arterial pressure (MAP) between the treatment groups at baseline (Fig. 4.2).

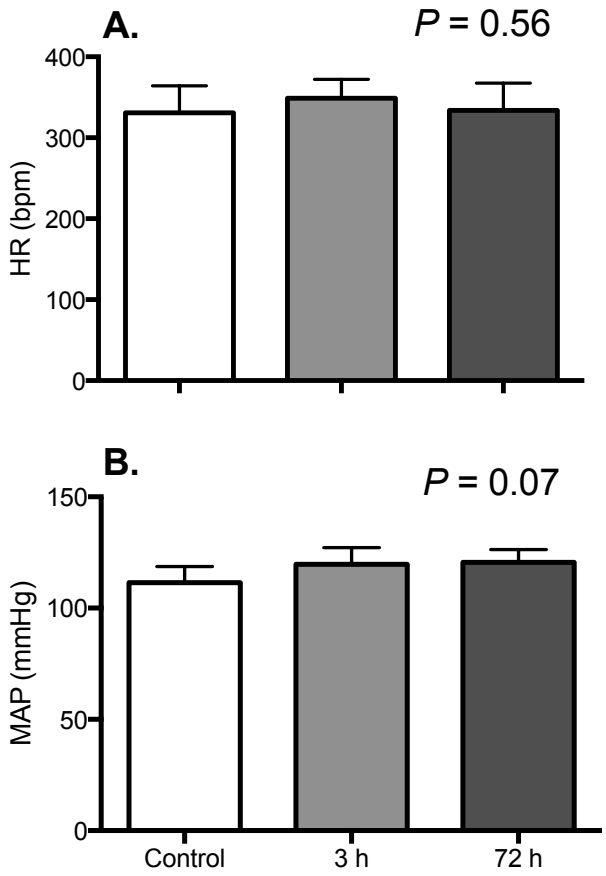

Figure 4.2 (A) Heart rate and (B) mean arterial pressure of the treatment at baseline. The three groups were rats subjected to myocardial infarction (MI) with vehicle treatment (Control), treatment with ONO-1301 at 3 hours post MI (3 h) and, treatment with ONO-1301 at 72 hours post MI (72 h). Values expressed as mean ± SEM (n = 6 in each group). *P* values are the outcomes of one-way ANOVA. MAP = mean arterial pressure; HR = heart rate.

In control animals ACh reduced MAP (by 39 ± 6 mmHg) and HR (by 36 ± 19 bpm), SNP induced reductions in MAP (by 39 ± 5 mmHg) and HR (by 54 ± 18 bpm), and Dob increased HR (by 47 ± 14 bpm) but had little effect on MAP. In rats treated with ONO-1301, the effects of ACh, SNP and Dob on MAP and HR were similar to those observed in control rats (see Fig. 4.3).

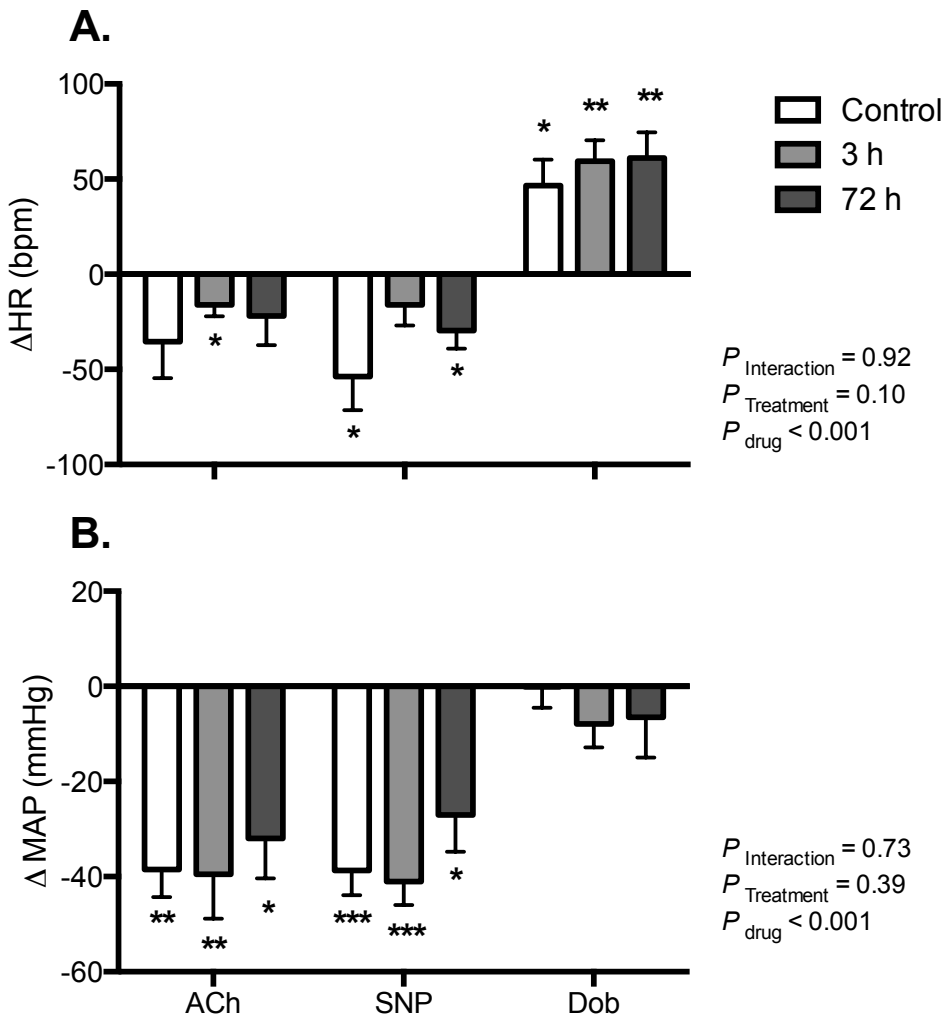

Figure 4.3 Relative changes in (A) heart rate and (B) mean arterial pressure in response to vasoactive agents in the various treatment groups The three groups were rats subjected to myocardial infarction (MI) with vehicle treatment (Control), treatment with ONO-1301 at 3 hours post MI (3 h) and, treatment with ONO-1301 at 72 hours post MI (72 h). Data are shown as mean ± SEM, n = 6 in each group. P values are the outcomes of two-way analysis of variance. * denotes $P < 0.05$, ** $P < 0.01$, *** $P < 0.001$ vs baseline (Student's paired t-test). Acetylcholine = ACh; sodium nitroprusside = SNP, dobutamine = Dob; MAP = mean arterial pressure; HR = heart rate.

4.5.2 Number and Caliber of Vessels Visible Under Baseline Conditions

Typical angiograms of the coronary circulation in the three groups were similar at baseline and during drug administration (Fig. 4.4). The number of visualized vessels progressively increased across order 1-3, but fewer 4th order vessels were observed than 3rd order vessels (Fig. 4.5 A). Across all 4 orders, similar numbers of vessels was observed in rats treated with ONO-1301 at 3 h post MI (1st: 4.7 ± 0.6, 2nd: 10.8 ± 1.4, 3rd: 13.0 ± 1.5 and 4th: 5.7± 2.1) as were observed in rats treated with vehicle. There were fewer visible 3rd order vessels in rats treated with ONO-1301 at 72 h post MI (8.2 ± 0.7) than rats treated with vehicle (12.5 ± 2.2). As expected vessel ID at baseline progressively decreased with branching order (P < 0.001). The basal ID of vessels was similar in the three groups (Fig. 4.5 B).

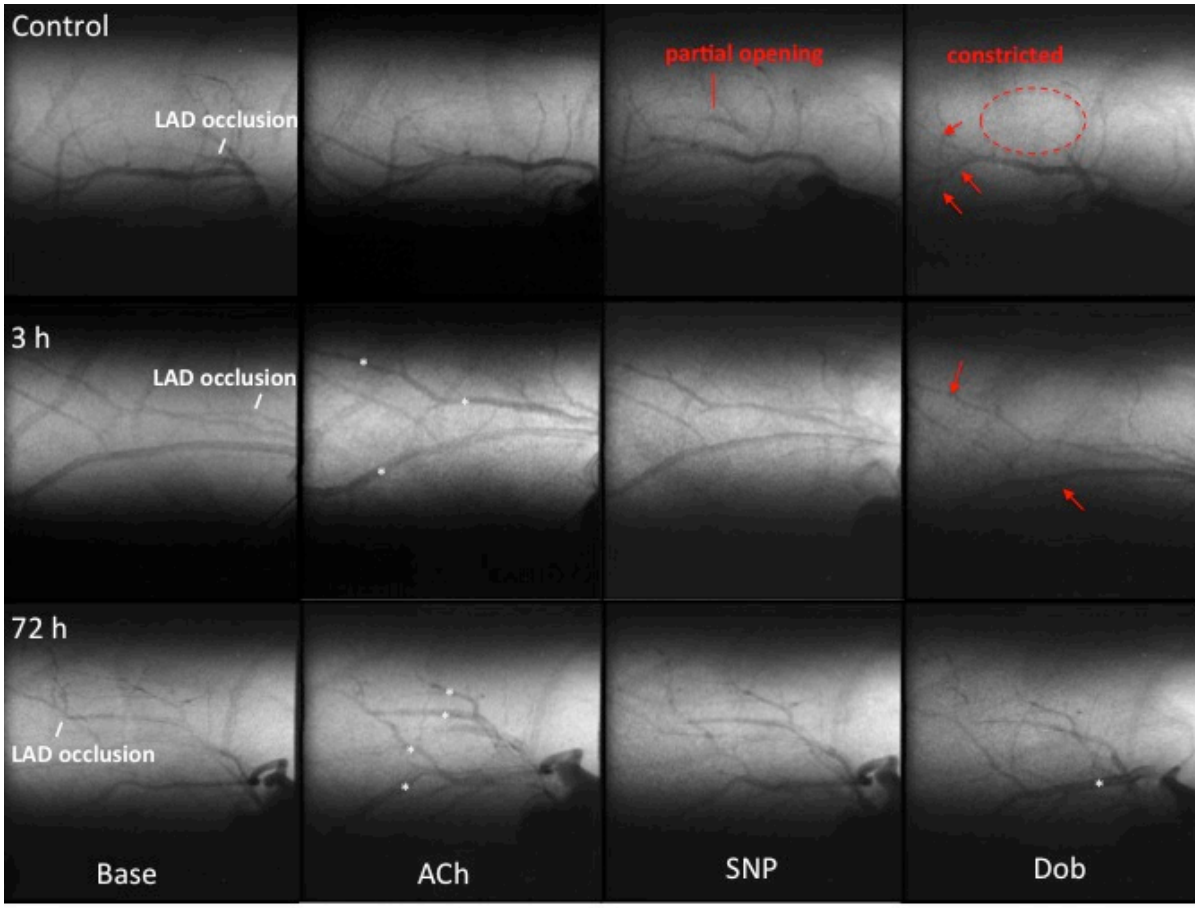

Figure 4.4 Representative synchrotron radiation angiograms of the coronary vasculature. Images were generated during sequential infusion of vehicle, acetylcholine (ACh), sodium nitroprusside (SNP), and dobutamine (Dob). Sprague Dawley rats were treated with either vehicle (control) or ONO-1301 3 hours (3 h) after MI, or treated with ONO1301 at 3 days post MI (72 h). Images are presented for individual rats in rows. Red arrows = vasoconstriction, white asterisk = vasodilation relative to baseline.

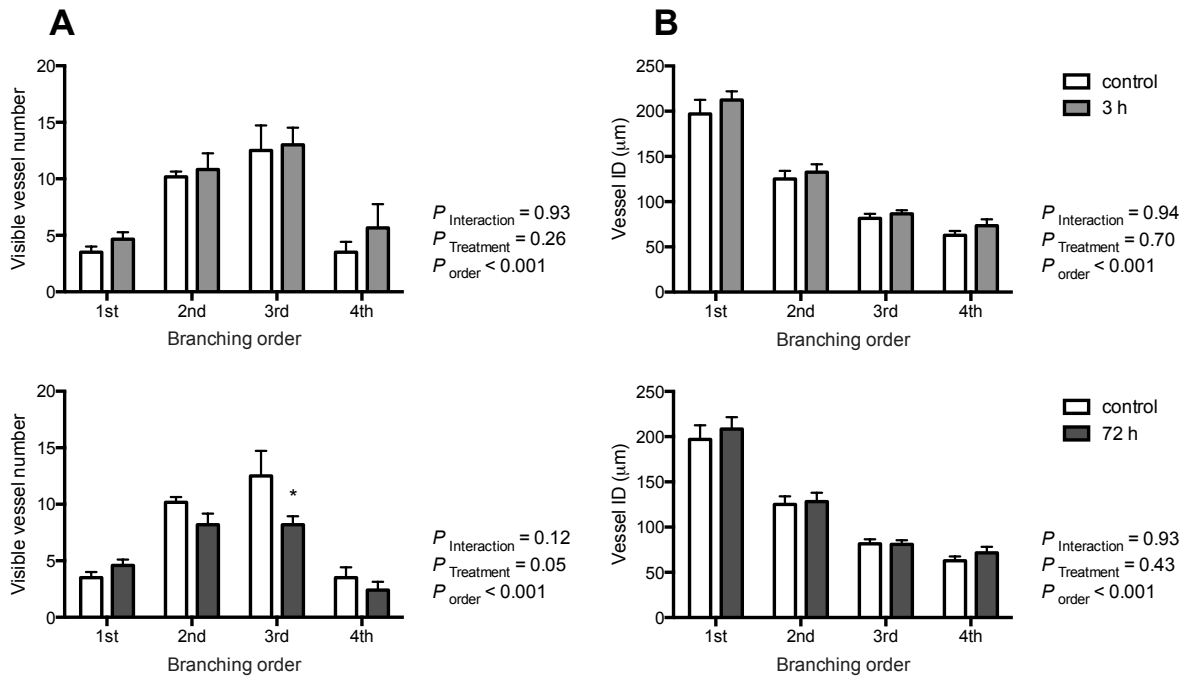

Figure 4.5 (A) The number of visible vessels and (B) internal diameter (ID) in the field of view categorized by branching order in all the treatment groups. The treatment groups were rats subjected to myocardial infarction (MI) treated with vehicle microspheres (Control, n = 6), rats treated with ONO-1301 3 hours post MI (3 h, n = 6), and rats treated with ONO-1301 72 hours post MI (72 h, n = 5). Data are shown as mean ± SEM. *P* values are the outcomes of two-way ANOVA. *P* values are the outcomes of two-way ANOVA. * denotes $P < 0.05$ vs corresponding vessels in control animals (after application of the Dunn Sidak procedure to account for the fact that both the 3 h and 72 h group were contrasted against the control group).

4.5.3 Changes in the Number of Perfused Vessels During Drug Stimulation

We examined relative change in vessel number in response to administration of ACh, SNP and the β_1-adrenergic agonist (Dob). Infusion of ACh, SNP and Dob did not significantly alter the number of visible 1st or 2nd order coronary vessels in angiograms in any of the groups. Infusion of ACh tended to increase the number of visible 3rd order vessels in rats treated with ONO-1301 at 3 h post MI (11.8 ± 4.6 %; $P = 0.09$ vs baseline, Fig.4.6) but this apparent effect was not observed in vehicle-treated rats or rats treated with ONO-1301 72 h post MI. The number of perfused 3rd and 4th order vessels in control rats was similar to baseline during infusion of SNP and Dob. In rats treated with ONO-1301, the effects of SNP and Dob on perfused vessels were similar to those in control rats.

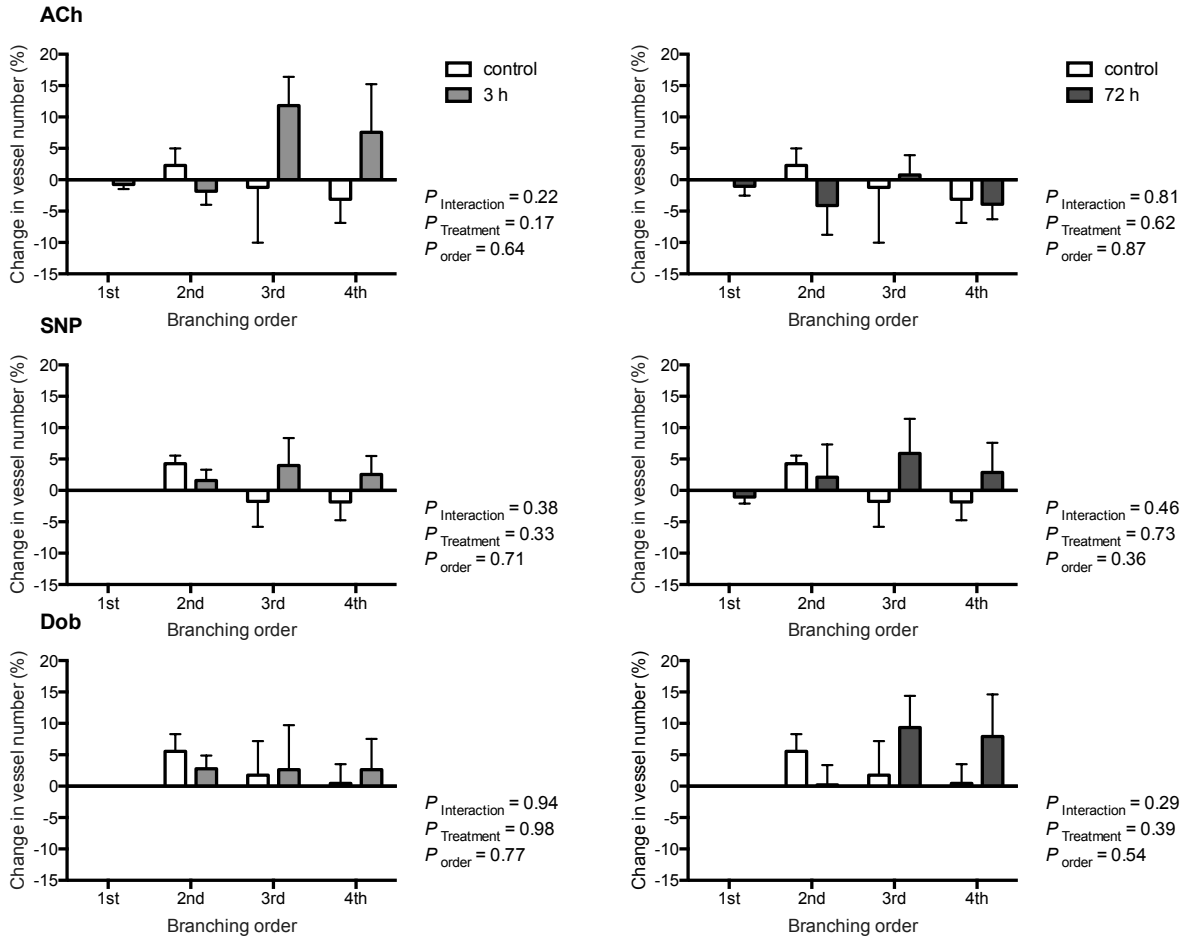

Figure 4.6 Relative change in vessel number in response to vasoactive agents in the various treatment groups. The treatment groups were: rats subjected to myocardial infarction (MI) treated with vehicle microspheres (Control, n = 6), rats treated with ONO-1301 3 hours post MI (3 h, n = 6), and rats treated with ONO-1301 72 hours post MI (72 h, n = 5). Data are shown as mean ± SEM. *P* values are the outcomes of two-way analysis of variance. Acetylcholine = ACh; sodium nitroprusside = SNP, dobutamine = Dob.

4.5.4 Changes in Vessel Caliber During Drug Stimulation

ACh increased the calibers of coronary vessels to a similar degree in all branching orders in the control animals (1^{st}: 25.7 ± 10.8 %, 2^{nd}: 24.7 ± 8.5 % and 3^{rd}: 17.5 ± 6.1 %). In response to SNP and Dob infusion, the caliber of coronary vessels in the control animals increased similarly to those during infusion of ACh. In rats treated with ONO-1301, the effects of ACh, SNP and Dob on vessel caliber were similar to those in control rats (Fig. 4.7).

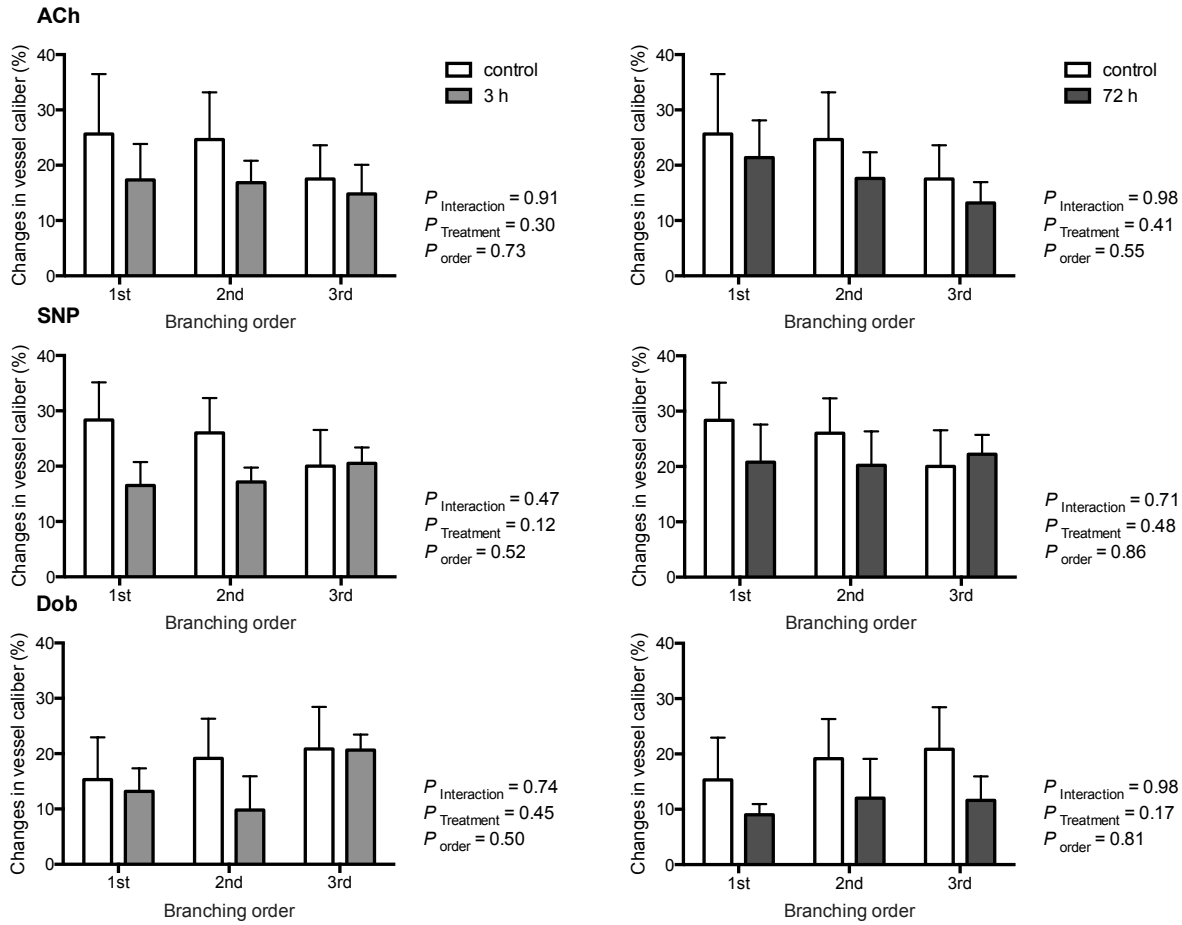

Figure 4.7 Relative change in vessel caliber in 3rd and 4th order vessels number in response to vasoactive agents in the various treatment groups. The treatment groups were: rats subjected to myocardial infarction (MI) treated with vehicle microspheres (Control, n = 6), rats treated with ONO-1301 3 hours post MI (3 h, n = 6), and rats treated with ONO-1301 72 hours post MI (72 h, n = 5). Data are shown as mean ± SEM. *P* values are the outcomes of two-way analysis of variance. Acetylcholine = ACh; sodium nitroprusside = SNP, dobutamine = Dob.

4.6 Discussion

In the current study, we were unable to detect significant differences, in the number of perfused vessels or vessel caliber, between rats treated with ONO-1301 and rats treated with vehicle, during baseline recordings. When we examined the vasodilatory response to ACh, SNP and Dob, there was no significant difference between groups. Thus, we were unable to detect a beneficial effect of ONO-1301 on vasodilatory function in the coronary circulation after MI.

Further, in the current study, we were not able to detect a beneficial effect of ONO-1301 on revascularization post MI. In contrast, a previous study provided evidence that subcutaneous administration of ONO-1301, 3 days after ligation of the coronary artery, increased angiogenesis and reduced the size of the fibrotic area in the ischemic myocardium (11). ONO-1301 also improved cardiac function after MI, as demonstrated by a lower HR, decreased systolic and diastolic left ventricular pressure, and improvement in contractility of the LV in rats treated with ONO-1301 relative to vehicle-treated controls (11). ONO-1301 has also been shown to inhibit hypertrophy of the pulmonary arteries in rats with pulmonary hypertension (21). It also had a beneficial effect in the canine coronary circulation subjected to chronic MI (16). Indeed, in these dogs both myocardial blood flow and capillary density increased at 8 weeks post MI (16). Taken together, these studies indicate that ONO-1301 can induce angiogenesis and is beneficial for regeneration of cardiac structure and function after MI and cardiopulmonary disease.

How can we reconcile our inability to detect a beneficial effect of treatment with ONO-1301 in the current study, with the observations described above? One possibility is that the relatively mild HF in the rats we studied was not severe enough to overcome the intrinsic capacity of the heart for revascularisation. This proposition merits future study, in animals with more severe HF.

One important limitation of our current study was the omission of a control group not subjected to MI. Without such a group it is not possible to quantify the degree of vascular dysfunction induced by MI. It may be that only mild dysfunction was present. Notably, coronary vasodilatory responses in the rats we studied were of similar magnitude to those we have previously observed in healthy rats of a similar age (13). Furthermore, even in rats that were untreated after MI, coronary vasodilatation was

observed in response to both endothelium-independent and endothelium-dependent agents, and these responses are comparable to that reported by Jenkins *et al* in normal rats (13). Thus, it may be that the function of both vascular smooth muscle and endothelium was preserved across the three groups. Furthermore, the vasodilatory responses to infusion of Dob showed that the ability to regulate coronary perfusion under changing conditions of heart work was not appreciably blunted in these animals.

Another major limitation of our approach should be acknowledged. *In vivo* angiography does not necessarily visualize all vessels segments in the coronary vasculature. Contrast media flows through vessels with the least resistance. Thus, high vascular resistance in some segments might prevent or greatly reduce the entry of contrast media into the vessel, so that its concentration might be below the level of detection. Nakamura et al found that capillary density increased significantly at the border zone of the heart of mice with MI when ONO-1301 was injected directly into the anterior and lateral myocardium (19). In addition, Hirata *et al* showed that treatment with ONO-1301 had an angiogenic effect in the border zone of the ischemic myocardium in Wistar rats with MI (11). Importantly, the diameter of capillary vessels is less than 20 μm, so these small vessels are not detectable with our *in vivo* approach. Therefore, in the rats treated with ONO-1301 in our current study, there might have been many smaller newly developed vessels, which we were not able to detect by angiography. Future studies would benefit by combining *in vivo* synchrotron microangiography with *ex vivo* 3D-computed tomography (CT) of vascular casts. Injection of gelatine containing barium into the vasculature after the dynamic studies would allow subsequent CT reconstruction for much improved visualization of arterial vessels down to capillary level (23). This would allow more accurate determination of the number of newly developed arterial vessels.

To conclude, we were not able to detect a beneficial effect of ONO-1301 on revascularization and vasodilatory responses to endothelium-dependent and endothelium-independent agents. One potential explanation for this negative finding is that the function of both vascular smooth muscle and endothelium may have been relatively well preserved in the model of mild MI we studied. Future studies, including an additional protocol to produce vascular casts from the same animals used for

synchrotron microangiography would allow more accurate assessment of the microvasculature.

4.7 References

1. **Camici PG, d'Amati G, and Rimoldi O**. Coronary microvascular dysfunction: mechanisms and functional assessment. *Nat Rev Cardiol* 12: 48-62, 2015.
2. **Chiu JJ, and Chien S**. Effects of disturbed flow on vascular endothelium: pathophysiological basis and clinical perspectives. *Physiol Rev* 91: 327-387, 2011.
3. **Doppler SA, Deutsch MA, Lange R, and Krane M**. Cardiac regeneration: current therapies-future concepts. *J Thorac Dis* 5: 683-697, 2013.
4. **Ertl G, and Frantz S**. Healing after myocardial infarction. *Cardiovasc Res* 66: 22-32, 2005.
5. **Frangogiannis NG**. The inflammatory response in myocardial injury, repair, and remodelling. *Nat Rev Cardiol* 11: 255-265, 2014.
6. **Frangogiannis NG, Smith CW, and Entman ML**. The inflammatory response in myocardial infarction. *Cardiovasc Res* 53: 31-47, 2002.
7. **Fukushima S, Miyagawa S, Sakai Y, and Sawa Y**. A sustained-release drug-delivery system of synthetic prostacyclin agonist, ONO-1301SR: a new reagent to enhance cardiac tissue salvage and/or regeneration in the damaged heart. *Heart Fail Rev* 20: 401-413, 2015.
8. **Furie B, and Furie BC**. Mechanisms of thrombus formation. *N Engl J Med* 359: 938-949, 2008.
9. **Giblett JP, West NE, and Hoole SP**. Cardioprotection for percutaneous coronary intervention—reperfusion quality as well as quantity. *Int J Cardiac* 177: 786-793, 2014.
10. **Golino P, Ashton JH, Buja LM, Rosolowsky M, Taylor AL, McNatt J, Campbell WB, and Willerson JT**. Local platelet activation causes vasoconstriction of large epicardial canine coronary arteries in vivo. Thromboxane A2 and serotonin are possible mediators. *Circulation* 79: 154-166, 1989.
11. **Hirata Y, Soeki T, Yamada H, Shiota A, Shimabukuro M, Sakai Y, Nakayama M, Matsumoto K, Igarashi T, and Sata M**. A synthetic prostacyclin agonist, ONO-1301, ameliorates ventricular remodeling after acute myocardial infarction via upregulation of HGF in rat. *Biomedicine & Aging Pathology* 1: 90-96, 2011.
12. **Imawaka H, and Sugiyama Y**. Kinetic study of the hepatobiliary transport of a new prostaglandin receptor agonist. *J Pharmacol Exp Ther* 284: 949-957, 1998.
13. **Jenkins MJ, Edgley AJ, Sonobe T, Umetani K, Schwenke DO, Fujii Y, Brown RD, Kelly DJ, Shirai M, and Pearson JT**. Dynamic synchrotron imaging of diabetic rat coronary microcirculation in vivo. *Arterioscler Thromb Vasc Biol* 32: 370-377, 2012.
14. **Jin YN, Inubushi M, Masamoto K, Odaka K, Aoki I, Tsuji AB, Sagara M, Koizumi M, and Saga T**. Long-term effects of hepatocyte growth factor gene therapy in rat myocardial infarct model. *Gene Ther* 19: 836-843, 2012.
15. **Kilian EG, Sadoni S, Vicol C, Kelly R, van Hulst K, Schwaiger M, Kupatt C, Boekstegers P, Pillai R, Channon K, Hetzer R, and Reichart B**. Myocardial transfection of hypoxia inducible factor-1alpha via an adenoviral vector during coronary artery bypass grafting. *Circ J* 74: 916-924, 2010.
16. **Kubota Y, Miyagawa S, Fukushima S, Saito A, Watabe H, Daimon T, Sakai Y, Akita T, and Sawa Y**. Impact of cardiac support device combined with slow-release prostacyclin agonist in a canine ischemic cardiomyopathy model. *J Thorac Cardiovasc Surg* 147: 1081-1087, 2014.
17. **Kuwabara K, Ogawa S, Matsumoto M, Koga S, Clauss M, Pinsky DJ, Lyn P, Leavy J, Witte L, and Joseph-Silverstein J**. Hypoxia-mediated induction of acidic/basic fibroblast growth factor and platelet-derived growth factor in mononuclear phagocytes stimulates growth of hypoxic endothelial cells. *Proc Natl Acad Sci USA* 92: 4606-4610, 1995.

18. **Losordo DW, and Dimmeler S**. Therapeutic Angiogenesis and Vasculogenesis for Ischemic Disease : Part I: Angiogenic Cytokines. *Circulation* 109: 2487-2491, 2004.
19. **Nakamura K, Sata M, Iwata H, Sakai Y, Hirata Y, Kugiyama K, and Nagai R**. A synthetic small molecule, ONO-1301, enhances endogenous growth factor expression and augments angiogenesis in the ischaemic heart. *Clin Sci* 112: 607-616, 2007.
20. **Nakamura K, Sata M, Iwata H, Sakai Y, Hirata Y, Kugiyama K, and Nagai R**. A synthetic small molecule, ONO-1301, enhances endogenous growth factor expression and augments angiogenesis in the ischaemic heart. *Clinical Science* 112: 607-616, 2007.
21. **Obata H, Sakai Y, Ohnishi S, Takeshita S, Mori H, Kodama M, Kangawa K, Aizawa Y, and Nagaya N**. Single injection of a sustained-release prostacyclin analog improves pulmonary hypertension in rats. *Am J Respir Crit Care Med* 177: 195-201, 2008.
22. **Raczka E, and Quintana A**. Effects of intravenous administration of prostacyclin on regional blood circulation in awake rats. *Br J Pharmacol* 126: 1325-1332, 1999.
23. **Sangaralingham SJ, Ritman EL, McKie PM, Ichiki T, Lerman A, Scott CG, Martin FL, Harders GE, Bellavia D, and Burnett JC, Jr.** Cardiac micro-computed tomography imaging of the aging coronary vasculature. *Circ Cardiovasc Imaging* 5: 518-524, 2012.
24. **Stitham J, Midgett C, Martin KA, and Hwa J**. Prostacyclin: an inflammatory paradox. *Front Pharmacol* 2: 24, 2011.
25. **Tanouchi T, Kawamura M, Ohyama I, Kajiwara I, Iguchi Y, Okada T, Miyamoto T, Taniguchi K, Hayashi M, Iizuka K, and Nakazawa M**. Highly selective inhibitors of thromboxane synthetase. 2. Pyridine derivatives. *J Med Chem* 24: 1149-1155, 1981.
26. **Uchida T, Hazekawa M, Morisaki T, Yoshida M, and Sakai Y**. Effect of antioxidants on the stability of ONO-1301, a novel long-acting prostacyclin agonist, loaded in PLGA microspheres. *J Microencapsul* 30: 245-256, 2013.
27. **Uchida T, Hazekawa M, Yoshida M, Matsumoto K, and Sakai Y**. A novel long-acting prostacyclin agonist (ONO-1301) with an angiogenic effect: promoting synthesis of hepatocyte growth factor and increasing cyclic AMP concentration via IP-receptor signaling. *J Pharmacol Sci* 123: 392-401, 2013.
28. **Uren NG, Crake T, Lefroy DC, de Silva R, Davies GJ, and Maseri A**. Reduced coronary vasodilator function in infarcted and normal myocardium after myocardial infarction. *N Engl J Med* 331: 222-227, 1994.
29. **Yang ZJ, Chen B, Sheng Z, Zhang DG, Jia EZ, Wang W, Ma DC, Zhu TB, Wang LS, Li CJ, Wang H, Cao KJ, and Ma WZ**. Improvement of heart function in postinfarct heart failure swine models after hepatocyte growth factor gene transfer: comparison of low-, medium- and high-dose groups. *Mol Biol Rep* 37: 2075-2081, 2010.

CHAPTER 5

Overexpression Of The APJ Receptor on Vascular Smooth Muscle Promotes Apelin-Induced Vasoconstriction In The Coronary Circulation *In Vivo*

Chapter 5

5.1 Chapter Preface and Author Contribution

This chapter describes a preliminary study performed in collaboration with the University of Tsukuba, Tsukuba, Ibaraki, Japan and the SPring-8 Synchrotron Radiation Research Institute, Harima, Hyogo, Japan.

Apelin is an endogenous peptide ligand for the G-protein-coupled receptor, APJ. Both apelin and the apelin receptor (APJ) are expressed in a wide range of tissues, including the brain, heart, blood vessels and the gastrointestinal tract (6, 13, 16, 23). Previously, our colleagues from the University of Tsukuba provided evidence that APJ mediates coronary vasospasm. They administered apelin to anesthetized mice before filling their coronary circulation with Microfil® to allow visualization of the coronary circulation *ex vivo*. They observed evidence of vasospasm, in the hearts of mice over-expressing APJ, after exposure to apelin (Fukamizu et al, unpublished). In the study described in this chapter of my thesis we investigated whether the same response can be observed in coronary vessels *in vivo*. Synchrotron-based contrast microangiography was used for the assessment of changes in caliber of vessels and number of visible vessels.

Our colleagues from the University of Tsukuba developed a mouse model that overexpresses the APJ receptor on vascular smooth muscle cells (SMA-APJ mouse), which was used in the current study, performed at the Japanese synchrotron. My primary supervisor, Dr. Pearson, performed the preparative surgery on the mice on the day of the acute experiment. He and I performed the subsequent contrast angiography of the coronary circulation together. I conducted the analysis of the data generated from this study and made a major contribution to their interpretation.

5.2 Abstract

A recent study performed by our colleagues (Prof Fukamizu and Assoc Prof. Ishida from the University of Tsukuba) provided evidence that apelin induces vasoconstriction of the coronary vasculature. However, major limitations of the previous study discussed above were that (i) vascular caliber was assessed *ex vivo* rather than *in vivo*, and (ii) that only between-animal comparisons were made. In the current study we tested the hypothesis that APJ receptors on vascular smooth muscle (VSM) mediate coronary vasoconstriction *in vivo*. The aim of the current study was to determine whether or not coronary vasoconstriction occurs in a mouse model that overexpresses the APJ receptor on VSM. Synchrotron-based contrast microangiography was used to allow the assessment of coronary vascular diameter and number in both wild type mice (WT) and mice with overexpression of APJ (TG). More 3rd order vessels were visible in TG than WT mice (55 ± 16 %). In WT mice, administration of apelin was followed by little or no change in the number of observable vessels or their caliber. In contrast, in the TG mice, administration of apelin was followed by a -38.6 ± 6.6 % reduction in the number of observable 3rd order vessels and vasoconstriction in 1st (-18.8 ± 6.2 % reduction in diameter), 2nd (-18.0 ± 4.5 %) and 3rd (-11.0 ± 3.8 %) order vessels. To conclude, our current findings provide evidence that the apelin/APJ pathway on VSM leads to vasoconstriction and possibly also angiogenesis in the coronary circulation in mice.

5.3 Introduction

Apelin is an endogenous peptide ligand for the G-protein-coupled receptor, APJ (20, 24). G-protein-coupled receptors are the largest group of transmembrane receptors, mediating transduction of a diverse array of extracellular signals (24). Apelin and APJ are distributed in various tissues including the brain, heart, blood vessels and gastrointestinal tract (6, 13, 16, 23).

The physiological roles of apelin and APJ are not fully understood. Four lines of evidence support the hypothesis that the APJ/apelin system plays important roles in the regulation of cardiovascular function. Firstly, the APJ receptor shares a close homology to the angiotensin II type 1 (AT_1) receptor, which mediates major cardiovascular effects, such as vasoconstriction and secretion of aldosterone from the adrenal cortex (17). Secondly, apelin itself has been shown to modulate cardiac contractility and vascular tone *in vitro* (17). Upregulation of apelin also has been shown to cause potent vasoconstriction in the human coronary artery (22). Thirdly, levels of apelin mRNA were shown to increase in the left ventricle (LV) in chronic heart failure (HF) associated with coronary heart disease and dilated cardiomyopathy (4). Fourthly, plasma levels of apelin increase in the early stage of all forms of left ventricular dysfunction (2).

A recent study performed by our colleagues (Prof Fukamizu and Assoc Prof. Ishida from the University of Tsukuba) provided evidence that apelin induces vasoconstriction of the coronary vasculature. Specifically, they found evidence that apelin can induce stenosis and focal vessel constriction in the coronary arteries of mice that overexpressed APJ in vascular smooth muscle (VSM) (Fig. 5.1, Fukamizu et al unpublished). Vasospasm is the sudden constriction of an artery, leading to decreased perfusion of the vessel. Thus, vasospasm can lead to tissue ischemia and necrosis (3, 11, 18). Myocardial ischemia caused by coronary vasospasm can lead to angina, myocardial infarction (MI), HF and even death (18).

Major limitations of the previous study discussed above (Fig. 5.1) were that (i) vascular caliber was assessed *ex vivo* rather than *in vivo*, and (ii) that only between-animal comparisons were made. That is, because it was necessary to remove the heart from animals to assess vascular caliber, it was not possible to make

observations, in the same vessels, before and after administration of apelin. To overcome these limitations, in the current study we tested the hypothesis that APJ receptors mediate coronary vasoconstriction *in vivo*.

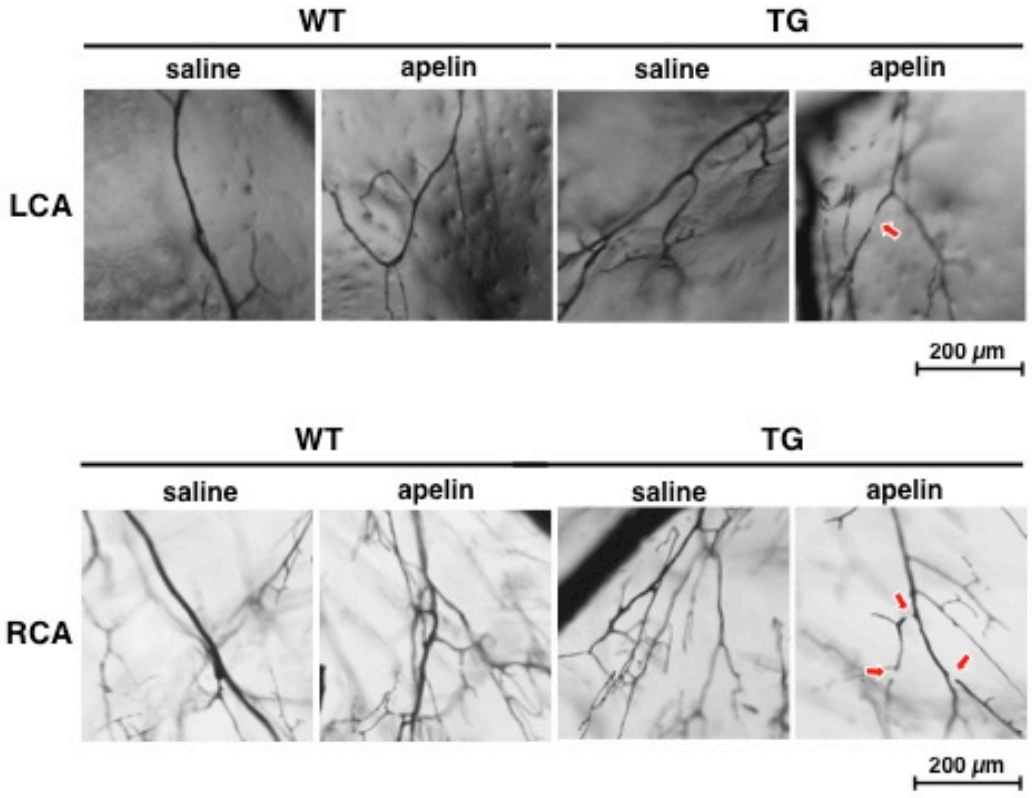

Figure 5.1 Angiograms of Microfil® within coronary vessels, showing evidence of vasospasm induced by apelin. Ex vivo studies were performed using wild type mice (WT) and a transgenic mouse model with overexpression of the APJ receptor (TG). Mice of approximately 14 weeks of age received an intraperitoneal injection of either apelin (296 μg/kg) or saline. Ten minutes later, they were anesthetized with an intraperitoneal injection of sodium pentobarbital (1:10 dilution with sodium lactate, 50 mg/kg). Two minutes after anesthesia, 700~800 μl of Microfil® (MV-112, Flow Tech Inc., Carver, MA, USA) was injected directly into the left ventricle, with a 1 ml syringe, to enable visualization of the coronary vessels. Hearts were fixed in 10% formalin at 4 °C overnight, then stored in 70% ethanol at 4 °C for 12 hours to promote dehydration. Hearts were then made transparent using a clearing agent (methyl salicylate), so the vessels could be visualized in the intact heart, using a stereoscopic microscope, without the need for sectioning. LCA = left coronary artery; RCA = right coronary artery. Red arrows indicate localized vasospasms. (Fukamizu *et al* unpublished).

5.4 Methods

5.5 Preparation of the Experimental Model

All procedures were approved in advance by the SPring-8 Animal Experiment Review Committee and the National Cerebral and Cardiovascular Center Animal Experiment Committee. Our colleagues from the University of Tsukuba developed a mouse model that overexpresses the APJ receptor on VSM cells (SMA-APJ mouse) (19). Briefly, to generate the transgenic mouse, the human genomic DNA containing the APJ gene locus was attached to the human smooth muscle α-actin promoter with a bovine growth hormone poly-A tail (Fig. 5.2). The linearized DNA was microinjected as a transgene into the pronuclei of eggs from imprinting control region (ICR) mice.

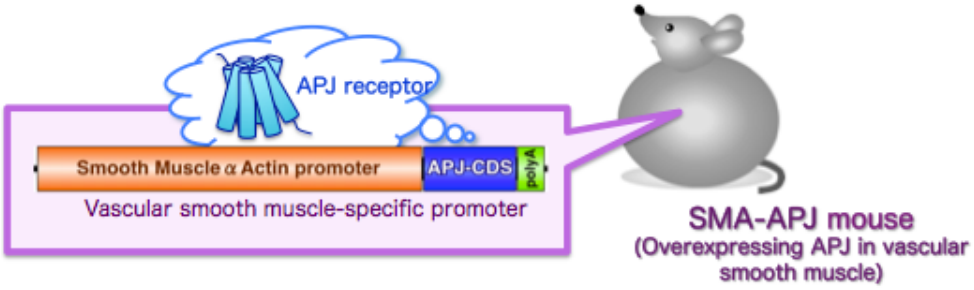

Figure 5.2 Schematic diagram of the gene locus in the mouse model that overexpresses the APJ receptor. The genomic DNA containing the APJ gene locus was attached to the human smooth muscle α-actin promoter with a bovine growth hormone poly-A tail (19). CDS = protein coding DNA sequences, SMA = smooth muscle α-actin.

Male SMA-APJ and control WT mice (14 weeks old) were bred by our colleagues and delivered by courier to the Biomedical Animal Holding Facility of SPring-8 prior to the start of angiography experiments.

Experimental treatment groups:

1. Wild type mice (WT, n = 4)
2. SMA-APJ transgenic mice (TG, n = 4)

5.5.1 Surgical Preparation for Angiography

All coronary microangiography was conducted at Beamline 28B2 of SPring-8, the Synchrotron Radiation Research Institute in Hyogo, Japan. Microangiography was performed with synchrotron radiation to visualize the coronary circulation *in vivo* as has been described in detail previously (8). Imaging of the coronary circulation was performed with monochromatic synchrotron radiation at 33.2 keV, just above the iodine K-edge energy for producing maximal absorption of the iodine contrast agent in the vascular lumen.

Each mouse was anesthetized with sodium pentobarbital (1:10 dilution with sodium lactate, 50 mg/kg) intraperitoneally, and supplementary doses of anesthetic (~20 mg/kg/h) were periodically administered to maintain the level of anesthesia. After induction of anesthesia, the mice were intubated for artificial ventilation (~40% oxygen) with a MiniVent rodent ventilator (Hugo-Sachs, Germany). A rectal thermistor coupled with a thermostatically controlled heating pad was used to maintain body temperature at approximately 37 °C.

An Instech-Solomon catheter (Instech-Solomon, Plymouth Meeting, PA, United States) was used to cannulate the right carotid artery. The tip of the catheter was positioned close to left descending coronary artery, near the aortic valve, to facilitate selective injection of contrast media into the coronary circulation. Arterial pressure and heart rate were also recorded from the Instech-Solomon catheter inserted into the carotid artery. The analogue arterial pressure signal was digitized at 1000 Hz and recorded by CHART software (Version 5.4.1, AD Instruments, NSW, Australia) to allow determination of mean arterial pressure and heart rate. Body fluids were maintained during the period of imaging by infusion of sodium lactate (Otsuka, Tokyo, Japan) via a catheter inserted into the jugular vein.

5.5.2 Protocol for Angiography

After the preparatory surgery, each animal was moved into the X-ray hutch for coronary microangiography. The mouse was placed in a supine position in front of the X-ray detector in the path of the X-ray beam. Iodinized contrast medium (Iomeron 350, Bracco-Eisai Co. Ltd., Tokyo, Japan) was delivered through the carotid artery using a PHD200 syringe pump (0.1-0.2 ml bolus 11 ml/min, Harvard Apparatus, Holliston, Massachusetts, United States). Each cine recording of 100 frames, at 30 frames/s, was recorded on a SATICON detector (Hitachi Denshi Techno-System, Ltd., Tokyo, Japan) with 1.5-2 ms/frame shutter open time. Images with 1024 x 1024 pixel format and 10-bit resolution were recorded from a field of view of approximately 10 mm^2.

Baseline vessel calibers, across the first three branching orders of arterial vessels in each mouse, were determined after 5 minutes of vehicle infusion (sodium lactate 0.2 ml/h; baseline). After the baseline imaging, each mouse received an intraperitoneal injection of apelin (296 µg/kg). Contrast images were again recorded 12 minutes after injection of apelin.

5.5.3 Statistical Analysis

Data are expressed as mean ± SEM unless otherwise stated. For each individual mouse the mean vessel ID and vessel number of each branching order was used for group comparisons. Two-way ANOVA was used to assess the main effects of genotype and branching order and their interaction. Student's unpaired t-test was carried out to assess and difference between baseline and after injection of apelin. GraphPad Prism (GraphPad Software, Inc., La Jolla, CA, USA) was used for all analysis. Two-tailed $P \leq 0.05$ was considered statistically significant.

5.6 Results

5.6.1 General Characteristics

Body weight (BW, g) was measured on the day of experiment prior to synchrotron angiography. TG mice weighed 22 ± 4 % less than WT mice (Fig. 5.3).

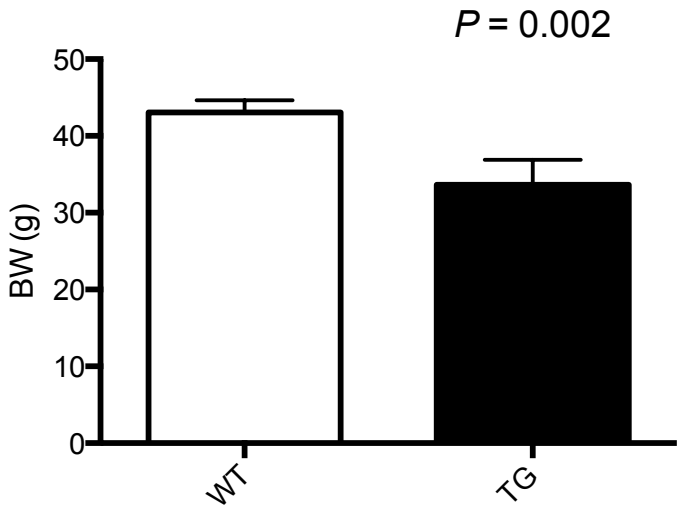

Figure 5.3 Body weight in the two groups. WT = wild type mice and TG = mice with overexpression of APJ. Columns and error bars show mean ± SEM of n = 4 in each group. The *P* value is the outcome of an unpaired t-test.

5.6.2 Baseline Vessel Number and Vessel Caliber

Typical angiograms show that coronary vessels in the two groups of mice responded differently after administration of apelin (Fig. 5.4). The number of visualized vessels progressively increased across order 1-3 (Fig. 5.5). More 3rd order vessels were visible in TG than WT mice (55 ± 16 %). As expected, vessel ID at baseline progressively decreased with branching order. The ID of vessels during the baseline period was similar in the two groups of mice (Fig. 5.5).

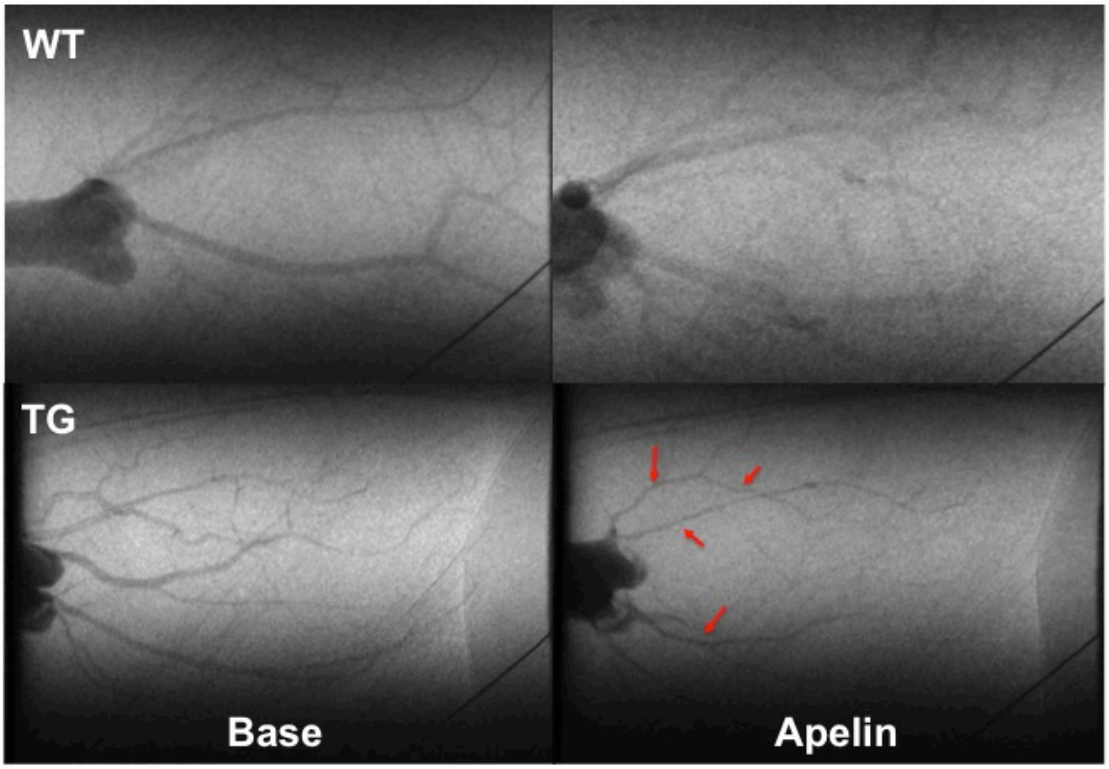

Figure 5.4 Representative synchrotron radiation angiograms of the coronary vasculature. Images were captured during infusion of the vehicle and 12 minutes after apelin injection (296 µg/kg). The two groups of mice were wild type mice (WT) and transgenic mice (TG). Horizontally aligned images are from the same mouse. Red arrows = vasoconstriction.

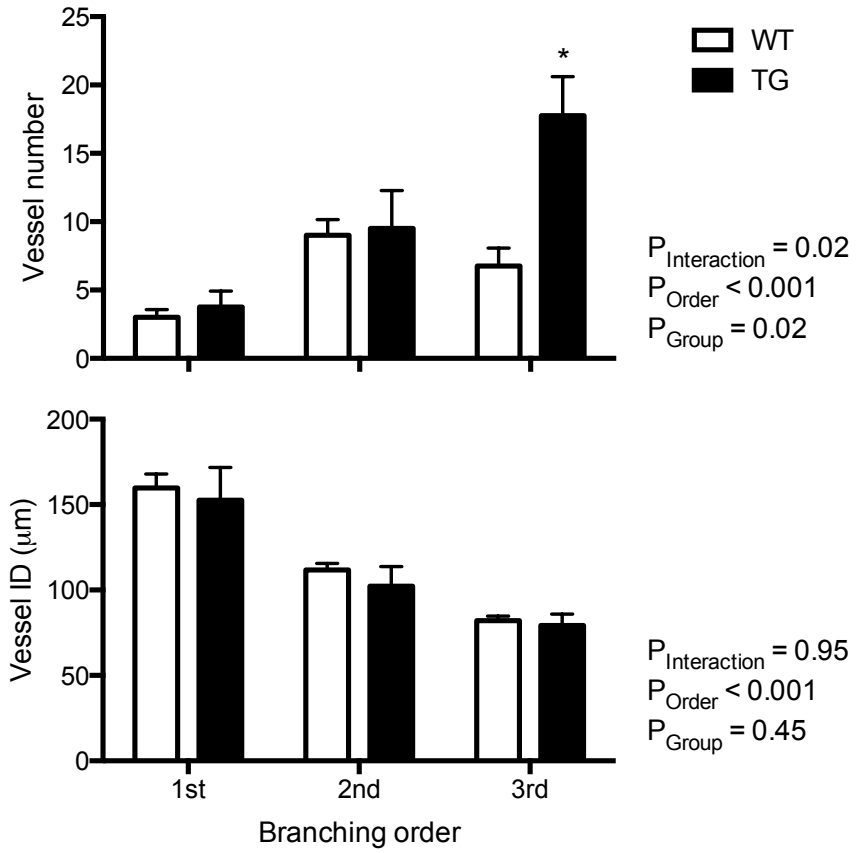

Figure 5.5 The number of visible vessels and internal diameter (ID) in the field of view categorized by branching order in two groups. WT = wild type mice and TG = mice with overexpression of APJ. Data are shown as mean ± SEM. *P* values are the outcomes of two-way ANOVA. * denotes $P \leq 0.05$ vs WT by unpaired t-test.

5.6.3 Vessel Recruitment and Vessel Caliber in Response to Apelin

We examined relative change in the number and caliber of vessels in response to administration of apelin. In WT mice, administration of apelin was followed by little or no change in the number of observable vessels or their caliber. In contrast, in the TG mice, administration of apelin was followed by a -38.6 ± 6.6 % reduction in the number of observable 3rd order vessels and vasoconstriction in 1st (-18.8 ± 6.2 % reduction in diameter), 2nd (-18.0 ± 4.5 %) and 3rd (-11.0 ± 3.8 %) order vessels (Fig. 5.6).

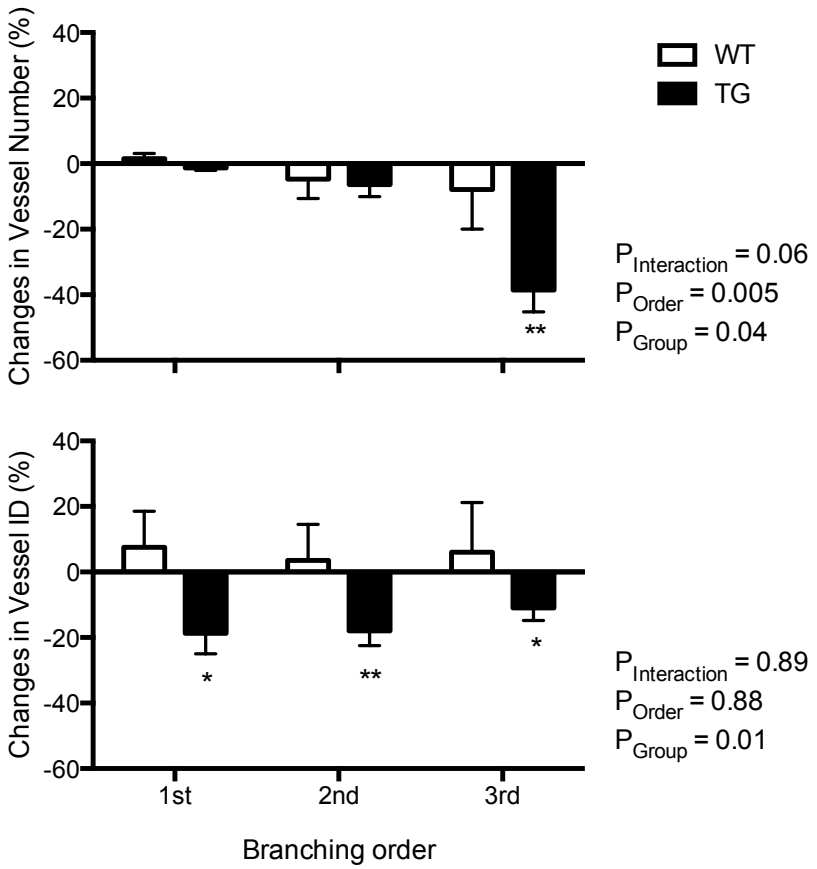

Figure 5.6 Relative change in vessel number and vessel caliber after administration of apelin in wild type mice and transgenic mice. WT = wild type mice and TG = mice with overexpression of APJ. Data are presented as mean ± SEM, n = 4 in each group. * denotes $P \leq 0.05$ and ** denotes $P \leq 0.01$ vs baseline by paired t-test. *P* values are the outcomes of two-way ANOVA.

5.7 Discussion

In the current *in vivo* study, we found that apelin induced marked vasoconstriction in the coronary circulation of mice that overexpress APJ in VSM, but not in WT mice. However, the baseline caliber of coronary vessels in mice that overexpress APJ in VSM was not appreciably different from that of WT mice. These results indicate that apelin and its receptor APJ may play little role in the tonic physiological regulation of coronary vascular tone. However, apelin and its receptor APJ may contribute to the control of coronary vascular tone under pathophysiological conditions associated with upregulation of APJ and increased circulating levels of apelin. Such conditions include atherosclerosis, stenosis of the calcified aortic valve and ischemic heart failure HF (1, 5, 21). Thus, antagonists of APJ might be beneficial in the treatment of these cardiovascular diseases.

Our current findings indicate that apelin and its receptor make little contribution in the acute physiological regulation of coronary vascular tone *in vivo*. Nonetheless, several previous studies have provided evidence that APJ also has the potential to mediate the phosphorylation of endothelial nitric oxide synthase (eNOS) in both mice and rats and thus has the potential to contribute to endothelium-dependent vasodilation (7, 25). Others have shown that apelin primarily functions as a regulator of vascular tone via APJ receptors in VSM (5, 12). Taken together with our current results, these previous findings indicate that apelin has opposing effects on arterial blood vessels via endothelium-mediated vasodilation and VSM-dependent vasoconstriction. Thus, we cannot exclude the possibility that the absence of an effect of apelin on coronary vascular tone in WT mice reflects a balance between endothelium-mediated vasodilation and VSM-dependent vasoconstriction.

In the current study, marked vasoconstriction in the coronary circulation, induced by administration of apelin, was apparent in mice that overexpress APJ in VSM. This could indicate that vasoconstrictor responses to apelin can only be observed under conditions of artificially induced upregulation of the APJ receptor. However, upregulation of APJ in VSM can occur in response to endothelial damage (26). Constriction of an artery leads to decreased perfusion of the vessel, and thus to tissue ischemia and potentially necrosis (3, 11, 18). Myocardial ischemia can lead to angina, MI, HF and even death (18). Strategies for treatment for these cardiovascular

diseases should not only include the use of direct vasodilators, but should also include use of antagonists of constrictor factors. Thus, antagonists of APJ may be beneficial in the treatment of ischemic heart disease with coronary spasm.

Interestingly, our data provide evidence that chronic overexpression of APJ on the VSM may have led to angiogenesis. That is, we observed considerably more 3rd order vessels in mice that over-express APJ than in WT mice. However, the ID of coronary arterial vessels was similar in mice that overexpressed APJ on VSM and WT mice. Taken at face value, these observations may indicate that chronic upregulation APJ in VSM leads to angiogenesis in the coronary circulation but not enlargement of the caliber of vessels. This explanation is feasible, since apelin is considered to be an angiogenic factor (9, 10). Furthermore, the apelin/APJ pathway has been shown to regulate proliferation and assembly of vascular cells during embryogenesis in mice (15). In contrast to our current findings, a study performed by Kidoya et al in the dorsal skin in mice provided evidence that upregulation of APJ expression in endothelial cells induces vascular enlargement but not angiogenesis (14). Taken together with our current results, these previous findings indicate that apelin can have disparate effects on the formation of blood vessels, perhaps depending on the vascular territory being studied, the stage of development of the experimental animals being studied, and the experimental conditions. Perhaps APJ-receptors on the endothelium modulate vessel caliber, while APJ-receptors on VSM modulate angiogenesis. This proposition merits further investigation.

The two major limitations of our current pilot study should be acknowledged. Firstly, we did not examine the regulation of coronary vasodilatory function in these mice. Therefore, we do not know whether these vessels have normal vasomotor function. Secondly, a small number of mice was used for this study, due to their limited availability. In the future, we would like to examine endothelium-dependent and endothelium-independent vasodilator responses in these mice with a larger number of mice for each drug treatment utilizing infusions of acetylcholine and sodium nitroprusside.

To conclude, our current findings provide evidence that the apelin/APJ pathway on VSM leads to vasoconstriction and possibly also angiogenesis in the coronary circulation in mice. Future studies, that include an additional protocol to examine

vasodilatory function in these animals using synchrotron microangiography, would provide a more complete understanding of the role of the apelin/APJ pathway in regulation of the function of the coronary circulation.

5.8 Reference

1. **Atluri P, Morine KJ, Liao GP, Panlilio CM, Berry MF, Hsu VM, Hiesinger W, Cohen JE, and Joseph Woo Y**. Ischemic heart failure enhances endogenous myocardial apelin and APJ receptor expression. *Cell Mol Biol Lett* 12: 127-138, 2007.
2. **Chen MM, Ashley EA, Deng DX, Tsalenko A, Deng A, Tabibiazar R, Ben-Dor A, Fenster B, Yang E, and King JY**. Novel role for the potent endogenous inotrope apelin in human cardiac dysfunction. *Circulation* 108: 1432-1439, 2003.
3. **Fisher C, Kistler J, and Davis J**. Relation of cerebral vasospasm to subarachnoid hemorrhage visualized by computerized tomographic scanning. *J Neurosurg* 6: 1, 1980.
4. **Földes G, Horkay F, Szokodi I, Vuolteenaho O, Ilves M, Lindstedt KA, Mäyränpää M, Sármán B, Seres L, and Skoumal R**. Circulating and cardiac levels of apelin, the novel ligand of the orphan receptor APJ, in patients with heart failure. *Biochem Biophys Res Commun* 308: 480-485, 2003.
5. **Hashimoto T, Kihara M, Ishida J, Imai N, Yoshida S, Toya Y, Fukamizu A, Kitamura H, and Umemura S**. Apelin stimulates myosin light chain phosphorylation in vascular smooth muscle cells. *Arterioscler Thromb Vasc Biol* 26: 1267-1272, 2006.
6. **Hosoya M, Kawamata Y, Fukusumi S, Fujii R, Habata Y, Hinuma S, Kitada C, Honda S, Kurokawa T, and Onda H**. Molecular and functional characteristics of APJ Tissue distribution of mRNA and interaction with the endogenous ligand apelin. *J Biol Chem* 275: 21061-21067, 2000.
7. **Ishida J, Hashimoto T, Hashimoto Y, Nishiwaki S, Iguchi T, Harada S, Sugaya T, Matsuzaki H, Yamamoto R, Shiota N, Okunishi H, Kihara M, Umemura S, Sugiyama F, Yagami K, Kasuya Y, Mochizuki N, and Fukamizu A**. Regulatory roles for APJ, a seven-transmembrane receptor related to angiotensin-type 1 receptor in blood pressure in vivo. *J Biol Chem* 279: 26274-26279, 2004.
8. **Jenkins MJ, Edgley AJ, Sonobe T, Umetani K, Schwenke DO, Fujii Y, Brown RD, Kelly DJ, Shirai M, and Pearson JT**. Dynamic synchrotron imaging of diabetic rat coronary microcirculation in vivo. *Arterioscler Thromb Vasc Biol* 32: 370-377, 2012.
9. **Kälin RE, Kretz MP, Meyer AM, Kispert A, Heppner FL, and Brändli AW**. Paracrine and autocrine mechanisms of apelin signaling govern embryonic and tumor angiogenesis. *Dev Biol* 305: 599-614, 2007.
10. **Kasai A, Shintani N, Oda M, Kakuda M, Hashimoto H, Matsuda T, Hinuma S, and Baba A**. Apelin is a novel angiogenic factor in retinal endothelial cells. *Biochem Biophys Res Commun* 325: 395-400, 2004.
11. **Kassell NF, Peerless SJ, Durward QJ, Beck DW, Drake CG, and Adams HP**. Treatment of ischemic deficits from vasospasm with intravascular volume expansion and induced arterial hypertension. *J Neurosurg* 11: 337, 1982.
12. **Katugampola SD, Maguire JJ, Matthewson SR, and Davenport AP**. [125I]-(Pyr1) Apelin-13 is a novel radioligand for localizing the APJ orphan receptor in human and rat tissues with evidence for a vasoconstrictor role in man. *Br J Pharmacol* 132: 1255-1260, 2001.
13. **Kawamata Y, Habata Y, Fukusumi S, Hosoya M, Fujii R, Hinuma S, Nishizawa N, Kitada C, Onda H, and Nishimura O**. Molecular properties of apelin: tissue distribution and receptor binding. *Biochim Biophys Acta* 1538: 162-171, 2001.
14. **Kidoya H, Naito H, and Takakura N**. Apelin induces enlarged and nonleaky blood vessels for functional recovery from ischemia. *Blood* 115: 3166-3174, 2010.
15. **Kidoya H, Ueno M, Yamada Y, Mochizuki N, Nakata M, Yano T, Fujii R, and Takakura N**. Spatial and temporal role of the apelin/APJ system in the caliber size regulation of blood vessels during angiogenesis. *EMBO J* 27: 522-534, 2008.

16. **Kleinz MJ, Skepper JN, and Davenport AP**. Immunocytochemical localisation of the apelin receptor, APJ, to human cardiomyocytes, vascular smooth muscle and endothelial cells. *Regul Pept* 126: 233-240, 2005.
17. **Lee DK, Cheng R, Nguyen T, Fan T, Kariyawasam AP, Liu Y, Osmond DH, George SR, and O'Dowd BF**. Characterization of apelin, the ligand for the APJ receptor. *J Neurochem* 74: 34-41, 2001.
18. **Maseri A, L'Abbate A, Baroldi G, Chierchia S, Marzilli M, Ballestra AM, Severi S, Parodi O, Biagini A, and Distante A**. Coronary vasospasm as a possible cause of myocardial infarction. *N Engl J Med* 299: 1271-1277, 1978.
19. **Murata K, Ishida J, Ishimaru T, Mizukami H, Hamada J, Saito C, and Fukamizu A**. Lactation Is a Risk Factor of Postpartum Heart Failure in Mice with Cardiomyocyte-specific Apelin Receptor (APJ) Overexpression. *J Biol Chem* 291: 11241-11251, 2016.
20. **O'Dowd BF, Heiber M, Chan A, Heng H, Tsui L-C, Kennedy JL, Shi X, Petronis A, George SR, and Nguyen T**. A human gene that shows identity with the gene encoding the angiotensin receptor is located on chromosome 11. *Gene* 136: 355, 1993.
21. **Peltonen T, Napankangas J, Vuolteenaho O, Ohtonen P, Soini Y, Juvonen T, Satta J, Ruskoaho H, and Taskinen P**. Apelin and its receptor APJ in human aortic valve stenosis. *J Heart Valve Dis* 18: 644-652, 2009.
22. **Pitkin SL, Maguire JJ, Kuc RE, and Davenport AP**. Modulation of the apelin/APJ system in heart failure and atherosclerosis in man. *Br J Pharmacol* 160: 1785-1795, 2010.
23. **Reaux A, De Mota N, Skultetyova I, Lenkei Z, El Messari S, Gallatz K, Corvol P, Palkovits M, and Llorens-Cortes C**. Physiological role of a novel neuropeptide, apelin, and its receptor in the rat brain. *J Neurochem* 77: 1085-1096, 2001.
24. **Tatemoto K, Hosoya M, Habata Y, Fujii R, Kakegawa T, Zou M-X, Kawamata Y, Fukusumi S, Hinuma S, and Kitada C**. Isolation and characterization of a novel endogenous peptide ligand for the human APJ receptor. *Biochem Biophys Res Commun* 251: 471-476, 1998.
25. **Tatemoto K, Takayama K, Zou MX, Kumaki I, Zhang W, Kumano K, and Fujimiya M**. The novel peptide apelin lowers blood pressure via a nitric oxide-dependent mechanism. *Regul Pept* 99: 87-92, 2001.
26. **Wang L-Y, Zhang D-L, Zheng J-F, Zhang Y, Zhang Q-D, and Liu W-H**. Apelin-13 passes through the ADMA-damaged endothelial barrier and acts on vascular smooth muscle cells. *Peptides* 32: 2436-2443, 2011.

CHAPTER 6

Chronic Intermittent Hypoxia Accelerates Coronary Microcirculatory Dysfunction In Insulin-resistant Goto-Kakizaki Rats

Am J Physiol Regul Integr Comp Physiol 311: R426–R439, 2016.
First published June 1, 2016; doi:10.1152/ajpregu.00112.2016.

Chronic intermittent hypoxia accelerates coronary microcirculatory dysfunction in insulin-resistant Goto-Kakizaki rats

Yi Ching Chen,[1] Tadakatsu Inagaki,[2] Yutaka Fujii,[2] Daryl O. Schwenke,[3] Hirotsugu Tsuchimochi,[2] Amanda J. Edgley,[1,4] Keiji Umetani,[5] Yuan Zhang,[4] Darren J. Kelly,[4] Misa Yoshimoto,[2] Hisashi Nagai,[6] Roger G. Evans,[1] Ichiro Kuwahira,[7] Mikiyasu Shirai,[2]* and James T. Pearson[1,8,9]*

[1]*Cardiovascular Disease Program, Biosciences Discovery Institute and Department of Physiology, Monash University, Melbourne, Australia;* [2]*Department of Cardiac Physiology, National Cerebral and Cardiovascular Center Research Institute, Suita, Japan;* [3]*Department of Physiology-Heart Otago, University of Otago, Dunedin, New Zealand;* [4]*St Vincent's Hospital, University of Melbourne, Melbourne, Australia;* [5]*Japan Synchrotron Radiation Research Institute, Harima, Japan;* [6]*Departments of Clinical Laboratory Medicine and Forensic Medicine, University of Tokyo, Tokyo, Japan;* [7]*Department of Pulmonary Medicine, Tokai University Tokyo Hospital, Tokai University, Tokyo, Japan;* [8]*Monash Biomedical Imaging Facility, Melbourne, Australia; and* [9]*Australian Synchrotron, Melbourne, Australia*

Submitted 18 March 2016; accepted in final form 30 May 2016

Chen YC, Inagaki T, Fujii Y, Schwenke DO, Tsuchimochi H, Edgley AJ, Umetani K, Zhang Y, Kelly DJ, Yoshimoto M, Nagai H, Evans RG, Kuwahira I, Shirai M, Pearson JT. Chronic intermittent hypoxia accelerates coronary microcirculatory dysfunction in insulin-resistant Goto-Kakizaki rats. *Am J Physiol Regul Integr Comp Physiol* 311: R426–R439, 2016. First published June 1, 2016; doi:10.1152/ajpregu.00112.2016.—Chronic intermittent hypoxia (IH) induces oxidative stress and inflammation, which impair vascular endothelial function. Long-term insulin resistance also leads to endothelial dysfunction. We determined, in vivo, whether the effects of chronic IH and insulin resistance on endothelial function augment each other. Male 12-wk-old Goto-Kakizaki (GK) and Wistar control rats were subjected to normoxia or chronic IH (90-s N_2, 5% O_2 at nadir, 90-s air, 20 cycles/h, 8 h/day) for 4 wk. Coronary endothelial function was assessed using microangiography with synchrotron radiation. Imaging was performed at baseline, during infusion of acetylcholine (ACh, 5 $\mu g \cdot kg^{-1} \cdot min^{-1}$) and then sodium nitroprusside (SNP, 5 $\mu g \cdot kg^{-1} \cdot min^{-1}$), after blockade of both nitric oxide (NO) synthase (NOS) with N^{ω}-nitro-L-arginine methyl ester (L-NAME, 50 mg/kg) and cyclooxygenase (COX, meclofenamate, 3 mg/kg), and during subsequent ACh. In GK rats, coronary vasodilatation in response to ACh and SNP was blunted compared with Wistar rats, and responses to ACh were abolished after blockade. In Wistar rats, IH blunted the ability of ACh or SNP to increase the number of visible vessels. In GK rats exposed to IH, neither ACh nor SNP were able to increase visible vessel number or caliber, and blockade resulted in marked vasoconstriction. Our findings indicate that IH augments the deleterious effects of insulin resistance on coronary endothelial function. They appear to increase the dependence of the coronary microcirculation on NO and/or vasodilator prostanoids, and greatly blunt the residual vasodilation in response to ACh after blockade of NOS/COX, presumably mediated by endothelium-derived hyperpolarizing factors.

intermittent hypoxia; insulin resistance; microangiography; EDHF

SLEEP APNEA SYNDROME (SAS) is a sleep disorder characterized by repeated episodes of apnea during sleep and is present in ~4% of the general population (30). SAS is highly prevalent in patients with obesity and type-2 diabetes (45). The prevalence of SAS in the general population is likely to increase in the future due to the increasing prevalence of obesity and type-2 diabetes (30). Chronic intermittent hypoxia (IH) is an important factor in the development of SAS (2). The consequences of chronic IH include an increase in inflammation and oxidative stress in multiple organs, necrosis, apoptosis, metabolic dysfunction, and endothelial dysfunction leading to elevated blood pressure, arrhythmias, and increased vulnerability to myocardial infarction (17, 24, 35). While SAS is characterized by the presence of chronic IH and hypercapnia, the contribution of chronic IH to vascular dysfunction is thought to be large (2). Many patients with SAS develop heart failure due to suspected changes in β-adrenergic and nitric oxide (NO) signaling. SAS is thought to promote atherosclerosis, which appears to be exacerbated when combined with metabolic syndrome and causes more severe vascular dysfunction than in patients without metabolic syndrome, possibly as a result of greater reductions in NO bioavailability due to elevated oxidative stress (18, 26, 40). Whether chronic exposure to IH alone drives exacerbation of vascular dysfunction in the presence of metabolic syndrome remains to be determined.

IH induces oxidative stress through the production of reactive oxygen species (ROS) and activation of inflammatory mediators, in particular the redox-sensitive transcription factor NF-κB, which impairs vascular endothelial function and promotes atherogenesis (19). Factors that have been shown to drive endothelial dysfunction in chronic IH include both a decline in vasodilator production and an increase in vasoconstrictor tone (41, 44). Oscillations in arterial oxygen levels also increase ROS and reactive nitrogen species, which promote endothelial dysfunction in part through NF-κB, and in part through decreased expression of endothelial NO synthase (NOS) and consequently decreased NO bioavailability (43). In addition, increased production of vascular adhesion molecules and increased sensitivity to endothelin-1 has also been observed in response to IH (1, 44). Impaired endothelium-mediated relaxation after IH is frequently attributed to decreased NO-mediated vasodilation and increased sensitivity to vasoconstrictors (41, 44, 46). Whether chronic IH evokes changes in the residual vasodilator response to endothelial stimulation, presumed to

* M. Shirai and J. T. Pearson contributed equally to this work.

Address for reprint requests and other correspondence: J. T. Pearson, Dept. of Cardiac Physiology, National Cerebral and Cardiovascular Center Research Institute, 5-7-1 Fujishirodai Suita-shi 565-8565, Japan (e-mail: jpearson@ncvc.go.jp).

be chiefly mediated by endothelium-derived hyperpolarization factor (EDHF), has not been investigated.

Other adverse effects of chronic IH include metabolic dysregulation. It has been shown that increased ROS causes apoptosis of pancreatic β-cells and reduces insulin sensitivity (20, 31). Long-term insulin resistance also leads to endothelial dysfunction (3, 39). Therefore it is of interest to determine whether the effects of exposure to chronic IH and insulin resistance augment each other, leading to the exacerbation of endothelial dysfunction and acceleration towards a state of diabetic heart failure.

In the current study, we tested the hypothesis that the onset of coronary vascular dysfunction in insulin-resistant rats is accelerated by medium-term exposure to severe chronic IH. The Goto-Kakizaki (GK) rat is a nonobese model of Type-2 diabetes, derived from an inbred strain of Wistar rats selected for glucose intolerance (14). We therefore investigated the effects of IH for 4 wk in 16-wk-old male GK rats and aged-matched Wistar control rats. Coronary endothelial function was assessed using microangiography with synchrotron radiation. It is well established that coronary blood flow is determined by the resistance of microvessels, including small arteries and large arterioles, and therefore the internal diameter (ID) of these vessels. However, agonist-mediated flow increases can evoke local dilation responses (caliber changes) and/or an increase in the number of perfused vessels, which is primarily the result of conducted dilation. Therefore, to assess local changes in dilation we measured vessel ID. To assess global perfusion changes that result from conducted dilation we counted the number of angiographically visible vessels as an index of the spread of dilation along vessel segments, which results in a reduction of microvessel resistance and the opening of further visible vessel branches. Further, we examined the effect of chronic IH on cardiac remodeling with immunohistochemistry.

METHODS

Animals. All experiments were approved by the SPring-8 and the National Cerebral and Cardiovascular Center Animal Ethics Committees and conducted in accordance with the guidelines of the Physiological Society of Japan. Male Wistar ($n = 14$) and GK ($n = 14$) rats (12 wk old) were housed in groups in acrylic chambers. Rats were exposed to either continuous normoxia (21% oxygen) or IH (cycles of 5% O_2 at the nadir of N_2 exposure for 90 s followed by 90 s of normoxia, for 8 h/day) for 4 wk (22, 37). This protocol results in severe hypoxemia (Pa_{O_2} of 25 mmHg) and transient hypocapnia (Pa_{CO_2} of 18 mmHg) and acute respiratory alkalosis (pH ~7.6) during the hypoxic period of each cycle (22). Microangiogram quality was not suitable for analysis in 3 rats and was not included in the analyses (final $n = 6$ and 7 for normoxia and IH treated Wistar, $n = 5$ and 7 for normoxia and IH treated GK rats, respectively).

Microangiography with synchrotron radiation. All coronary microangiography was conducted at Beamline 28B2 of SPring-8, the Synchrotron Radiation Research Institute in Hyogo, Japan. Microangiography was performed with synchrotron radiation to visualize the coronary circulation in vivo and has been described in detail previously (16, 34). Imaging of the coronary circulation was performed with monochromatic synchrotron radiation at 33.2 keV, just above the iodine K-edge energy for producing maximal absorption contrast of the iodine contrast agent in the vascular lumen.

Surgical preparation. Rats were anesthetized with pentobarbital sodium (50 mg/kg ip). Supplementary doses of anesthetic (~20 $mg \cdot kg^{-1} \cdot h^{-1}$) were periodically administered to maintain the level of anesthesia. After inducing anesthesia, the rats were intubated by tracheotomy for artificial ventilation with a rodent ventilator (tidal volume = 1 ml/100 g body wt, 70 strokes/min, ~40% oxygen, Shinano, Tokyo). A rectal thermistor coupled with a thermostatically controlled heating pad was used to maintain body temperature at ~37°C.

A 20-gauge Angiocath catheter (Becton Dickinson, Sandy, UT) was used to cannulate the right carotid artery. The tip of the cannula was positioned close to the left descending coronary artery near the aortic valve for selective angiography of the coronary circulation (16). Arterial pressure and heart rate were recorded from a catheter filled with heparinized saline (12 U/ml) inserted into the femoral artery, and connected to a disposable transducer (MLT0699, AD Instruments, NSW, Australia). The analog arterial pressure signal was digitized at 1,000 Hz and recorded by CHART software (v5.4.1, AD Instruments, NSW, Australia) to determine mean arterial pressure and heart rate. Body fluid was maintained during the period of imaging by sodium lactate (Otsuka, Tokyo) infused via a catheter inserted into the jugular vein (3 ml/h). Drug infusions were also delivered via the jugular vein catheter.

Angiography protocol. After the preparatory surgery, each animal was moved into the X-ray hutch at BL28B2 for coronary microangiography (16). The rat was placed in a supine position in front of the X-ray detector in the path of the X-ray beam. Iodinized contrast medium (Iomeron 350, Bracco-Eisai, Tokyo) was delivered through the carotid artery using a high-speed injector (0.3–0.5 ml bolus, ~11 ml/s, Nemoto Kyorindo, Tokyo). The ventilator was turned off for a period of ~3 s immediately before the start of each cine recording of 100 frames at 30 frames/s recorded on a SATICON detector (Hitachi Denshi Techno-System, Tokyo) with 1.5–2 ms/frame shutter open time. Images with 1,024 × 1,024 pixel format and a 10-bit resolution were recorded from a ~10 mm^2 field of view. Approximately 10 min was allowed between each imaging sequence for renal clearance of the contrast agent.

Cine images of the coronary circulation were acquired at the end of a 5-min infusion of vehicle (sodium lactate 3 ml/h), acetylcholine (ACh; Ovisot, Daiichi Sankyo, Japan, 5 $\mu g \cdot kg^{-1} \cdot min^{-1}$), and sodium nitroprusside (SNP, Sigma-Aldrich, 5 $\mu g \cdot kg^{-1} \cdot min^{-1}$). The NOS inhibitor N^{ω}-nitro-L-arginine methyl ester (L-NAME, Sigma-Aldrich, 50 mg/kg) and the cyclooxygenase (COX) inhibitor sodium meclofenamate (Meclo, Sigma-Aldrich, 3 mg/kg) were then administered and a repeat cine sequence recorded during a vehicle infusion 30 min later. Responses to an infusion of ACh (5 $\mu g \cdot kg^{-1} \cdot min^{-1}$) were then reassessed during NOS/COX blockade. At the end of the experiments, rats were killed by overdose with pentobarbital sodium, and their hearts were removed, dissected into left and right ventricles, weighed and then fixed in 4% buffered paraformaldehyde.

Assessment of vessel caliber and vessel number. ImageJ (ver. 1.41, NIH, Bethesda, MD) was used to identify coronary vessels and determine their caliber. Vessels were labeled and classified according to branching orders from the first-order main segment. The visible vessel number for each branching order and the internal diameter (ID) of each vessel were determined from a single field of view for all cine sequences (16). The ID of each vessel was measured repeatedly and averaged over 15 consecutive frames.

Histology and immunohistochemistry. Rat hearts were fixed with paraformaldehyde, and stored in 70% ethanol and later embedded in paraffin. Paraffin sections (4 μm thick) were then stained with picrosirus red to examine the extent of fibrosis. All non-round vessels were excluded from analysis. Immunohistochemical staining with the endothelial cell marker isolectin B4 (Vector Laboratories, Burlingame, CA; diluted 1:100) was performed to assess capillary density (16). Capillary density was evaluated by histological examination of the myocardium to detect positively stained endothelial cells from 10 nonoverlapping fields randomly selected from within two sections of the subepicardial region of the middle of LV. After using proteinase K to digest the tissues for 4 min, sections were then incubated with biotinylated isolectin B4 at room temperature for 1 h, followed by streptavidin-HRP (Dako, Golstrup, Denmark) for 30 min and diaminobenzidine (Dako) as described previously (16). An Aperio

ScanScope XT Slide Scanner (Aperio Technologies) system was used to capture digital images with a 20× objective. Quantification was performed automatically with Aperio Imagescope (v11.0.2.725, Aperio Technologies) using the Positive Pixel Count v9 algorithm (Aperio Technologies) for perivascular fibrosis and capillary density (9).

Statistical analysis. Data are expressed as means ± SE unless otherwise stated, and *n* represents the number of rats in each group. For each individual rat a within-rat mean vessel ID and vessel number for each branching order was calculated and the between-rat means were then used for group comparisons. Three-way ANOVA was used to determine differences between treatments and strains in different branching orders or during the various drug infusions (Systat 13, Systat Software, San Jose, CA). Two-way ANOVA was carried out to assess differences between and within groups, and Student's paired *t*-test was used to access the difference between baseline and drug infusion using GraphPad Prism (GraphPad Software, La Jolla, CA). Two-tailed $P < 0.05$ was considered statistically significant.

RESULTS

General characteristics. Body weight and nonfasted blood glucose were measured on the day of experiment prior to microangiography. GK rats were on average 13.6% heavier and had greater blood glucose concentration than Wistar rats. Rats treated with IH were lighter than rats treated with normoxia (Table 1). The deficit in body weight associated with IH was greater in GK rats (−13.6%) than Wistar rats (−6.8%). GK rats also had greater left ventricular mass (22.6%) and right ventricular mass (38.1%) than the Wistar rats (Table 1). There was no apparent impact of IH on blood glucose concentration, or left or right ventricular mass (Table 1).

Histological changes in response to intermittent hypoxia. Exposing the rats to IH resulted in markedly greater capillary density score in the left ventricle than in rats subjected to normoxic conditions (Fig. 1*A*), but there was no apparent strain effect. The media-lumen ratio of coronary vessels (vessel ID of 1–100 μm) was on average 17% greater in GK rats than Wistar rats (Fig. 1*B*). Treatment with IH in both Wistar and GK rats resulted in significantly greater media-lumen ratio (15.6%) than in rats subjected to normoxic conditions.

Interstitial fibrosis in the left ventricle of GK rats was greater than in Wistar rats (Fig. 2*A*). Exposure to IH did not have any significant effect on the extent of interstitial fibrosis in either Wistar or GK rats. In contrast to interstitial fibrosis, there was more pronounced perivascular fibrosis when rats were exposed to IH than normoxia, but insulin resistance did not appreciably influence this effect (Fig. 2*B*).

Hemodynamic changes in response to drug infusion. Prior to any drug intervention, the mean arterial pressure (MAP) was not significantly different between Wistar and GK rats nor was it significantly different in rats exposed to IH compared with those exposed to normoxia (Table 2). Heart rate (HR) on the other hand showed a trend to be elevated only in Wistar rats subjected to IH than in those exposed to normoxia.

During infusion of either ACh or SNP, across the various treatment groups, MAP fell by 28–48 mmHg and HR fell by 16–34 beats/min relative to their baseline levels (Table 2). For the most part, these changes were similar in Wistar and GK rats. However, during infusion of ACh, MAP was appreciably higher in GK rats (109.8 ± 4.3 mmHg, averaged across rats exposed to normoxia and IH) than in Wistar rats (92.8 ± 5.4 mmHg, $P = 0.02$). Decreases in MAP observed during infusion of SNP were significantly smaller in GK rats than Wistar rats. Chronic IH was associated with a greater MAP and HR during ACh and SNP infusions than in rats subjected to normoxia.

HR was decreased markedly following NOS/COX blockade as we have previously observed in anesthetized rats (16). The magnitude of the decrease in HR was significantly smaller in GK rats than Wistar rats, and was largest in IH-treated Wistar rats. Upon infusion of ACh postblockade, MAP and HR decreased further in both Wistar and GK rats of both exposure groups (normoxia and IH). Nevertheless, in response to ACh infusion postblockade, MAP was markedly (17–30 mmHg) higher in GK rats than Wistar rats.

Baseline vessel number and internal diameter in normoxic and IH groups. Figure 3 shows typical angiograms of the coronary circulation in the four treatment groups at baseline and during drug administration. The number of visualized vessels progressively increased across orders 1–3, but fewer 4th-order vessels were observed than 3rd-order vessels (Fig. 4). Across all 4 orders, more vessels were visible in GK (34.2 ± 1.9) than Wistar rats (26.8 ± 2.2) for combined normoxic and IH groups ($P < 0.01$, Fig. 4). There was no apparent effect of IH on the number of visible vessels ($P = 0.18$). As expected, vessel ID at baseline progressively decreased with branching order ($P < 0.001$). The basal ID of vessels was similar in GK and Wistar rats and in rats subjected to IH compared with those subjected to normoxia (Fig. 4).

Perfused vessel number changes during drug stimulation in normoxic and IH rats. The number of angiographically visible arterial microvessels increased during ACh and SNP infusions in both Wistar and GK normoxic rat groups. However, IH greatly blunted this response in both strains. Only a small number of newly visualized arteries and large arterioles (1st- and 2nd-order branches) were seen during infusion of ACh and SNP (−2 to 2% change across all groups; Fig. 5). In contrast, ACh increased the number of visible 3rd- and 4th-order vessels in both Wistar and GK rats exposed to normoxia (mean response = 6.2 ± 6.3% vs. 16.2 ± 5.1%). These responses were abolished in rats exposed to IH (mean response = −2.8 ± 5.8% Wistar vs.

Table 1. *Characteristics of the rats in this study*

	Wistar		GK		*P*		
Variable	Normoxia	IH	Normoxia	IH	Treatment (Tr)	Strain (S)	Tr × S
BW, g	322 ± 6	300 ± 5	379 ± 2	333 ± 6	<0.001	<0.001	0.05
BG, mmol/l	7.1 ± 0.4	6.4 ± 0.4	10.9 ± 1.0	11.2 ± 0.6	0.70	<0.001	0.40
RLVW, g/kg BW	1.75 ± 0.04	1.74 ± 0.11	2.11 ± 0.06	2.15 ± 0.16	0.74	<0.001	0.59
RRVW, g/kg BW	0.29 ± 0.02	0.34 ± 0.03	0.40 ± 0.04	0.48 ± 0.04	0.07	0.002	0.53

Values are expressed as means ± SE, $n = 7$ in each group. IH, intermittent hypoxia; GK, Goto-Kakizaki rats; BW, body weight; BG, blood glucose; RLVW, relative left ventricle weight; RRVW. relative right ventricle weight. *P* values are the outcomes of 2-way ANOVA.

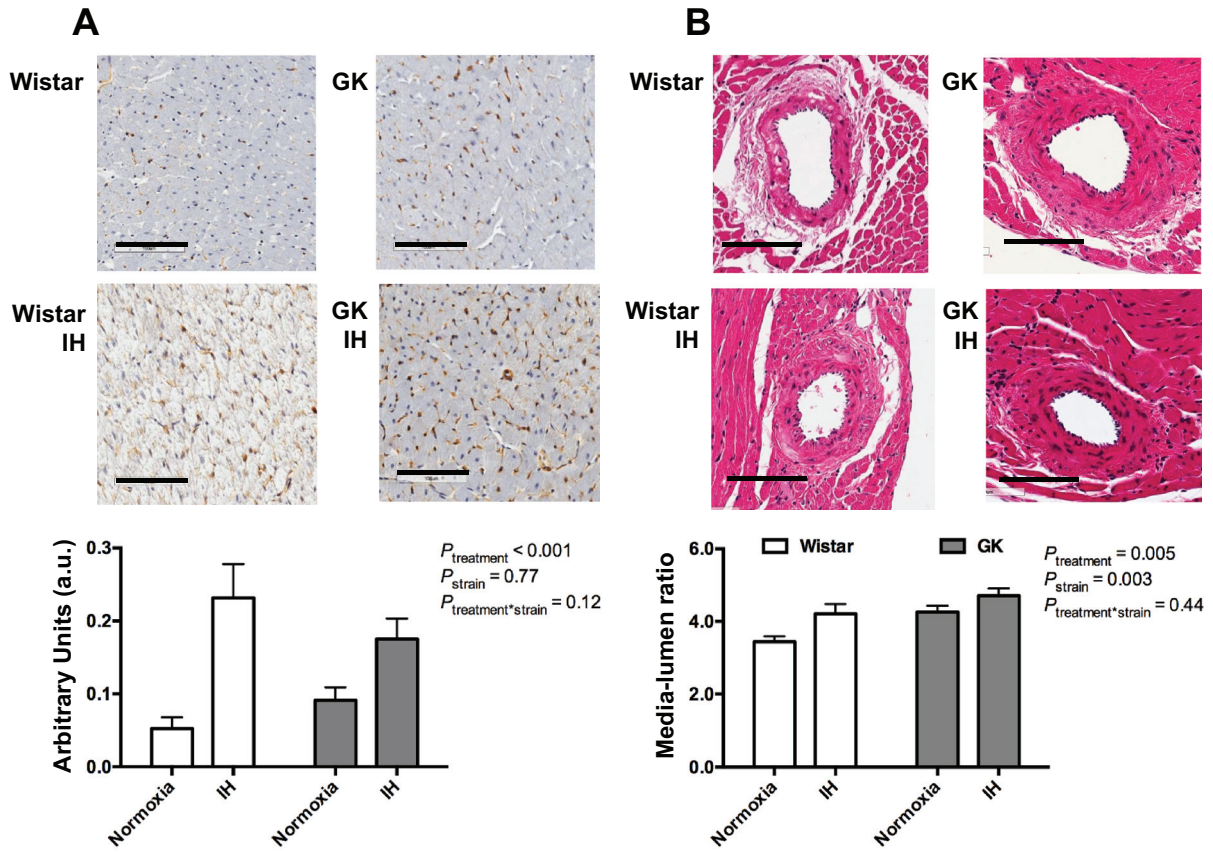

Fig. 1. Myocardial capillary density determined by isolectin β (*A*) and the media-lumen ratio (*B*) of arterial vessels 1–100 μm in Wistar (open bars) and Goto-Kakizaki (GK) rats (filled bars) subjected to either normoxia or intermittent hypoxia (IH). Values are presented as means ± SE; $n = 7$ in each group. *P* values are the outcomes of a 2-way ANOVA with factors strain, treatment, and their interaction. Black bar represents 100 μm.

−1.4 ± 3.8% GK, treatment $P = 0.002$, Fig. 6*A*). In general, SNP increased the number of visible 3rd- and 4th-order vessels in Wistar and GK rats exposed to normoxia (mean response = 12.1 ± 8.7% vs. 13.0 ± 6.9%), but reduced the number of visible vessels in the corresponding rats exposed to IH (mean response = −6.9 ± 4.8% Wistar vs. −5.0 ± 4.6% GK, treatment $P = 0.001$, Fig. 6*B*). Thus exposure to IH appears to greatly blunt the ability of both ACh and SNP to increase the number of angiographically detectable arterioles.

In Wistar rats exposed to normoxia, NOS/COX blockade had little effect on the number of visible arterial vessels across any branching order (Figs. 5 and 6), and the subsequent response to ACh infusion (mean response for 3rd and 4th orders = 29.4 ± 13.1%, Fig. 6). Similarly, NOS/COX blockade had little effect on the number of angiographically visible vessels in GK rats in general (Figs. 5 and 6), but there was a tendency for the number of visible 2nd-order vessels to be reduced ($P = 0.06$). ACh normalized visible 2nd-order vessel number in GK rats following NOS/COX blockade (Fig. 5*D*). Notably, NOS/COX blockade tended to reduce the number of perfused 2nd-, 3rd-, and 4th-order vessels more in IH rats, although this apparent effect was not statistically significant (mean response for both strains = −16.2 ± 3.5%, treatment $P = 0.08$, Fig. 5*C*). NOS/COX blockade blunted the ACh-mediated increase in vessel number in IH rats relative to normoxia rats (treatment $P = 0.003$), and tended to increase the reduction in 3rd-order vessels in GK rats exposed to IH (−15.6 ± 5.5%, branching order × strain $P = 0.08$).

Vessel caliber changes during drug stimulation in normoxic and IH rats. ACh increased the caliber of 1st-order conduit vessels, similarly in all four treatment groups (mean = 23.1 ± 3.6%; Fig. 7*A*). While a strong dilatory response to ACh was evident in all branching orders in Wistar rats, the increase in vessel caliber in GK rats was blunted in 3rd-order vessels (Fig. 8*A*). SNP evoked an increase in caliber that tended to decrease in relative magnitude with increasing branching order in Wistar and GK rats (strain $P = 0.02$, Figs. 7*B* and 8*B*). SNP increased the caliber of 3rd-order vessels in Wistar rats but not GK rats (Fig. 8*B*). Thus vasodilatation in response to SNP was in general blunted in GK rats compared with in Wistar rats. Interestingly, IH treatment per se did not blunt the increase in caliber in response to SNP in conduit or microvessels. In Wistar rats exposed to IH the dilatory response to SNP was robust (mean of all orders = 16.7 ± 4.2%). On the other hand, in GK rats exposed to IH, SNP did not significantly increase vessel caliber (Figs. 7*B* and 8*B*). Thus ACh and SNP responses were blunted in GK rats and this effect was exacerbated by IH.

NOS/COX blockade did not consistently alter vessel caliber in Wistar rats (Figs. 7*C* and 8*C*). In contrast, following NOS/COX blockade there was more pronounced vasoconstriction in GK rats than Wistar rats in both 3rd- and 4th-order vessels (mean of both orders = −8.0 ± 4.8 vs. −16.6 ± 6.1%, strain $P = 0.001$, Fig. 8*C*). In Wistar rats, IH treatment did not significantly alter the response of vessel caliber to NOS/COX blockade. In striking contrast, NOS/COX blockade resulted in a significantly more pronounced constrictor response across all

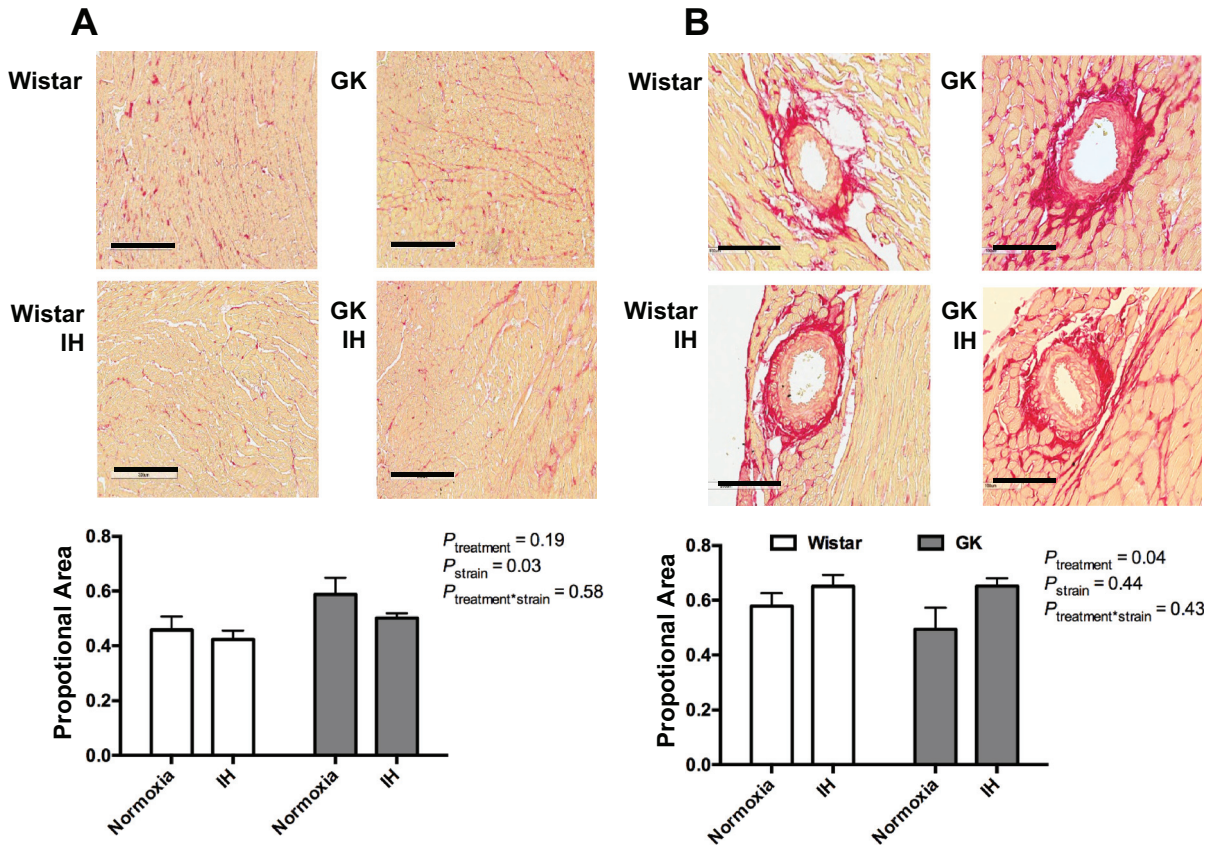

Fig. 2. Interstitial fibrosis (*A*) and perivascular fibrosis (*B*) scores in picrosirius stained sections from Wistar (open bars) and Goto-Kakizaki (GK) rats (closed bars) subjected to either normoxia or intermittent hypoxia (IH). Values are presented as means ± SE; $n = 7$ in each group. *P* values are the outcomes of a 2-way ANOVA with factors strain, treatment, and their interaction. Black bar in *A* represents 300 μm and *B* represents 100 μm.

branching orders in GK rats exposed to IH than the corresponding Wistar rats, particularly in the microvessels (mean of 3rd and 4th orders = −20.4 ± 5.4 vs. 12.4 ± 11.8% Wistar IH, treatment × strain $P = 0.04$). Postblockade, in Wistar rats exposed to normoxia, ACh infusion increased vessel caliber chiefly in the 1st-, 2nd-, and 3rd-order vessels, but had little effect in GK rats (Figs. 7*D* and 8*D*). In Wistar rats, IH treatment blunted the vasodilator response to ACh postblockade to a small extent in 3rd-order vessels only (treatment $P = 0.02$). In GK rats, IH treatment had little impact on the postblockade response to ACh, although if anything it tended to enhance vasodilatation in 1st-order vessels (Fig. 7).

DISCUSSION

In the present study, we showed that the onset of coronary vascular dysfunction in young insulin-resistant rats is exacerbated by medium-term exposure to severe chronic IH. This

Table 2. *Mean arterial pressure and heart rate during the various stages of the microangiographic study*

	Wistar	Wistar IH	GK	GK IH	Treatment (Tr)	Strain (S)	Tr × S
MAP, mmHg							
Baseline	138 ± 9	128 ± 9	137 ± 6	147 ± 7	0.99	0.30	0.23
ACh	90 ± 8	96 ± 8	108 ± 8	111 ± 5	0.68	0.02*	0.43
SNP	99 ± 7	109 ± 10	118 ± 7	123 ± 5	0.50	0.03*	0.47
Blockade	155 ± 10	136 ± 13	151 ± 1	140 ± 8	0.25	0.48	0.28
Blockade + ACh	120 ± 7	102 ± 11	137 ± 3	143 ± 3	0.09	0.02*	0.21
HR, beats/min							
Baseline	372 ± 11	415 ± 10	395 ± 17	396 ± 6	0.05*	0.82	0.06
ACh	351 ± 15	380 ± 18	366 ± 17	379 ± 9	0.02*	0.61	0.12
SNP	351 ± 19	384 ± 17	385 ± 15	390 ± 10	0.04*	0.25	0.07
Blockade	288 ± 11	287 ± 7	301 ± 21	344 ± 11	0.01*	0.03*	0.95
Blockade + ACh	275 ± 8	264 ± 9	252 ± 25	279 ± 17	0.15	0.13	0.04*

Values are expressed as means ± SE. Response of mean arterial pressure (MAP) and heart rate (HR) of Wistar rats treated with normoxia, $n = 6$, Wistar rats treated with intermittent hypoxia (IH), $n = 7$, Goto-Kakizaki (GK) rats treated with normoxia, $n = 5$ and GK rats treated with IH, $n = 7$ in response to infusion of acetylcholine (ACh), sodium nitroprusside (SNP) and meclofenamate and N^{ω}-nitro-L-arginine methyl ester (L-NAME) (Blockade). *P* values are the outcomes of 2-way ANOVA. *Effects where $P < 0.05$.

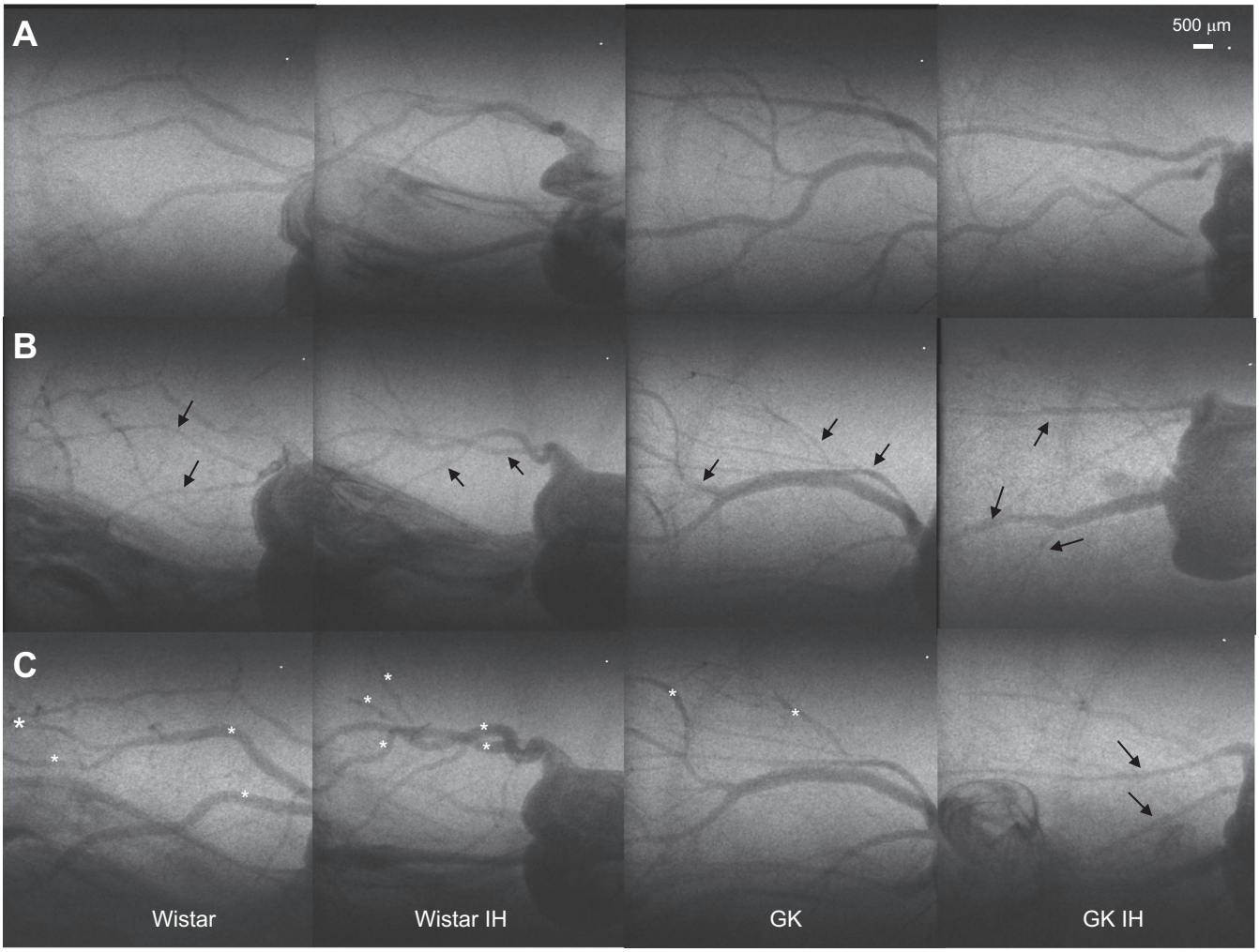

Fig. 3. Representative synchrotron radiation angiograms of the coronary vasculature during infusion of the vehicle (*A*), following administration of N^{ω}-nitro-L-arginine methyl ester (L-NAME) and meclofenamate (Blockade; *B*), and subsequent infusion of ACh (*C*). Wistar and Goto-Kakizaki (GK) rats were treated chronically with either normoxia or intermittent hypoxia (IH). Images are presented for individual rats in columns. Black arrows = vasoconstriction; white asterisk = vasodilation relative to baseline.

effect is particularly prominent in the resistance microvessels. Coronary endothelial function was assessed using cine microangiography with synchrotron radiation in vivo in anesthetized rats. Our main findings were as follows. First, we found that chronic IH greatly blunted the increases in global coronary perfusion, induced by the agonist ACh and nitric oxide donor SNP, as assessed by the number of angiographically visible vessels. Second, we found that local dilator responses of the resistance microvessels, as assessed by measurement of their caliber, were blunted in insulin-resistant GK rats relative to control Wistar rats. Thus, while coronary vascular function appears to be impaired by both IH and insulin resistance, and they appear to exacerbate each other's influence, the precise mechanisms underlying their effects may differ.

The abilities of ACh and SNP to increase the number of angiographically visible vessels were greatly blunted by chronic IH. However, changes in the number of visible vessels, in response to ACh and SNP, were little different in GK rats compared with Wistar rats. In stark contrast, the ability of ACh and SNP to increase the caliber of resistance vessels was greatly blunted in GK rats compared with Wistar rats, but little affected by IH treatment. Transmission of a dilatory signal along vessels and smaller branching microvessels is an important mechanism that results in an increase in the number of microvessels that are perfused. An increase in visible vessel number during endothelium-dependent stimulation with agonists such as ACh implies that vascular resistance decreased significantly in, and potentially downstream of, the newly visualized vessels, which permits contrast agent entry. Transmission of the dilatory signal across the length of vessels and their side branches relies predominantly on the EDHF-mediated signal being transmitted by conducted dilation from one endothelial cell to its neighboring endothelial cell and/or abutting smooth muscle cells (4, 12, 13, 32). Thus our data indicate that IH most likely impairs this mechanism. On the other hand, since IH did not impair caliber increases in response to ACh after blockade it suggests that EDHF-mediated dilation through K ion influx and hyperpolarization spread through myoendothelial gap junctions is not impaired. These findings are consistent with the hypothesis that chronic IH

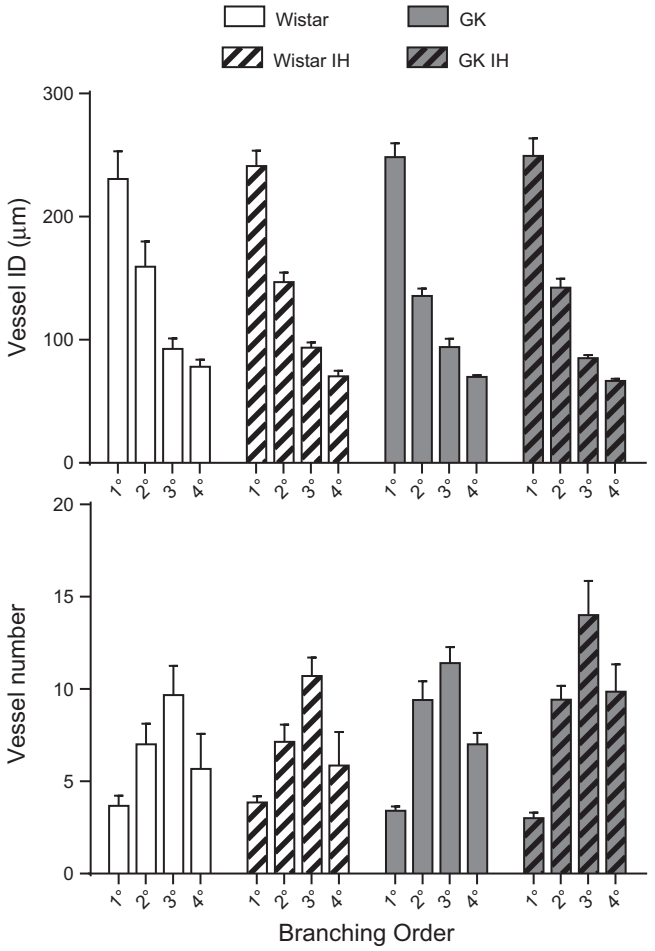

Fig. 4. The baseline internal diameter (ID) of coronary arterial vessels and the number of visible vessels in the field of view categorized by branching order observed during infusion of the vehicle. Wistar and Goto-Kakizaki (GK) rats were treated chronically with either normoxia or intermittent hypoxia (IH). Wistar rats treated with normoxia, $n = 6$, Wistar rats treated with IH, $n = 7$, GK rats treated with normoxia, $n = 5$ and GK rats treated with IH, $n = 7$.

affects the ability of dilatory signals to be transmitted along the vascular tree through endothelial cell-cell connections, but not radially from endothelial cells to smooth muscle cells.

In particular, microangiograms revealed that IH appears to differentially affect the coronary circulation as IH most affected the ability of dilator factors to increase perfusion distribution to subepicardial and subendocardial layers. Transmural arterioles that arise from the epicardial conduit arteries were less visible in IH-treated rats and generally did not increase in number during ACh following blockade. Our findings also suggest that, even though chronic IH blunted conducted dilation, it did not directly impair endothelium-dependent or endothelium-independent dilation in the vessels visible at baseline. Hence, our data raise the possibility that insulin resistance and IH might act to impair coronary vascular function through independent mechanisms, since the effects of chronic IH were mostly seen on the number of perfused vessels that were visualized and the effects of insulin resistance were mostly seen on vessel caliber. These two variables that determine coronary flow might therefore reflect different physiological factors. We speculate that caliber changes reflect the state of endothelial function and the local balance of dilator and constrictor factors, whereas a change in the number of perfused vessels that are angiographically visible reflects the ability to increase global perfusion of the myocardium with changing metabolic requirements.

Using synchrotron microangiography, which provides unique insights into vasomotor responses in the intact heart in vivo, we provide evidence that the EDHF mechanisms that mediate local dilation and conducted dilation may differ. Although many details remain unresolved, in common to both forms of dilation, close cell-cell connections through various gap junctions, and hyperpolarization currents generated by calcium-activated K channels are important for the spread of hyperpolarization in the radial direction (endothelial to smooth muscle cells) and along arteries and arterioles (resulting in conducted dilation) (4, 12, 13, 32).

We speculate that our findings could indicate that chronic IH greatly blunts the transmission of hyperpolarization along the resistance microvessels, possibly associated with remodeling of the arterial wall in Wistar and GK rats. Increased wall thickness might contribute in part to increased myogenic tone following exposure to IH. Whether there are significant changes in the expression of connexins, calcium-activated K channels or K currents in the microvessels after exposure to IH remains to be established. In Wistar rats, IH did not prevent local vasodilation in response to ACh, following NOS/COX blockade, as increases in caliber were still observed. Hence, chronic IH may selectively impair communication longitudinally along the endothelium more than radial transmission of the hyperpolarizing current through myoendothelial gap junctions to smooth muscle cells. Others have shown that small- and intermediate-conductance calcium-activated K channels in normoglycemic animals are important for the transmission of hyperpolarization along the endothelium of microvessels (4), as well as through gap junctions (12). Alternatively, IH might act to reduce hyperpolarization in the coronary microcirculation by attenuating dilation through the large-conductance calcium-activated K channel pathway. Jackson-Weaver et al. (15) have previously shown that vascular hydrogen sulfide production from endogenous cysteine is reduced by chronic IH, leading to less dilation through large-conductance calcium-activated K channels.

In this study we found that multiple mechanisms that contribute to the regulation of local dilation, through changes in microvessel caliber, are impaired in the insulin-resistant GK rat. Coronary microvessels in the GK rats did not significantly increase caliber in response to the NO donor SNP. Further, ACh failed to increase the caliber of macro- or microvessels in GK rats during NOS/COX blockade. A reduction in NO-sensitive soluble guanylyl cyclase (sGC) activity has been detected in the aorta in GK rats at 5 wk of age (47). Moreover, the same authors also suggest that dysfunction of vascular sGC signaling is likely to be responsible for blunted endothelium-independent vasodilation (47). Therefore, the sensitivity of nitrergic signaling appears to be depressed, even though NO and/or prostanoids appear to be the main contributors to the regulation of vasomotor tone in the GK rat. Our data also suggest that some components, that are assumed to be regulated by EDHF pathways, are impaired by insulin resistance. In GK rats exposed to normoxia, the response of vessel caliber to

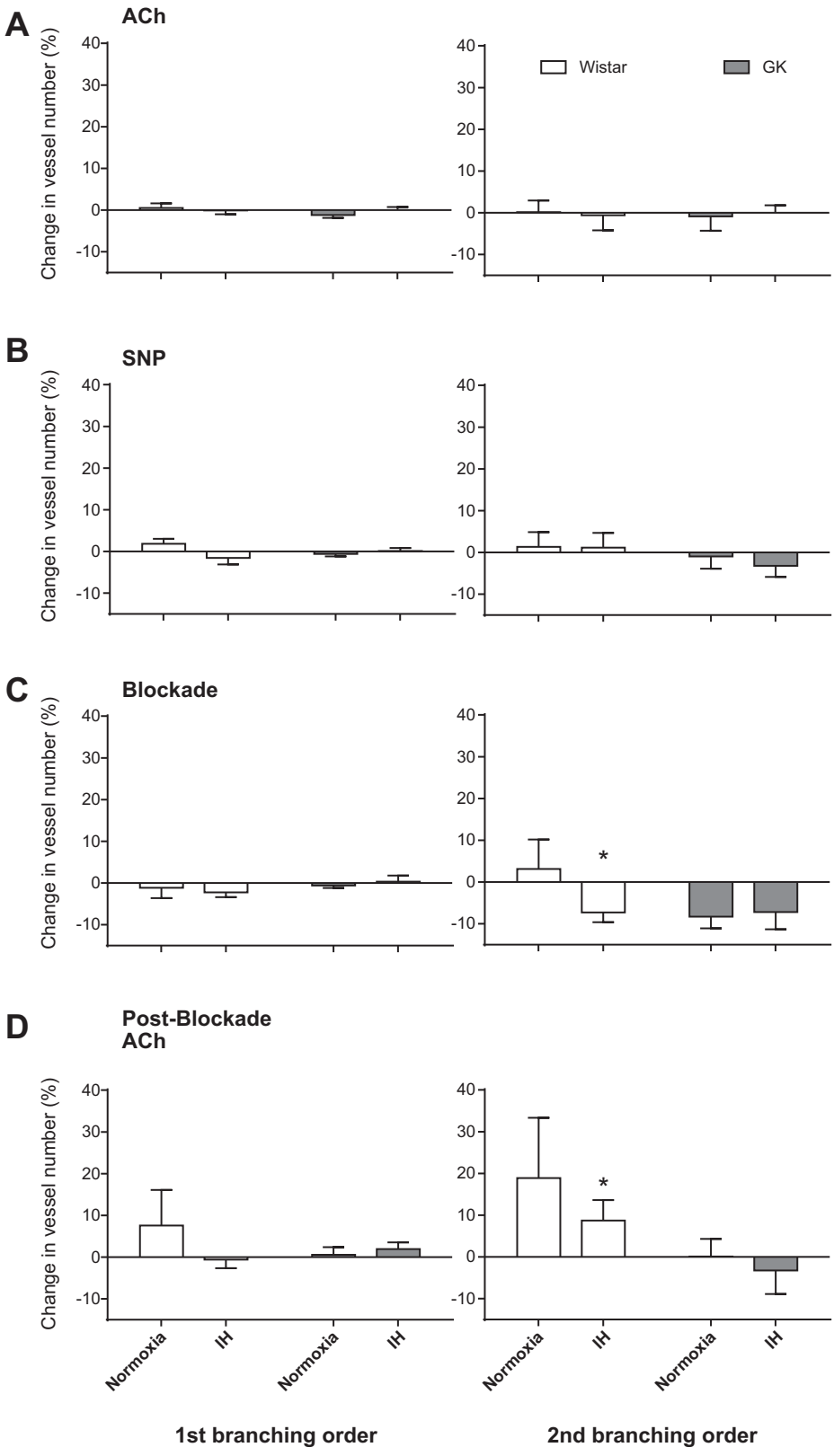

Fig. 5. Relative change in vessel number from baseline in 1st- and 2nd-order branch vessels in Wistar and Goto-Kakizaki (GK) rats subjected to either normoxia or intermittent hypoxia (IH) in response to infusion of acetylcholine (ACh, *A*), sodium nitroprusside (SNP, *B*), meclofenamate and L-NAME (Blockade, *C*), and ACh following Blockade (*D*). Wistar rats treated with normoxia, $n = 6$, Wistar rats treated with IH, $n = 7$, GK rats treated with normoxia, $n = 5$ and GK rats treated with IH, $n = 7$. Values are presented as means ± SE. $*P < 0.05$ vs. baseline (Student's paired *t*-test).

ACh after NOS/COX blockade was blunted, but the increase in the number of visible vessels was similar to that observed in Wistar rats. These observations suggest that insulin resistance impairs the transmission of hyperpolarization in the radial direction but not along vessels, in direct contrast to the effects of chronic IH that we report here. Whether the local impairment of dilation, which we assume to be due to EDHF, by the insulin-resistant state is due to a change in a diffusible factor or

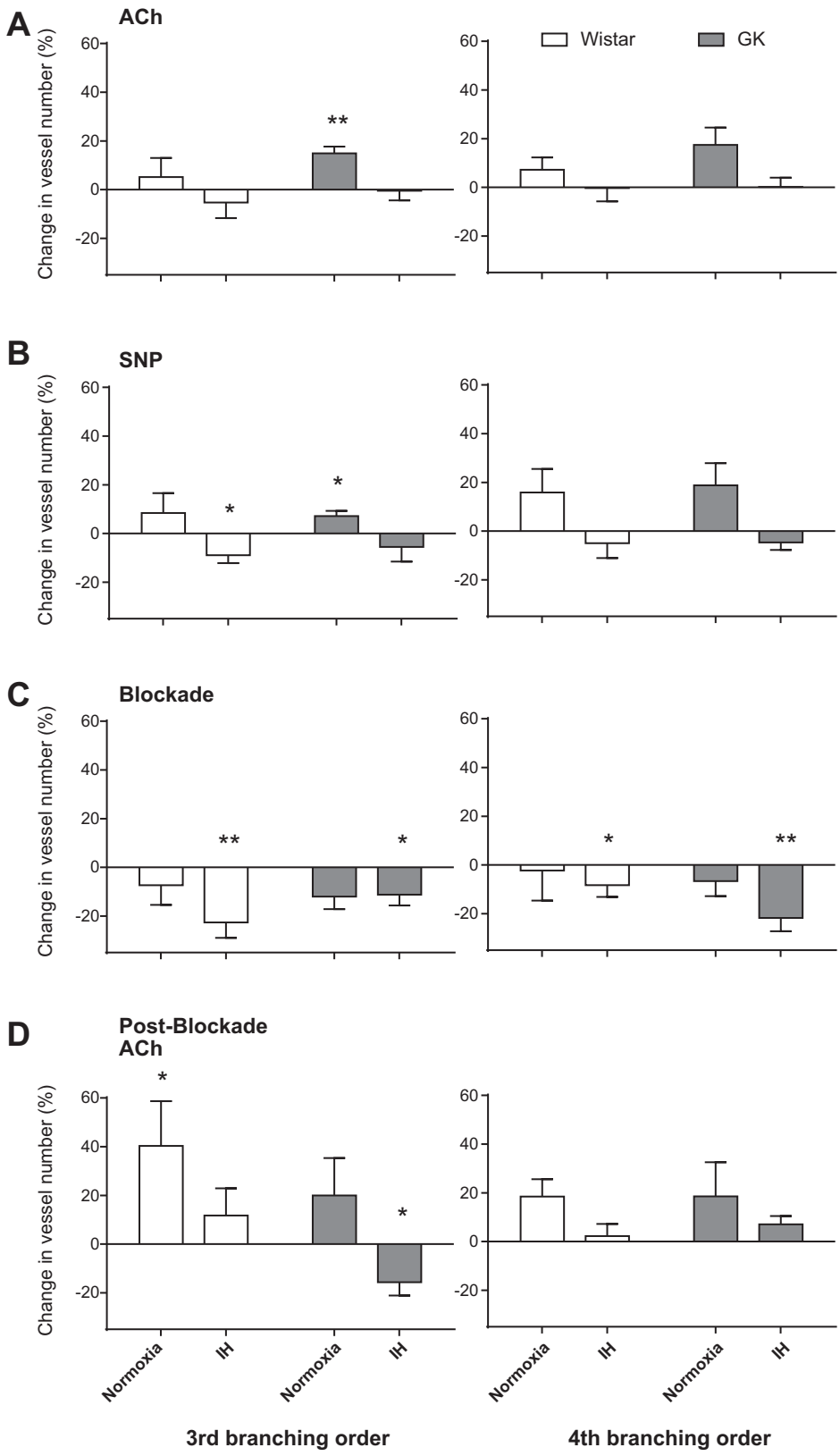

Fig. 6. Relative change in vessel number from baseline in 3rd- and 4th-order branch vessels in Wistar and Goto-Kakizaki (GK) rats subjected to either normoxia or intermittent hypoxia (IH) in response to infusion of acetylcholine (ACh, *A*), sodium nitroprusside (SNP, *B*), meclofenamate and L-NAME (Blockade, *C*), and ACh following Blockade (*D*). Wistar rats treated with normoxia, $n = 6$, Wistar rats treated with IH, $n = 7$, GK rats treated with normoxia, $n = 5$ and GK rats treated with IH, $n = 7$. Values are presented as means ± SE. $^{*}P < 0.05$, $^{**}P < 0.01$ vs. baseline (Student's paired *t*-test).

impaired transmission through K channels and/or gap junctions also merits further investigation.

In situ imaging reveals that both insulin resistance and chronic IH blunt endothelial function, and their combined effects are at least additive. NO and/or vasodilatory prostaglandins were found to be important for maintaining local vasomotor tone and the extent of perfusion across the coronary vascular tree following chronic exposure to IH. Notably, the

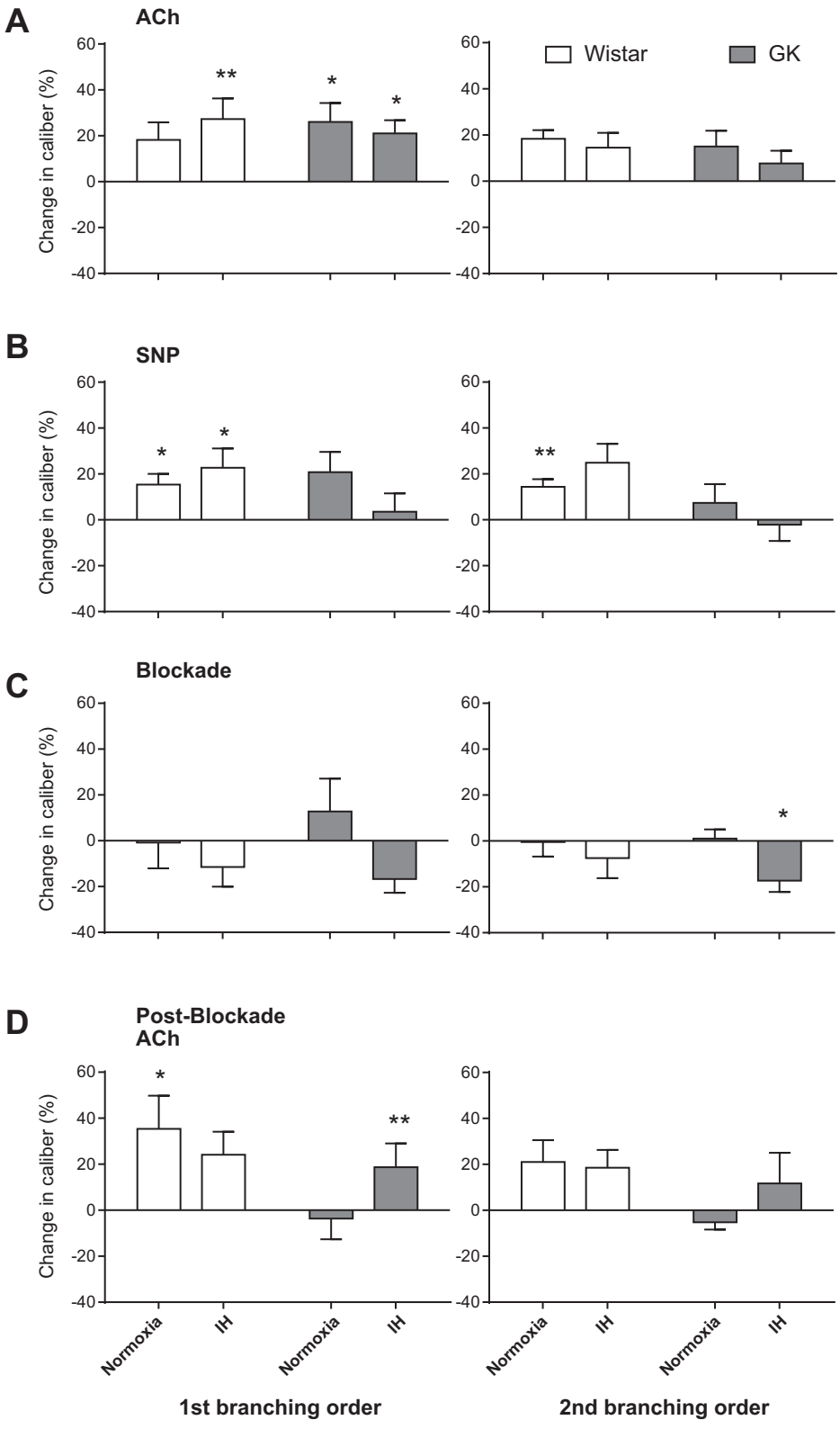

Fig. 7. Relative change in vessel ID of 1st- and 2nd-order branches in Wistar and Goto-Kakizaki (GK) rats subjected to either normoxia or intermittent hypoxia (IH) in response to infusion of acetylcholine (ACh, *A*), sodium nitroprusside (SNP, *B*), meclofenamate and L-NAME (Blockade, *C*), and ACh following Blockade (*D*). Wistar rats treated with normoxia, $n = 6$, Wistar rats treated with IH, $n = 7$, GK rats treated with normoxia, $n = 5$ and GK rats treated with IH, $n = 7$. Values are presented as means ± SE. $^{*}P < 0.05$, $^{**}P < 0.01$ vs. baseline. (Student's paired *t*-test).

vasoconstrictor effect of L-NAME and meclofenamate was exaggerated in the GK rat. After blockade of NOS/COX, ACh was still able to increase the number of visible vessels and vessel caliber in the control Wistar rats, but less able in GK rats and rats exposed to IH. Thus EDHF appears able to compensate for the acute inhibition of NO and/or vasodilator prostanoids in the normal rat heart. But both IH and insulin resistance augmented the ability of NOS/COX blockade to reduce the number of visible vessels, and reduce vessel caliber. We conclude from these findings that both IH and insulin resistance increase the dependence of

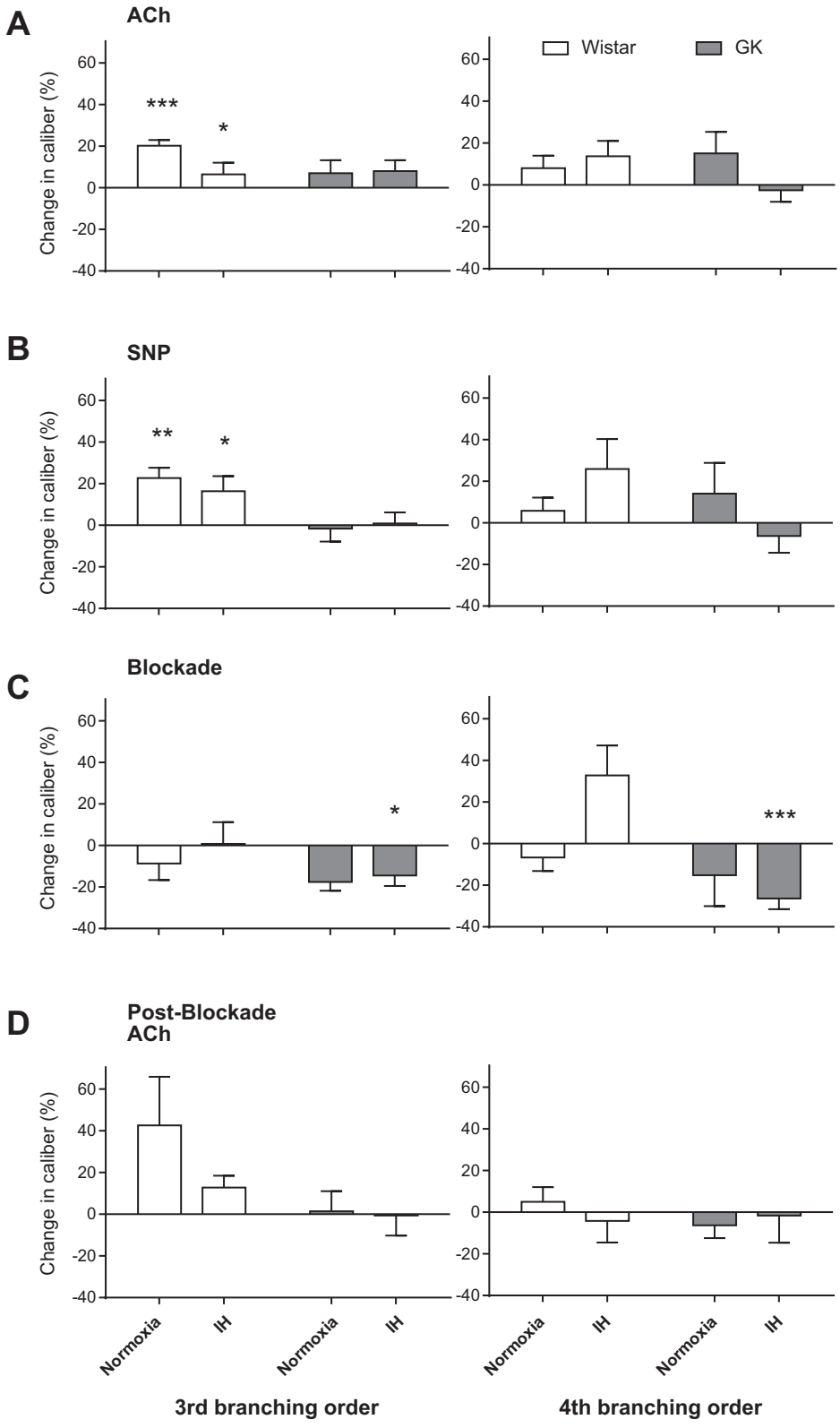

Fig. 8. Relative change in vessel ID of 3rd- and 4th-order branches in Wistar and Goto-Kakizaki (GK) rats subjected to either normoxia or intermittent hypoxia (IH) in response to infusion of acetylcholine (ACh, *A*), sodium nitroprusside (SNP, *B*), meclofenamate and L-NAME (Blockade, *C*) and ACh following Blockade (*D*). Wistar rats treated with normoxia, $n = 6$, Wistar rats treated with IH, $n = 7$, GK rats treated with normoxia, $n = 5$ and GK rats treated with IH, $n = 7$. Values are presented as means ± SE. $*P < 0.05$, $**P < 0.01$, $***P < 0.001$ vs. baseline. (Student's paired *t*-test).

the coronary circulation on vasodilator tone originating from NO and/or prostanoids, and appear to reduce the contribution of EDHF.

Available evidence from this and other studies suggests that risk factors for endothelial dysfunction, including chronic IH and insulin resistance, have additive effects (10, 23, 26, 33, 42). Chronic IH not only reduced the number of perfused vessels visualized at baseline, but it essentially eliminated the dilator response and the increase in the number of visible vessels in response to either ACh or SNP in rats with insulin

resistance. Others have shown that chronic IH reduces the bioavailability of NO in the cerebral and skeletal muscle circulation in Sprague-Dawley rats (28, 29). More recently, Nara et al. (23) showed that chronic IH did not reduce NO bioavailability in the pulmonary circulation in young rats, but did so in middle-aged rats through upregulation of arginase. Further, impaired endothelium-dependent vasodilation was observed in the forearm of patients with obstructive sleep apnea (OSA), and an additional defect in endothelium-independent vasodilation was found in patients with both OSA and hypertension (10). These findings support the argument that chronic IH itself causes a reduction of endothelium-dependent vasodilation and chronic IH in the presence of other risk factors can exacerbate this vascular dysfunction, as has been suggested previously (26, 33, 42).

Advantages of synchrotron radiation angiography and limitations of this study. Currently available preclinical imaging techniques do not permit imaging of the microcirculation of dynamic organs under conscious conditions. In a recent review the advantages and limitations of synchrotron radiation microangiography for imaging dynamic organs, such as the heart and lungs, in anesthetized animals have been put forward (36). In adult rats, utilizing this approach with available X-ray detectors capable of 10- to 15-μm-pixel resolution it is possible to visualize arterioles in vivo without motion artefacts (coronary ~40 μm, pulmonary vessels ~50 μm) (16, 34). While longitudinal synchrotron microangiography studies have been performed on the same rats over periods varying from days to months for assessment of cerebral vascular dysfunction (7, 8) repeated imaging of the coronary circulation is likely to be difficult to achieve as contrast agent is administered through a cannula placed in the carotid artery (36).

Within the limitations of the synchrotron facilities, we have utilized pentobarbital anesthesia in our studies (16, 34, 37), which is known to depress myocardial contractility (21). We report here only the responses of rats after a similar period of stable anesthesia that has been shown to slightly reduce coronary and pulmonary vascular resistances in anesthetized dogs relative to conscious conditions (21, 25). Therefore basal coronary flow in our anesthetized rats is likely to be slightly enhanced compared with conscious rats. This might have contributed to an exaggerated constrictor response to combined L-NAME and meclofenamate blockade, as reported for the canine pulmonary circulation (25), albeit we found no significant change in coronary caliber in normoxia-treated Wistar (this study) or Sprague-Dawley rats (16). However, there is no evidence to suggest that pentobarbital reduces the ability of coronary vessels to dilate in response to NO, or in response to ACh after combined blockade of COX and NOS, presumed to be mediated by EDHF. Importantly, ACh evoked dilation both before and after COX and NOS blockade in normoxia-treated rats. Moreover, others have shown that pentobarbital does not reduce nitrite/nitrate production in lung tissue (23) or NOS activity in the periphery (27).

We investigated the effects of chronic hypocapnic IH on the coronary circulation in combination with and without insulin resistance to understand how severe hypoxemia alters coronary endothelial function. Chronic IH is a critical factor in the pathophysiology of SAS, but hypercapnia also contributes to SAS and is likely to induce different neurohormonal responses both in the short and long term than IH. Based on the findings of this study, investigating the effects of hypercapnic IH or utilizing other models of airway obstruction in the future might then allow one to separate the influences of hypoxia and hypercapnia in SAS.

Perspectives and Significance

Our findings provide a clear demonstration that coronary dysfunction following exposure to chronic IH is exacerbated by insulin resistance in young rats. The generation of ROS plays an important role in the pathogenesis of vascular complications (5, 6, 38). Cheng et al. (11) demonstrated that an elevation in oxidative stress and perivascular inflammation evokes systemic endothelial dysfunction and leads to hypertension in young GK rats on a high-salt diet. This systemic vascular dysfunction is likely to be in part due to chronic activation of the sympathetic nervous system, as endothelial dysfunction persisted in GK rats treated with angiotensin receptor blockade. Furthermore, we have shown directly by nerve activity recordings in Sprague-Dawley rats that chronic IH for 6 wk induces sympathetic overactivation (37). Therefore, in the future it will be important to determine, in insulin-resistant GK rats, whether sympathetic overactivation might be an important driver of endothelial and smooth muscle dysfunction in the coronary microvessels following chronic IH.

One recent study lends weight to the idea that with aging, insulin-resistant and diabetic animals might be unable to sustain compensatory responses that are seen in young adults (23). Hence, another direction for future study is to determine whether chronic IH treatment in middle-aged insulin-resistant rats exacerbates coronary function more than in young rats. It will also be important to determine the roles of ROS and NF-kB in the endothelial dysfunction and remodeling of coronary resistance microvessels induced by insulin resistance/diabetes and IH.

ACKNOWLEDGMENTS

Experiments were conducted on BL28B2 (Proposals 2011B1324, 2011B1588, 2012B1536, and 2013A1267) at SPring-8 Synchrotron, Japan Synchrotron Radiation Research Institute, Hyogo, Japan.

GRANTS

This work was supported by an Intramural Research Fund (11-1-2) for Cardiovascular Disease from the National Cerebral and Cardiovascular Center to M. Shirai. Travel support was provided to Y. C. Chen and J. T. Pearson by the International Synchrotron Access Programme (AS/IA113 and AS/IA123) managed by the Australian Synchrotron and funded by the Australian Government.

DISCLOSURES

No conflicts of interest, financial or otherwise, are declared by the author(s).

AUTHOR CONTRIBUTIONS

Y.C.C., T.I., Y.F., D.O.S., H.T., K.U., Y.Z., M.Y., M.S., and J.T.P. performed experiments; Y.C.C., A.J.E., Y.Z., and R.G.E. analyzed data; Y.C.C., H.T., D.J.K., H.N., R.G.E., I.K., M.S., and J.T.P. interpreted results of experiments; Y.C.C. and J.T.P. prepared figures; Y.C.C., H.T., R.G.E., and J.T.P. drafted manuscript; Y.C.C., D.O.S., H.T., A.J.E., R.G.E., I.K., M.S., and J.T.P. edited and revised manuscript; Y.C.C., T.I., Y.F., D.O.S., H.T., A.J.E., K.U., Y.Z., D.J.K., M.Y., H.N., R.G.E., I.K., M.S., and J.T.P. approved final version of manuscript; D.O.S., H.T., H.N., I.K., M.S., and J.T.P. conception and design of research.

REFERENCES

1. **Allahdadi KJ, Duling LC, Walker BR, Kanagy NL.** Eucapnic intermittent hypoxia augments endothelin-1 vasoconstriction in rats: role of PKCδ. *Am J Physiol Heart Circ Physiol* 294: H920–H927, 2008.
2. **Almendros I, Wang Y, Gozal D.** The polymorphic and contradictory aspects of intermittent hypoxia. *Am J Physiol Lung Cell Mol Physiol* 307: L129–L140, 2014.
3. **Balletshofer BM, Rittig K, Enderle MD, Volk A, Maerker E, Jacob S, Matthaei S, Rett K, Häring HU.** Endothelial dysfunction is detectable in young normotensive first-degree relatives of subjects with type 2 diabetes in association with insulin resistance. *Circulation* 101: 1780–1784, 2000.
4. **Behringer EJ, Segal SS.** Tuning electrical conduction along endothelial tubes of resistance arteries through Ca^{2+}-activated K^+ channels. *Circ Res* 110: 1311–1321, 2012.
5. **Bleeke T, Zhang H, Madamanchi N, Patterson C, Faber JE.** Catecholamine-induced vascular wall growth is dependent on generation of reactive oxygen species. *Circ Res* 94: 37–45, 2004.
6. **Cai H, Harrison DG.** Endothelial dysfunction in cardiovascular diseases: the role of oxidant stress. *Circ Res* 87: 840–844, 2000.
7. **Cai J, He C, Yuan F, Chen L, Ling F.** A novel haemodynamic cerebral aneurysm model of rats with normal blood pressure. *J Clin Neurosci* 19: 135–138, 2012.
8. **Cai J, Sun Y, Yuan F, Chen L, He C, Bao Y, Chen Z, Lou M, Xia W, Yang GY, Ling F.** A novel intravital method to evaluate cerebral vasospasm in rat models of subarachnoid hemorrhage: a study with synchrotron radiation angiography. *PloS One* 7: e33366, 2012.
9. **Campbell DJ, Somaratne JB, Jenkins AJ, Prior DL, Yii M, Kenny JF, Newcomb AE, Kelly DJ, Black MJ.** Differences in myocardial structure and coronary microvasculature between men and women with coronary artery disease. *Hypertension* 57: 186–192, 2011.
10. **Carlson JT, Rangemark C, Hedner JA.** Attenuated endothelium-dependent vascular relaxation in patients with sleep apnoea. *Hypertension* 14: 577–584, 1996.
11. **Cheng ZJ, Vaskonen T, Tikkanen I, Nurminen K, Ruskoaho H, Vapaatalo H, Muller D, Park JK, Luft FC, Mervaala EM.** Endothelial dysfunction and salt-sensitive hypertension in spontaneously diabetic Goto-Kakizaki rats. *Hypertension* 37: 433–439, 2001.
12. **Czikora I, Feher A, Lucas R, Fulton DJ, Bagi Z.** Caveolin-1 prevents sustained angiotensin II-induced resistance artery constriction and obesity-induced high blood pressure. *Am J Physiol Heart Circ Physiol* 308: H376–H385, 2015.
13. **Garland CJ, Dora KA.** EDH: Endothelium-dependent hyperpolarization and microvascular signaling. *Acta Physiol (Oxf)* 2016 Jan 11. doi:10.1111/apha.12649. [Epub ahead of print]
14. **Goto Y, Kakizaki M, Masaki N.** Production of spontaneous diabetic rats by repetition of selective breeding. *Tohoku J Exp Med* 119: 85–90, 1976.
15. **Jackson-Weaver O, Paredes DA, Gonzalez Bosc LV, Walker BR, Kanagy NL.** Intermittent hypoxia in rats increases myogenic tone through loss of hydrogen sulfide activation of large-conductance Ca^{2+}-activated potassium channels. *Circ Res* 108: 1439–1447, 2011.
16. **Jenkins MJ, Edgley AJ, Sonobe T, Umetani K, Schwenke DO, Fujii Y, Brown RD, Kelly DJ, Shirai M, Pearson JT.** Dynamic synchrotron imaging of diabetic rat coronary microcirculation in vivo. *Arterioscler Thromb Vasc Biol* 32: 370–377, 2012.
17. **Joyeux-Faure M, Stanke-Labesque F, Lefebvre B, Beguin P, Godin-Ribuot D, Ribuot C, Launois SH, Bessard G, Levy P.** Chronic intermittent hypoxia increases infarction in the isolated rat heart. *J Appl Physiol* 98: 1691–1696, 2005.
18. **Kasai T, Floras JS, Bradley TD.** Sleep apnea and cardiovascular disease a bidirectional relationship. *Circulation* 126: 1495–1510, 2012.
19. **Kohler M, Stradling JR.** Mechanisms of vascular damage in obstructive sleep apnea. *Nat Rev Cardiol* 7: 677–685, 2010.
20. **Loh K, Deng H, Fukushima A, Cai X, Boivin B, Galic S, Bruce C, Shields BJ, Skiba B, Ooms LM.** Reactive oxygen species enhance insulin sensitivity. *Cell Metabolism* 10: 260–272, 2009.
21. **Manders WT, Vatner SF.** Effects of sodium pentobarbital anesthesia on left ventricular function and distribution of cardiac output in dogs, with particular reference to the mechanism for tachycardia. *Circ Res* 39: 512–517, 1976.
22. **Nagai H, Tsuchimochi H, Yoshida K, Shirai M, Kuwahira I.** A novel system including an N_2 gas generator and an air compressor for inducing intermittent or chronic hypoxia. *Int J Clin Exp Physiol* 1: 307–310, 2014.
23. **Nara A, Nagai H, Shintani-Ishida K, Ogura S, Shimosawa T, Kuwahira I, Shirai M, Yoshida K.** Pulmonary arterial hypertension in rats due to age-related arginase activation in intermittent hypoxia. *Am J Respir Cell Mol Biol* 53: 184–192, 2014.
24. **Nieto FJ, Young TB, Lind BK, Shahar E, Samet JM, Redline S, D'Agostino RB, Newman AB, Lebowitz MD, Pickering TG.** Association of sleep-disordered breathing, sleep apnea, and hypertension in a large community-based study. *JAMA* 283: 1829–1836, 2000.
25. **Nyhan DP, Chen BB, Fehr DM, Goll HM, Murray PA.** Pentobarbital augments pulmonary vasoconstrictor response to cyclooxygenase inhibition. *Am J Physiol Heart Circ Physiol* 257: H1140–H1146, 1989.
26. **Ohike Y, Kozaki K, Iijima K, Eto M, Kojima T, Ohga E, Imai K, Hashimoto M, Yoshizumi M, Ouchi Y.** Amelioration of vascular endothelial dysfunction in obstructive sleep apnea syndrome by nasal continuous positive airway pressure-possible involvement of nitric oxide and asymmetric N^G,N^G-dimethylarginine. *Circ J* 69: 221–226, 2005.
27. **Omote K, Hazama K, Kawamata T, Kawamata M, Nakayaka Y, Toriyabe M, Namiki A.** Peripheral nitric oxide in carrageenan-induced inflammation. *Brain Res* 912: 171–175, 2001.
28. **Phillips SA, Olson E, Lombard JH, Morgan BJ.** Chronic intermittent hypoxia alters NE reactivity and mechanics of skeletal muscle resistance arteries. *J Appl Physiol* 100: 1117–1123, 2006.
29. **Phillips SA, Olson E, Morgan BJ, Lombard JH.** Chronic intermittent hypoxia impairs endothelium-dependent dilation in rat cerebral and skeletal muscle resistance arteries. *Am J Physiol Heart Circ Physiol* 286: H388–H393, 2004.
30. **Punjabi NM.** The epidemiology of adult obstructive sleep apnea. *Proc Am Thorac Soc* 5: 136–143, 2008.
31. **Sakai K, Matsumoto K, Nishikawa T, Suefuji M, Nakamaru K, Hirashima Y, Kawashima J, Shirotani T, Ichinose K, Brownlee M.** Mitochondrial reactive oxygen species reduce insulin secretion by pancreatic β-cells. *Biochem Biophys Res Commun* 300: 216–222, 2003.
32. **Sandow SL, Neylon CB, Chen MX, Garland CJ.** Spatial separation of endothelial small- and intermediate-conductance calcium-activated potassium channels (K_{Ca}) and connexins: possible relationship to vasodilator function? *J Anat* 209: 689–698, 2006.
33. **Savransky V, Nanayakkara A, Li J, Bevans S, Smith PL, Rodriguez A, Polotsky VY.** Chronic intermittent hypoxia induces atherosclerosis. *Am J Respir Crit Care Med* 175: 1290–1297, 2007.
34. **Schwenke DO, Pearson JT, Umetani K, Kangawa K, Shirai M.** Imaging of the pulmonary circulation in the closed-chest rat using synchrotron radiation microangiography. *J Appl Physiol* 102: 787–793, 2007.
35. **Shahar E, Whitney CW, Redline S, Lee ET, Newman AB, Javier Nieto F, O'Connor GT, Boland LL, Schwartz JE, Samet JM.** Sleep-disordered breathing and cardiovascular disease: cross-sectional results of the Sleep Heart Health Study. *Am J Respir Crit Care Med* 163: 19–25, 2001.
36. **Shirai M, Schwenke DO, Tsuchimochi H, Umetani K, Yagi N, Pearson JT.** Synchrotron radiation imaging for advancing our understanding of cardiovascular function. *Circ Res* 112: 209–221, 2013.
37. **Shirai M, Tsuchimochi H, Nagai H, Gray E, Pearson JT, Sonobe T, Yoshimoto M, Inagaki T, Fujii Y, Umetani K, Kuwahira I, Schwenke DO.** Pulmonary vascular tone is dependent on the central modulation of sympathetic nerve activity following chronic intermittent hypoxia. *Basic Res Cardiol* 109: 1–10, 2014.
38. **Somers MJ, Mavromatis K, Galis ZS, Harrison DG.** Vascular superoxide production and vasomotor function in hypertension induced by deoxycorticosterone acetate-salt. *Circulation* 101: 1722–1728, 2000.
39. **Stühlinger MC, Abbasi F, Chu JW, Lamendola C, McLaughlin TL, Cooke JP, Reaven GM, Tsao PS.** Relationship between insulin resistance and an endogenous nitric oxide synthase inhibitor. *JAMA* 287: 1420–1426, 2002.
40. **Sydow K, Mondon CE, Cooke JP.** Insulin resistance: potential role of the endogenous nitric oxide synthase inhibitor ADMA. *Vasc Med* 10: S35–S43, 2005.
41. **Tahawi Z, Orolinova N, Joshua IG, Bader M, Fletcher EC.** Altered vascular reactivity in arterioles of chronic intermittent hypoxic rats. *J Appl Physiol* 90: 2007–2013, 2001.
42. **Von Känel R, Dimsdale JE.** Hemostatic alterations in patients with obstructive sleep apnea and the implications for cardiovascular disease. *Chest* 124: 1956–1967, 2003.

43. **Wang B, Yan B, Song D, Ye X, Liu SF.** Chronic intermittent hypoxia down-regulates endothelial nitric oxide synthase expression by an NF-κB-dependent mechanism. *Sleep Med* 14: 165–171, 2013.
44. **Wang Z, Li AY, Guo QH, Zhang JP, An Q, Guo YJ, Chu L, Weiss JW, Ji ES.** Effects of cyclic intermittent hypoxia on ET-1 responsiveness and endothelial dysfunction of pulmonary arteries in rats. *PloS One* 8: e58078, 2013.
45. **West SD, Nicoll DJ, Stradling JR.** Prevalence of obstructive sleep apnoea in men with type 2 diabetes. *Thorax* 61: 945–950, 2006.
46. **Williams SB, Cusco JA, Roddy M, Johnstone MT, Creager MA.** Impaired nitric oxide-mediated vasodilation in patients with non-insulin-dependent diabetes mellitus. *J Am Coll Cardiol* 27: 567–574, 1996.
47. **Witte K, Jacke K, Stahrenberg R, Arlt G, Reitenbach I, Schilling L, Lemmer B.** Dysfunction of soluble guanylyl cyclase in aorta and kidney of Goto-Kakizaki rats: influence of age and diabetic state. *Nitric Oxide* 6: 85–95, 2002.

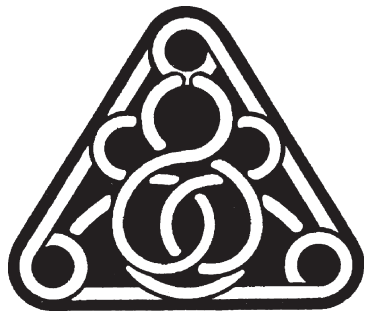

CHAPTER 7

Final Discussion and Conclusions

Chapter 7 Final Discussion and Conclusions

In the studies described in this thesis, synchrotron based microangiography was used to evaluate the efficacy of several therapies aimed at preventing the development of chronic heart failure (HF) after myocardial infarction (MI). I also used synchrotron based microangiography to assess coronary vascular function in animal models with various risk factors for development of HF, such as intermittent hypoxia, insulin resistance, and vasospasm, to improve our understanding of the contributions of each of these risk factors to coronary vascular dysfunction and the progression of HF.

7.1 Application of Regenerative Therapies for Preventing Heart Failure After Myocardial Infarction

The major strategies and goals for preventing the progression of chronic HF are to minimize risk factors of HF, improve status of symptoms, and increase survival rate. Following these strategies, various therapies have been used to prevent development of HF. In the past decade, cell based regenerative therapies are continuing to be explored to improve cardiac function in end-stage HF. The question of which regenerative approaches are best has been widely debated. Importantly, the function of the coronary microvessels, in regenerative therapy trials involving small animals, has received little attention. This issue was the chief focus of the experiments described in Chapters 3 and 4 of this thesis. I investigated whether revascularization of the ischemic myocardium can be augmented by a cell-based (Chapter 3) and a pharmacological (Chapter 4) therapy, and whether these new vessels have normal vasomotor function.

In the studies described in Chapter 3, we tested whether combined therapy with cell sheets and omentum could be an effective therapy for preventing HF after MI, by promoting re-establishment of coronary blood flow to prevent ongoing ischemia. We found that combined treatment with omentum and myoblast cell sheets increased vascularization of the ischemic myocardium, and that these new microvessels had better dilatory responses to endothelium-dependent agents than rats without treatment. Moreover, the data obtained from the same animals by our colleagues showed that combined therapy with myoblast sheets with omentum attenuated

cardiac hypertrophy and fibrosis, provided improved global coronary flow reserve, and induced the formation of structurally mature blood vessels (16). These outcomes were not achieved with either therapy alone. Thus, combined therapy with omentum and myoblast cell sheets is a promising approach for the prevention of the progression of HF after MI. Although combined therapy with omentum and myoblast cell sheets was shown to provide beneficial effects on the coronary circulation 4 weeks post MI, the therapeutic effects at other time points after treatment remain unknown. Ideally multiple time points should be evaluated longitudinally, with the same cohorts of animals, to establish whether there is more arteriolar-small artery development beyond 2 weeks post MI. MRI can be used as the additional approach to evaluate net coronary blood flow at different time point after treatment and before the final microangiography. This would also allow us to determine the time window during which the benefits of combination therapy are maximal and the size of the benefit that can be obtained with this regenerative approach. We also should consider studies in older animals to evaluate the effect of these treatments on recovery from MI, since the potential for angiogenesis is blunted with age (21, 26).

In the studies described in Chapter 4, we tested whether the novel prostacyclin analogue, ONO-1301 (developed by ONO Pharmaceutical Co Ltd), improves coronary vascular structure and function after MI. We were not able to detect a beneficial effect of ONO-1301 on revascularization or on vasodilatory responses to endothelium-dependent and endothelium-independent agents. Our findings contrast with those of others, who found beneficial effects of ONO-1301 on the coronary circulation of dogs subjected to experimental MI (20). They showed that both myocardial blood flow and capillary density was greater in dogs treated with ONO-1301 than in dogs without treatment, 8 weeks after MI (20). It is possible that our failure to detect beneficial effects of ONO-1301 on coronary function after MI is related to the relatively mild nature of the HF in the rats we studied, which might not have been severe enough to overcome the intrinsic capacity for revascularisation. This proposition should be tested in future studies.

7.2 Contribution of Vasospasm, Intermittent Hypoxia, and Insulin Resistance to Coronary Dysfunction

MI is an important risk factor for development of HF (15). However, other risk factors such as hypertension, obesity, pulmonary dysfunction, vasospasm, sleep apnea, diabetes and aging also contribute to the development of HF, in large part by inducing coronary dysfunction (3, 5, 18, 31, 35, 40, 43). By improving our understanding of how these risk factors contribute to the pathological processes underlying progression of HF, particularly changes in the structure and function of the coronary circulation, it should be possible to develop better therapies for delaying the progression of HF.

Vasospasm can lead to tissue ischemia and necrosis due to prolonged vasoconstriction (12, 17, 24). Previously, our colleagues from the University of Tsukuba established that delivery of apelin causes stenosis and focal vessel constriction in hearts that overexpressed APJ in vascular smooth muscle (Fukamizu et al, unpublished). In these studies, they assessed vascular tone *ex vivo*, by analysis of the coronary vasculature filled with a silicone polymer (Mircofil®). In the preliminary study described in Chapter 5, I examined the role of the APJ receptor in mediating vasoconstriction induced by apelin, by imaging the coronary vasculature *in vivo*. My findings indicate that apelin and its receptor APJ play little role in the tonic physiological regulation of coronary vascular tone. However, apelin and its receptor APJ might contribute to the control of coronary vascular tone under pathophysiological conditions associated with upregulation of APJ and increase circulating levels of apelin. Such conditions include atherosclerosis, stenosis of calcified aortic valves and ischemic HF (4, 13, 33). Thus, antagonists of APJ might be beneficial in the treatment of these cardiovascular conditions and preventing the acute onset of HF. However, we did not examine the regulation of coronary vasodilatory function in these mice. Therefore, we do not know whether these vessels have normal vasomotor function. In the future, we would like to examine endothelium-dependent and endothelium-independent vasodilator responses in these mice utilizing infusions of acetylcholine and sodium nitroprusside. This additional protocol to examine vasodilatory function in these animals, using synchrotron microangiography, would provide a more complete understanding of the role of the apelin/APJ pathway in regulation of the function of the coronary circulation.

Diabetes is associated with life-long cardiovascular complications, being a major risk factor for mortality due to stroke, myocardial infarction or heart failure (25, 39). Approximately 80-90% of patients with diabetes have type-2 diabetes (42). In recent years there has been an alarming increase in the prevalence of type-2 diabetes globally (37). There is also growing evidence that insulin resistance, in the presence of additional risk factors, accelerates endothelial dysfunction (8, 32). Sleep apnea syndrome is a sleep disorder characterized by repeated episodes of apnea during sleep and is highly prevalent in patients with type-2 diabetes (34). Chronic intermittent hypoxia (IH) is an important factor in the development of sleep apnea syndrome (SAS), and contributes to systemic vascular dysfunction (2). Therefore, in the studies described in Chapter 6, I determined whether chronic IH accelerates the progression of vascular dysfunction in adult rats with insulin resistance. My results indicate that coronary vascular function is impaired, in an additive manner, by chronic IH and insulin resistance. Furthermore, chronic IH and insulin resistant may impair coronary vascular function through independent mechanisms. One recent study lends weight to a future direction of study that with aging, insulin resistant animals might be unable to sustain compensatory responses that are seen in young adults (28).

7.3 Future Directions

In this thesis, synchrotron based microangiography was used to evaluate coronary vascular function in experimental animals. At least one major limitation of our approach should be acknowledged. *In vivo* microangiography does not necessarily visualize all vessels segments in the coronary vasculature. Contrast media flows through vessels with the least resistance. Thus, high vascular resistance in some segments might prevent or greatly reduce the entry of contrast media into downstream vascular elements, so that concentrations of the contrast agent are below the level of detection. Future studies would benefit by combining *in vivo* synchrotron microangiography with *ex vivo* CT of vascular casts. Injection of gelatine containing barium into the vasculature after the dynamic imaging would allow subsequent 3D-computed tomographic (CT) reconstruction for much improved visualization of vessels down to the level of the pre-capillary arterioles. This would allow more accurate determination of the number of newly developed

vessels in regeneration studies and also establish the proportion of vessels that are assessed during *in vivo* microangiography.

In this thesis, I evaluated the impact of insulin resistance, and intermittent hypoxia on the development of coronary dysfunction. There are three other risk factors that have also been shown to greatly contribute to the development of HF; hypertension, aging and obesity (22, 29). There are growing epidemics of hypertension (especially due to increasing prevalence in low to middle income countries) and obesity around the world (1, 6, 7, 14, 23). Therefore, we also need to consider how obesity and hypertension additively contribute to the acceleration of HF. There is growing evidence to suggest that increased activities of rho-kinase (ROCK) and protein kinase C-β (PKC-β) leads to coronary vascular dysfunction in animals with these risk factors (27, 30, 36, 41). Therefore, it is crucial to determine the contribution of ROCK and PKC-β to HF in animal models with hypertension or obesity by evaluating the expression of ROCK and PKC-β in the heart. On the other hand, it is well established that potassium (K^+) channels play an important role in endothelium-dependent vasodilation through endothelial-derived hyperpolarization (10, 19, 38). However, under pathological conditions, altered function of vascular K^+ channels could be either a consequence of HF or an important contributor to the origins of HF (9-11). Therefore, it is also necessary to evaluate how K^+ channels contribute to vascular dysfunction in these disease states. Further studies into these pathways might allow us to gain more understanding of the pathological progress of HF caused by hypertension and obesity, and provide us with new insights into preventing the development of HF induced by these risk factors.

Collectively, in studies of rodents, using synchrotron microangiography, we were able to demonstrate how risk factors for HF and novel potential treatments for HF affect the function of the coronary circulation. These studies provide novel insights into the mechanisms that drive progression of coronary dysfunction, particularly the relative roles of major risk factors for HF. They also demonstrate that it is possible to assess the efficacy of potential therapies for HF in preclinical studies by evaluating coronary function *in vivo*.

7.4 References

1. **Adeloye D, and Basquill C**. Estimating the prevalence and awareness rates of hypertension in Africa: a systematic analysis. *PLoS One* 9: e104300, 2014.
2. **Almendros I, Wang Y, and Gozal D**. The polymorphic and contradictory aspects of intermittent hypoxia. *Am J Physiol Lung Cell Mol Physiol* 307: L129-140, 2014.
3. **Artham SM, Lavie CJ, Milani RV, and Ventura HO**. Obesity and hypertension, heart failure, and coronary heart disease-risk factor, paradox, and recommendations for weight loss. *Ochsner J* 9: 124-132, 2009.
4. **Atluri P, Morine KJ, Liao GP, Panlilio CM, Berry MF, Hsu VM, Hiesinger W, Cohen JE, and Joseph Woo Y**. Ischemic heart failure enhances endogenous myocardial apelin and APJ receptor expression. *Cell Mol Biol Lett* 12: 127-138, 2007.
5. **Baena-Diez JM, Byram AO, Grau M, Gomez-Fernandez C, Vidal-Solsona M, Ledesma-Ulloa G, Gonzalez-Casafont I, Vasquez-Lazo J, Subirana I, and Schroder H**. Obesity is an independent risk factor for heart failure: Zona Franca Cohort study. *Clin Cardiol* 33: 760-764, 2010.
6. **Basu S, and Millett C**. Social epidemiology of hypertension in middle-income countries: determinants of prevalence, diagnosis, treatment, and control in the WHO SAGE study. *Hypertension* 62: 18-26, 2013.
7. **Bromfield S, and Muntner P**. High blood pressure: the leading global burden of disease risk factor and the need for worldwide prevention programs. *Curr Hypertens Rep* 15: 134-136, 2013.
8. **Cheng ZJ, Vaskonen T, Tikkanen I, Nurminen K, Ruskoaho H, Vapaatalo H, Muller D, Park JK, Luft FC, and Mervaala EM**. Endothelial dysfunction and salt-sensitive hypertension in spontaneously diabetic Goto-Kakizaki rats. *Hypertension* 37: 433-439, 2001.
9. **Climent B, Simonsen U, and Rivera L**. Effects of obesity on vascular potassium channels. *Curr Vasc Pharmacol* 12: 438-452, 2014.
10. **Fedele F, Severino P, Bruno N, Stio R, Caira C, D'Ambrosi A, Brasolin B, Ohanyan V, and Mancone M**. Role of ion channels in coronary microcirculation: a review of the literature. *Future Cardiol* 9: 897-905, 2013.
11. **Feletou M**. Calcium-activated potassium channels and endothelial dysfunction: therapeutic options? *Br J Pharmacol* 156: 545-562, 2009.
12. **Fisher C, Kistler J, and Davis J**. Relation of cerebral vasospasm to subarachnoid hemorrhage visualized by computerized tomographic scanning. *J Neurosurg* 6: 1, 1980.
13. **Hashimoto T, Kihara M, Ishida J, Imai N, Yoshida S, Toya Y, Fukamizu A, Kitamura H, and Umemura S**. Apelin stimulates myosin light chain phosphorylation in vascular smooth muscle cells. *Arterioscler Thromb Vasc Biol* 26: 1267-1272, 2006.
14. **Hruby A, and Hu FB**. The Epidemiology of Obesity: A Big Picture. *Pharmacoeconomics* 33: 673-689, 2015.
15. **Jhaveri RR, Reynolds HR, Katz SD, Jeger R, Zinka E, Forman SA, Lamas GA, and Hochman JS**. Heart failure in post-MI patients with persistent IRA occlusion: prevalence, risk factors, and the long-term effect of PCI in the Occluded Artery Trial (OAT). *J Card Fail* 18: 813-821, 2012.
16. **Kainuma S, Miyagawa S, Fukushima S, Pearson J, Chen YC, Saito A, Harada A, Shiozaki M, Iseoka H, Watabe T, Watabe H, Horitsugi G, Ishibashi M, Ikeda H, Tsuchimochi H, Sonobe T, Fujii Y, Naito H, Umetani K, Shimizu T, Okano T, Kobayashi E, Daimon T, Ueno T, Kuratani T, Toda K, Takakura N, Hatazawa J, Shirai M, and Sawa Y**. Cell-sheet therapy with omentopexy promotes

arteriogenesis and improves coronary circulation physiology in failing heart. *Mol Ther* 23: 374-386, 2015.
17. **Kassell NF, Peerless SJ, Durward QJ, Beck DW, Drake CG, and Adams HP**. Treatment of ischemic deficits from vasospasm with intravascular volume expansion and induced arterial hypertension. *J Neurosurg* 11: 337, 1982.
18. **Khan H, Kalogeropoulos AP, Georgiopoulou VV, Newman AB, Harris TB, Rodondi N, Bauer DC, Kritchevsky SB, and Butler J**. Frailty and risk for heart failure in older adults: the health, aging, and body composition study. *Am Heart J* 166: 887-894, 2013.
19. **Ko EA, Han J, Jung ID, and Park WS**. Physiological roles of K+ channels in vascular smooth muscle cells. *J Smooth Muscle Res* 44: 65-81, 2008.
20. **Kubota Y, Miyagawa S, Fukushima S, Saito A, Watabe H, Daimon T, Sakai Y, Akita T, and Sawa Y**. Impact of cardiac support device combined with slow-release prostacyclin agonist in a canine ischemic cardiomyopathy model. *J Thorac Cardiovasc Surg* 147: 1081-1087, 2014.
21. **Lahteenvuo J, and Rosenzweig A**. Effects of aging on angiogenesis. *Circ Res* 110: 1252-1264, 2012.
22. **Lavie CJ, Alpert MA, Arena R, Mehra MR, Milani RV, and Ventura HO**. Impact of obesity and the obesity paradox on prevalence and prognosis in heart failure. *JACC Heart Fail* 1: 93-102, 2013.
23. **Lifshitz F, and Lifshitz JZ**. Globesity: the root causes of the obesity epidemic in the USA and now worldwide. *Pediatr Endocrinol Rev* 12: 17-34, 2014.
24. **Maseri A, L'Abbate A, Baroldi G, Chierchia S, Marzilli M, Ballestra AM, Severi S, Parodi O, Biagini A, and Distante A**. Coronary vasospasm as a possible cause of myocardial infarction. *N Engl J Med* 299: 1271-1277, 1978.
25. **McMurray JJ, Gerstein HC, Holman RR, and Pfeffer MA**. Heart failure: a cardiovascular outcome in diabetes that can no longer be ignored. *Lancet Diabetes Endocrinol* 2: 843-851, 2014.
26. **Min JY, Chen Y, Malek S, Meissner A, Xiang M, Ke Q, Feng X, Nakayama M, Kaplan E, and Morgan JP**. Stem cell therapy in the aging hearts of Fisher 344 rats: synergistic effects on myogenesis and angiogenesis. *J Thorac Cardiovasc Surg* 130: 547-553, 2005.
27. **Mochly-Rosen D, Das K, and Grimes KV**. Protein kinase C, an elusive therapeutic target? *Nat Rev Drug Discov* 11: 937-957, 2012.
28. **Nara A, Nagai H, Shintani-Ishida K, Ogura S, Shimosawa T, Kuwahira I, Shirai M, and Yoshida K**. Pulmonary arterial hypertension in rats due to age-related arginase activation in intermittent hypoxia. *Am J Respir Cell Mol Biol* 53: 184-192, 2015.
29. **Oktay AA, Rich JD, and Shah SJ**. The emerging epidemic of heart failure with preserved ejection fraction. *Curr Heart Fail Rep* 10: 401-410, 2013.
30. **Palaniyandi SS, Sun L, Ferreira JC, and Mochly-Rosen D**. Protein kinase C in heart failure: a therapeutic target? *Cardiovasc Res* 82: 229-239, 2009.
31. **Palano F, Paneni F, Sciarretta S, Tocci G, and Volpe M**. The progression from hypertension to congestive heart failure. *Recenti Prog Med* 102: 461-467, 2011.
32. **Paulus WJ, and Tschope C**. A novel paradigm for heart failure with preserved ejection fraction: comorbidities drive myocardial dysfunction and remodeling through coronary microvascular endothelial inflammation. *J Am Coll Cardiol* 62: 263-271, 2013.
33. **Peltonen T, Napankangas J, Vuolteenaho O, Ohtonen P, Soini Y, Juvonen T, Satta J, Ruskoaho H, and Taskinen P**. Apelin and its receptor APJ in human aortic valve stenosis. *J Heart Valve Dis* 18: 644-652, 2009.

34. **Punjabi NM**. The epidemiology of adult obstructive sleep apnea. *Proc Am Thorac Soc* 5: 136-143, 2008.
35. **Reishtein JL**. Obstructive sleep apnea: a risk factor for cardiovascular disease. *J Cardiovasc Nurs* 26: 106-116, 2011.
36. **Shi J, and Wei L**. Rho kinases in cardiovascular physiology and pathophysiology: the effect of fasudil. *J Cardiovasc Pharmacol* 62: 341-354, 2013.
37. **Shi Y, and Hu FB**. The global implications of diabetes and cancer. *Lancet* 383: 1947-1948, 2014.
38. **Sobey CG**. Potassium channel function in vascular disease. *Arterioscler Thromb Vasc Biol* 21: 28-38, 2001.
39. **Stamler J, Vaccaro O, Neaton JD, and Wentworth D**. Diabetes, other risk factors, and 12-yr cardiovascular mortality for men screened in the Multiple Risk Factor Intervention Trial. *Diabetes Care* 16: 434-444, 1993.
40. **Sueda S, Kohno H, Oshita A, Izoe Y, Nomoto T, and Fukuda H**. Vasospastic heart failure: multiple spasm may cause transient heart failure? *J Cardiol* 54: 452-459, 2009.
41. **Yao L, Romero MJ, Toque HA, Yang G, Caldwell RB, and Caldwell RW**. The role of RhoA/Rho kinase pathway in endothelial dysfunction. *J Cardiovasc Dis Res* 1: 165-170, 2010.
42. **Zaccardi F, Webb DR, Yates T, and Davies MJ**. Pathophysiology of type 1 and type 2 diabetes mellitus: a 90-year perspective. *Postgrad Med J* 92: 63-69, 2016.
43. **Zinman B, Lachin JM, and Inzucchi SE**. Empagliflozin, Cardiovascular Outcomes, and Mortality in Type 2 Diabetes. *N Engl J Med* 374: 1094, 2016.

Cell-sheet Therapy With Omentopexy Promotes Arteriogenesis and Improves Coronary Circulation Physiology in Failing Heart

Satoshi Kainuma[1], Shigeru Miyagawa[1], Satsuki Fukushima[1], James Pearson[2], Yi Ching Chen[2], Atsuhiro Saito[1], Akima Harada[1], Motoko Shiozaki[1], Hiroko Iseoka[1], Tadashi Watabe[3], Hiroshi Watabe[3], Genki Horitsugi[4], Mana Ishibashi[4], Hayato Ikeda[4], Hirotsugu Tsuchimochi[5], Takashi Sonobe[5], Yutaka Fujii[5], Hisamichi Naito[6], Keiji Umetani[7], Tatsuya Shimizu[8], Teruo Okano[8], Eiji Kobayashi[9], Takashi Daimon[10], Takayoshi Ueno[1], Toru Kuratani[1], Koichi Toda[1], Nobuyuki Takakura[6], Jun Hatazawa[4], Mikiyasu Shirai[5] and Yoshiki Sawa[1]

[1]Department of Cardiovascular Surgery, Osaka University Graduate School of Medicine, Osaka, Japan; [2]Monash Biomedical Imaging Facility and Department of Physiology, Monash University, Melbourne, Australia; [3]Department of Molecular Imaging in Medicine, Osaka University Graduate School of Medicine, Osaka, Japan; [4]Department of Nuclear Medicine and Tracer Kinetics, Osaka University Graduate School of Medicine, Osaka, Japan; [5]Department of Cardiac Physiology, National Cerebral and Cardiovascular Center Research Institute, Osaka, Japan; [6]Department of Signal Transduction, Research Institute for Microbial Diseases, Osaka University, Osaka, Japan; [7]Japan Synchrotron Radiation Research Institute, Harima, Japan; [8]Institute of Advanced Biomedical Engineering and Science, Tokyo Women's Medical University, Tokyo, Japan; [9]Division of Organ Replacement Research, Center for Molecular Medicine, Jichi Medical School, Tochigi, Japan; [10]Department of Biostatistics, Hyogo College of Medicine, Hyogo, Japan

Cell-sheet transplantation induces angiogenesis for chronic myocardial infarction (MI), though insufficient capillary maturation and paucity of arteriogenesis may limit its therapeutic effects. Omentum has been used clinically to promote revascularization and healing of ischemic tissues. We hypothesized that cell-sheet transplantation covered with an omentum-flap would effectively establish mature blood vessels and improve coronary microcirculation physiology, enhancing the therapeutic effects of cell-sheet therapy. Rats were divided into four groups after coronary ligation; skeletal myoblast cell-sheet plus omentum-flap (combined), cell-sheet only, omentum-flap only, and sham operation. At 4 weeks after the treatment, the combined group showed attenuated cardiac hypertrophy and fibrosis, and a greater amount of functionally ($CD31^+$/$lectin^+$) and structurally ($CD31^+$/α-SMA^+) mature blood vessels, along with myocardial upregulation of relevant genes. Synchrotron-based microangiography revealed that the combined procedure increased vascularization in resistance arterial vessels with better dilatory responses to endothelium-dependent agents. Serial ^{13}N-ammonia PET showed better global coronary flow reserve in the combined group, mainly attributed to improvement in the basal left ventricle. Consequently, the combined group had sustained improvements in cardiac function parameters and better functional capacity. Cell-sheet transplantation with an omentum-flap better promoted arteriogenesis and improved coronary microcirculation physiology in ischemic myocardium, leading to potent functional recovery in the failing heart.

Received 27 August 2014; accepted 16 November 2014; advance online publication 13 January 2015. doi:10.1038/mt.2014.225

INTRODUCTION

Heart failure following myocardial infarction (MI) is a major cause of death and disability worldwide. Despite advances in drug and device therapy, recovery of cardiac function and prevention of transition to heart failure in MI patients remain unsatisfactory, indicating the need for development of novel therapeutic alternatives.[1] Myocardial regenerative therapy with cell-sheet transplantation has been shown to induce angiogenesis via paracrine effects in a chronic MI model.[2,3] However, the proangiogenic effect of the stand-alone cell-sheet treatment may be insufficient to fully relief ischemia in the chronic MI heart that involves a large territory of the left ventricle (LV), since the coronary inflow of the ischemic/infarct myocardium is dependent upon collateral arteries from other territories.[4,5] In addition, microvascular dysfunction is present in critical chronic MI heart across a wide range of the peripheral coronary tree.[6] This highlights the need for a comprehensive understanding of the mechanism of angiogenesis induced by a cell-sheet therapy in ischemic hearts.

For successful therapeutic neovascularization of ischemic tissues, it is essential to induce robust angiogenic responses (angiogenesis), and establish functionally and structurally mature arterial vascular networks (arteriogenesis) that show long-term stability and control perfusion.[5] Establishment of mature vessels is a complex process that requires several angiogenic factors to stimulate vessel sprouting and remodeling (endothelial tubulogenesis accompanied with a pericyte recruitment) of the primitive vascular network. Endothelial vasodilator function of coronary microvessels (resistance arterial vessels) is also an important determinant of myocardial perfusion in response to increased myocardial oxygen demand, playing a critical role in neovascular therapies.[6–8] The attenuated therapeutic effects observed in the previous clinical trials were caused by multiple factors including

Correspondence: Yoshiki Sawa, Chairman of Department of Cardiovascular Surgery, Osaka University Graduate School of Medicine, 2-2-E1, Yamadaoka, Suita, Osaka 565–0871, Japan. E-mail: sawa-p@surg1.med.osaka-u.ac.jp

generation of unstable blood vessels that regress over time or functionally immature vessels accompanied with endothelial dysfunction in ischemic areas.[5,9]

The omentum (OM), historically used in surgical revascularization for patients with ischemic heart disease, is also known to release a number of angiogenic cytokines and attenuate inflammation.[10–14] In addition, the gastroepiploic artery involved in the OM-flap can play an important role as an extracardiac blood source with high perfusion capacity for developing effective collateral vessels for advanced coronary artery disease. We established a combination strategy of cell-sheet transplantation covered with a pedicle OM-flap in porcine models, allowing us to implant large numbers of cells and improve cell survival.[13,14] However, data are scarce regarding the therapeutic effects of such combined treatment on vessel maturity and coronary microcirculation physiology in ischemic territory. We hypothesized that cell-sheet transplantation with a pedicle OM-flap will better promote arteriogenesis and stabilize blood vessels in ischemic myocardium along with improved coronary microcirculation physiology, consequently enhancing the therapeutic effects of cell-sheet therapy. Herein, we focused on vessel maturation induced by cell-sheet therapy with an OM-flap and evaluated the physiological benefits in coronary microcirculation utilizing modern modalities such as *in vivo* synchrotron-based microangiography and positron emission tomography (PET).

RESULTS

Histological analysis of host myocardium

Four weeks after treatment, myocardial structural components, collagen accumulation and cardiomyocyte hypertrophy, were assessed by hematoxylin-eosin, Masson trichrome, and Periodic acid-Schiff staining (n = 11 for each group). LV myocardial structure was better maintained in the combined group as compared with the others (**Figure 1c**). The combined group had a significantly thickened anterior LV wall (anterior wall thickness, control 392 ± 31 versus combined 912 ± 34 versus sheet-only 688 ± 27 versus OM-only 500 ± 28 μm) (**Figure 1d**). That group also had a significantly attenuated collagen accumulation (percent fibrosis, 18 ± 1 versus 8 ± 4 versus 13 ± 6 versus 14 ± 1%, respectively) (**Figure 1e**) and cardiac hypertrophy (myocyte size, 23 ± 1 versus 16 ± 1 versus 20 ± 3 versus 21 ± 2 μm, respectively) (**Figure 1f**) in the peri-infarct regions (ANOVA $P < 0.001$ for all).

Gene expressions in peri-infarct myocardium during acute treatment phase

The myocardial gene expressions related to angiogenesis, vessel maturation, and anti-inflammation were analyzed at 3 days after each treatment using real-time PCR (n = 6 for each group). As compared to the others, the combined group showed substantially higher gene expressions of *vascular endothelial growth factor (VEGF)-A*, *VEGF receptor-1*, *VEGF receptor-2*, *Akt-1*, *platelet-derived growth factor (PDGF)-β*, *angiopoietin (Ang)-1*, *Tie-2*, *vascular endothelial (VE)-cadherin*, *platelet endothelial cell adhesion molecule (PECAM)-1*, and *stromal cell-derived factor (SDF)-1* in peri-infarct myocardium at the early stage of transplantation (**Figure 2**).

Vessel recruitment in transplanted cell-sheets and donor cell survial

To evaluate the effect of adding OM-flap to the cell-sheet therapy on the vessel recruitment (angiogenesis) in the transplanted area that should be related to the donor cell survival, we serially assessed the number of functional blood vessels with patent endothelial layers (CD31/lectin double-positive cells) in the transplanted area of the sheet-only and combined groups at 3, 7, and 28 days after each treatment (n = 6 for each group and each time point) (**Figure 3a–f**). At 3 days after treatment, in the sheet-only group, several blood vessels were just located at the border between the sheet and infarct area (**Figure 3a**), whereas a large number of functional vessels was detected proximal to the border between the cell-sheet and OM and within the sheet in the combined group (**Figure 3d**), suggesting that the cell-sheet received blood supply directly from the infarct myocardium and OM. Consequently, the combined group had greater numbers of functional blood vessels in the cell-sheet than the sheet-only group at any follow-up point, although both groups showed steady decrease in the number of vessels during the 28 days (**Figure 3g**).

The quantitative assessments of the donor (GFP-positive) cell presence were also serially performed to elucidate the donor cell dynamics in the sheet-only (**Figure 3a–c**) and combined (**Figure 3d–f**) groups. We traced the transplanted donor cells and found that there was no significant difference in the engrafted area at 3 days after transplantation between the groups, while the subsequent changes in each group were apparently distinctive (**Figure 3h**). During the 7days after the treatment, the amount of decrease in the engrafted area was substantially smaller in the combined group than that in the sheet-only group, resulting in 4.3-fold increased retention of donor cells in the former group. This led to the greater donor cell presence in the combined group persistently (at least until day 28), which was consistent with the amount of vessel recruitment in the cell-sheet.

Vessel remodeling and maturation in peri-infarct myocardium

We serially assessed neovascular vessel maturity in peri-infarct areas at 3 (n = 6 for each group) and 28 days (n = 11 for each group) after treatment (**Figure 4**). Vessel density and structural maturity were quantified as the number of CD31 positive and CD31/α-smooth muscle actin (SMA) double-positive vessels per mm^2, respectively. A maturation index was calculated as the percentage of CD31/α-SMA double-positive vessels to total vessel number. Functionally mature vessels with patent endothelial layers were assessed by lectin injection, which binds uniformly and rapidly to the luminal surface of endothelium, thus labeling patent blood vessels. Vessels positive for CD31 but negative for lectin were regarded as functionally immature and undergoing regression, or that had lost patency.[15,16]

In general, α-SMA signals were located at the outer edges of CD31 staining, indicating pericyte attachment to newly formed endothelium. Three days after treatment, there was no difference in number of CD31-positive cells among the groups, though the combined group showed a trend of greater number of functional blood vessels with patent endothelial layers (CD31/lectin double-positive) and structurally (CD31/α-SMA double-positive) mature vessels, with a higher maturation index (**Figure 4a–g**). Notably, the percentage without lectin staining (CD31$^+$/lectin$^-$) was significantly smaller in the combined group.

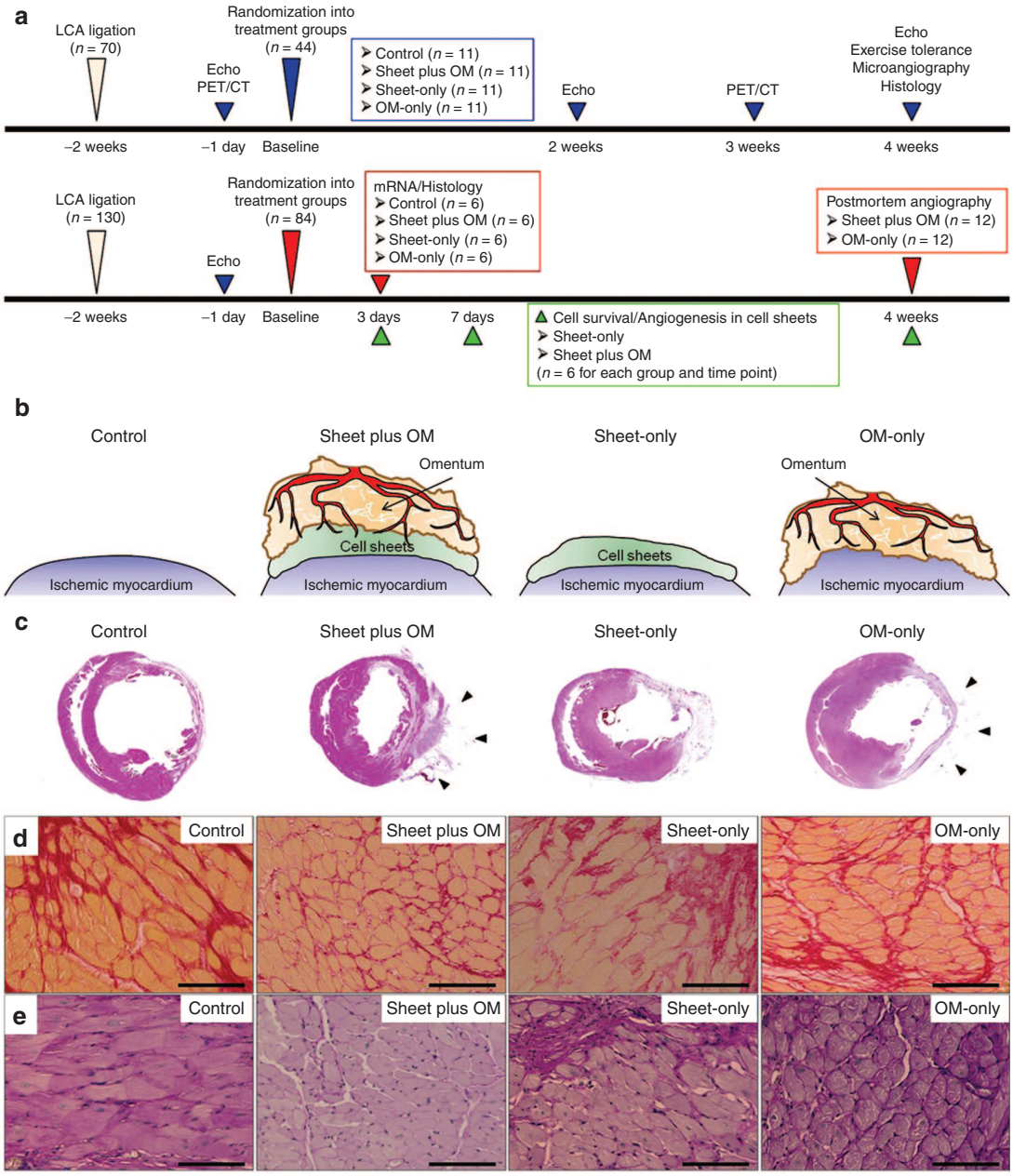

Figure 1 Study protocol and histological analysis of host myocardium. (**a**) Experimental protocols. (**b**) Procedural schemes for treatment groups. (**c**) Macroscopic images of HE-stained whole sections of the left ventricle and (**d**) anterior wall thickness (40×, scale bar = 1,000 μm). Black arrows indicate the omentum tissue. Photomicrographs of Sirius red- (**e**) and periodic acid-Schiff-stained (**f**) sections of peri-infarct myocardium (400×, scale bar = 100 μm) (n = 11 for each group).

The number of endothelial (CD31 positive) cells in the control and single treatment groups decreased with time, while that in the combined remained unchanged. Consequently, the angiogenic effects induced in the latter were more profound at 28 days after treatment, with a significantly greater amount of mature vessels (Figure 4h–n).

Number of resistance vessels and relative dilatory responses to endothelium-dependent stimulation in ischemic myocardium

To evaluate the effects of each treatment on microcirculation physiology in terms of relative dilatory responses to acetylcholine and dobutamine hydrochloride in the resistance vessels, synchrotron radiation microangiography was performed after 3 weeks after the treatment (control: n = 11, combined: n = 11, cell-sheet: n = 5, OM: n = 6). Using iodinated agents, coronary microcirculation in ischemic areas was clearly visualized in anesthetized closed-chest rats (Figure 5a). Vessel internal diameter (ID) at baseline (before agent administration) tended to decrease according to branching order and differed among the groups with larger first branching order arteries observed in the combined group (Figure 5b). Moreover, the combined group had a greater number of third and fourth branching order arterial vessels (resistance arterial vessels) at baseline (Figure 5c).

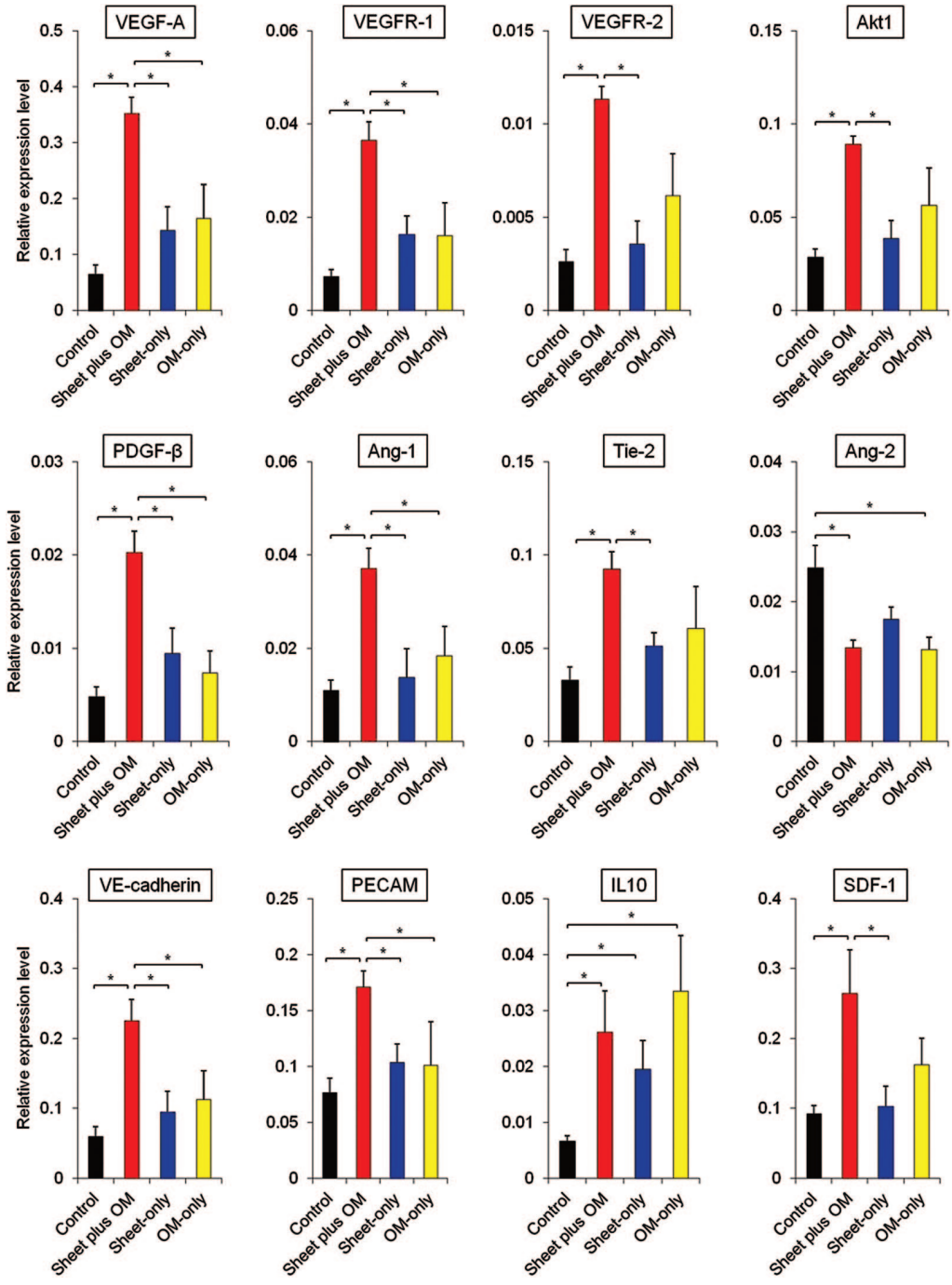

Figure 2 Gene expressions in peri-infarct myocardium during acute treatment phase. Quantitative reverse transcription PCR showing gene expressions related to angiogenesis, vessel maturation, and anti-inflammation in peri-infarct myocardium 3 days after treatment (n = 6 for each group) (*P < 0.05). Data were normalized to β-actin expression level. As compared to the others, the combined group showed substantially higher gene expressions associated with angiogenesis, vessel remodeling and anti-inflammation in peri-infarct myocardium at 3 days after treatment.

Acetylcholine-mediated dilation in the third and fourth branching orders was significantly different among the groups. The mean caliber changes in response to acetylcholine in the combined group were 28±8% and 32±8% for the third and fourth order branches respectively, which were greater than in the others (**Figure 5d**). Similarly, the mean caliber changes in response to dobutamine hydrochloride in the combined group were 31±7% and 34±7%, respectively, which were greater than in the others (**Figure 5e**).

The distributions of individual segment caliber changes in response to acetylcholine are described in **Supplementary Figure S1**. The control group had a relatively high frequency of third and fourth branching order arterial vessels showing localized segmental vasoconstriction (ID constriction >5% of baseline). The frequency of abnormal vasoconstriction with acetylcholine in the control group was about eight- and fourfold for the third and fourth branching order, respectively, as compared

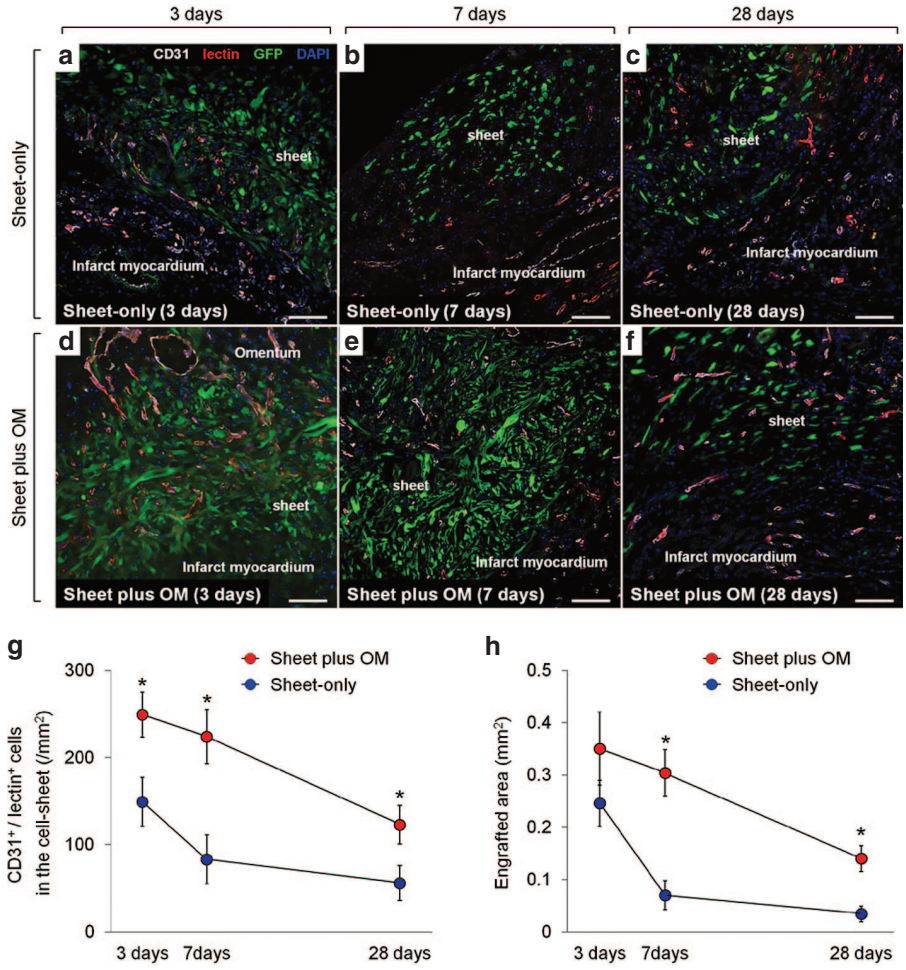

Figure 3 Vessel recruitment in transplanted cell-sheets and donor cell survial. Serial representative images of functional blood vessels with patent endothelial layers (CD31/lectin double-positive) vessels in the transplanted donor (GFP-positive) cells in sheet-only (**a–c**) and combined groups (**d–f**) at 3, 7, and 28 days after each treatment (200×, scale bar = 100 μm). Quantitative analyses of functionally mature vessels in the transplanted area (**g**) and the donor (GFP-positive) cell presence (**h**) at 3, 7, and 28 days after each treatment (n = 6 for each group and each time point) (* $P < 0.05$ versus sheet-only group). At 3 days after treatment, in the sheet-only group, several blood vessels were just located at the border between the sheet and infarct area (**a**), whereas a large number of functional vessels was detected proximal to the border between the cell-sheet and OM and within the sheet in the combined group (**d**). Consequently, the combined group had greater numbers of functional blood vessels in the cell-sheet than the sheet-only group at any follow-up point (**g**). There was no significant difference in the engrafted area at 3 days after transplantation between the groups, while the subsequent changes in each group were apparently distinctive (**h**). During the 7 days after the treatment, the amount of decrease in the engrafted area was substantially smaller in the combined group than that in the sheet-only group, resulting in 4.3-fold increased retention of donor cells in the former group. This led to the greater donor cell presence in the combined group persistently (at least until day 28), which was consistent with the amount of vessel recruitment in the cell-sheet.

with the combined group (third order: control 49% versus combined 6% versus sheet-only 22% versus OM-only 25%; fourth order: control 18% versus combined 4% versus sheet-only 13% versus OM-only 17%).

Global and regional changes in myocardial blood flow and coronary flow reserve

To evaluate global and regional myocardial blood flow (MBF), and coronary flow reserve (CFR), ^{13}N-ammonia PET measurements were serially performed 1 day before and 3 weeks after the treatments (control: n = 5, combined: n = 8, cell-sheet: n = 7, OM: n = 7) (**Figure 6a–f**). In normal rats used for the validation study, global MBF at rest and during stress was 5.1 ± 0.5 and 7.1 ± 1.3 ml/min/g respectively, while global CFR was 1.4 ± 0.3.

Two weeks after coronary ligation (before treatment), global MBF at rest and during stress were substantially decreased in all groups, with no significant differences. Similarly, global CFR was not different among the groups. Three weeks after treatment, global MBF at rest was not different, while that during stress was significantly greater in the combined and single treatment groups as compared to the control (control 2.5 ± 0.4 versus combined 3.8 ± 0.6 versus sheet-only 3.3 ± 0.5 versus OM-only 3.8 ± 0.3, respectively, ANOVA p=0.0003). Postoperative global CFR was also substantially higher in the treatment groups as compared with the control (control 1.1 ± 0.2 versus combined 1.4 ± 0.2 versus sheet-only 1.4 ± 0.2 versus OM-only 1.4 ± 0.2, respectively, ANOVA p=0.015).

With regard to the magnitude of change in the global CFR (pre- versus post-treatment), the combined group offered the

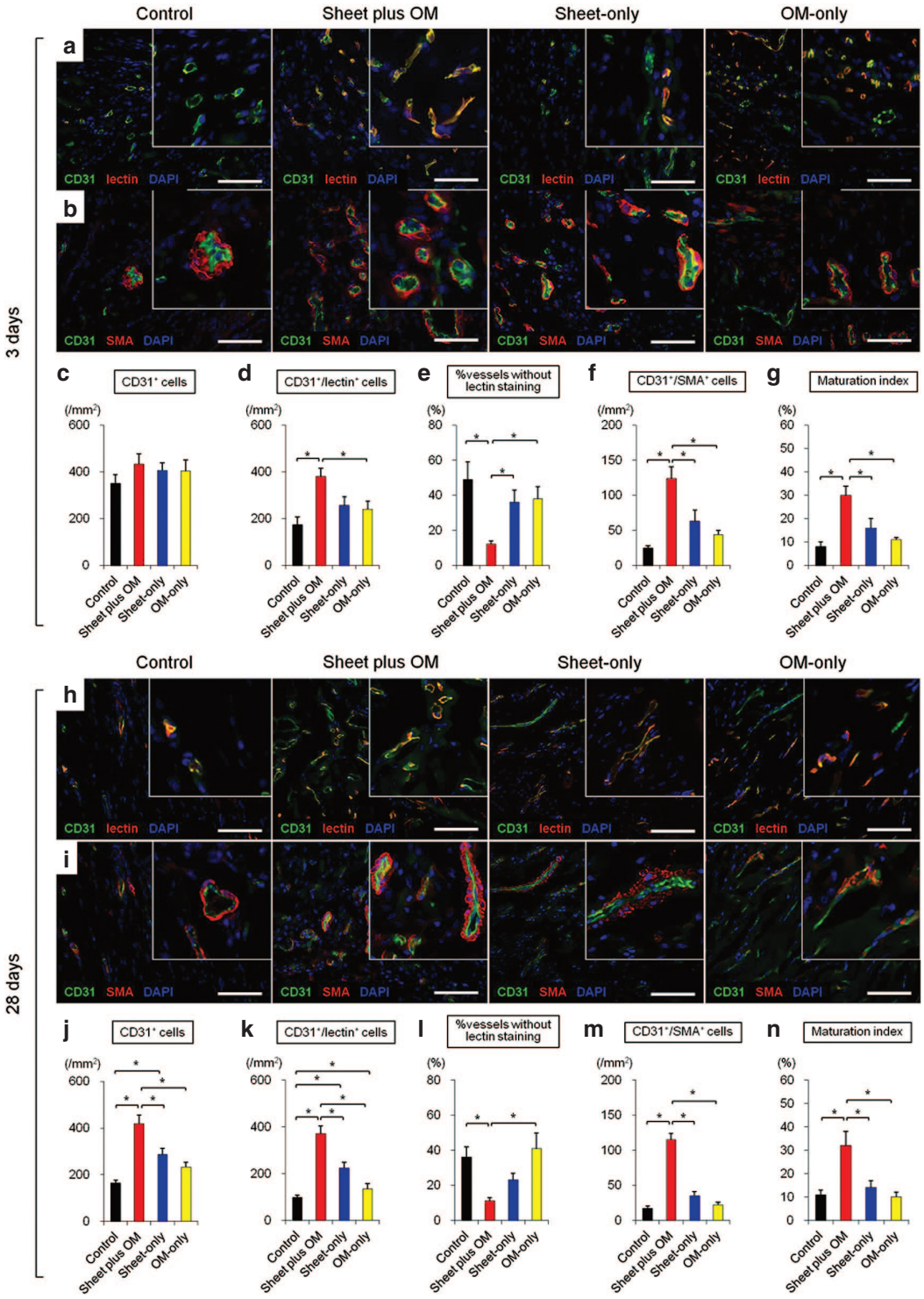

Figure 4 Vessel remodeling and maturation in peri-infarct myocardium. Immunohistochemical analyses of functionality (patency) and vessel maturation observed in peri-infarct myocardium at 3 (n = 6 for each group) (**a–g**) and 28 (n = 11 for each group) (**h–n**) days after treatments (* $P < 0.05$). Representative CD31/lectin and CD31/α-SMA staining at 3 (**a,b**) and 28 (**h,i**) days after treatments (400×, scale bar= 100 μm). Three days after treatment, there was no difference in number of CD31-positive cells among the groups, though the combined group showed a trend of greater number of functional blood vessels with patent endothelial layers (CD31/lectin double-positive) and structurally (CD31/α-SMA double-positive) mature vessels, with a higher maturation index (**c–g**). Notably, the percentage without lectin staining ($CD31^+/lectin^-$) was significantly smaller in the combined group. The number of endothelial (CD31 positive) cells in the control and single treatment groups decreased with time, while that in the combined remained unchanged. Consequently, the angiogenic effects induced in the latter were more profound at 28 days after treatment, with a significantly greater amount of mature vessels (**j–n**).

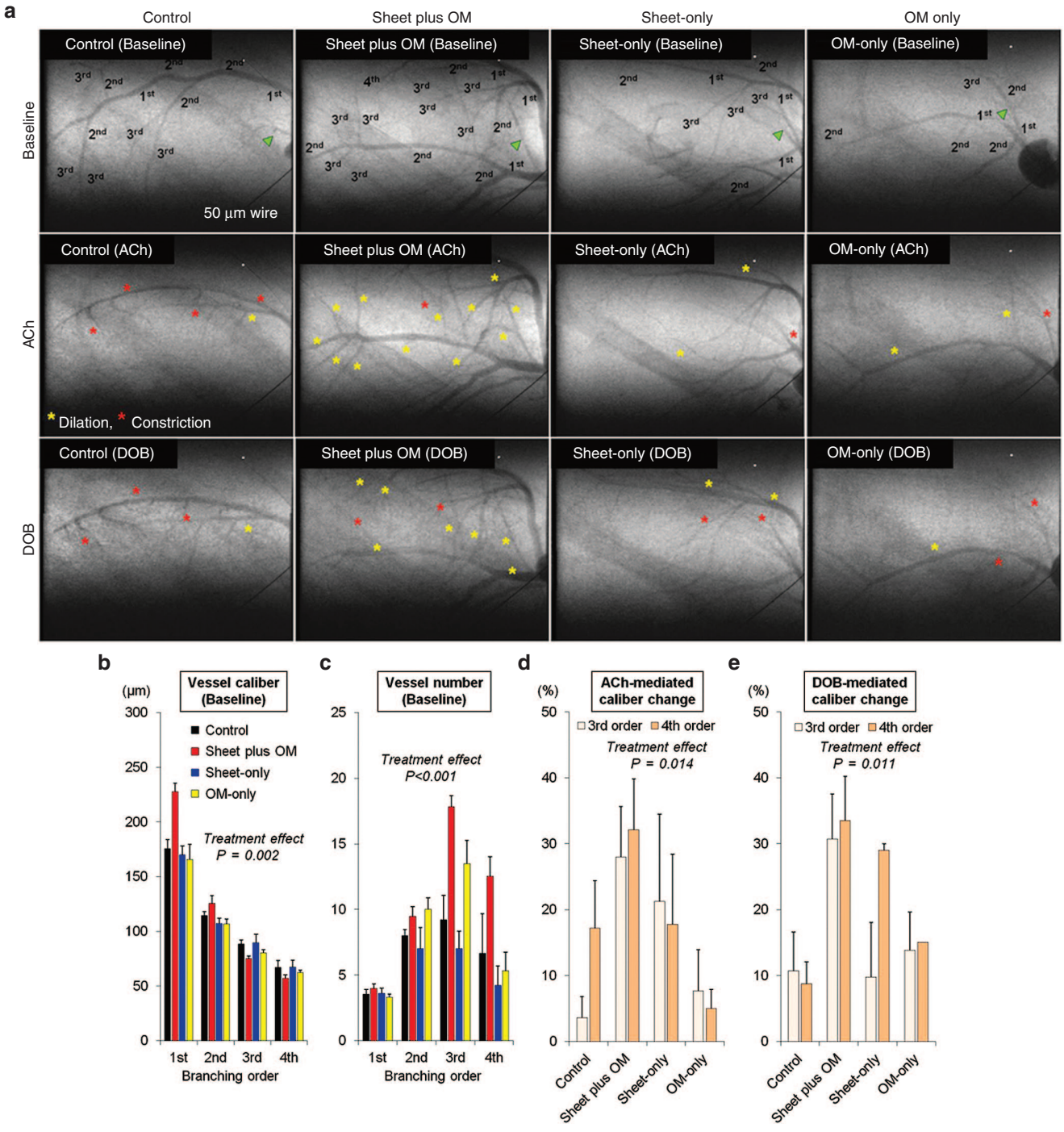

Figure 5 Number of resistance vessels and relative dilatory responses to endothelium-dependent stimulation in ischemic myocardium. Synchrotron radiation microangiography was performed to evaluate vessel number and caliber and relative dilatory responses to acetylcholine and dobutamine hydrochloride in resistance vessels (control: $n = 11$, combined: $n = 11$, cell-sheet: $n = 5$, OM: $n = 6$). Using iodinated agents, coronary microcirculation in ischemic areas was clearly visualized in anesthetized closed-chest rats. Representative angiogram frames for all treatment groups at baseline, and in response to acetylcholine and dobutamine hydrochloride (**a**). Yellow and red asterisks indicate vessels showing dilation and constriction in response to acetylcholine and dobutamine hydrochloride, respectively. Quantitative analyses of (**b**) vessel internal diameter and (**c**) visible vessel number at baseline according to branching order. Vessel internal diameter at baseline (before agent administration) tended to decrease according to branching order and differed among the groups with larger first branching order arteries observed in the combined group (**b**). Moreover, the combined group had a greater number of third and fourth branching order arterial vessels (resistance arterial vessels) at baseline (**c**). Mean caliber changes in response to (**d**) acetylcholine and (**e**) dobutamine hydrochloride. Acetylcholine-mediated dilation in the third and fourth branching orders was significantly different among the groups. The mean caliber changes in response to acetylcholine in the combined group were 28 ± 8% and 32 ± 8% for the third and fourth order branches respectively, which were greater than in the others (**d**). Similarly, the mean caliber changes in response to dobutamine hydrochloride in the combined group were 31 ± 7% and 34 ± 7%, respectively, which were greater than in the others (**e**).

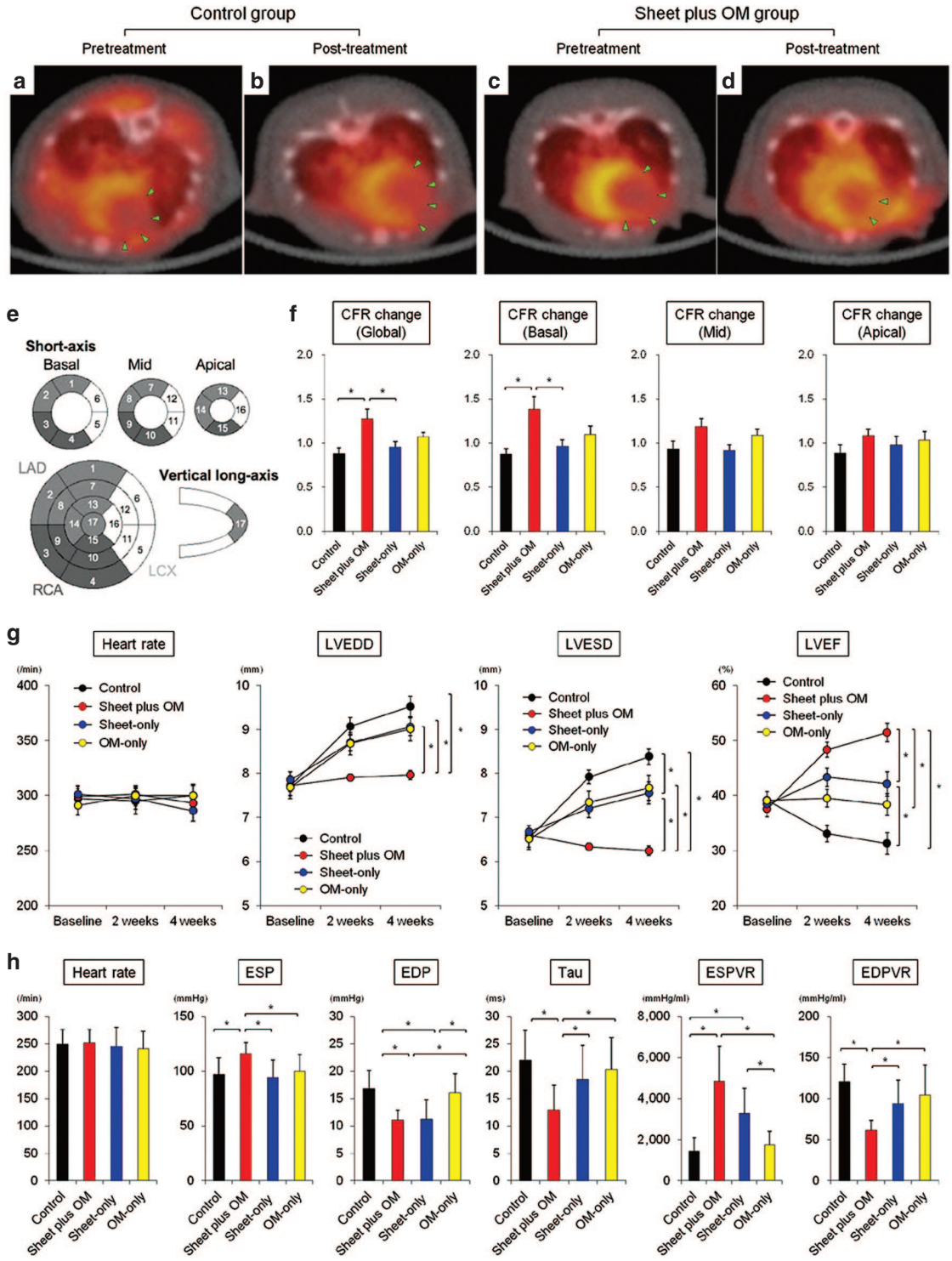

Figure 6 Serial changes in the global and regional coronary flow reserve and cardiac function parameters. Representative serial PET/CT fusion images of $^{13}N\text{-}NH_3$ PET during stress in control (**a,b**) and combined (**c,d**) groups. Recovery of MBF in large portion of basal left ventricle (anterior and lateral segments) was observed in the combined but not control group (green triangles). Quantitative analyses of changes in CFR calculated as a ratio of post-treatment to pretreatment CFR in global, basal, mid, and apical LV segments (control: $n = 5$, combined: $n = 8$, cell-sheet: $n = 7$, OM: $n = 7$) (*$P < 0.05$) (**e,f**). The combined group offered the most remarkable improvement in the global CFR, as evidenced by a higher ratio of post- to pretreatment CFR. Notably, that beneficial change was mainly caused by significant improvement in the basal left ventricle. CFR, coronary flow reserve; MBF, myocardial blood flow. (**g**) Serial assessments of cardiac function parameters at baseline (before treatment), and 2 and 4 weeks after treatments (*$P < 0.05$). In the combined group, remarkable improvements in LV function parameters occurred promptly and were sustained for up to 4 weeks, resulting in significantly smaller LV dimensions and greater LV ejection fraction as compared with other treatment groups. (**h**) Quantitative analyses of hemodynamic function parameters for each treatment (*$P < 0.05$). The basic hemodynamic indices revealed that LV end-systolic pressure was higher, whereas LV end-diastolic pressure and time constant were lower in the combined group as compared to the others. Pressure–volume loop analysis revealed that end-systolic pressure–volume relationship was higher, while end-diastolic pressure–volume relationship was lower in the combined group.

most remarkable improvement in the global CFR, as evidenced by a higher ratio of post- to pre-treatment CFR. Notably, that beneficial change was mainly caused by significant improvement in the basal left ventricle (control 0.9 ± 0.1 versus combined 1.4 ± 0.4 versus sheet-only 1.0 ± 0.1 versus OM-only 1.1 ± 0.1, respectively, ANOVA $P = 0.012$) (**Figure 6e**,**f**).

Global LV function and hemodynamic performance

The cardiac function was evaluated by echocardiography before (at baseline) and 2 and 4 weeks after each treatment ($n = 11$ for each group) (**Figure 6** g,h). Two weeks after left coronary artery ligation, severe dilatation of the LV chamber and severe systolic dysfunction were observed, with no significant differences among the groups (**Figure 6g**). In the control, LV dimensions increased and LV ejection fraction deteriorated in a time-dependent manner, suggesting progressive LV remodeling. In the sheet-only and OM-only groups, LV ejection fraction initially improved, then tended to deteriorate in association with gradual LV dilatation. In the combined group, remarkable improvements in LV function parameters occurred promptly and were sustained for up to 4 weeks, resulting in significantly smaller LV dimensions and greater LV ejection fraction as compared with other treatment groups.

Consistently, the basic hemodynamic indices revealed that LV end-systolic pressure was higher, whereas LV end-diastolic pressure and time constant were lower in the combined group as compared to the others. Load-independent parameters assessed by pressure–volume loop analysis revealed that end-systolic pressure–volume relationship was higher, while end-diastolic pressure–volume relationship was lower in the combined group (**Figure 6h**). These results confirmed that cell-sheet therapy combined with OM-flap improved the therapeutic effects of single treatment group (cell-sheet only or OM-flap only) for the treatment of chronic MI.

Functional capacity assessment

There was no difference in running distance at 4 rpm (control 125 ± 15 versus combined 148 ± 9 versus sheet-only 133 ± 10 versus OM-only 135 ± 15 m, ANOVA $P = 0.63$) ($n = 11$ in each). In contrast, the combined group showed more improved functional capacity in terms of longer running distance at 8 rpm (54 ± 5 versus 178 ± 17 versus 81 ± 10 versus 76 ± 7 m, respectively, ANOVA $P < 0.001$).

Angiographic assessment of communication between coronary arteries and pedicle omentum

Communication between the coronary arteries and branches of the gastroepiploic artery in the OM specimens was evaluated using three different methods with a different series of OM-only and combined group animals ($n = 12$ in each) (**Figure 1a**).

A postmortem angiography examination from the aortic root was performed to verify antegrade flow from the OM into the heart in the combined and OM-only groups ($n = 4$ for each group). In the combined group, aortography revealed that the gastroepiploic artery branches feeding the OM expanded into the heart, and established several tight junctions between the native coronary arteries and OM (**Figure 7a**). In contrast, in the OM-only group, the gastroepiploic artery branches failed to penetrate the heart, accompanied by immature leaky collateral vessel formation between the coronary artery and OM, evidenced by considerable leakage of contrast agent (**Figure 7b**).

We selectively injected India ink into the celiac artery to visually and histologically confirm vessel communication between the pedicle OM and native coronary artery ($n = 4$ for each group). Numerous collaterals filled with India ink were clearly identified between the gastroepiploic artery and native coronary arteries in the combined group, while that was not seen in the OM-only group (data not shown) (**Figure 7c–e**). Histological analysis confirmed vessel communication between those in the combined group (**Figure 7f**,**g**).

Finally, a selective perfusion via aortic root and celiac artery using two different MICROFIL colors was performed ($n = 4$ for each group). In the combined group, MICROFIL solution injected in a retrograde manner into the aortic root (MV-117 Orange) was easily shown expanded into the OM to communicate with the gastroepiploic artery (**Figure 7h**). That solution injected into the celiac artery (MV-120 Blue) was also found to expand into the myocardium and communicated with native coronary arteries (**Figure 7i**). Those findings were not seen in the OM-only group (data not shown).

Vessel migration into cell-sheet from host myocardium and omentum

To further confirm whether the OM- and host myocardium-derived endothelial cells migrated toward the cell-sheet, we established two types of parabiotic pair models ($n = 4$ for each).

In parabiotic pairs of wild-type MI rats that received transplantation of cell-sheets labeled with Cell Tracker TM Orange CMTMR followed by coverage with a GFP-transgenic rat oriented pedicle OM, a large number of OM-derived endothelial cells (isolectin/GFP double-positive cells) had migrated toward the cell-sheet (**Figure 8a–d**). Similarly, in another parabiotic pair of GFP-transgenic MI rats that received cell-sheet transplantation covered with a wild-type rat oriented pedicle OM, a large number of host myocardium-derived endothelial cells (isolectin/GFP double-positive cells) had migrated toward the cell-sheet (**Figure 8e–h**).

Cell-sheet stimulated vascular cell migration

We performed an *in vitro* migration assay using HUVECs to evaluate the effects of skeletal myoblast cell-sheet derived growth factors on vessel recruitment (**Figure 8i**). The number of migrating cells was significantly greater in the 100% conditioned medium group, followed by the 10% conditioned medium and control groups, suggesting that SM cell-sheet derived growth factors stimulate vascular cell migration in a concentration-dependent manner (**Figure 8j**,**k**).

DISCUSSION

The major findings of this study can be summarized as follows. As compared to the single treatment groups, the cell-sheet plus OM group showed (i) improved donor cell retention along with amplified angiogenesis in the cell-sheet through the follow-up (at least day 28), (ii) attenuated cardiac hypertrophy and

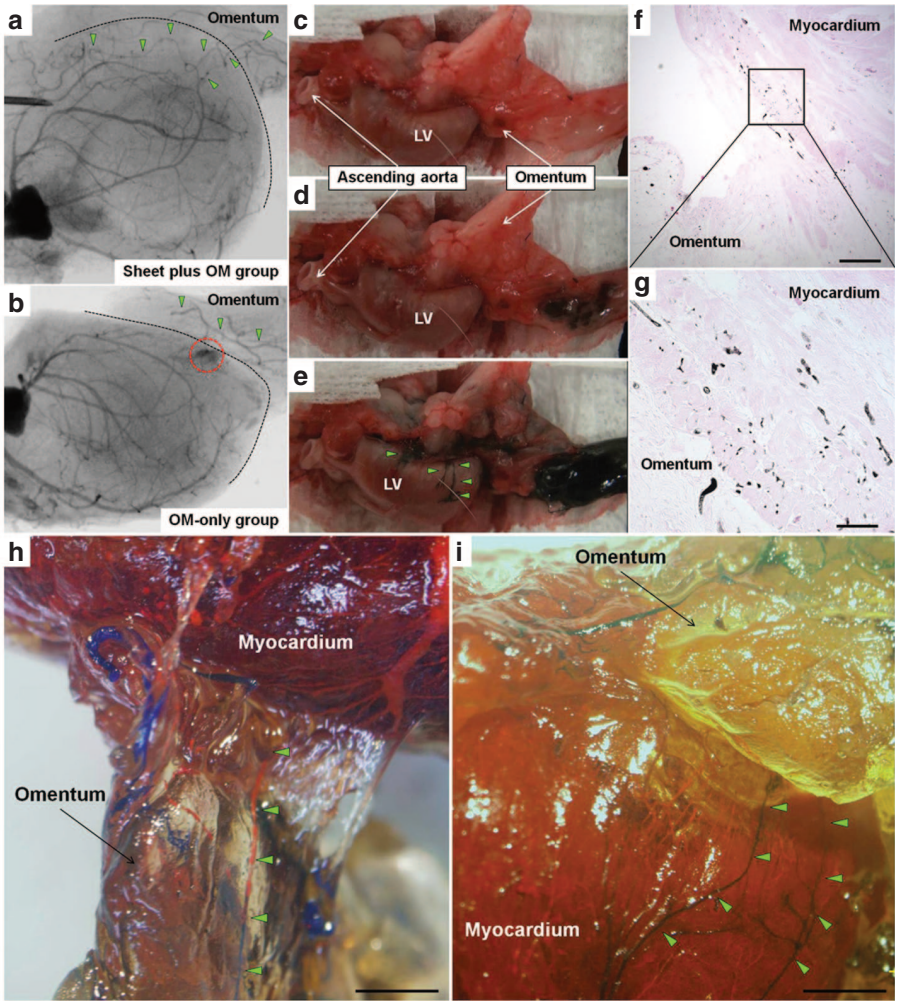

Figure 7 Angiographic assessment of communication between coronary arteries and pedicle omentum. Communication between the coronary arteries and branches of the gastroepiploic artery was evaluated using three different methods with a different series of OM-only and combined group animals. A postmortem angiography examination from the aortic root in the combined (**a**) and OM-only (**b**) groups ($n = 4$ for each group). In the combined group, aortography revealed that the gastroepiploic artery branches feeding the OM expanded into the heart, and established several tight junctions between the native coronary arteries and OM (**a**). In contrast, in the OM-only group, the gastroepiploic artery branches failed to penetrate the heart, accompanied by immature leaky collateral vessel formation between the coronary artery and OM, evidenced by considerable leakage of contrast agent (red dotted circle) (**b**). Black dotted line indicates heart surface. Green triangles indicate the branches of the gastroepiploic artery. Selective India ink injection into the celiac artery to visually and histologically confirm vessel communication between the pedicle OM and native coronary artery ($n = 4$ for each group). Numerous collaterals filled with India ink were clearly identified between the gastroepiploic artery and native coronary arteries in the combined group (**c–e**), while that was not seen in the OM-only group (data not shown). Histological analysis confirmed vessel communication between those in the combined group (**f**: 40×, scale bar = 500 µm, **g**: 200×, scale bar = 100 µm). A selective perfusion via aortic root and celiac artery using two different MICROFIL colors ($n = 4$ for each group). In the combined group, MICROFIL solution injected in a retrograde manner into the aortic root (MV-117 Orange) was easily shown expanded into the OM to communicate with the gastroepiploic artery (**h**, 7.5×, scale bar = 2 mm). That solution injected into the celiac artery (MV-120 Blue) was also found to expand into the myocardium and communicated with native coronary arteries (**i**, 7.5×, scale bar = 2 mm). Those findings were not seen in the OM-only group (data not shown). Green triangles show visible vessel communication in the OM-flap (**h**) and host myocardium (**i**).

fibrosis, and a greater amount of functionally and structurally mature blood vessels in the ischemic myocardium, along with myocardial upregulation of relevant genes, (iii) increased vascularization in resistance arterial vessels with better dilatory responses to endothelium-dependent agents, (iv) more remarkable improvement in the global CFR, mainly caused by significant improvement in the basal left ventricle, (v) sustained improvements in cardiac function parameters and better functional capacity, and (vi) creation of robust vascular communication between the OM and native coronary arteries, shown by *in vivo* angiography.

The retention, survival, and engraftment of transplanted cells in the cell-sheet therapy are largely influenced by the degree of vascularization in the transplanted area and subsequent myocardial inflammation after cell-sheet transplantation.[2,17] The concept of combining OM-flap with the current cell-sheet therapy is likely to be reasonable because the OM is known to play a key role in controlling the spread of inflammation, and promoting revascularization, reconstruction and tissue regeneration. Our data suggest that the combined treatment improved the hypoxic environment in the transplanted area to a greater degree, potentially improving initial cell engraftment and enhancing the paracrine effects induced by

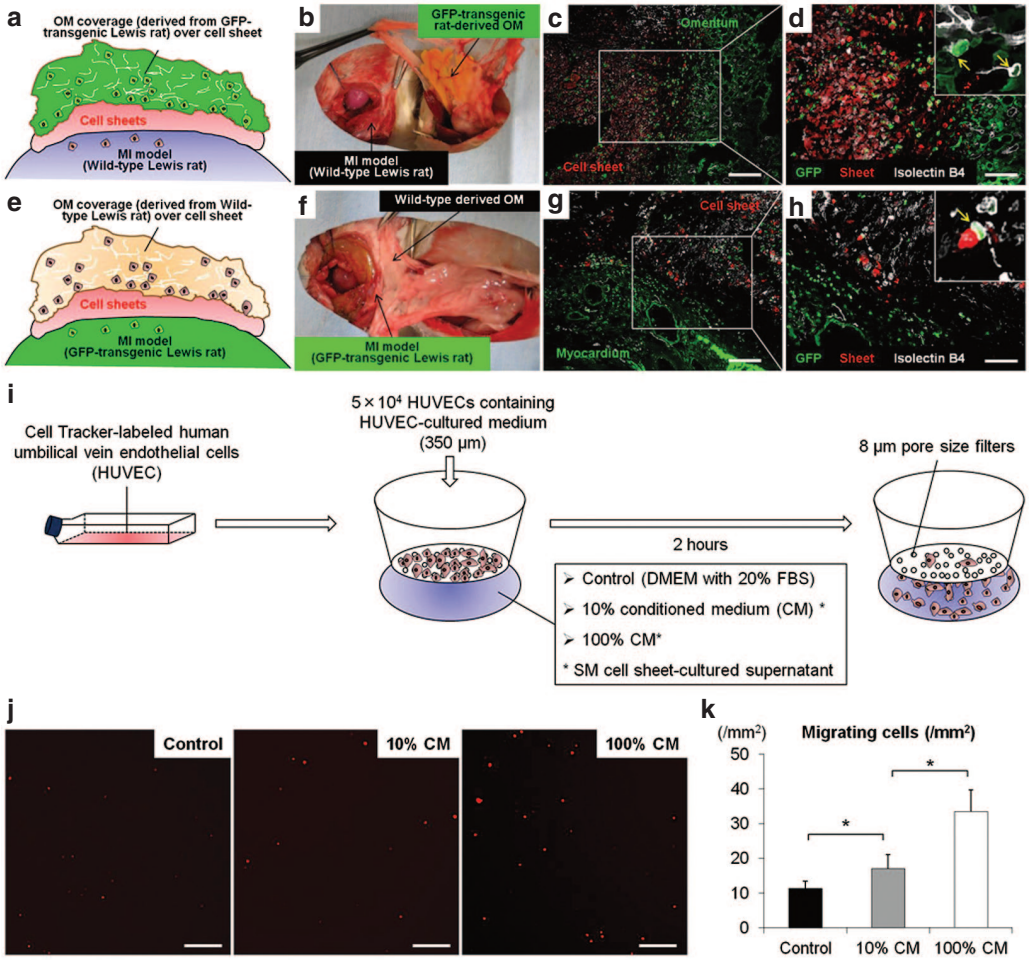

Figure 8 Vessel migration into cell-sheet from host myocardium and omentum. Schematic representation of experimental design to form parabiotic pairs of wild-type MI model rats (recipient) for transplantation of wild-type oriented cell-sheets labeled with Cell Tracker TM Orange CMTMR, followed by coverage with pedicle OM derived from GFP-transgenic rat (donor). (**a,b**) Representative GFP/isolectin staining in parabiotic pairs model (**c**: 100×, scale bar = 200 μm, **d**: 200×, scale bar = 100 μm). Schematic representation of experimental design to form second parabiotic pairs of GFP-transgenic MI rats for cell-sheet transplantation covered with wild-type oriented pedicle OM (**e,f**). Representative GFP/isolectin staining in second parabiotic pairs (**g**: 100×, scale bar = 200 μm, **h**: 200×, scale bar = 100 μm). *In vitro* migration assay (**i**). To investigate cell migration in response to skeletal myoblast cells cultured in conditioned medium, a modified Boyden chamber migration assay was performed using an HTS FluoroBlok Multiwell Insert System containing filters with a pore size of 8 μm. Human umbilical vein endothelial cells (HUVECs) were grown in EGM-2 culture medium. After incubation at 37 °C for 2 hours, the number of migrated cells was counted in 15 randomly chosen fields under 100× magnification using fluorescence microscopy. Two replicate samples were used in each experiment, which were performed at least twice. Migrating cells were analyzed using a light microscope and reported as numbers of migrating cells per mm^2 (**j**). Representative images show migrating cells labeled with Cell Tracker TM Orange CMTMR (100×, scale bar = 200 μm). Quantitative analyses of migrating cells according to concentration in the skeletal myoblast-cultured conditioned medium (**k**). Asterisk indicates statistical significance ($P < 0.05$).

cell-sheet therapy in terms of higher expressions of relevant genes, subsequently stabilizing therapeutic effect of cell-sheet therapy. The discrepancy between functional improvement and donor cell engraftment suggests that the improvement of cardiac function is not mainly mediated by direct contribution of transplanted donor cells but other indirect roles, possibly paracrine effects, offered by the cell-sheet at the early stage of transplantation.

The histological findings demonstrated that the rats receiving the cell-sheet implantation plus OM-flap had a significantly thickened anterior LV wall that was augmented by cardiomyocyte layers as compare to the other groups. Potential mechanisms may include cardiomyogenic differentiation of the donor-derived cells or endogenous stem cells, or paracrinal inhibition of progressive necrosis and/or apoptosis of the native cardiomyocytes. We speculate that both mechanisms might have contributed to the thickening of the targeted LV wall, although cardiomyogenic differentiation was not clearly identified in this study. Improved regional blood flow by the combined therapy could reduce the number of the necrotic/apoptotic cardiomyocytes, while reduced accumulation of fibrous components would inhibit thinning of the LV wall.[5,18] In addition, girdling effects from the covered OM might have reduced wall stress of the LV, leading to maintenance of the LV thickness.[19] Further studies to focus on the cardiomyogenic transdifferentiation using genetically labeled rodent models are warranted.

When blood vessels grow, endothelial cells migrate out first and assemble in a primitive network of immature channels (angiogenesis).[5] As these nascent vessels only consist of endothelial cells,

they rupture easily and are leaky, prone to regression, and poorly perfused.[18,20–22] Recruitment of mural cells around nascent vessels essentially contributes to remodeling and maturation of the primitive vascular network (arteriogenesis), subsequently causing therapeutic improvement of blood perfusion.[5,18] We found a larger percentage of vessels without lectin staining and lower maturation index in the control and single treatment groups, indicating that promotion of angiogenesis, but failure to effectively induce arteriogenesis. Consequently, the single treatments showed only transient effects on global cardiac function and limited functional capacity, possibly due to irregular capillary networks and increased vascular permeability. In the combined treatment group, greater numbers of functionally and structurally mature vessels were established promptly after treatment and maintained in ischemic myocardium. This might be primarily attributed to upregulated expressions of genes related to angiogenesis (*VEGF*, *VEGFR-1*, *VEGF-R2, Akt-1*) and/or endogenous regeneration (*SDF-1*). Moreover, elevated expressions of *Ang-1* and its receptor *Tie-2*, and *PDGF, VE-cadherin*, and *PECAM* might play key roles in promoting maturation processes such as "stabilization" of cell junctions and tight pericyte recruitment (arteriogenesis).[5,15,16,18,20–22] Interestingly, the elevated expression of the those relevant genes shown in the combined group was mostly reduced after 28 days after treatment (data not shown), corresponding with reduced donor cell presence. We found, however, the combined treatment group showed more sustained positive effects on vessel maturity and cardiac function recovery as compared with the control and single treatment groups at 28 days after treatment, indicating that paracrine mediators contribute to the myocardial recovery mainly during the early phase after the treatment and the effects on cardiac function and vessel structure, once established, could last for a longer time.[2] These data suggest that OM-flap covering the cell-sheet played a key role in accomplishing the maturity of the new vessels in the targeted myocardial territory, leading to formation of more organized and durable vascular network, as compared to the control and the single treatment groups.

Endothelial vasodilator function of coronary microvessels (resistance arterial vessels) is an important determinant of myocardial perfusion in response to increased myocardial oxygen demand, playing a critical role in neovascular therapies.[6–8] Vasodilation in response to specific endothelium-dependent and endothelium-independent stimuli within the coronary circulations can be measured to assess endothelial function. To the best of our knowledge, this is the first to verify that cell-sheet treatment with and without OM-flap could improve endothelial vasodilator function of resistance arterial vessels in a rat MI model, utilizing *in vivo* synchrotron-based microangiography that has proved an effective method for clearly visualizing resistance arterioles and accurately identifying neurohumoral modulation of coronary blood flow within the microcirculation for assessing therapy efficacy.[7,23,24] Microangiography revealed attenuated dilatation and a strong trend toward increased incidence of paradoxical constrictions in the control, followed by the single treatment group, suggesting that the endothelial-dependent vasodilator function in resistance arterial vessels was progressively impaired in those groups.[25,26] In contrast, combined treatment effectively restored endothelial function in resistance arterial vessels, evidenced by better dilatory responses to acetylcholine, an endothelium-dependent vasodilator.[27] This corresponds with PET/CT findings demonstrating substantial improvement in CFR, which indicated the ability of the myocardium to increase blood flow in response to increasing myocardial oxygen demand. Adenosine causes vasodilation by stimulating receptors in the microcirculation, facilitating measurement of the endothelium-independent CFR in the microcirculation. Interestingly, a remarkable improvement in CFR was observed in basal, but not apical LV, indicating that the combined treatment might be capable of improving microvasculature functionality of hibernating myocardium, rather than scar cardiac tissue. These physiological benefits in the coronary microcirculation may activate collateral growth through increased flow and shear stress, a powerful driving force of arteriogenesis, leading to enhanced functional capacity under a high load.[28,29] Therefore, we speculate that the present combined treatment strategy has potential to effectively prevent progression of endothelial dysfunction, which independently predicts major clinical adverse events in patients with heart failure.[28–30]

Our data suggest that the combination of cell sheet transplantation and OM-flap acts synergistically, rather than additively, on vessel maturation, coronary microcirculation physiology, functional capacity, and cardiac reverse remodeling, whereas the OM-only strategy failed to stabilize its long-term effect. These results encouraged us to investigate the role of the cell-sheet transplantation in activating the effects of OM-flap. Postmortem angiography findings demonstrated visible collateral vessels between the native coronary arteries and OM-flap in the combined group, whereas no tight junctions were shown in the OM-only group, indicating that formation of collateral vessels between native coronary arteries and OM was accelerated by the interposed cell-sheets. The possible mechanism of those findings might be explained by our *in vitro* migration assay demonstrating that growth factors and cytokines secreted by the cell-sheet stimulate migration of endothelial cells derived from both host myocardium and the OM toward the sheet, subsequently establishing robust vessel connections with persistent blood flow between the native coronary arteries and OM. In contrast, in the OM-only group, lack of that process caused immature leaky collateral vessel formation and thus inadequate collateral blood flow in the ischemic myocardium. Based on those findings, we speculate that the therapeutic effects of the combined treatment strategy might be responsible for increased donor cell survival and stimulation of donor cells induced by OM-flap as well as for cell-sheet–mediated activation of OM-flap as a donor artery with high perfusion capacity. Nevertheless, further studies are absolutely needed to determine the main molecular mechanism of therapeutic effects induced by the combined treatment.

LIMITATIONS

Considering the potential molecular mechanisms behind the beneficial histological and physiological alterations observed with the combined strategy, we found that a group of possibly relevant molecules including *VEGF-A*, *VEGF receptor-1*, *VEGF receptor-2*, *Akt-1*, *SDF-1*, *PDGF-β*, *Ang-1*, *Tie-2*, *VE-cadherin*, and *PECAM* were upregulated in the combined group, suggesting that the effects may be attributed to activation of several paracrine molecules,

rather than a single molecule. Although some may argue what kinds of cytokines play a major role in generating therapeutic effects among the many complex molecular and cellular mechanisms involved, we consider that establishment of mature vessels is a complex process that is not regulated by specific factors, but rather numerous multiple factors that also dynamically change in response to the process of angiogenesis or vessel maturation. We believe that use of a cell-sheet and pedicle-OM as synergistic intelligent engineered tissues can efficiently support the regenerative process by dynamic cross-talk with ischemic cardiac tissue.

Although we did not experience any complication such as torsion of omentum flap or diaphragmatic hernia in the rats receiving the combined treatment, it is considered that a conventional lapalotomy itself may adversely affect general conditions particularly in critically-ill heart failure patients. An endoscopic approach may be useful in minimizing the OM-flap procedure-related complications in clinical settings.

CONCLUSION

We demonstrated that cell-sheet transplantation with an omentum-flap better promoted arteriogenesis and improved coronary microcirculation physiology in ischemic myocardium tissue, leading to potent functional recovery in a rat MI model. Further development of this treatment strategy toward clinical application is encouraged.

MATERIALS AND METHODS

All experimental procedures were approved by an institutional ethics committee. Animal care was conducted humanely in compliance with the Principles of Laboratory Animal Care formulated by the National Society for Medical Research and the Guide for the Care and Use of Laboratory Animals, prepared by the Institute of Animal Resources and published by the National Institutes of Health (publication no. 85-23, revised 1996).

Two weeks after left coronary artery ligation, rats were divided into four groups: (i) skeletal myoblast cell-sheet transplantation covered with an OM-flap (combined group), (ii) cell-sheet transplantation only, (iii) OM-flap only, and (iv) sham operation (control group). The protocol of this study is shown in **Figure 1a**,**b**. All *in vivo* and *in vitro* assessments were carried out in a blinded manner. A detailed description of all methods and reagents used for the experiments is provided in the **Supplementary Materials and Methods**.

SUPPLEMENTARY MATERIAL

Figure S1. Frequency distribution charts showing individual segment caliber changes in response to acetylcholine in **(a)** third and **(b)** fourth branching order vessels.
Materials and Methods.

ACKNOWLEDGMENTS

We thank Tsuyoshi Ishikawa, Yuuka Fujiwara, Yuka Kataoka, Hiromi Nishinaka, Toshika Senba, and staff of the PET Molecular Imaging Center for their excellent technical assistance. This research was supported by Research on Regenerative Medicine for Clinical Application from the Ministry of Health, Labour and Welfare of Japan and the Australian Synchrotron International Synchrotron Access Program (ISAP AS-IA111). Experiments were performed at the Japan Synchrotron Radiation Research Institute (SPring-8, BL28B2, Proposal 2011A1169). T.S. is a consultant for CellSeed, Inc., and T.O. is an Advisory Board Member of CellSeed, Inc. and an inventor/developer holding a patent for temperature-responsive culture surfaces. The authors have no conflicts of interest to report.

REFERENCES

1. Shah, AM and Mann, DL (2011). In search of new therapeutic targets and strategies for heart failure: recent advances in basic science. *Lancet* **378**: 704–712.
2. Narita, T, Shintani, Y, Ikebe, C, Kaneko, M, Harada, N, Tshuma, N *et al.* (2013). The use of cell-sheet technique eliminates arrhythmogenicity of skeletal myoblast-based therapy to the heart with enhanced therapeutic effects. *Int J Cardiol* **168**: 261–269.
3. Sekiya, N, Matsumiya, G, Miyagawa, S, Saito, A, Shimizu, T, Okano, T *et al.* (2009). Layered implantation of myoblast sheets attenuates adverse cardiac remodeling of the infarcted heart. *J Thorac Cardiovasc Surg* **138**: 985–993.
4. Habib, GB, Heibig, J, Forman, SA, Brown, BG, Roberts, R, Terrin, ML *et al.* (1991). Influence of coronary collateral vessels on myocardial infarct size in humans. Results of phase I thrombolysis in myocardial infarction (TIMI) trial. The TIMI Investigators. *Circulation* **83**: 739–746.
5. Carmeliet, P and Jain, RK (2011). Molecular mechanisms and clinical applications of angiogenesis. *Nature* **473**: 298–307.
6. Gutiérrez, E, Flammer, AJ, Lerman, LO, Elízaga, J, Lerman, A and Fernández-Avilés, F (2013). Endothelial dysfunction over the course of coronary artery disease. *Eur Heart J* **34**: 3175–3181.
7. Shirai, M, Schwenke, DO, Tsuchimochi, H, Umetani, K, Yagi, N and Pearson, JT (2013). Synchrotron radiation imaging for advancing our understanding of cardiovascular function. *Circ Res* **112**: 209–221.
8. Furchgott, RF and Zawadzki, JV (1980). The obligatory role of endothelial cells in the relaxation of arterial smooth muscle by acetylcholine. *Nature* **288**: 373–376.
9. Banquet, S, Gomez, E, Nicol, L, Edwards-Lévy, F, Henry, JP, Cao, R *et al.* (2011). Arteriogenic therapy by intramyocardial sustained delivery of a novel growth factor combination prevents chronic heart failure. *Circulation* **124**: 1059–1069.
10. O'Shaugnessy, L (1937). Surgical treatment of cardiac ischemia. *Lancet* **232**: 185–194.
11. Takaba, K, Jiang, C, Nemoto, S, Saji, Y, Ikeda, T, Urayama, S *et al.* (2006). A combination of omental flap and growth factor therapy induces arteriogenesis and increases myocardial perfusion in chronic myocardial ischemia: evolving concept of biologic coronary artery bypass grafting. *J Thorac Cardiovasc Surg* **132**: 891–899.
12. Shrager, JB, Wain, JC, Wright, CD, Donahue, DM, Vlahakes, GJ, Moncure, AC *et al.* (2003). Omentum is highly effective in the management of complex cardiothoracic surgical problems. *J Thorac Cardiovasc Surg* **125**: 526–532.
13. Shudo, Y, Miyagawa, S, Fukushima, S, Saito, A, Shimizu, T, Okano, T *et al.* (2011). Novel regenerative therapy using cell-sheet covered with omentum flap delivers a huge number of cells in a porcine myocardial infarction model. *J Thorac Cardiovasc Surg* **142**: 1188–1196.
14. Kawamura, M, Miyagawa, S, Fukushima, S, Saito, A, Miki, K, Ito, E *et al.* (2013). Enhanced survival of transplanted human induced pluripotent stem cell-derived cardiomyocytes by the combination of cell sheets with the pedicled omental flap technique in a porcine heart. *Circulation* **128**(11 Suppl 1): S87–S94.
15. Mancuso, MR, Davis, R, Norberg, SM, O'Brien, S, Sennino, B, Nakahara, T *et al.* (2006). Rapid vascular regrowth in tumors after reversal of VEGF inhibition. *J Clin Invest* **116**: 2610–2621.
16. Inai, T, Mancuso, M, Hashizume, H, Baffert, F, Haskell, A, Baluk, P *et al.* (2004). Inhibition of vascular endothelial growth factor (VEGF) signaling in cancer causes loss of endothelial fenestrations, regression of tumor vessels, and appearance of basement membrane ghosts. *Am J Pathol* **165**: 35–52.
17. Shimizu, T, Sekine, H, Yang, J, Isoi, Y, Yamato, M, Kikuchi, A *et al.* (2006). Polysurgery of cell sheet grafts overcomes diffusion limits to produce thick, vascularized myocardial tissues. *FASEB J* **20**: 708–710.
18. Carmeliet, P and Conway, EM (2001). Growing better blood vessels. *Nat Biotechnol* **19**: 1019–1020.
19. Hagège, AA, Vilquin, JT, Bruneval, P and Menasché, P (2001). Regeneration of the myocardium: a new role in the treatment of ischemic heart disease? *Hypertension* **38**: 1413–1415.
20. Weis, SM and Cheresh, DA (2005). Pathophysiological consequences of VEGF-induced vascular permeability. *Nature* **437**: 497–504.
21. Cao, Y, Hong, A, Schulten, H and Post, MJ (2005). Update on therapeutic neovascularization. *Cardiovasc Res* **65**: 639–648.
22. Adams, RH and Alitalo, K (2007). Molecular regulation of angiogenesis and lymphangiogenesis. *Nat Rev Mol Cell Biol* **8**: 464–478.
23. Jenkins, MJ, Edgley, AJ, Sonobe, T, Umetani, K, Schwenke, DO, Fujii, Y *et al.* (2012). Dynamic synchrotron imaging of diabetic rat coronary microcirculation in vivo. *Arterioscler Thromb Vasc Biol* **32**: 370–377.
24. Iwasaki, H, Fukushima, K, Kawamoto, A, Umetani, K, Oyamada, A, Hayashi, S *et al.* (2007). Synchrotron radiation coronary microangiography for morphometric and physiological evaluation of myocardial neovascularization induced by endothelial progenitor cell transplantation. *Arterioscler Thromb Vasc Biol* **27**: 1326–1333.
25. Ludmer, PL, Selwyn, AP, Shook, TL, Wayne, RR, Mudge, GH, Alexander, RW *et al.* (1986). Paradoxical vasoconstriction induced by acetylcholine in atherosclerotic coronary arteries. *N Engl J Med* **315**: 1046–1051.
26. Marti, CN, Gheorghiade, M, Kalogeropoulos, AP, Georgiopoulou, VV, Quyyumi, AA and Butler, J (2012). Endothelial dysfunction, arterial stiffness, and heart failure. *J Am Coll Cardiol* **60**: 1455–1469.
27. Bonetti, PO, Lerman, LO and Lerman, A (2003). Endothelial dysfunction: a marker of atherosclerotic risk. *Arterioscler Thromb Vasc Biol* **23**: 168–175.
28. Poelzl, G, Frick, M, Huegel, H, Lackner, B, Alber, HF, Mair, J *et al.* (2005). Chronic heart failure is associated with vascular remodeling of the brachial artery. *Eur J Heart Fail* **7**: 43–48.
29. Meyer, B, Mörtl, D, Strecker, K, Hülsmann, M, Kulemann, V, Neunteufl, T *et al.* (2005). Flow-mediated vasodilation predicts outcome in patients with chronic heart failure: comparison with B-type natriuretic peptide. *J Am Coll Cardiol* **46**: 1011–1018.
30. Heitzer, T, Baldus, S, von Kodolitsch, Y, Rudolph, V and Meinertz, T (2005). Systemic endothelial dysfunction as an early predictor of adverse outcome in heart failure. *Arterioscler Thromb Vasc Biol* **25**: 1174–1179.